
Dublin City University
Ollscoil Chathair Bhaile Átha Cliath

# DEVELOPMENTS IN MODIFIED ELECTRODES FOR SENSING APPLICATIONS

by

**Aoife Morrin B.Sc.**

**Thesis submitted for the Degree of Doctor of Philosophy**

**Supervisors:**
**Prof. Malcolm R. Smyth**
**&**
**Dr. Anthony J. Killard**

**Dublin City University** **July 2004**

## Declaration

I hereby certify that this material, which I now submit for assessment on the programme of study leading to the award of PhD. is entirely my own work and has not been taken from the work of others save and to the extend that such work has been cited and acknowledged within the text of my work.

Signed: _____

ID No.: 50161792

Date: 14 September 2004

## Acknowledgements

First and foremost I want to thank Prof. Malcolm Smyth and Dr. Anthony Killard for all the mentoring, guidance, encouragement and positivity over the past few years. A special thanks to all my fellow postgrads for sharing the highs and the lows - especially Máire, Kathleen, Tom, Blánaid and Gill. I'd also like to thank the rest of the students and staff in the Chemistry department in DCU for all their help, in particular the technicians, whom I could always count on for help.

I also wish to acknowledge the people with whom I collaborated – Dr. Alicia Guzman, Orawan Ngamna and Frank Weilbeer. Also, all the past and present members of Malcolm's group including Niamh, Emily, Clodagh, John, Eimear, Padraic and Adriano.

I was lucky enough to spend some time at Inverness Medical in Scotland and the University of the Western Cape (UWC), South Africa, over the course of my PhD. I want to thank everyone I met during these times. In particular, the Research Team in Inverness Medical, who gave me an invaluable insight into research in the 'real world' and Prof. Iwuoha for giving me the opportunity to work for him in South Africa – a truly memorable time. Also, Prof. Darkwa, Dr. Richard Moutlaoli, and Gretta Mathebe and everyone else that helped me in the Department of Chemistry at UWC.

Finally, I would like to thank my family, especially my Mum, for all the encouragement, support (and the odd few bob!) during my long time in college!

# TABLE OF CONTENTS

## Abbreviations

| | |
|---|---|
| 2,4 D | 2,4 Dichlorophenoxyacetic acid |
| A | Area of electrode |
| a.c. | Alternating current |
| A.U. | Absorbance unit |
| Ab | Antibody |
| ABTS | 2,2'-Azino-bis(3-ethylbenzthiazoline-6-sulphonic acid) |
| AFM | Atomic force microscopy |
| Ag | Antigen |
| Ag/AgCl | Saturated silver/silver chloride electrode |
| $a_i$ | Ion activity |
| APTES | 3-Aminopropyltriethoxysilane |
| bpy | Bipyridyl |
| BSA | Bovine serum albumin |
| C | Concentration of redox active species in bulk solution |
| $c_i$ | Analyte ion concentration |
| CME | Chemically modified electrode |
| CNT | Carbon nanotubes |
| cp | Cyclopentadienyl |
| CPE | Carbon paste electrode |
| CV | Cyclic voltammetry |
| d.c. | Direct current |
| $D^0$ | Diffusion coefficient |
| DBSA | Dodecylbenzene sulphonic acid |
| DCPIP | Dichlorophenolindophenol |
| DNA | Deoxyribonucleic acid |
| $D_O$ | Diffusion coefficient of an oxidised species |
| $D_R$ | Diffusion coefficient of a reduced species |
| dtc | Diethyldithiocarbamato |
| E | Applied Potential |
| $E_{1/2}$ | Half-wave potential |

| | |
|---|---|
| EC | Electrochemical process |
| EDC | 1-Ethyl-3-(3-dimethylaminopropyl)carbodiimide hydrochloride |
| EDX | Electron dispersive x-ray |
| $E_{eq}$ | Equilibrium potential |
| EFM | Electrochemical force microscopy |
| ELISA | Enzyme-linked immunosorbent assay |
| EM | Emeraldine |
| $EM^{\bullet+}$ | Emeraldine radical cation |
| $E^{o}$ | Standard electrode potential |
| $E_{p,a}$ | Anodic peak potential |
| $E_{p,c}$ | Cathodic peak potential |
| F | Faraday's constant |
| FET | Field effect transistor |
| FIA | Flow injection analysis |
| GOD | Glucose oxidase |
| HCG | Human chorionic gonadotropin |
| HF | Hydrofluoric acid |
| His-tag | Histidine tag |
| HOPG | Highly ordered pyrolytic graphite |
| HRP | Horseradish peroxidase |
| i | Current |
| $I_{max}$ | Maximum current |
| $i_{p,a}$ | Anodic peak current |
| $i_{p,c}$ | Cathodic peak current |
| ISFET | Ion-selective field effect transistor |
| ITO | Indium tin oxide |
| j | Current density |
| $j_{p,a}$ | Anodic peak current density |
| $j_{p,c}$ | Cathodic peak current density |
| $K_m^{app}$ | Apparent Michaelis-Menten constant |
| $\vec{k}$ | Rate constant for an anodic process |
| $k^0$ | Electron rate transfer constant |
| $k^{0'}$ | Apparent electron rate transfer constant |

| | |
|---|---|
| LB | Langmuir–Blodgett |
| LDH | L-lactate dehydrogenase |
| LM | Leucoemeraldine |
| $LM^{\bullet+}$ | Leucoemeraline radical cation |
| m | Slope |
| MB | Meldola's Blue |
| MoAb | Monoclonal antibody |
| $M_w$ | Molecular weight |
| MWNT | Multi-walled nanotubes |
| n | Number of electrons transferred |
| NADH | Nicotinamide-adenine dinucleotide |
| $[n\text{-}Bu_4N][BF_4]$ | Tributylammonium tetrafluoroborate |
| NHS | N-hydroxysuccinimide |
| NMR | Nuclear magnetic resonance |
| NTA | Nitrilotriacetic acid |
| O | Oxidized form of an electrochemically active species |
| OSWV | Osteryoung square wave voltammetry |
| PANI | Polyaniline |
| PBS | Phosphate buffered saline |
| PCA | Principal component analysis |
| PEDOT | Poly 3,4-ethylenedioxythiophene |
| PET | Polyethylene terephthalate |
| ppb | Parts per billion |
| PPD | *p*-phenylenediamine |
| ppm | Parts per million |
| ppt | Parts per trillion |
| PPy | Polypyrrole |
| PVC | Polyvinylchloride |
| PVS | Polyvinylsulphonate |
| Q | Charge |
| $Q_{Bare}$ | Charge at a bare gold electrode |
| $Q_{SAM}$ | Charge under the gold oxide stripping peaks |
| R | (a) Reduced form of an electrochemically active species |
| | (b) Universal gas constant |

| | |
|---|---|
| RVC | Reticulated vitreous carbon |
| SAM | Self-assembled monolayer |
| SAMMS | Self-assembled monolayer on mesoporous silica |
| SCE | Saturated calomel electrode |
| SDS | Sodium dodecyl sulphate |
| SECM | Scanning electrochemical microscopy |
| SEM | Scanning electron microscopy |
| SMO | Semi-conducting metal oxide |
| SPE | Screen-printed electrode |
| SPR | Surface plasmon resonance |
| SWNT | Single-walled nanotubes |
| T | Temperature |
| t | Time |
| TCNQ | Tetracyanoquinodimethane |
| THF | Tetrahydrofuran |
| TPA | Tripropylamine |
| TTF | Tetrathiafulvalene |
| UV | Ultra violet |
| WE | Working electrode |
| Y | Yttrium |
| z | Number of electrons per polymeric unit |
| $\Delta Ep$ | Peak potential separation |
| $\Phi$ | Kinetic parameter |
| $\Gamma$ | Surface concentration |
| $\Gamma_{ibf}$ | Film ion barrier factor |
| $\alpha$ | Transfer coefficient |
| $\alpha_a$ | Transfer coefficient of an anodic species |
| $\alpha_c$ | Transfer coefficient of a cathodic species |
| $\gamma$ | Activity coefficient |
| $\rho$ | Specific density |
| $\sigma_p$ | Hammett substituent constant |
| $\upsilon$ | Scan rate |

# Chapter 1

## Chemically Modified Electrodes for Electroanalytical Applications: A Literature Review

## 1.1 INTRODUCTION

Chemically modified electrodes (CMEs) represent a modern approach to electrochemical systems, in particular, electroanalytical systems. Compared with other electrode concepts in electrochemistry, the distinguishing feature of a CME is that quite a thin film (from monomolecular to perhaps a few micrometers in thickness) of a selected substance is bonded to or coated to the electrode surface, to impart the behaviour of that substance to the electrode. This behaviour may be chemical, electrochemical, optical or electrical in nature The ability to control and manipulate the properties of the bonded or coated substance leads to a tailoring of the electrode that can benefit many applications such as electroanalysis and other sensing devices. These include acceleration of electron-transfer reactions, prevention of electrode fouling, selective binding, preferential accumulation and selective membrane permeation. Such steps can impart higher selectivity, sensitivity or stability to electrochemical devices. Other important applications of CMEs include energy conversion and storage, controlled release of drugs, electrochromic displays, corrosion protection and electro-organic synthesis (Wang, 2000).

In this chapter, a brief introduction to some of the techniques that are commonly used in electroanalysis will first be presented and discussed in relation to chemically modified electrodes An insight into the processes that can occur at CMEs, specifically for electroanalytical applications will then be discussed as well as their preparation routes. Considering the scope of the CME field and the amount of publications over the years, this review focuses on research and application of CMEs in the past three years, with key issues relating to electroanalytical chemistry

## 1.2 ELECTROANALYTICAL TECHNIQUES

Electroanalytical techniques are concerned with the measurement of electrical quantities such as current, potential, or charge, and their relationship to chemical parameters Such use of electrical measurements for analytical purposes, in conjunction with CMEs has found a vast range of applications including environmental monitoring, industrial quality control, and biomedical analysis (Wang *et al*, 2000).

This section describes some of the techniques used to monitor both electroactive bulk solution species and attached films, and also how these techniques, in conjunction with CMEs, are applied to quantitative analysis, or sensing. The methods are divided up into three main categories.

1 Voltammetry
2 Potentiometry
3 Conductimetry

### *1.2.1 Voltammetry*

Voltammetry functions by measurement of a current response ($i$) at a working electrode as a function of applied potential ($E$) with respect to a reference electrode, usually a silver/silver chloride (Ag/AgCl) or a saturated calomel electrode (SCE), by means of a potentiostat. When a potential is applied between the working and reference electrodes, the current that is produced then passes between the working electrode and a third auxiliary electrode. Platinum is frequently used as the material for this auxiliary electrode A schematic of this setup is given in *Figure 1 1*.

Potential excitations that can be applied to the working electrode in the solution of interest include ramps, potential steps, pulse trains, sine waves, and various combinations thereof. These excitations survey the potential range of interest Under certain conditions, when a potential is reached where a species present in the bulk electrolyte is oxidised or reduced, current flows between the working and auxiliary electrode at a rate proportional to the concentration of electroactive species.

The current, measured by the potentiostat, as well as giving quantitative information, gives information concerning a large number of physical and chemical parameters about the species of interest.

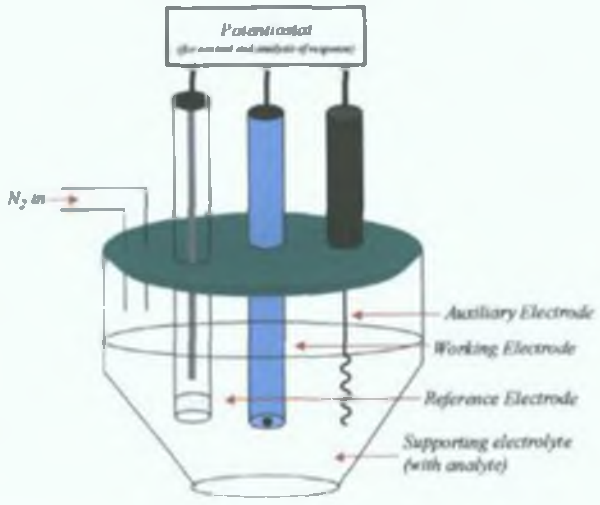


***Figure 1.1.*** A three-electrode electrochemical cell set-up for a typical voltammetric experiment.

### 1.2.1.1 Cyclic Voltammetry

Of all the electrochemical methods available for studying electrode processes, cyclic voltammetry is probably the most widely used. It offers a rapid location of redox potentials of the electroactive species of interest and convenient evaluation of the effect of the media upon the redox process.

Cyclic voltammetry (CV) consists of linearly scanning the potential of a stationary working electrode at a particular scan rate in the forward direction, and then reversing over the same scan range but in the opposite direction. In CVs of reversible reactions, i.e. those with fast electrode kinetics relative to the timescale of the experiment, the product of the initial oxidation or reduction is then reduced or oxidised, respectively, on reversing the scan direction. A schematic of a cyclic voltammogram at a planar electrode for a reversible redox species in solution is given in *Figure 1.2a*. Theoretical analysis of the wave shape leads to the Randles-Sevcik equation for peak current in cyclic voltammetry:

$$i_p = 2.69 \times 10^5 n^{3/2} A D^{0.1/2} C v^{1/2} \qquad \textbf{Equation 1.1}$$

where $n$ is the number of electrons transferred, $A$ is the electrode area ($cm^2$), $D^0$ is the diffusion coefficient ($cm^2\ s^{-1}$), $C$ is the concentration of the redox active species in bulk solution (mmol $cm^{-3}$), and $\upsilon$ is the scan rate ($V\ s^{-1}$)

Of particular note is the proportionality between peak current and $\upsilon^{1/2}$ for a reversible system In practice, however, the systems examined are not always ideally reversible due to slower kinetics, and hence the CVs are not as symmetric as those given in *Figure 1 2a*. These systems are termed quasi-reversible systems For completely irreversible systems, only the oxidation or reduction corresponding to the initial sweep direction appears, since no re-reduction or re-oxidation can occur, i.e. there is no reverse peak. By measuring peak potentials for forward and reverse scans it is possible to deduce standard rate constants from values of peak separation for simple electrode processes, $O + ne^- \longrightarrow R$, where O is the oxidized form of an electrochemically active species, and R is the reduced form of the same species. A method for calculation of these rate constants (Nicholson, 1965) is given in *Chapter 2*. In addition to this computational method, there also are computer simulation and fitting procedures which fit the whole curve, and not just the peak potentials (Bard & Faulkner, 2001).

Electroactive layers immobilised on the electrode surface lead to changes in the shape of the cyclic voltammogram, since they do not have to diffuse to the electrode surface In particular, in the case of fast kinetics, the CV is symmetrical, with oxidation and reduction peak potentials coincident (*Figure 1 2b*). As the kinetics become slower, some peak separations begin to occur. In contrast to *Equation 1 1*, current should be directly proportional to scan rate for an adsorbed, reversible species that shows no intermolecular interactions and fast electron transfers (Brett & Oliveira-Brett, 1993). The behaviour and performance of CMEs based on surface-confined modifiers and conducting polymers are commonly investigated by cyclic voltammetry The blocking/barrier properties of insulating films such as insulating self-assembled monolayers are often monitored by changes in the CV response using a redox marker (e.g. ferrocyanide) in solution (Vergheese & Berchmans, 2004).

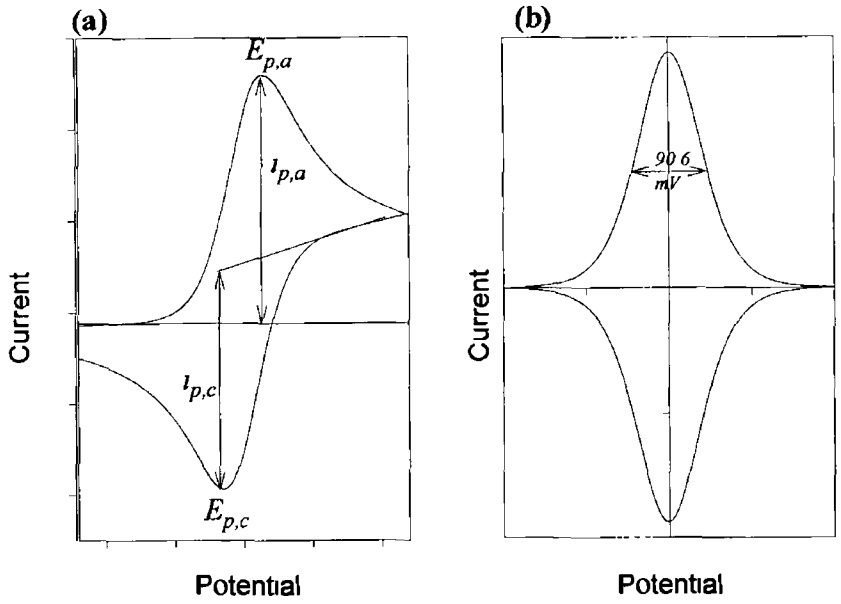


***Figure 1.2.*** Cyclic voltammogram for (a) a reversible redox species in solution at a planar electrode and (b) a reversible redox species in an electroactive layer immobilised on an electrode. $E_{p,a}$ and $E_{p,c}$ represent the anodic and cathodic peak potentials, respectively, and $i_{p,a}$ and $i_{p,c}$ represent the anodic and cathodic peak current heights, respectively.

Cyclic voltammetry is an excellent tool for investigating the mechanism of electrode reactions but in terms of quantitative measurements, limits of detection are not very low ($10^{-5}$ mol $dm^{-3}$) (Wang *et al*, 2000) This is due to the relative contributions to the total cell current of the faradaic and non-faradaic (or capacitive) currents As such, cyclic voltammetry is generally not used for chemical sensing, but rather for characterisation purposes.

### 1.2.1.2 Chronoamperometry

Chronoamperometry involves stepping the potential of the working electrode from a value at which no faradaic reaction occurs, to a fixed potential where oxidation or reduction of some species in solution can occur (Wang *et al*, 2000) This results in a flow of current between the working and auxiliary electrodes that is proportional to parameters, such as concentration of redox active species and the diffusion coefficient, $D^0$, of this species, as governed by the Cottrell equation

$$i = \frac{nFAD^{0^{1/2}}C}{\pi^{1/2}t^{1/2}} \qquad \textit{Equation 1 2}$$

where $n$, $A$, $D^0$ and $C$ are as before, $F$ is Faraday's Constant (C) and $t$ is time.

In terms of analysis, chemically modified electrodes may be employed to induce reduction or oxidation of analyte in solution For instance, when conditions of steady state are reached (i e. when current is independent of scan direction and time), analyte may be added to the electrochemical cell which generates a current flow proportional to the concentration of analyte. Additionally, the CME may serve as a platform for binding of analyte, such as in immunosensors (Moore *et al*, 2003). Bound analyte, usually labelled with a redox active marker, can subsequently be oxidised or reduced and measured quantitatively.

### *1.2.2 Potentiometry*

Potentiometry is another quantitative technique wherein measurements involve the determination of an equilibrium potential generated under conditions of zero current flow, between an indicator and reference electrode (Wang *et al*, 2000) The indicator electrode is modified with a suitable membrane selective to the ion of interest. On the inside of this electrode is an inner solution containing the ion of interest at a constant activity. The equilibrium potential, $E_{eq}$, corresponds to a potential difference across the membrane and is a function of the activity of the ions present in solution, due to the gradient of activity of analyte ions in the inner and bulk solutions. By careful choice of membrane, the selectivity of the response can be increased with minimal interference from other ions. $E_{eq}$ is logarithmically related to the activity of the ion for which the membrane is selective, via the Nernst equation·

$$E_{eq} = E^{o} + \left(\frac{RT}{nF}\right)\log a_i \qquad \textbf{\textit{Equation 1.3}}$$

where $E^{o}$ is the standard electrode potential, $R$ is the universal gas constant ($JK^{-1}mol^{-1}$), T is the temperature (K) and $a_i$ refers to the activity of the ion The ion activity can then be related to concentration using the following equation

$$a_i = \gamma_i c_i \qquad \textbf{\textit{Equation 1.4}}$$

where $\gamma_i$ is the activity coefficient of the ion and $c_i$ is concentration.

Selective electrodes using this measurement principle include primary ion-selective electrodes and multiple membrane electrodes (including gas-sensing and enzyme electrodes) Glass electrodes are examples of ion-selective electrodes that are mainly used to measure pH. The functioning of this glass electrode is by exchange of protons in solution with sodium ions at the surface region of the glass membrane The potential difference generated at this interface is proportional to the concentration of protons in solution.

Multiple membrane electrodes are simple selective electrodes, the membrane of which is covered by a second membrane. This membrane could be gas-permeable (for gas sensing) or contain enzyme (for enzyme sensors) Luo & Do (2004) have developed a potentiometric urea sensor based on the degradation of urea by urease leading to the formation of ammonium ions, which can be detected at an ammonium-selective polyaniline-Nafion membrane-modified working electrode

### *1.2.3 Conductimetry*

Conductimetry is a voltammetric technique used for electroanalytical sensing. It involves the application of an a c. or d c potential between two electrodes immersed in solution. Addition of an ionic species to the solution can lead to a change in the electrical impedance (a.c.) or conductivity (d.c ) of the electrode pair. Chemical modification of the electrodes is necessary to make this sensing technique selective. This type of sensor is most commonly constructed by coating a planar interdigitated electrode array with a thin film of material designed to respond to the analyte of interest. Electrical conductivity changes in this film as a result of interaction with the analyte are monitored, and are proportional to concentration.

Conductimetric gas sensors make use of inorganic or organic films whose electrical conductivity changes in the presence of organic vapours Sahm *et al.* (2004) used a nanoparticulate $SnO_2$ thick film for conductimetric sensing of propanal and $NO_2$. Enzyme-based biosensors use an enzyme immobilised in proximity to the electrode surface in order to achieve specificity for a particular analyte. The catalytic enzymatic reaction leads to the formation of ionic products, which increases the conductivity of the solution proximal to the electrodes (Sheppard *et al*, 1996). An alternative approach to construct conductimetric biosensors exploits the pH-dependent conductivity of conducting polymers. Kim *et al* (2002) constructed a membrane strip

immunosensor based on conductimetric detection using polyaniline-bound gold colloids as the signal generator. Human albumin in buffer solution was used as a model system Important matrices such as blood and urine pose serious problems for conductimetric techniques due to the large fluctuations in ionic activity. As such, a blank electrode is required. One commercial system for the measurement of urea in serum, plasma and urine is the BUN analyser (Beckman-Coulter) based on the enzyme urease. The initial rate of change in conductivity is measured to compensate for the background conductivity of the sample. The instrument is limited to the measurement of analytes at relatively high concentration due to the small changes in conductivity produced by low levels of analyte.

## 1.3 PROCESSES AT MODIFIED ELECTRODES

To prepare a CME, a thin film of a selected chemical is either bound or coated onto the electrode surface to endow the desirable properties of the film to the electrode in a chemically designed manner This can be done in order to facilitate an electrode process that can otherwise only be carried out at a high over-potential, $\eta$, (such as the electrocatalytic oxidation of methanol), or to inhibit a reaction (such as metallic corrosion), or to produce selectivity toward a particular process (such as enzyme-catalysed oxidative determination of glucose in blood) These ends are achieved by developing within the structure of the CME a favourable interplay of the dynamics by which electrons are conveyed between the electrode and the species whose oxidation or reduction is ultimately required to achieve that goal (Bard & Faulkner, 2001). This section classifies some the electrochemical processes, desirable for electroanalysis, that can occur at suitably modified electrodes.

### *1.3.1 Accumulation*

From dilute solutions, accumulation (or preconcentration) of analyte from bulk solution can be performed at an electrode modified with a suitable layer This analyte accumulation at the CME is followed by detection, and its main purpose is to improve detectability. If this accumulation is preferential, because of selective interactions between the analyte and immobilised reagent, then it can serve additionally as a separation step and hence improve the selectivity Yantasee *et al* (2004) developed a highly selective voltammetric method for detection of $Cd^{2+}$, $Cu^{2+}$ and $Pb^{2+}$, based on a carbamoylphosphonic acid self-assembled monolayer on mesoporous silica (SAMMS) Preconcentration allowed detection limits of 0.5 ppb to be reached.

### *1.3.2 Electrocatalysis*

For electroanalytical purposes, electrocatalysis is used to amplify a detection signal. Slow electrode reactions for many important analytes require a

potential greatly exceeding their formal redox potentials in order that these reactions proceed at desirably high rates. The acceleration of such kinetically hindered electrode reactions by electrode-confined mediators permits the quantification of these analytes at less extreme potentials, because catalysed electrode reactions usually occur near the formal potential of the mediator (Kutner *et al.*, 1998). By applying less extreme potentials, both sensitivity and selectivity can be improved significantly. This type of CME is not only selective and sensitive, but also fast and reusable in analytical measurements.

Examples of mediated processes (that may or may not be electrocatalytic) within electroactive films are given in *Figure 1.3*. Primary reactant, A, in the external solution can be converted to product B using the reversible redox mediator P/Q where electron transfer can occur by electron diffusion or electron hopping (*Figure 1.3a*) or by movement (or mass transfer) (*Figure 1.3b*) within the film. Electron transfer from Q to A can then occur in order to produce product B. The mediator Q contained within the film is renewed electrochemically resulting in a cyclic mechanism.

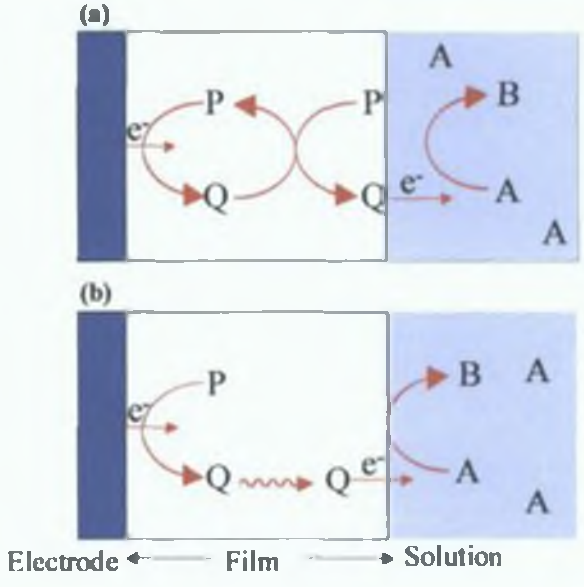


***Figure 1.3.*** Schematic diagram of mediated electrode processes that can occur at a modified electrode. (a) Electron transfer from primary reactant A to product B using immobilised redox mediator P/Q, by electron diffusion and (b) by movement.

The theory of mediated charge transfer has been widely studied by many authors. The electrocatalytic signal dependence on the analyte and/or mediator concentration is governed by four conceivable rate determining steps (or their combination) (Kutner *et al.*, 1998):

1 Convective diffusion of analyte from bulk solution to the film-solution interface

2 Diffusion of analyte through the film

3 Diffusion-like propagation of charge within the film by self-exchange redox reaction

4 Mediator/analyte cross-exchange redox reaction in the film

Several different CMEs have been fabricated for electrocatalysis including mediators attached to monolayer films such as a ferrocene–tethered β-cyclodextrin self-assembled monolayer (Favero *et al*, 2004), conducting polymers such as polyaniline (Grennan *et al*, 2003), and metal or semi-conducting nanoparticles dispersed in a host matrix such as carbon nanoparticles in polyaniline (Zimer *et al*, 2003).

Electrocatalysis is commonly used in biosensing applications where electrochemically active biomolecules (e.g. redox enzyme) are used as the mediator. Usually electrocatalytic biosensors operate amperometrically. However, potentiometric detection has also been used (Rotariu *et al*, 2004). The charge exchange between the electrode and the immobilised biomolecule involved in a catalytic sequence with biological analyte in solution is either direct (Rotariu *et al*, 2004) or it is aided by an additional surface-bound mediator (Grennan *et al*, 2003).

The improvements in sensitivity and selectivity that accrue from electrocatalytic CMEs have been illustrated for numerous analytical problems including the sensing of nicotinamide-adenine dinucleotide (NADH) using a Meldola's Blue modified electrode (Prieto-Simon & Fabregas, 2004), detection of sulphur dioxide on a silver-dispersed self-assembly (Shankaran *et al*, 2002), and DNA hybridisation detection using methylene blue and zirconia thin films (Zhu *et al*, 2004)

### *1 3 3 Permeability*

Permeability provides discriminative transport through a membrane coating that controls access of analyte and interfering substances to the electrode surface (Kutner *et al*, 1998) Mechanisms of the permeability transport are based on

differences in properties, such as charge, size, polarity, shape, or chirality of the analyte from interfering substances. For instance, a cation exchange polymer film on an electrode is a membrane barrier to anions in solution while cations freely partition into it (*Figure 1.4*). Polyanionic perfluorosulphonated ionomers, e.g., Nafion and poly(estersulphonic acid) of the Kodak AQ series are examples of widely used cation-exchange permselective membranes. The permeability of membranes can be combined with other properties such as electrocatalysis. For example, a conducting polymer, polycarbazole modified with tyrosinase was used for electrocatalytic detection of D- and L-norepinephrine, where the polymer could exhibit a chiral differentation, due to a better permeation of the D-form (Cosnier *et al.*, 2003).

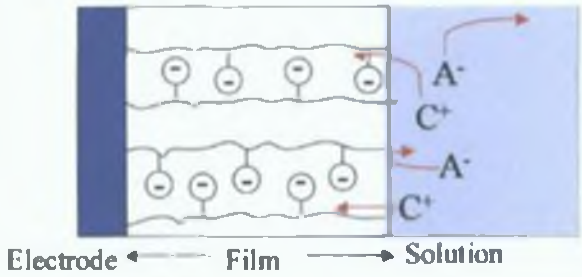


***Figure 1.4.*** Schematic of a CME using a negatively charged polymer film to exclude anionic interferences.

### *1.3.4 Ionic equilibria*

CMEs with selective ion-exchange (ionophore) films are used as asymmetric ion-selective electrodes. That is, an electrolyte solution containing analyte ion is on one side of the membrane and a solid electrode on the other. These CMEs are predominantly used as potentiometric sensors (*Section 1.2.2*).

## 1.4 MODIFICATION METHODS AND THEIR APPLICATIONS

Methods to modify electrodes with behaviours such as these discussed in *Section 1.3* include adsorption and covalent attachment of monolayers, deposition of polymer (by methods such as casting, spin-coating, or electropolymerisation), and bulk modification of carbon composite materials. For the case of adsorption-based CMEs, physical and chemical interaction properties are utilized as the modifying procedures to form monolayer structures. Thiol self-assembled monolayers (SAM) on Au are a well-known example. Easy surface modification and functional group attachment are the chief advantages of this approach. Covalent modification of the electrode surface that uses a specific functional group is also of particular interest in the preparation of CMEs. For example >C=O and >C-O$^-$ functional groups formed on glassy carbon electrodes and –OH groups from oxide electrodes are often utilised for monolayer modification in various applications (Zen *et al*, 2003). Alternatively, thicker polymer-based layers can be used for formation of CMEs. A wide variety of polymers have been used for this approach such as ionomers, redox polymers and inorganic polymers. CMEs are also constructed in supports such as clay, zeolite, $SiO_2$, carbon paste, and other epoxy resins (Zen *et al*, 2003).

This section discusses the different types of CMEs according to the nature of the modification method. Recent applications of these methods relating to analytical chemistry are discussed.

### *1.4.1 Adsorption*

#### 1.4.1.1 Physisorption

Many substances spontaneously adsorb on a substrate surface from solution, generally because the substrate environment is energetically more favourable than in solution (Bard & Faulkner, 2002). Physisorption from solution onto substrates by drop-coating followed by solvent evaporation is a simple route for monolayer CME fabrication. Several redox mediators such as potassium hexacyanoferrate (II),

Meldola's Blue (MB) and dichlorophenolindophenol (DCPIP) have been adsorbed on to glassy carbon electrodes for the electrocatalysis of the oxidation of NADH (Prieto-Simon & Fabregas, 2004) However, the modified electrodes were found to generate continuous desorption of the mediator from the surface resulting in electrode fouling and high standard deviations. Techniques such as mediator-entrapped composites and electrodeposition were found to be more suitable for prevention of leaching.

Carbon nanotubes (CNT), a new promising electrode support material, can be physisorbed onto substrates such as gold (Guo *et al*, 2004) or carbon (Gong *et al*, 2004). Both single-walled nanotubes (SWNT) and multi-walled nanotubes (MWNT) exist They have a hollow-like cylindrical structure, which has appreciable adsorption ability for unique application in electroanalytical sensors, in particular gas sensors (Wang *et al*, 2004) Cantalini *et al* (2003) have developed a carbon nanotube $NO_2$ gas sensor based on resistance measurements. The electrical resistance of the nanotubes was found to decrease on adsorption of $NO_2$, due to the electron withdrawing properties of this gaseous molecule. A detection limit of 10 ppb for $NO_2$ was reached with this method Other important sensor applications of the CNTs are NADH (Musameh *et al*, 2002) and DNA (Gong *et al*, 2004) sensors.

#### 1.4.1.2 Chemisorption

Even though physisorbed systems are useful for analytical applications, stability is always a critical problem for such electrodes Chemisorbed routes provide more thermally stable CMEs. A good example is self-assembled monolayers (SAMs) of organosulphur compounds with long chain groups on Au. The thiol group binds tightly to the gold electrode, and the lateral interactions between neighbouring chains create a regular structure in which the chains are extended in parallel at an angle from the normal. The well-ordered monolayers formed by alkanethiols can be used to immobilise proteins close to an electrode surface with a high degree of control over the molecular architecture of the recognition interface (Gooding & Hibbert, 1999) As a consequence of this ability, SAMs have been used for fundamental investigations of the interactions of proteins and electrodes (Faucheux *et al.*, 2004) and for the fabrication of biosensors (Campuzano *et al.*, 2002). Further literature on SAM technology and a novel electroactive SAM for catalysis in a biosensor is presented in

*Chapter 5* Other applications of SAMs include corrosion prevention, chemical catalysis and controlling of surface energy.

### *1.4.2 Covalent Attachment*

Stronger attachment to the substrate surfaces can be accomplished by covalent linking of the desired component to surface groups present on, or formed on, the substrate to form a monolayer The surface functional group of base electrodes can be derivatised either by synthetic route or by controlling the oxidation/reduction potentials in a suitable medium. Carbon surfaces are found to be efficient for covalent modifications due to their alterable functionalities. Ammo, aryl, diazonium and acrylacetate-based compounds have all been used for the development of stable, compact films. The compounds may then be suitably coupled with redox groups for further electroanalytical applications. Components linked to electrode surfaces in this way include various ferrocenes, viologens and $M(bpy)_n^x$ species (M = Ru, Os, Fe, bpy = bipyridyl), as they show easily detectable electrochemical reactions, These mediators have been used extensively in electroanalytical applications. An electrochemically stable monolayer of $Ru(bpy)_3^{2+}$ was obtained on glassy carbon for the first time by Wang *et al.* (2001) It was based on the electrostatic attachment of $Ru(bpy)_3^{2+}$ to benzene sulphonic acid monolayer film covalently bound to glassy carbon electrode by the electrochemical reduction of diazobenzene sulphonic acid using cyclic voltammetry. The good stability of this Ru modified electrode allowed the sensitive determination of tripropylamine (TPA) in a flow injection analysis (FIA) system.

Covalent attachment of protein monolayers on electrode surfaces has also been carried out. With intimate contact between the redox active biomolecule and the electrode using covalent attachment, direct electron transfer can be observed This electronic coupling between the protein and the electrode can be used for the construction of biosensors that eliminate the need for mediation (Gorton *et al.*, 1999). Quan *et al* (2004) have examined several covalent immobilisation methods for laccase on both glassy carbon and platinum. In the case of glassy carbon, the surface was modified by electrochemical oxidation of 1,5-pentanediol or by direct electrochemical oxidation to introduce the carboxylic acid functional group Peptide coupling between laccase and the functional groups of the modified surface was done

by the use of 1-ethyl-3-(3-dimethylaminopropyl)carbodiimide hydrochloride (EDC) and N-hydroxysuccinimide (NHS). In the case of platinum, the surface was modified to introduce hydroxyl functional groups, followed by coupling the enzyme with cyanuric chloride Another method tested was the modification of the surface by silanization with 3-aminopropyltriethoxysilane (APTES), which was followed by coupling the enzyme with glutaraldehyde. The silanization method was the most effective with respect to long-term stability (60 successive measurements) and fast response times (< 2 s) for *p*-phenylenediamine (PPD) detection. Covalent attachments have also been successfully carried out for glucose oxidase (GOD) on indium tin oxide (ITO) (Fang *et al.*, 2003), and oligonucleotides on silicon (Yin *et al.*, 2004). Covalent attachment of enzymes to vertically orientated carbon nanotubes was reported for the first time by Yu *et al.* (2003). Quasi-reversible Fe(III)/Fe(II) voltammetry was observed for the iron heme enzymes myoglobin and horseradish peroxidase coupled to the carboxylated ends of the nanotubes by amide linkages

### *1.4.3 Modification with polymers*

Polymeric modifying layers result in fairly thick films, typically a few micrometers Polymer films can be formed on an electrode surface from solutions of either the polymer or the monomer Methods that start with dissolved polymer include casting, spin-coating, electrodeposition and covalent attachment via functional groups. Starting with the monomer, one can produce films by thermal, chemical, electrochemical, plasma or photochemical polymerisation

#### 1.4.3.1 Conducting Polymers

Conducting polymers have attracted much interest in recent years. Conducting polymers contain π-electron backbones responsible for their unusual electronic properties such as electrical conductivity, low energy optical transitions, low ionisation potential and high electron affinity. The π-conjugated system of these polymers have single and double bonds alternating along the polymer chain which make them capable of functioning as electron transfer mediators. With these materials, redox changes are not localised at a specific centre but rather delocalised

over a number of conducting polymer groups (Gerard *et al.*, 2002). Examples of these species are polyacetylene, polypyrrole (PPy), polyaniline (PANI), and polythiophene (*Figure 1 5)* Electropolymerisation of monomer onto electrodes is the most commonly reported method to develop this type of CME in electroanalytical applications. Incorporation of modifiers such as biomolecules can be achieved by encapsulation, adsorption or covalent attachment at a functional group (Cosnier & Lapellec, 1999).

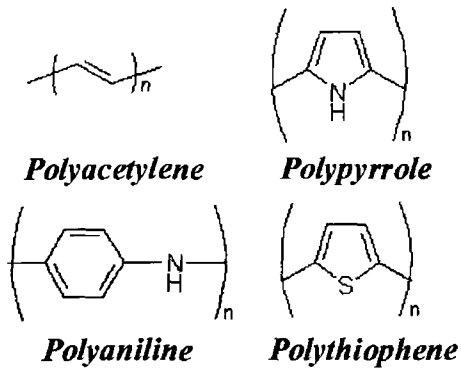


***Figure 1.5.*** Structures of electronically conducting polymers

Conducting polymers can be synthesised by both electrochemical and chemical oxidative polymerisation (Gerard *et al.*, 2002). Electrochemical synthesis is rapidly becoming the preferred method because of its simplicity and increased reproducibility (the mechanism of which will be discussed in *Section 2 1 1* in relation to polyaniline). Electrochemical polymerisation is generally employed by galvanostatic, potentiostatic or potentiodynamic methods.

The ability to synthesise some of these polymers, such as PPy, under mild conditions enables a range of biological moieties (enzymes, antibodies and even whole living cells) to be encapsulated into the polymer structure (Mailley *et al.*, 2004). Polythiophene, another conducting heterocyclic polymer, cannot be synthesied from aqueous media due to the insolubility of its monomer. Substitutions to thiophene with flexible alkyl or alkoxy side chains have served to increase the solubility of the monomer (Udum *et al*, 2004). Vedrine *et al.* (2003) used the functionalised polythiophene, poly 3,4-ethylenedioxythiophene (PEDOT), in an enzyme-based biosensor. PEDOT was synthesised electrochemically from an aqueous medium, providing stable, homogenous films. PEDOT served both as an electrocatalytic non-diffusional mediator and as an entrapment matrix for the enzyme. Polyaniline can be

synthesised readily from aqueous media However, acidic conditions are required for formation of the most highly conductive form Because of this, entrapment is not generally used, as the activity of the biomolecule may be affected. A novel polyaniline uricase biosensor prepared by a template process was recently reported by Kan *et al* (2004). Electrochemical polymerisation was carried out in an acidic aniline solution containing uricase. The electrode was then hydrolysed in acid to remove the uricase to form cavities Active uricase was then doped into the uricase cavities available Biomolecules can also be doped onto the surface of the polymer (e.g polyaniline) by electrostatic interactions with the polymer backbone (Grennan *et al.*, 2003) In this way, diffusion of substrates and biorecognition molecules does not have to take place into and out of a polymer matrix as traditionally occurs in polymer entrapment systems which is important when dealing with high molecular weight species as often occurs with biosensors.

Abtech Scientific Inc (Pennsylvania, USA) market polymer-modified interdigitated microsensor electrode array devices possessing surface-available groups for the specific covalent attachment of biomolecules such as enzymes, NA and antibodies. These microsensors are amenable to conductimetric, potentiometric and amperometric formats.

### 1.4.3.2 Ion-exchange polymers

Ion-exchange polymers (polyelectrolytes) contain charged sites that can bind ions from solution via an ion-exchange process Typical examples are Nafion, Toflex, polystyrene sulphonate and protonated poly(4-vinylpyridine) These types of polymer-modified electrodes are generally prepared by the drop-coating technique Solid electrodes coated with thin films of ion-exchange polymers allow the quick preconcentration and simultaneous voltammetric detection of small electroactive inorganic and organic ions This approach can also be used for incorporation of electroactive species within the polymer. In addition to incorporation capabilities, the ionic interactions between the ion-exchanger and enzymes can promote the direct electrochemistry of the enzyme without requiring mediator Ugo *et al* (2002) demonstrated this principle for cytochrome *c* using a polyestersulphonated ionomer-coated glassy carbon.

### 1.4.3.3 Encapsulation polymers

Sol-gel polymers are another new and attractive material for tailoring electrode surfaces for electroanalytical applications Low temperature encapsulation of the recognition species and/or redox mediator can be achieved with the sol-gel technique Such ceramic films are prepared by the hydrolysis of an alkoxide precursor such as $Si(OCH_3)_4$ under acidic or basic condensation, followed by polycondensation of the hydroxylated monomer to form a three-dimensional interconnected porous network. The resulting porous glass-like material can physically retain the desired modifier but permits interaction with the analyte that diffuses into the matrix Besides their ability to entrap modifier, sol-gel processes offer tunability of their physical characteristics such as permselectivity, thermal stability and mechanical rigidity Sol-gel derived composite electrodes have also been prepared by dispersing carbon or gold powders in the initial sol-gel mixture (Salimi & Abdi, 2004) Non-conducting polymers such as polyphenol, polyphenylenediamines and overoxidised polypyrrole have also been used for encapsulation of desired modifiers (Iwuoha *et al*, 2004, Yuqing *et al*, 2004).

### *1.4.4 Bulk modification of carbon composite materials*

Carbon paste electrodes (CPEs) have been extensively used for electroanalytical applications since their introduction by Adams in 1958. These electrodes can be fabricated under mild conditions consisting of blending a carbon powder with a hydrophobic binder. Entrapment of modifiers such as enzymes and inorganic catalysts within the paste during the fabrication process to develop another type of CME has been effectively used in recent years. The electrodes are nonporous and their surfaces can be renewed mechanically. Thus the electrode surfaces can be restored reproducibly after fouling or loss of catalytic activity. Calvo-Marzal *et al.* (2004) used a carbon paste electrode chemically modified with tetrathiafulvalene-tetracyanoquinodimethane (TTF/TCNQ) for amperometric detection of reduced glutathione. Serban & El Murr (2004) have shown that bulk modification of a carbon composite with zeolites of the type NaY (Y = yttrium), can effectively lower the overpotential required for oxidation of NADH. This was attributed to higher

hydrophilicity of the electrode surface when these zeolite particles were dispersed in it, favouring electron transfer. The utility of CPEs modified with cobalt(II) phthalocyanine for electrocatalytic oxidation of guanine and single stranded DNA in aqueous solution has also been demonstrated (Abbaspour *et al.*, 2004).

Although there have been many electroanalytical applications of this CME technique, it has been argued that the modification method is mechanically unstable leading to leakage of modifier and hence, irreproducibility. Proposals to prepare a carbon paste electrode by *in situ* electropolymerisation of polypyrrole within a paste containing enzyme, pyrrole monomer, carbon particles, and Nujol by Mailley *et al* (2004) has been shown to remarkably improve the mechanical stability of the modifier. With this *in situ* generated polymer network, leaching of enzyme can be prevented. Over a 72 h period of immersion, 0.1 μg of enzyme leached from a CPE in the presence of polypyrrole, while 150 μg leached from a CPE containing no polymer network, showing the remarkable effect of this *in situ* generated polymer. In the case of Calvo-Marzal *et al* (2004), Nafion was incorporated into the carbon paste electrode m order to retain the mediator Other stabilising agents that have been used include epoxy resin, Kel-F and Teflon.

## 1.5 SUMMARY

The absence of any molecular character of a 'naked' electrode which results in a lack of molecular selectivity and specificity has been a major shortcoming of electrochemistry and, in particular, its application in analytical chemo- and bio-sensor development. Modification of electrode surfaces for CME fabrication is used to improve response to analyte compared with that obtained at an unmodified surface, to create a novel, selective response to analyte.

CMEs have potential for commercial application in many fields such as healthcare, environmental monitoring, and the food industry However, despite the voluminous fundamental research over the past years on this technology, only a few commercial uses of CMEs for analytical applications have been described These include for instance, amperometric glucose sensing electrodes (Johnson & Johnson), based on a disposable format, and an 'electronic nose' (MOSES), comprised of up to 64 selective gas sensors for bench-top use

The ideal sensor should be easy to use, sensitive, selective and free from interferences. Simplification and short analysis times are also important Present research is focusing on the long-term stability and reproducibility of CMEs in order to develop superior CMEs for reliable use in analytical applications Amenability of CMEs to cheap mass-production is another important criterion that must be met before their widespread commercialisation Modifications of electrodes with SAMs, carbon nanotubes and conducting polymers all have potential in this respect.

## 1.6 THESIS OUTLINE

The purpose of this research was to investigate different electrode types and modifications to their surfaces for development of disposable electrochemical bio- and chemical sensors Various approaches are described which encompass technologies such as screen-printing, conducting polymers, and self-assembled monolayers. Moves towards mass production of these sensors is described, with the ultimate goal being the development of disposable electrodes that could be produced at large scales

*Chapter 2* of this thesis reports on commercial screen-printed electrodes (SPEs) and SPEs designed and fabricated in-house using various carbon inks They were characterized through electrochemical and microscopic techniques to yield electrodes with optimal properties for electrochemical sensing applications. The in-house design was pursued and the most suitable carbon ink chosen and optimized. The behaviour of electrochemically grown polyaniline films on these SPE surfaces was also described. Primarily, the thickness of this film was examined with a view to developing a more in-depth understanding of its charge transfer properties. Amperometry was the main experimental technique used where horseradish peroxidase (HRP) was incorporated into the system and hydrogen peroxide used as substrate.

*Chapter 3* investigates the protein binding capacity of this polymer-modified SPE using electrostatic adsorption. Both colorimetric and electrochemical techniques were employed to establish optimum working concentrations of bound protein to determine absolute mass of protein binding to the surface of the polymer, and a theory is put forward to connect the physical structure of the electrode with the optimum experimental characteristics

The properties of nanoparticulate conductmg polyaniline are examined in *Chapter 4* as an alternative to the monomer solution previously used for deposition of polyaniline (*Chapter 2*). Biosensor fabrication processes by means of electrodeposition and drop-coating were explored, and their application in an enzyme biosensor Long-term objectives of this work would be to develop a mass-producible sensor in a single fabrication step.

*Chapter 5* describes another electrocatalytic sensing platform using a novel spontaneously adsorbed cyclopentadienylnickel(II) thiolato Schiff base compound on gold The electrochemistry of this layer was explored, and the redox active layer was successfully applied as a novel electron transfer mediator in biosensing. The redox active layer was shown to effectively mediate the reaction of surface-bound HRP with substrate hydrogen peroxide, demonstrating another feasible sensor fabrication strategy.

*Chapter 6* reports on research into chemical sensors involving cyclopentadienylnickel thiolate complexes as sensing materials for sulphur dioxide. These redox active complexes form electrochemically stable $SO_2$ adducts A shift in formal potential upon the formation of this $SO_2$ adduct shows that the compounds are suitable for application as organic phase amperometric $SO_2$ sensor materials. Electrochemical, UV-Vis and $^1H$ NMR spectroscopic analyses show that the formation of $SO_2$ adducts causes the perturbation of the electronic density of the nickel metal centre, indicated by the shifts in the formal potentials of the redox couple that is dependent on $SO_2$ concentration.

Modifications of surfaces of electrodes in this research provides new and interesting properties in order for creation of new technological possibilities for both biochemical and chemical sensors in the future Recommendations for future work arising from this thesis are given in *Chapter 7*

## 1.7 REFERENCES


Abbaspour, A , Mehrgardı, M , Kıa, R (2004) Electrocatalytıc oxıdatıon of guanıne and ss-DNA at a cobalt(II) phthalocyanıne modıfied carbon paste electrode. *J Electroanal Chem* , **568** 261-266

Adams, R (1958). Carbon paste electrodes. *Anal Chem* **30** 1576-1576

Bard, A , Faulker, L (2001) Electrochemical Methods, Second Edıtion. *Wıley & Sons Inc , New York*

Brett, C., Brett, M. (1993) Electrochemıstry: prınciples, methods and applıcatıons *Oxford Scı Pub , Oxford* pp. 186

Calvo-Marzal, P , Torres, K , Hoehr, N , Neto, G , Kubota, L (2004) Determınation of reduced glutathione usıng an amperometrıc carbon paste electrode chemıcally modıfied wıth TTF-TCNQ. *Sens Actıat B ,* 100.337-344.

Campuzano, S , Galvez, R , M Pedrero, M , Manuel de Vıllena, F., Pıngarron, J M. (2002) Preparatıon, characterısatıon and applıcatıon of alkanethiol self-assembled modıfied with tetrathiafulvalene and glucose oxıdase at a gold dısk electrode. *J Electroanal Chem* , **526**:92-100.

Cantahni, C , Valentını, L , Armentano, I , Lozzi, L , Kenny, J , Santucci, S. (2003) Sensıtıvıty to $NO_2$ and cross-sensıtıvıty analysıs to $NH_3$, ethanol and humıdıty of carbon nanotubes thın film prepared by PECVD *Sens Actuat B,* **95** 195-202.

Cosnier, S , LePellec, A , Marks, R., Perıe, K., Lellouche, J (2003) A permselectıve biotinylated polydıcarbazole film for the fabrıcatıon of amperometrıc enzyme electrodes *Electrochem Comm* , **5**.973-977

Cosnier, S Lepellec, A. (1999) Poly(pyrrole-biotin) a new polymer for biomolecule grafting on electrode surfaces. *Electrochim Acta*, **44** 1833-1836

Fang, A , Ng, H., Fong, Li, S. (2003) A high-performance glucose biosensor based on monomolecular layer of glucose oxidase covalently immobilised on indium-tm oxide *Biosens Bioelectron* , **19** 43-49

Faucheux, N , Schweiss, R , Lutzow, K , Werner, C , Groth, T (2004) Self-assembled monolayers with different terminating groups as model substrates for cell adhesion studies *Biomater* , **25**·2721-2730

Favero, G , Campanella, L., D'Annibale, A , Ferri, T. (2004). Preparation and characterisation of a chemically modified electrode based on ferrocene-tethered β-cyclodextrin self-assembled monolayers. *Microchem J* , **76**.77-84.

Gerard, M., Chaubey, A , Malhotra, B (2002). Application of conducting polymers to biosensors. *Biosens Bioelectron* , **17** 345-359

Gong, K., Dong, Y , Xiong, S , Chen, Y., Mao, L. (2004). Novel electrochemical method for sensitive determination of homocysteine with carbon nanotube-based electrodes *Biosens Bioelectron* , **20**.253-259

Gooding, J , Hibbert, B (1999) The application of alkanethiol self-assembled monolayers to enzyme electrodes. *Tr Anal Chem* , **18** 525-533.

Gorton, L , Dominguez, E. (2002). Electrocatalytic oxidation of NAD(P)H at mediator-modified electrodes. *Rev Mol Biotech* , **82** 371-392.

Grennan, K., Strachan, G., Porter, A , Killard, A , Smyth, M.R. (2003) Atrazine analysis using an amperometric immunosensor based on single-chain antibody fragments and regeneration-free multi-calibrant measurement *Anal Chim Acta*, **500**·287-298.

Guo, M , Chen, J , Nie, L , Yao, S. (2004) Electrostatic assembly of calf thymus DNA on multi-walled carbon nanotube modified gold electrode and its interaction with chlorpromazine hydrochloride. *Electrochim Acta,* **49** 2637-2643

Iwuoha, E , Williams-Dottin, A , Hall, L., Morrin, A , Mathebe, G , Smyth, M.R , Killard, A J (2004) Electrochemistry and application of novel monosubstituted squarate electron transfer mediator in glucose oxidase-doped poly(phenol) sensor *Pure App Chem* , **76**:789-799.

Kan, J., Pan, X , Chen, C (2004) Polyaniline-uricase biosensor prepared with template process. *Biosens Bioelectron* , **19** 1635-1640

Kim, J , Cho, J , Cha, G , Lee, C , Kim, H., Paek, S (2002). Conductimetric membrane strip immunosensor with polyaniline-bound gold colloids as signal generator *Biosens Bioelectron* , **14**·907-915

Kutner, W., Wang, J , L'Her, M , Buck, R (1998) Analytical aspects of chemically modified electrodes. classification, critical evaluation and recommendations. *Pure App Chem* , **70**·1301-1318

Luo, Y , Do, J (2004). Urea biosensor based on PANI(urease)-Nafion/Au composite electrode *Biosens Bioelectron* , **20**:15-23

Mailley, P , Cummings, E , Mailley, S , Cosnier, S., Eggins, B., McAdams, E (2004). Amperometric detection of phenolic compounds by polypyrrole-based composite carbon paste electrodes. *Bioelectrochem* , **63** 291-296

Moore, E , Pravda, M., Guilbault, G (2003) Development of a biosensor for the quantitative detection of 2,4,6-trichloroanisole using screen-printed electrodes *Anal Chim Acta,* **484** 15-24

Musameh, M., Wang, J., Merkoci, A., Lin, Y (2002). Low-potential stable NADH detection at carbon nanotube-modified glassy carbon electrodes. *Electrochem Comm* , 4·743-746

Nicholson, R S (1965) Theory and application of the cyclic voltammetry of electrode reaction kinetics *Anal Chem* , **37** 1351-1355

Prieto-Simon, B , Fabregas, E (2004). Comparative study of electron mediators used in the electrochemical oxidation of NADH *Biosens Bioelectron* , **19** 1131-1138.

Rotariu, L , Bala, C., Magearu, V (2004). New potentiometric microbial biosensor for ethanol determination in alcoholic beverages. *Anal Chim Acta,* **513**:119-123

Quan, D., Shin, W. (2004). Modification of electrode surface for covalent immobilisation of laccase. *Mater Sci Eng C,* **24** 113-115

Sahm, T., Madler, L , Gurlo, A , Barsan, N., Pratsinus, S , Weimar, U (2004) Flame spray synthesis of tin dioxide nanoparticles for gas sensing. *Sens Actuat B,* **98** 148-153

Salimi, A., Abdi, K. (2004) Enhancement of the analytical properties and catalytic activity of a nickel hexacyanoferrate modified carbon ceramic electrode prepared by two-step sol-gel technique. application to amperometric detection of hydrazine and hydroxyl amine *Talanta,* **63**.475-483.

Serban, S , El Murr, N (2004). Synergetic effect for NADH oxidation of ferrocene and zeolite in modified carbon paste electrodes· New approach for dehydrogenase based biosensors *Biosens Bioelectron* , **20**.161-166

Shankaran, D., Uehera, N , Kato, T. (2002) Determination of sulphur dioxide based on a silver dispersed functional self-assembled electrochemical sensor. *Sens Actuat B,* **87** 442-447

Sheppard, N., Mears, D , Guiseppi-Elie, A (1996) Model of an immobilised enzyme conductimetric urea biosensor. Biosens. Bioelectron , 11·967-979

Udum, Y , Pekmez, K , Yıldız, A (2004) Electrochemical synthesis of soluble poly(3-methyl thiophene) *Eur Poly J*, **40**:1057-1062.

Ugo, P , Zangrando, V , Moretto, L , Brunetti, B. (2002) Ion-exchange voltammetry and electrocatalytic sensing capabilities of cytochrome c at polyestersulphonated ionomer coated glassy carbon electrode *Biosens Bioelectron*, **17**:479-487.

Vedrine, C , Fabiano, S , Tran-Minh, C (2003) Amperometric tyrosinase based biosensor using an electrogenerated polythiophene film as an entrapment support *Talanta,* **59** 535-544

Vergheese, T , Berchmans, S (2004). Evaluation of monolayers and mixed monolayers formed from mercaptobenzothiazole and decanethiol as sensing platforms *Mater Chem Phys*, **83**.229-238.

Wang, H., Xu, G., Dong, S (2001) Electrochemistry and electrochemiluminescence of stable (2,2'bipyridyl)ruthenium(II) monolayer assembled on benzene sulfonic acid modified glassy carbon electrode. *Talanta,* **55** 61-67

Wang, J (2000) Analytical Electrochemistry *Wiley-VCH, New York*

Wang, S., Zhang, Q , Yang, D , Zhong, G (2004). Multi-walled carbon nanotube-based gas sensors for $NH_3$ detection *Diam Rel Mater*, **13**:1327-1332

Yantasee, W , Lin, Y , Fryxell, G , Busche, B. (2004). Simultaneous detection of cadmium, copper and lead using a carbon paste electrode modified with carbamoylphosphonic acid self-assembled monolayer on mesoporous silica (SAMMS). *Anal Chim Acta,* **502**:207-212.

Yin, H , Brown, T., Greef, R , Wilkinson, J , Melvin, T (2004) Chemical modification and micropatterning of Si(100) with oligonucleotides. *Microelectron Eng*, **73-74**:830-836

Yu, X , Chattopadhyay, D , Galeska, I., Papadimitrakopoulos, F , Rusling, J (2003) Peroxidase activity of enzymes bound to the ends of single-wall carbon nanotube forest electrodes. *Electrochem Comm* , **5** 408-411

Yuqing, M , Jianrong, C, Xiaohua, W (2004) Using electropolymerised non-conducting polymers to develop enzyme amperometric biosensors *Tr Biotech*, **22**.227-231

Zen, J , Kumar, A , Tsai, D (2003) Recent updates of chemically modified electrodes in analytical chemistry. *Electroanal* , **15** 1073-1087

Zimer, A., Bertholdo, R , Grassi, M., Zarbin, A , Mascaro, L (2003). Template carbon dispersed in polyaniline matrix electrodes evaluation and application as electrochemical sensors to low concentrations of $Cu^{2+}$ and $Pb^{2+}$ *Electrochem Comm* , **5**:983-988

Zhu, N , Zhang, A., Wang, Q., He, P , Fang, Y (2004). Electrochemical detection of DNA hybridisation using methylene blue and electrodeposited zirconia thin films on gold electrodes *Anal Chim Acta,* **510**:163-168

# Chapter 2

## Characterisation and Optimisation of Screen-Printed Carbon Paste Electrodes and their Modification with Polyaniline

## 2.1 INTRODUCTION

Conducting polymer-modified electrodes have attracted much interest in recent times for application in molecular electronics for diodes, field-effect transistors and sensors The considerable flexibility of conductmg polymers m their chemical structures and their reversible redox characteristics make them attractive materials for sensing, in particular biosensing (Sharma *et al.*, 2003). They can act as excellent materials for immobilisation of biomolecules and have rapid electron transfer properties for the fabrication of efficient biosensors

Modification of electrodes such as carbon with conducting polymer is generally straightforward, and most commonly done by electrochemical synthesis. Traditionally, electrode modification experiments have used pyrolytic graphite and glassy carbon; surfaces that can be regenerated easily. Today, the sensing field demands further development of carbon as a cheap electrode platform for disposable, reproducible sensors, obviating the need for regeneration. Screen-printing of carbon pastes meets these criteria It holds many advantages over the other forms of carbon for electrode mass production in sensing applications

The aim of this work was to prepare and characterise screen-printed carbon electrodes and to examine their behaviour when modified with the conducting polymer, polyaniline/polyvinylsulphonate (PANI/PVS), for application in a biosensor format The electroactivity of both commercial electrodes and electrodes fabricated in-house from various commercial inks were examined in order to find the electrode most suited to amperometric sensor work The nature of the PANI/PVS film and its relationship with the electrode was then examined using electrochemical and physical techniques, to further elucidate the behaviour of the polymer as a non-diffusional mediator

A brief introduction into the theory behind screen printed electrodes and the conductmg polymer, polyaniline is given in the following section. The general areas are introduced and discussed m relation to previous work carried out by this, and other groups

### *2.1.1 The screen-printed electrode*

Research on carbon electrodes and their modifications for analytical purposes has undergone much activity in recent years (Huang *et al.*, 1993, Garjontye & Malinauskas, 1998, Gorton & Dominguez, 2002, Lu, 2004, Jin *et al*, 2004). Carbon electrodes can be obtained in a huge variety of forms. pyrolytic graphite, highly oriented pyrolytic graphite (HOPG), glassy carbon, powders, fibre, paste, and most recently, nanotubes and diamonds. There is a huge variation in the properties of these carbons as a result of differences in carbon crystalline size, orientation and extent of cross-linking between trigonally bonded regions. However, all these materials have a high chemical inertness and provide a wide range of anodic working potentials with low electrical resistivity. They also have a very pure crystalline structure that provides low residual currents and a high signal to noise ratio (Zhang *et al.*, 2000), making them ideal for electroanalytical applications. Carbon electrodes in general, are attractive for sensing applications. Specifically, screen-printing of carbon inks for the fabrication of electrodes has realised commercial success in the glucose sensing field (Hart *et al.*, 1997) Developed for the printing industry, this thick-film technology has been adapted for the electronics industry and biosensor research. Screen-printed electrodes have low unit costs and are capable of undergoing mass production, while still maintaining adequate levels of reproducibility. They also have the advantages of miniaturisation and versatility. A schematic of the screen-printing process is shown in *Figure 2 1.*

A wide range of substrates and inks are used to produce these electrodes Substrates may be flexible plastics such as polyethylene terephthalate (PET), polyvinyl chloride (PVC), or ceramic-based materials such as aluminium oxide or glass Carbon and metal inks are commonly used for printing working electrodes, and silver-based ink is usually used for obtaining reference and auxiliary electrodes and for forming conductive paths Insulating inks are often used in the fabrication of electrode strips for defining electrode areas, insulation and separating conductive components

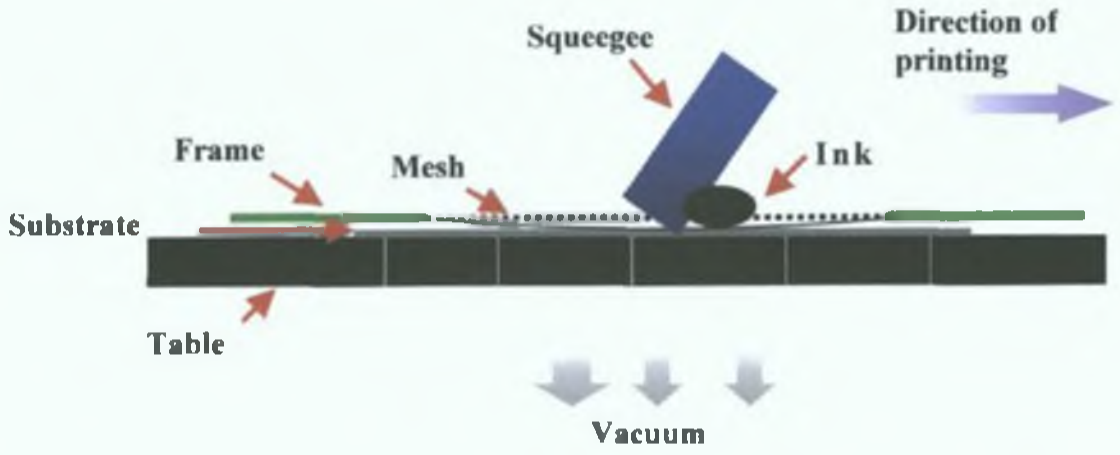


***Figure 2.1.*** The screen printing process. The screen itself is composed of a mesh of silk, synthetic or steel threads woven together, stretched tightly and mounted on a frame. The pores of the mesh are blocked in non-image areas and left open where the image is to be transferred. This is called a stencil. A rubber or metal squeegee is used to pass ink at a fixed speed and pressure over the screen, thereby transferring the image onto a substrate held in place underneath it by a vacuum.

Carbon ink used for the working electrode must contain a binder, solvent and graphite particles. What is still of some concern with screen printing, is the level of reproducibility in electrode production. This is mainly due to the nature of the carbon inks, the composition of which are proprietary and the lack of control of the microscopic structure of individual electrodes. Grennan *et al.* (2001) presented the effects of the curing temperature on the physical and electrochemical characteristics of the carbon paste. Improved sensor performance and decreased variability was demonstrated at elevated curing temperatures and this was associated with morphological changes to the carbon electrode surface. Wang *et al.* (1998) compared the electrochemical behaviour and electroanalytical performance of thick film carbon sensors on ceramic substrates fabricated from four different commercially available carbon inks. It was found that C10903D14 (supplied by Gwent Electronic Materials) was optimal for amperometric sensing. This ink possessed an attractive electrochemical reactivity but was found to have high residual currents. This would render it most suited to amperometric work as this method is not dependent on background contributions. It would be less suited, however, to voltammetric or stripping voltammetry work.

Killard *et al.* (1999) developed a carbon screen-printed working electrode comprising a silver conducting track, a carbon working electrode and an insulation layer This electrode was used in conjunction with external reference and auxiliary electrodes Cui *et al.* (2001) characterised a screen-printed strip comprising working, reference and auxiliary electrodes Silver acted as the conducting path Erlenkotter *et al* (2000) used a similar format with on-board reference and auxiliary electrodes However, the difference was that carbon acted as the conducing path for the working and auxiliary electrodes, and a platinum ink was printed to act as the working electrode. It is not just the interfacial region between solution and electrode that is important in determining the electrode's characteristics, but also the rest of the electrode, includmg the properties of the conducting path Carbon inks may have higher resistivities than other types of conducting inks and so may not be suitable as a conductive layer. Both strips described potentially have different charge transfer properties due to their very different compositions, and although both strips were successful for their respective applications, they may not necessarily be suited to other applications. It is important when designing any type of screen-printed electrode that the charge transfer properties are suited to the end-use application.

### *2.1.2 Polyaniline and its use as a non-diffusional type mediator*

Modifications of solid electrodes with conducting polymers is creating new technological possibilities in the development of chemical and biochemical sensors During the last two decades, polyaniline (PANI) has been studied extensively, a polymer that possesses interesting electrical, electrochemical and optical properties (Chiang & MacDiarmid, 1986; Cao *et al*, 1989) Modification of electrodes such as carbon with PANI is generally straightforward, and most commonly done by electrochemical synthesis The polymer can acts as a non-diffusional mediating species in enzyme biosensors, coupling electrons directly from the enzyme active site to the electrode. It can also be used as an effective substrate for immobilisation of biomolecules In this format, it allows direct electrical communication between the biomolecule and the electrode surface

PANI films are usually grown on electrode surfaces potentiodynamically or potentiostatically. The generally accepted mechanism for the electropolymerisation of aniline (Zotti *et al.*, 1988) is presented in *Figure* 2 2. Formation of the radical

cation of aniline by oxidation on the electrode surface (step 1) is considered to be the rate-determining step This is followed by coupling of radicals, mainly (*N*- and *para*-forms), and elimination of two protons The dimer (oligomer) formed then undergoes oxidation on the electrode surface along with aniline The radical cation of the oligomer couples with an aniline radical cation, resulting in propagation of the chain. The formed polymer is doped by the acid (HA) present m solution (step 4).

Electrochemical polymerisation is routinely carried out in an acidic aqueous solution of aniline as a low pH is required to solubilise the monomer. It may be electrochemically grown on electrode surfaces using potentiostatic or potentiodynamic techniques, although the latter result in more homogeneous films (Iwuoha *et al* , 1997).

*Figure 2 3* shows the cyclic voltammogram for the first cycle at a glassy carbon electrode in monomer solution. During this cycle, an increase in the anodic current is observed at about 0.8 V. This initial increase of current corresponds to the formation of the aniline radical cation (*Figure 2 2, Step 1*). These radicals couple to form dimers and eventually the insoluble conducting polymer precipitates onto the electrode surface. The current peaks at about 0 95 V, and the current decreases until the direction of the sweep is reversed at 1.2 V. On the return scan, the current continues to grow as a loop. This is characteristic of nucleation and growth phenomena as the current is larger on the return scan. The nucleation loop is due to the fact that the surface area of the electrode is increasing due to the electrochemical polymerisation of a high surface area polymer onto the glassy carbon surface (Naudin *et al.*, 1998)

*Step 1 Oxidation of monomer*

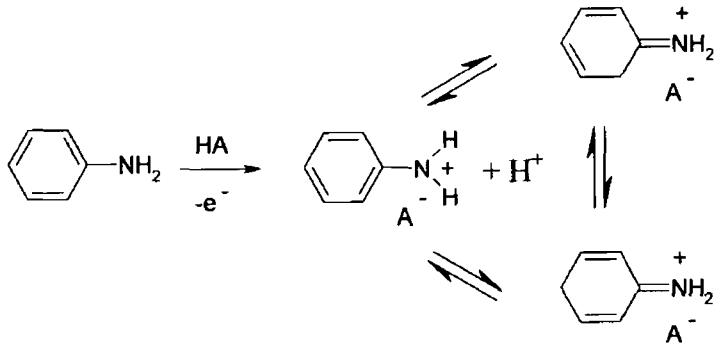

*Step 2 Radical coupling and rearomatisation*

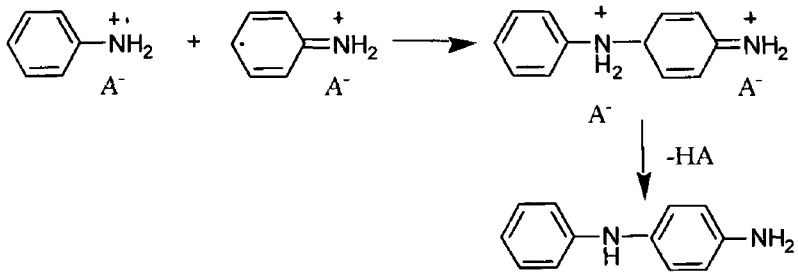

*Step 3 Chain propagation*

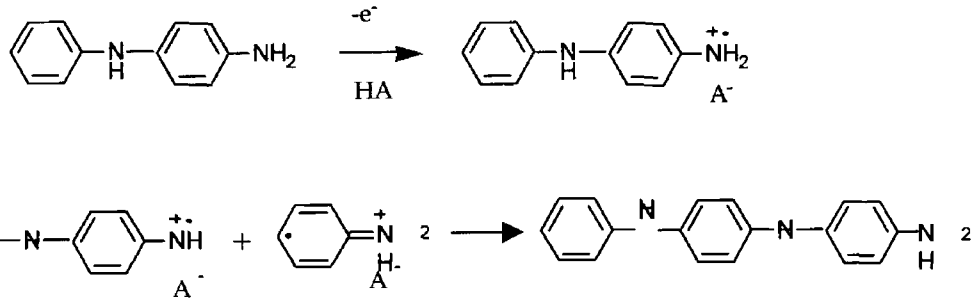

*Step 4 Doping of the polymer*

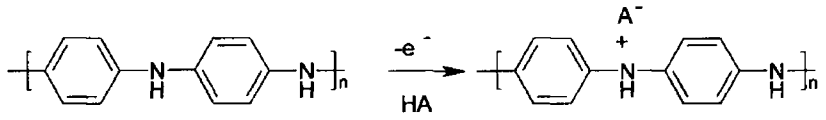

***Figure 2.2.*** Electropolymerisation of aniline (Wallace *et al*, 2003)

The addition of polyelectrolytes, such as polyvinylsulphonate (PVS), to the monomer solution for electropolymerisation can result in the incorporation of these larger molecules as dopants. This helps maintain electrical neutrality in the oxidised form of the polymer as well as leading to increases in structural stability and conductivity (Iwuoha *et al.*, 1997). A typical cyclic voltammogram for the electropolymerisation process of aniline from acidic media in the presence of PVS is shown in *Figure 2 4.* The oxidation peaks were assigned to the oxidation of leucoemeraldine (LM) to its radical cation, ($LM^{\bullet+}$) (a), and $LM^{\bullet+}$ to emeraldine (EM) (b). The reduction peaks were assigned to the reduction of EM to its emeraldine radical cation ($EM^{\bullet+}$) (c) and $EM^{\bullet+}$ to LM (d).

Electroactive PANI/PVS has been used as the mediator in a reagentless peroxide biosensor and operates at a pH of 6 8 (Killard *et al*, 1999). There has been previous research showing that polyanilme films are only efficient conductors under acidic conditions (Casella & Guascito 1997). However, Pekmez *et al.* (1994) have explained that reduced LM and the oxidised EM species exist in basic and neutral solutions, albeit with reduced conductivity Partial reduction of oxidised PANI films occur when the electrode is held at negative potentials and the polymer is thus a mixture of reduced and oxidised species, and their radical cations protonated to varying degrees, depending on the reaction medium. Thus, it is possible to use PANI/PVS in its reduced form as the electron transfer mediator in neutral buffer solutions. For all steady state amperometric experiments, the oxidised PANI/PVS/protein electrode was polarised at a potential of -100 mV vs. Ag/AgCl which allows for the presence of the reduced polyleucoemeraldine species.

Killard *et al.* (1999) have described a biosensor format where polyvinylsulphonate-doped aniline was electropolymerised onto the surface of a screen-printed carbon paste electrode. Biomolecules were then doped onto the surface of the polymer by electrostatic interactions with the polymer backbone. This effective biosensor format has examined the amperometric behaviour of immobilised horseradish peroxidase (Iwuoha *et al*, 1997), and has since been extended to develop rapid, single-step separation-free immunosensors for real-time monitoring (Killard *et al.*, 1999 and 2001) and incorporating multi-calibrant measurement (Grennan *et al*, 2003).

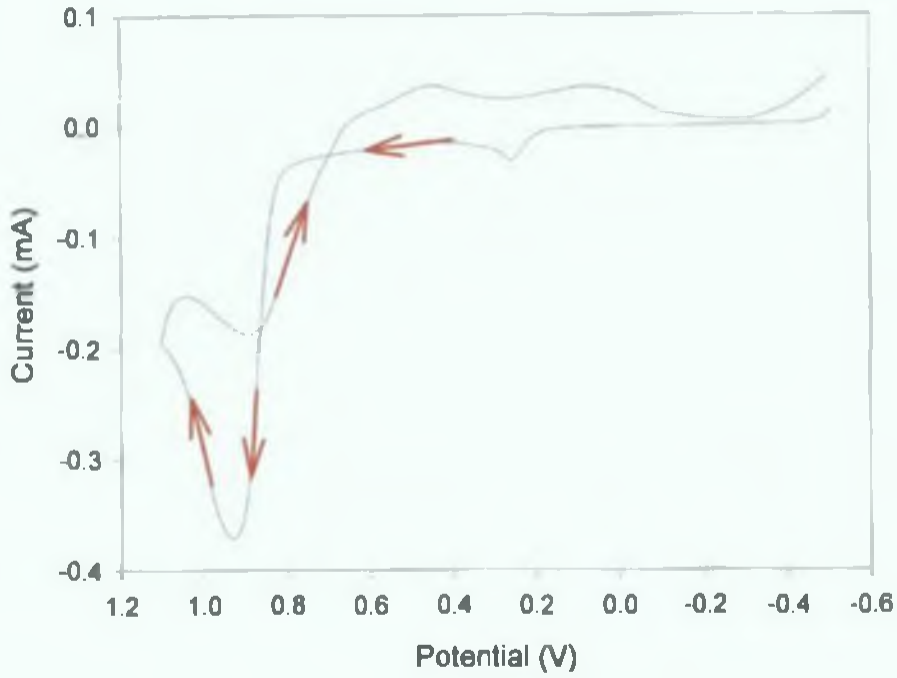


***Figure 2.3.*** Cyclic voltammogram for the first cycle at a glassy carbon electrode in an acidic aniline solution at a scan rate of 100 mV $s^{-1}$.

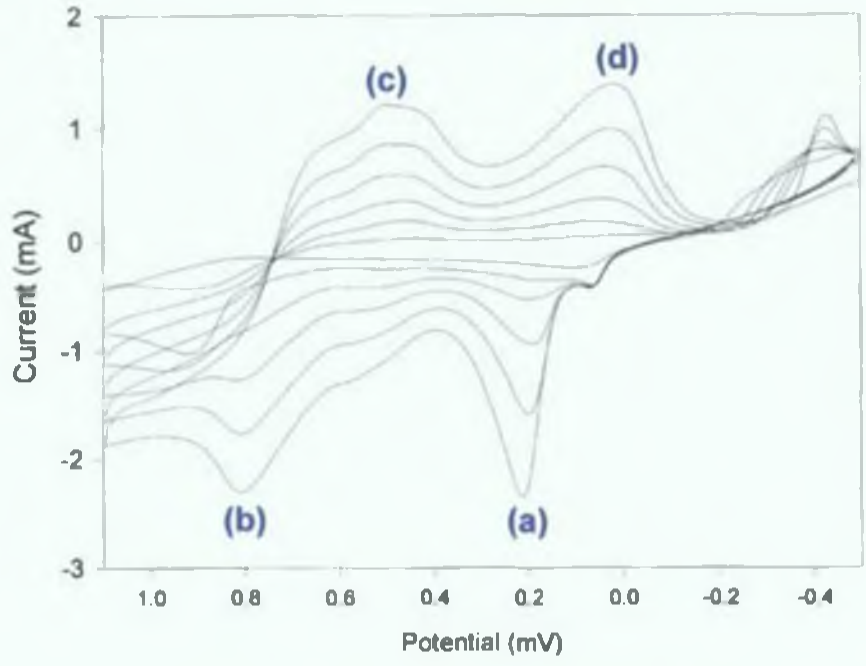


***Figure 2.4.*** Electrosynthesis of the PANI/PVS film in HCl (1 mol $dm^{-3}$) on an electrode surface. Successive polymerisation cycles are shown which correspond to increases in thickness of the film during deposition. The oxidation peaks were assigned to the oxidation of (a) LM to $LM^{\bullet+}$, and (b) $LM^{\bullet+}$ to EM. The reduction peaks were assigned to the reduction of (c) EM to its $EM^{\bullet+}$ and (d) $EM^{\bullet+}$ to LM.

## 2.2 MATERIALS AND METHODS

### *2 2 1 Materials*

Aniline was purchased from Aldrich (13,293-4), vacuum distilled and stored frozen under nitrogen Polyvinylsulphonate (PVS, 27,842-4), potassium hexacyanoferrate (II) (22,768-4) (potassium ferrocyanide trihydrate) and potassium hexacyanoferrate (III) (20,801-9) (potassium ferricyanide) were purchased from Aldrich Euroflash™, Ultra™, Ercon (661901) and LRH (C2010201R15) carbon paste inks were donated by Inverness Medical Ltd Gwent (C10903D14) carbon paste ink was donated by Gwent Electronic Materials Ltd (Gwent, UK) Electrodag® PF-410S and Lifescan™ silver silver chloride conductive inks were purchased from Acheson and donated by Inverness Medical Ltd , respectively Electrodag® 452 SS BLUE and Ercon insulation inks were purchased from Acheson or donated by Inverness Medical Ltd Poly(ethylene) terephthalate (PET) substrates were purchased from HiFi Industrial Film Ltd (Dublin, Ireland) Seriwash universal screen wash (ZT639) was obtained from Sericol Ltd , (Kent, UK) Horseradish peroxidase (HRP, 1,100 U/mg P8672), anti-biotin (B3640) and peroxidase biotmamidocaproyl conjugate (P9568) were purchased from Sigma-Aldrich (Poole, Dorset, UK) 30% (v/v) hydrogen peroxide solution was purchased from Merck Glassy carbon and silver/silver chloride (Ag/AgCl) electrodes were purchased from Bioanalytical Systems Ltd (Cheshire, UK) The platinum mesh (29,809-3) was purchased from Aldrich

### *2 2 2 Buffers and solutions*

Unless otherwise stated, all electrochemical measurements were carried out in phosphate buffered saline (PBS), (0 1 mol $dm^{-3}$ phosphate, 0 137 mol $dm^{-3}$, NaCl and 2 7 mmol $dm^{-3}$ KCl), pH 6 8 Unless otherwise stated, all immunochemicals were prepared in PBS

### *2 2.3 Instrumentation*

Screen-printing of in-house (non-commercial) electrodes was performed either with a semi-automated DEK 247 or DEK 248 printing machine (Weymouth, UK) Polyester screens with varying mesh thickness were used, and mounted at 45° to the print stroke Blade rubber squeegees were employed, and a flood blade was utilised on the DEK 248 All inks were cured in a conventional oven, apart from Electrodag® 452 SS BLUE which was cured with the UV lamp curing system from UV Process Supply, Inc (Cortland, Chicago, IL, USA)

All electrochemical protocols were performed either on a BAS100/W electrochemical analyser with BAS100/W software, or a CH1000 potentiostat with CH1000 software, using either cyclic voltammetry or time-based amperometric modes An Ag/AgCl pseudo reference electrode and a platinum mesh auxiliary electrode were used for bulk electrochemical experiments Electrochemical batch and flow cells were constructed according to Killard *et al* (1999) They were composed of polycarbonate, and designed to house the screen-printed electrodes Both cells incorporated internal Ag/AgCl reference and platinum wire auxiliary electrodes (*Figure 2 5*) Cell volumes of the batch and flow cells were 2 ml and 26 µl, respectively

Scanning electron microscopy (SEM) was performed with a Hitachi S 3000N scanning electron microscope An acceleration voltage of 20 KV was employed Energy Dispersive X-ray analysis (EDX) was carried out with an Oxford Instruments EDX system (Oxford Instruments Analytical Ltd , Bucks , UK) with LINK ISIS software and an SiLi detector

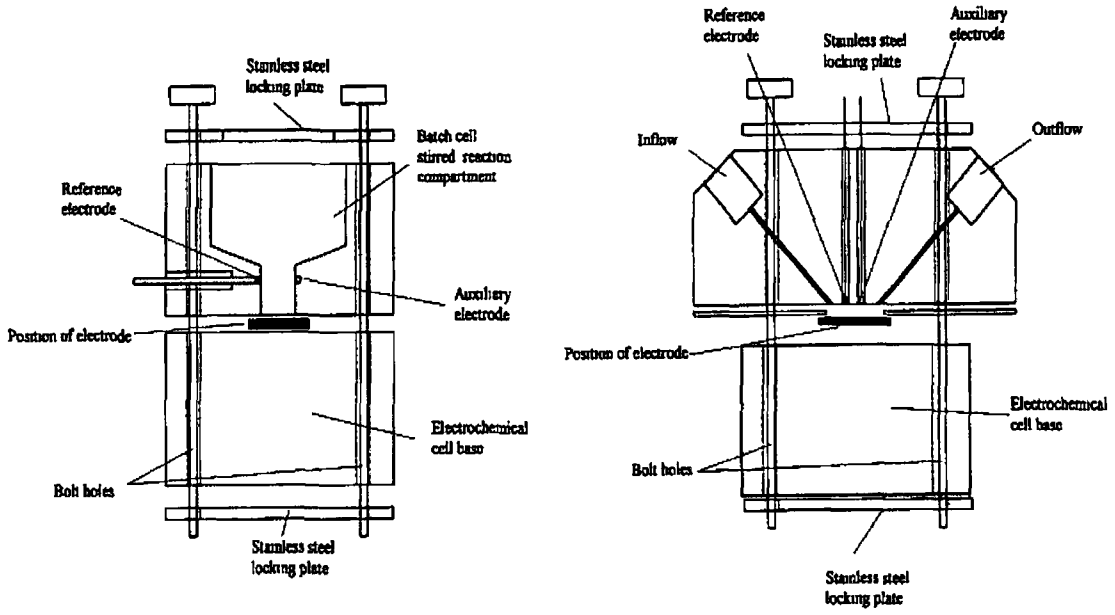


**(a)** **(b)**

***Figure 2.5.*** Batch and flow cell configurations (a) The polycarbonate batch cell comprised an upper reaction vessel and a lower base, between which was clamped the screen-printed electrode Platinum wire auxiliary and pseudo silver/silver chloride wire reference electrodes were incorporated into the reaction vessel with external connections as shown (b) The flow injection cell was composed of polycarbonate into which had been drilled holes for inflow and outflow Platinum and silver/silver chloride electrodes were placed at the base of the cell to come into close association with the screen-printed working electrode The flow chamber was formed by the use of a PET spacer (170 μm) The screen-printed electrode was clamped into place between the upper and lower sections as shown (Adapted from Killard *et al*, 1999)

### *2.2 4 Screen-printed electrode configuration and fabrication*

Six electrode types were fabricated for this study Two were manufactured commercially (Euroflash™ and Ultra™) and four by in-house screen-printing (designated Ultra-inH, Ercon-inH, LRH-inH and Gwent-inH, according to the working electrode carbon used) Their structural characteristics are summarised in *Table 2 1* and their fabrication is discussed in the following section The curing conditions for all inks are summarised in *Table 2 2*

#### 2.2 4 1 Euroflash™ fabrication procedure

*Figure 2 6* depicts a schematic of the commercial Euroflash™ electrode Electrodes were screen-printed onto a pre-shrunk substrate Initially, a layer of two Ag/AgCl tracks were deposited as part of the conducting paths from electrodes to contacts for the pseudo-reference and working electrodes (a) A layer of Euroflash™ carbon was deposited in three segments Two of which completed the conducting paths, and the third formed the working electrode (b) No further depositions were required for the reference electrode (a segment of the initial Ag/AgCl layer was defined for the pseudo-reference electrode) In the manufacturing process, a glucose oxidase layer is usually deposited at this stage However, this was not carried out for our purposes Finally, an insulation layer was deposited to eliminate cross-talk and to define the working electrode area (8 $mm^2$) (c)

#### 2 2 4.2 Ultra™ fabrication procedure

*Figure 2 7* depicts a schematic of the commercial Ultra™ electrode Electrodes were screen-printed onto a pre-shrunk substrate (a) Initially a layer of three Ultra™ carbon paths were deposited as the conducting paths from electrodes to contacts for the two working electrodes and the pseudo-reference electrode (b) Finally, an insulation layer was deposited to eliminate cross-talk and to define the working electrode area (10 $mm^2$) (c)

### 2.2.4 3 In-house fabrication procedure (three electrode strip)

*Figure 2 8* depicts a schematic of an in-house screen-printed electrode with onboard pseudo-reference and auxiliary electrodes (Ultra-inH, Ercon-inH and LRH-inH) Electrodes were screen-printed onto a pre-shrunk PET substrate Initially, a layer of three Ag/AgCl tracks were deposited as the conducting paths from electrodes to contacts for the pseudo-reference, auxiliary and working electrodes (a) A layer of carbon was deposited as the working electrode (b) The Ag/AgCl acted as both reference and auxiliary electrodes Finally, an insulation layer was deposited to eliminate cross-talk and to define the working electrode area (9 $mm^2$) (c)

### 2.2.4.4 In-house fabrication procedure (one electrode strip)

*Figure 2 9* depicts a schematic of an in-house screen-printed working electrode (Gwent-inH) Electrodes were screen-printed onto a pre-shrunk PET substrate Initially, a layer of silver was deposited as the conducting path from the working electrode to contact (a) A layer of Gwent carbon was deposited as the working electrode (b) Finally, an insulation layer (c) was deposited to eliminate cross-talk and to define the working electrode area (9 $mm^2$)

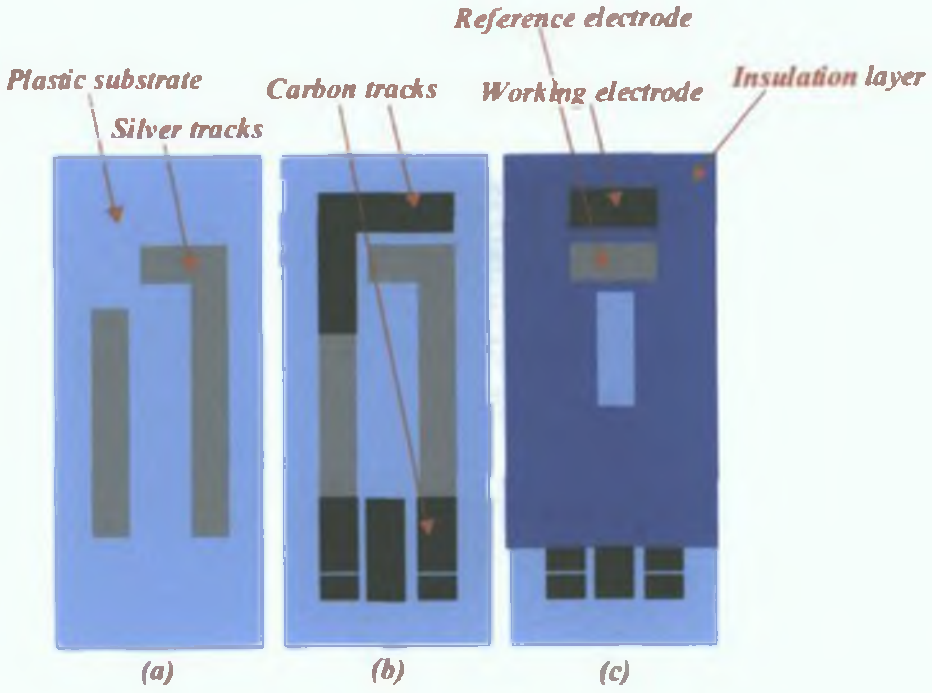


***Figure 2.6.*** Components of the Euroflash™ electrode strip: (a) Substrate with Ag/AgCl conducting path, (b) carbon print on top of (a), and (c) insulation layer printed on top of (b). (Working electrode area: 8mm$^2$)

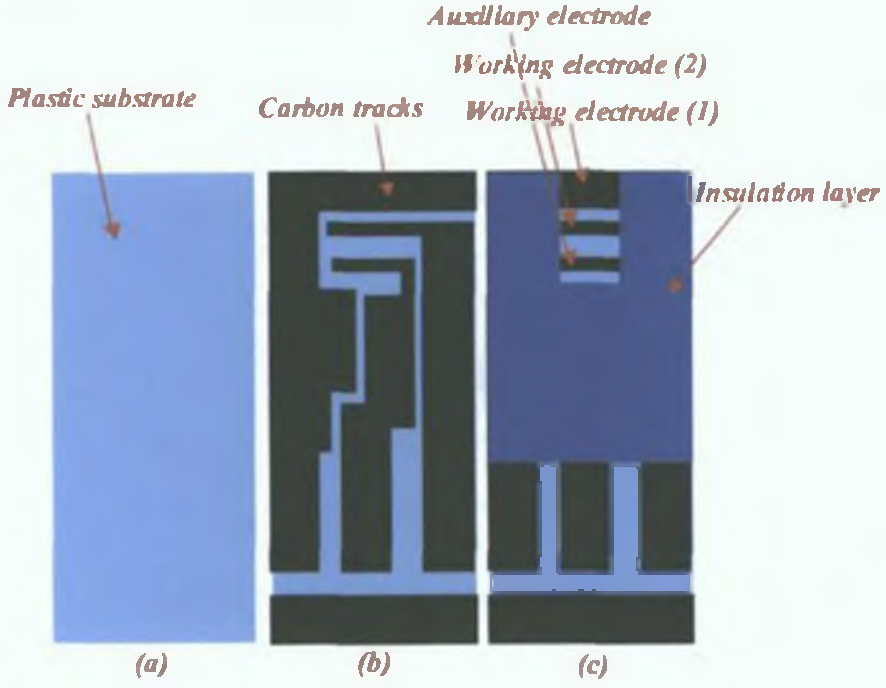


***Figure 2.7.*** Components of the Ultra™ electrode strip: (a) Substrate, (b) carbon tracks on top of (a) and (c) insulation layer on top of (b). (Working electrode (1) was utilised for all work described, working area: 10 mm$^2$).

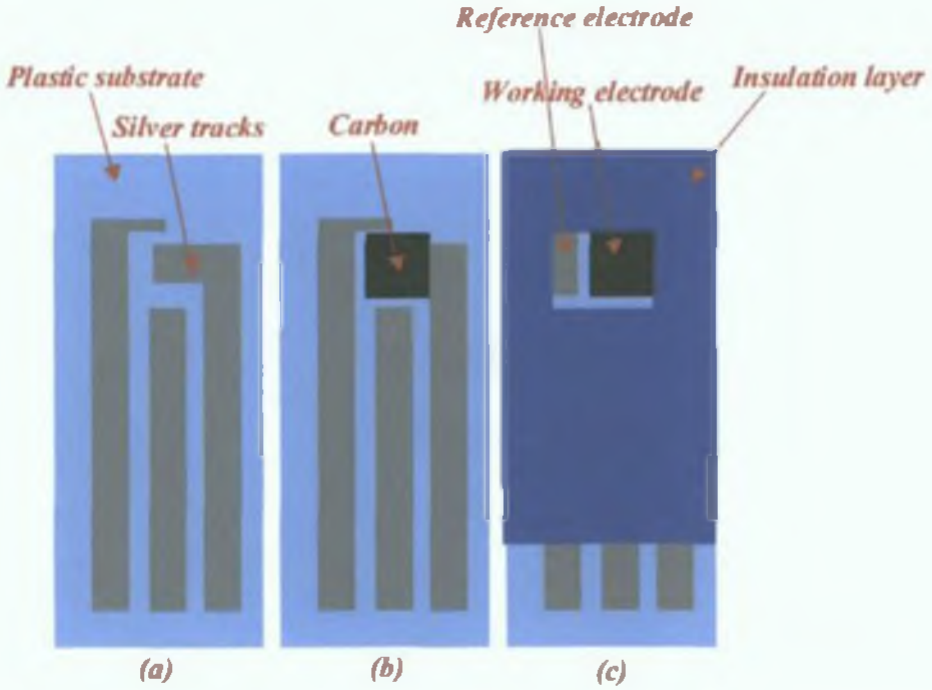


***Figure 2.8.*** Components of the in-house screen-printed electrode: (a) Substrate with Ag/AgCl conducting path, (b) carbon print on top of (a), and (c) insulation layer printed on top of (b). (Working electrode area: 9mm$^2$)

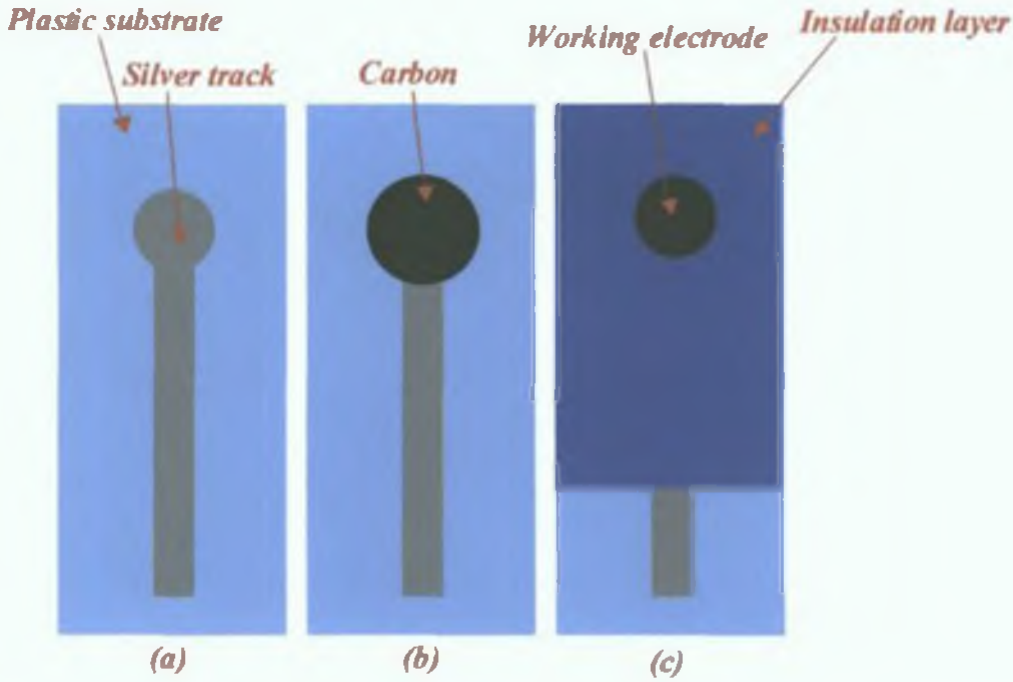


***Figure 2.9.*** Components of the in-house screen-printed electrode: (a) Substrate with Ag/AgCl conducting path, (b) carbon print on top of (a), and (c) insulation layer printed on top of (b). (Working electrode area: 7.07 mm$^2$)

***Table 2.1.*** Summary of the composition of all electrodes used

| *Electrode type* | *Fabrication method* | *Conducting layer* | *Working electrode layer* | *Working electrode area* | *Insulation layer* | *Name* |
|---|---|---|---|---|---|---|
| Euroflash™ | *Section 2.2.4.1* | Lifescan silver & Euroflash™ carbon | Euroflash™ carbon | 8mm$^2$ | Ercon | Euroflash™ |
| Ultra™ | *Section 2.2.4.2* | Ultra™ carbon | Ultra™ carbon | 10 mm$^2$ | " | Ultra™ |
| Ultra in-house | *Section 2.2.4.3* | Lifescan silver | Ultra™ carbon | 9mm$^2$ | " | Ultra-inH |
| Ercon in-house | *Section 2.2.4.3* | Lifescan silver | Ercon 661901 | " | " | Ercon-inH |
| LRH in-house | *Section 2.2.4.3* | Lifescan silver | LRH C2010201R15 | " | " | LRH-inH |
| Gwent in-house | *Section 2.2.4.4* | Acheson silver | Gwent C10903D14 | 7.07mm$^2$ | Electrodag ® 452 SS Blue | Gwent-inH |

***Table 2.2*** Curing conditions for all screen-printing inks used

| *Ink type* | *Curing conditions* |
|---|---|
| Lifescan silver ink | Conventional oven @ 70°C for 6 minutes |
| Electrodag ® PF-410 silver ink | Conventional oven @ 120°C for 5 minutes |
| Carbon inks donated by Inverness Medical Ltd<br>Euroflash™<br>Ultra™<br>Ercon 661901<br>LRH C2010201R15 | Conventional oven @ 70°C for 13 minutes |
| Carbon Paste No C10903D14 (Gwent Electronic Materials Ltd) | Conventional oven @ 150°C for 15 minutes |
| Ercon insulation ink | Conventional oven @ 70oC for 15 minutes |
| Electrodag® 452 SS BLUE insulation ink | UV curing 6 rpm, 762 W cm$^{-1}$, 2 cycles |

### *2.2 5 Electrode pre-treatment procedure*

Glassy carbon electrodes were cleaned by successive polishing on aqueous slurries of 1 μm, 0 3 μm and 0 05 μm alumina powder, followed by ultrasonic cleaning in Milli-Q water for ten minutes The electrodes were then placed in a solution of 0 2 mol $dm^{-3}$ $H_2SO_4$ A single voltammetric cycle was carried out between −1200 mV and +1500 mV at 100 mV $s^{-1}$ vs Ag/AgCl The same voltammetric procedure was employed for cleaning the screen-printed electrodes

### *2.2 6 Cyclic voltammetry*

Glassy carbon or screen-printed electrodes were cycled in equimolar amounts of potassium ferrocyanide and potassium ferricyanide ($1 \times 10^{-3}$ mol $dm^{3}$) using 1 mol $dm^{3}$ KCl as supporting electrolyte, unless otherwise stated Voltammograms were obtained using scan rates ranging from 10 to 100 mV $s^{1}$ and at a sensitivity of $1 \times 10^{-3}$ A $V^{1}$ vs Ag/AgCl under diffusion limited conditions

### *2 2 7 Determination of heterogeneous electron transfer rate constants*

Heterogeneous electron transfer rate constants ($k^0$) were calculated using the method of Nicholson (1965) according to *Equation 2 1*

$$k^0 = \Phi\left(D_0 \pi v\left(\frac{nF}{RT}\right)\right)^{\frac{1}{2}}\left(\frac{D_R}{D_0}\right)^{\frac{\alpha}{2}} \qquad \textit{Equation 2 1}$$

where $\Phi$ refers to a kinetic parameter, $D_0$ is the diffusion coefficient for the ferricyanide ($7\,6 \times 10^{-6}$ $cm^2$ $s^{1}$), $D_R$ is the diffusion coefficient for the ferrocyanide ($6\,3 \times 10^{6}$ $cm^2$ $s^{-1}$) (von Stackelberg *et al*, 1953) and $\alpha$ is the transfer coefficient (0 5), $R$ is the universal gas constant (8 314 J K $mol^{-1}$), $T$ is the absolute temperature (K), $n$ is the number of electrons transferred and $F$ is Faraday's constant (96,485 C)

### *2 2.8 Polymerisation of aniline on the electrode surface*

A solution of 186 µl aniline, 7 8 ml 1 mol $dm^{-3}$ HCl, and 2 ml PVS, was degassed for 10 mm Aniline was polymerised from this solution, onto the surface of the working electrode using cyclic voltammetry A platinum mesh auxiliary and a Ag/AgCl reference electrode were used The potential was cycled between –500 and +1100 mV at 100 mV $s^{-1}$, for the required number of scans, or until the current associated with the $LM^{\bullet+}$ radical cation (see peak (a) in *Figure 2 4*) reached the required current height

### *2.2.9 Immobilisation of protein*

Following polymerisation of aniline, the electrode was transferred to a 2 ml batch cell The surface of the polymer was reduced in 2 ml of PBS (degassed for 10 min under nitrogen or argon) at –500 mV vs Ag/AgCl, sample interval of 500 ms, over 1500 s at a sensitivity of $1 \times 10^{-4}$ A $V^{-1}$ Protein was prepared in PBS prior to use Very quickly after reduction was complete, PBS buffer was removed from the cell and quickly replaced with the protein solution, not under stirring or degassing Oxidation was then performed immediately at +700 mV vs Ag/AgCl for 1500 s During this oxidation, the protein becomes electrostatically attached to the polymer surface The protem solution was carefully recovered from the cell and re-stored for later use

### *2.2 10 Real-time monitoring of immunoaffinity interactions in the flow cell*

After the immobilisation of antibody (*Section 2 2 9*), the electrode was housed in the flow cell according to *Section 2 2 3* Amperometric experiments were performed at –100 mV vs Ag/AgCl wire electrode, with a sample interval of 100 ms and a sensitivity of $1 \times 10^{-4}$ A $V^{-1}$ PBS was passed over the surface of the electrode at a flow rate of 10 µl $sec^{-1}$ When a steady state was reached, HRP-labelled biotin (15 µg $ml^{-1}$) and $H_2O_2$ (1 mmol $dm^{-3}$) were passed over the surface of the electrode and the amperometric response monitored

## 2.3 RESULTS AND DISCUSSION

### *2 3.1 Electrochemical analysis of screen-printed electrodes fabricated from different inks*

Screen-printing technology is widely used for the mass-production of disposable electrochemical sensors The practical utility of screen-printed electrodes has been exploited, despite the fact that little is known about the nature of the electrode reactions (Wang *et al* , 1996) Given the complexity of carbon electrodes in general, and differences in the composition of commercial carbon inks, the question arises as to how such differences and complexity affect their electrochemical reactivity The aim of this work was to compare the electroactivity of both commercial electrodes and electrodes fabricated in-house from various commercial inks, in order to find the electrode most suited to amperometric sensor work Methods of analysis include cyclic voltammetry, amperometry and linear sweep voltammetry

Two commercially manufactured screen-printed working electrodes (WE) were examined, Euroflash™ and One Touch Ultra™ (*Figures 2 6 & 2 7*) These electrodes are manufactured by Inverness Medical Ltd, for glucose testing The WE of the Euroflash™ strip is composed of a silver and carbon conducting path, a carbon working electrode and an insulation layer to define the electrode area The Ultra™ WE electrode, contains only carbon and insulation layers It depends on only carbon to act as the conductor and the electrode The advantage of using less silver, or none at all, is to allow for reduced cost manufacturing A glucose oxidase layer is normally printed on top of the carbon layers of each of the electrodes, which allows for glucose measurements in blood The electrodes analysed for these purposes were withdrawn from the manufacturing process after the carbon print Electrochemical analyses were initially carried out on the commercial electrodes However, subsequently an in-house artwork was designed as a result of finding that the commercial electrodes suffered from severe charge transfer problems and were not suitable to this amperometric sensor work This in-house electrode design (*Figure 2 8*) did not encounter charge transfer difficulties as the conducting tracks were composed solely of silver It was used for the analysis of Ultra™, Ercon and LRH inks and these electrodes are referred to in this section as Ultra-inH, Ercon-inH and LRH-inH, respectively Summaries of

all inks used for fabrication and their respective curing conditions are given in *Tables 2 1 & 2 2*

### 2 3.1 1 Voltammetric performance of screen-printed electrodes

The ferri/ferrocyanide redox couple was the redox system used for comparing the voltammetric behaviour of screen-printed electrodes *Figure 2 10* displays the cyclic voltammograms of the redox couple at a glassy carbon electrode for comparison purposes, the commercial carbon strip electrodes (Euroflash™ and Ultra™) and the commercial inks printed in-house (Ercon-inH, LRH-inH, and Ultra-inH) The mean peak separations and anodic ($j_{p\,a}$) and cathodic ($j_{p\,c}$) peak current densities are also illustrated in *Figure 2 11* (n=3) The commercial electrodes, Euroflash™ and Ultra™, yielded very poor reversibility with $\Delta E_p$ values of 471 (± 56) mV and 416 (± 37) mV, respectively and $j_{p,a}$ values of –12 313 (± 2 025) μA $cm^{-2}$ and –15 107 (± 2 638) μA $cm^{-2}$, respectively This behaviour was attributed to the poor bulk charge transfer of the electrodes The conducting paths (composed of segments of silver and carbon for Euroflash™ and fully carbon for Ultra™ electrodes) from WEs to contacts had resistive properties that may have become a significant limiting factor in bulk charge transfer It resulted in the poor reversibility of the redox couple and low $j_{p\,a}$ values This initial work motivated the in-house electrode artwork to be designed where the conducting tracks were composed solely of silver Each in-house thick-film carbon electrode exhibited different electron-transfer reactivities towards $Fe^{2+}/Fe^{3+}$, with the Ultra-inH electrode yielding the most reversible behaviour For example, the redox couple gave a $\Delta E_p$ value of 264 (± 7) mV for Ultra-inH, as compared to 314 (± 25) mV and 562 (± 52) mV for Ercon-inH and LRH-inH, respectively The Ultra-inH also offered the highest $j_p$ values and lowest overvoltage of all the in-house electrodes (i e , anodic peak potentials for ferrocyanide of 392 mV, compared to 452, 460, 410 and 439 mV for Ultra™, Euroflash™, Ercon-inH and LRH-inH, respectively) Of all the electrodes examined, the Ultra-inH electrode exhibited the best behaviour towards the redox couple It was observed immediately that the commercial electrodes, manufactured by Inverness Medical Ltd , were not suited to present purposes because of high resistive properties The m-house design had more optimal bulk charge transfer properties, and in

conjunction with the Ultra™ commercial ink as the WE, behaved as the best screen-printed electrode This work demonstrates the importance of optimising *both* the conducting path and the carbon of the WE when designing a new screen-printed electrode Both parameters have profound effects on the behaviour of the electrode

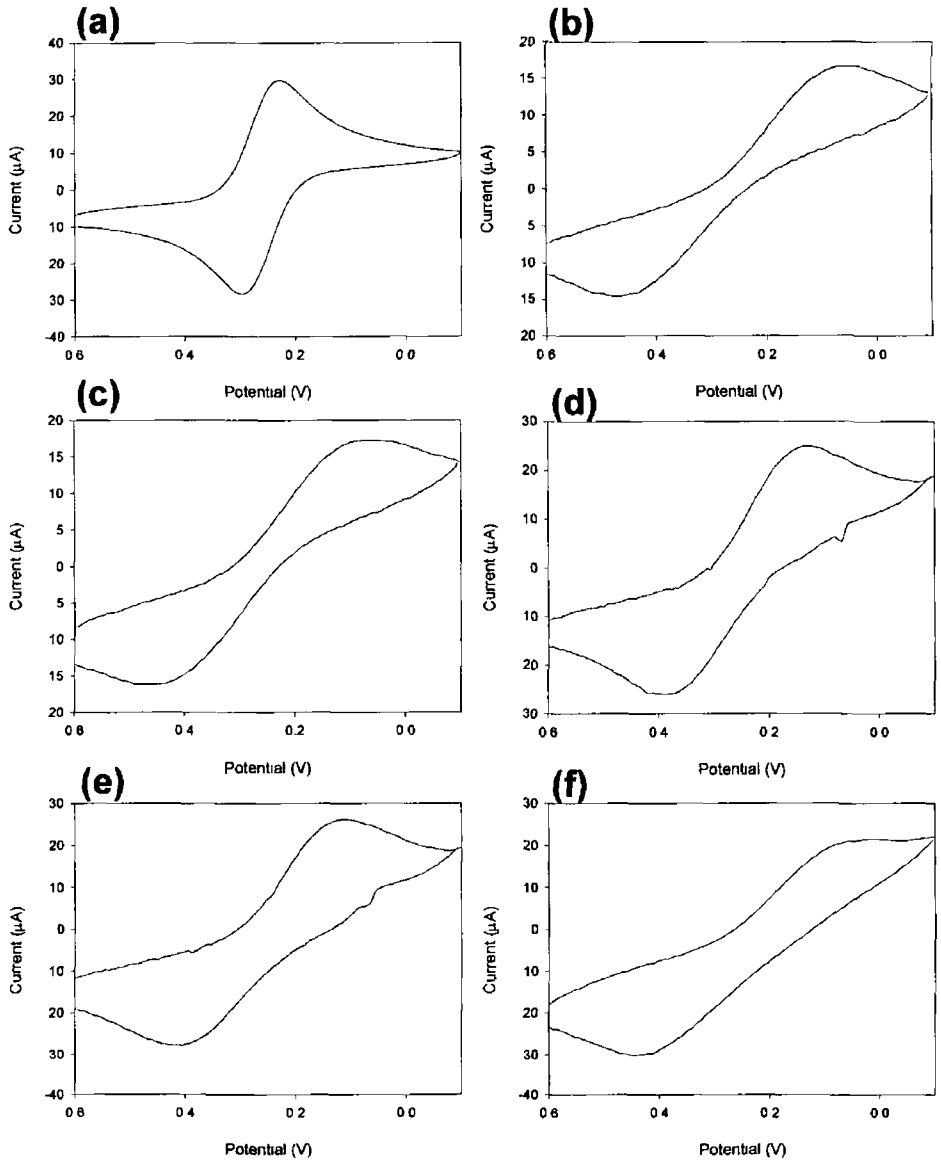


***Figure 2.10.*** Cyclic voltammograms for different electrodes in 1 × $10^{-3}$ mol $dm^{-3}$ ferri/ferrocyanide (a) Glassy carbon, (b) Euroflash™, (c) Ultra™, (d) Ultra-inH, (e) Ercon-inH and (f) LRH-inH The commercial electrodes ((b), (c)) showed very poor reversibility Using the in-house design, ((d), (e), (f)), reversibility improved, with the Ultra-inH exhibiting the best behaviour

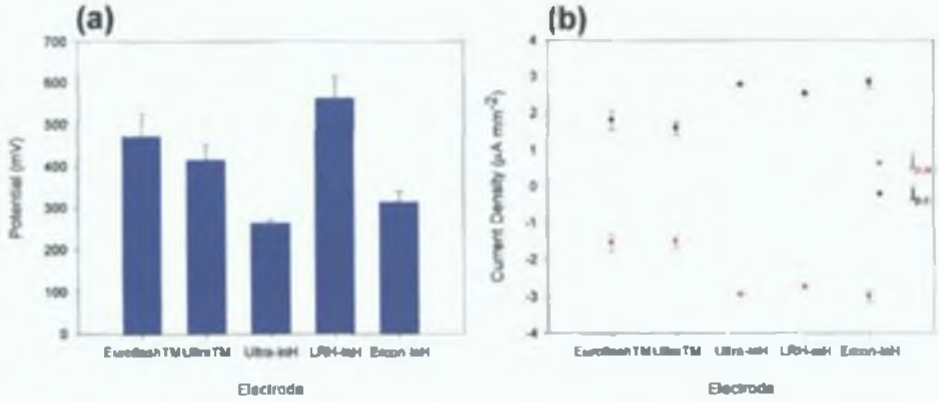


***Figure 2.11.*** (a) Cyclic voltammetric peak separations ($\Delta E_p$) and (b) anodic and cathodic peak current densities ($j_p$) for $1 \times 10^{-3}$ mol $dm^{-3}$ ferri/ferrocyanide for each of the screen-printed electrodes (n=3).

***Table 2.3.*** Kinetic parameter constants ($\Phi$) for varying $\Delta E_p$ values.

| $\Delta E_p$ (mV) | $\Phi$ | $\Delta E_p$ (mV) | $\Phi$ |
|---|---|---|---|
| 61 | 20 | 92 | 0.75 |
| 63 | 7 | 105 | 0.5 |
| 64 | 6 | 121 | 0.35 |
| 65 | 5 | 141 | 0.25 |
| 66 | 4 | 212 | 0.1 |
| 68 | 3 | 250 | 0.065 |
| 72 | 2 | 300 | 0.036 |
| 84 | 1 | 350 | 0.019 |

In order to measure both the bulk resistance of the electrodes and the interfacial charge transfer, apparent heterogeneous electron transfer rate constants ($k^0$) were calculated for each of the electrodes using the method of Nicholson (1965) This apparent rate constant should reflect both of these characteristics Working curves relating $\Delta E_p$ values to kinetic parameters ($\Phi$) are shown in *Table 2 3* $\Phi$ values for the electrode systems were calculated with the aid of a solver program that generated the sixth polynomial plot of $\Delta E_p$ vs log ($\Phi$)

All $k^0$ values are given in *Table 2 4* Recalling that for all the screen-printed electrodes the $\Delta E_p$ values were considerably greater than the 59 mV value expected for Nernstian one-electron reactions, $k^0$ values are then also inevitably low compared to glassy carbon Commercial electrodes (Euroflash™ and Ultra™) exhibited $k^0$ values 2000-fold and 1,250-fold lower than that obtained for glassy carbon, respectively The LRH-inH electrode proved the poorest with regard to $k^0$, being 3,500-fold lower than glassy carbon Ercon-inH and Ultra-inH both had the best $k^0$ values of the screen-printed electrodes, yielding $k^0$ values only 300-fold and 200-fold lower than glassy carbon, respectively Thus, Ultra-inH exhibited the best $k^0$ value, even if this was still two orders of magnitude lower than glassy carbon Such decreases in the electron-transfer reactivity may be consistent with the composition of the ink, being composed only partly of conductive carbon particles Attempts were made to fit the cyclic voltammetric data using CHI1000 software This fitting package uses the Butler-Volmer model and did not adequately fit this data (data not shown) This may be due to the capacitance present in the CVs, or it may be that the data tends towards the Marcus model, where the kinetics are affected by such factors as the nature and structure of the reacting species, the solvent, the electrode material and adsorbed layers on the electrode surface (Bard & Faulkner, 2001)

In view of the proprietary composition of all the inks, it is difficult to explain why the Ultra-inH electrode displayed the most favourable redox behaviour Observed changes in redox behaviour may be dictated by varying graphite content (good redox behaviour suggests a high graphite loading), the nature of the graphite particles, and the presence or absence of an adherent (inhibitory) organic layer An attempt to elucidate the physical properties of the inks is given in *Section 2 3 2*

Although Ultra-inH was shown to have the best behaviour of all the screen-printed electrodes to ferri/ferrocyanide, its behaviour was still far from ideal

Attempts to improve its behaviour (by electrochemical pre-treatment and optimisation of curing conditions) were carried out and these are outlined in *Section 2 3 3*

***Table 2.4.*** Table of heterogeneous electron transfer rate constants ($k^0$) for glassy carbon and each of the screen-printed electrodes

| *Electrode* | $k^0$ *(cm s$^{-1}$)* |
|---|---|
| Glassy Carbon | $5\,9 \times 10^{-2}$ |
| Euroflash™ | $2\,8 \times 10^{-5}$ |
| Ultra™ | $4\,7 \times 10^{-5}$ |
| Ercon-inH | $1\,7 \times 10^{-4}$ |
| LRH-inH | $1\,7 \times 10^{5}$ |
| Ultra-inH | $3\,1 \times 10^{-4}$ |

### 2 3 1 2 Performance of screen-printed electrodes in a biosensor format

The electrochemical performance of the screen-printed electrodes was investigated by incorporating them into the batch cell set-up shown in *Figure 2 5(a)* PANI/PVS was deposited on the surface of the electrode and the potential was cycled until the current associated with the $LM^{\bullet+}$ peak reached an anodic value of approx 2 8 mA (peak (a), *Figure 2 4*) No protein was immobilised onto the surface of the polymer Ultra-inH, Ercon-inH and LRH-inH electrodes were subjected to successive additions of 0 5 mmol dm$^{-3}$ added freshly hydrogen peroxide to a solution of 2 mg ml$^{-1}$ horseradish peroxidase and the amperometric response was monitored at –100 mV All three sensors responded to the changes in peroxide concentration (*Figure 2 12*) Similar response times and noise levels were observed (data not shown) Ultra-inH offered the highest sensitivity (4 μA (mmol dm$^{-3}$)$^{-1}$ peroxide), with Ercon-inH exhibiting a slightly lower sensitivity (3 2 μA (mmol dm$^{-3}$)$^{-1}$ peroxide) LRH-inH showed the poorest sensitivity (1 8 μA (mmol dm$^{-3}$)$^{-1}$ peroxide) This correlates with the voltammetric behaviour seen in *Section 2 3 1 1* Ultra-inH exhibited the highest sensitivity in terms of $j_p$ values while LRH-inH exhibited the lowest values

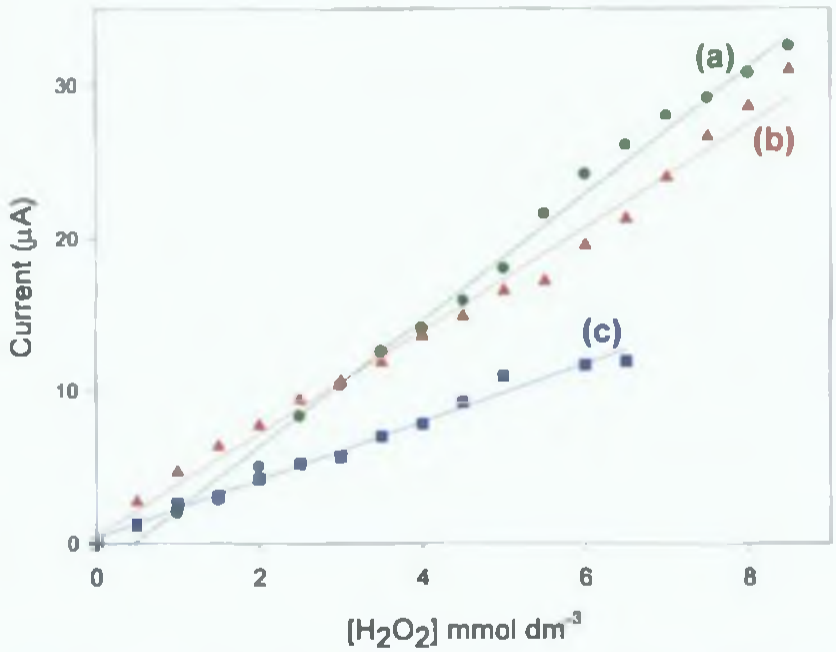


***Figure 2.12.*** Amperometric sensor responses for successive additions of 0.5 mmol $dm^{-3}$ $H_2O_2$ to a solution containing 2 mg $ml^{-1}$ HRP. Electrodes used were (a) Ultra-inH, (b) Ercon-inH and (c) LRH-inH. Electrodes were held at -100 mV vs. Ag/AgCl wire electrode.

Amperometric experiments could not be carried out on either of the commercial electrodes as the charge transfer properties of the electrodes hindered deposition of adequate polymer. For example, the in-house strips required seven cycles to immobilise polymer to the required thickness (LM peak height 2.8 mA, peak (a) in *Figure 2.4*), whereas the commercial electrodes needed twenty cycles in order to reach only one fifth the required thickness (LM peak height 0.56 mA, peak (a) in *Figure 2.4*). The experiments on these strips were abandoned at this point.

#### 2.3.1.3 Linear sweep voltammetric performance of screen-printed electrodes

The background current of thick-film carbon electrodes is strongly affected by the carbon ink employed (Wang *et al.*, 1998). *Figure 2.13* compares the background voltammograms for the different carbon electrodes in degassed phosphate buffer (pH 6.8). Several electrodes of each type were analysed and *Figure 2.13* shows data representative of all analyses.

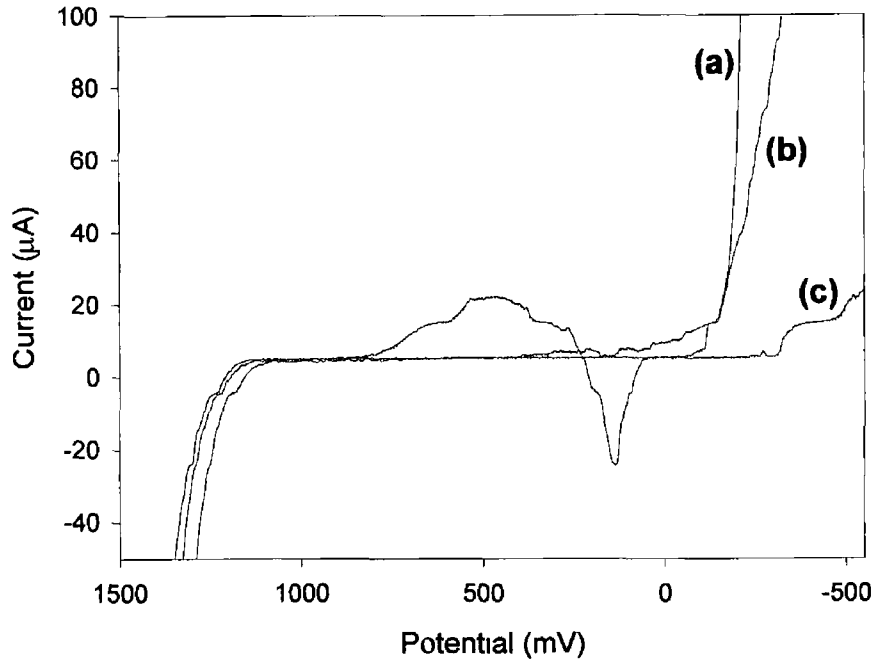


***Figure. 2.13.*** Linear sweep voltammograms in degassed PBS buffer (pH 6 8) Electrodes used were (a) Ultra-inH (green) (b) Ercon-inH (red) and (c) LRH-inH (blue)

LRH-inH exhibited the widest potential window particularly with respect to the cathodic potential limit (i e high hydrogen overvoltage) Its potential window had a range of +1150 to -300 mV, where the non-faradaic current remained constant (≈ 5 2 μA) in this electrolyte solution The background current of Ercon-inH was narrow and poor, exhibiting a lot of interference Ultra-inH also had a narrow potential window (+1097 to +60 mV) but was not affected by major interferences The non-faradaic current was of the same magnitude as for LRH-inH The anodic potential limits (i e oxygen overvoltage) were approximately the same for each of the inks

Carbon ink possessing a narrow potential is not necessarily a negative property for amperometric sensing It should be noted that an electrode of choice for fixed potential amperometric biosensors need not necessarily have the widest potential window as amperometric measurements are less affected by differences in the background contributions, as they are usually performed after the decay of transient currents to steady state values (Wang *et al*, 1998) However, the non-faradaic background current measured in linear sweep voltammetry, could potentially

have an effect on the sensitivity of the electrode The background current can limit the lowest current that can be measured, and so could affect the detection limits of an assay

### *2.3.2 Physical Characterisation of the screen-printed electrodes*

Ultra-inH, Ercon-inH and LRH-inH were compared in terms of their physical properties Due to the proprietary nature of the inks, very little information was known about their physical characteristics SEM (Scanning Electron Microscope) was employed in order to compare the morphology of each of the electrodes, and Energy Dispersive X-ray (EDX) analysis was used to elucidate if there were differences in the carbon contents of each of the inks Constant-height Scanning Electrochemical Microscopy (SECM), an electrochemical imaging technique, was also carried out in order to ascertain a visual image of spatially-confined variations in the chemical reactivity of the screen-printed carbon paste surface However, this technique has certain limitations on heterogeneous surfaces with variations in both conductivity and topography since current changes associated with distance variations cannot be distinguished from ones due to alterations in conductivity In order to circumvent these problems, instrumentation such as a constant-distance SECM or an SECM-AFM (Atomic Force Microscopy) would be required

#### 2.3.2 1 Scanning electron microscopy (SEM)

*Figure 2 14* depicts SEM images of (a) Ultra™ (b) Ercon™ and (c) LRH™ inks cured at 70°C for 13 minutes Each of the inks have varying degrees of surface roughness While the LRH™ ink has the smoothest structure of all the inks, the Ultra ink shows the roughest, most defined topography This result demonstrates that Ultra-inH has the highest surface area of all electrodes This is in agreement with the results from *Sections 2 3 1 1 & 2 3 1 2*, where it was shown that the Ultra-inH electrode exhibited the highest sensitivity, attributed to the increased surface area and hence, electrocatalytic sites

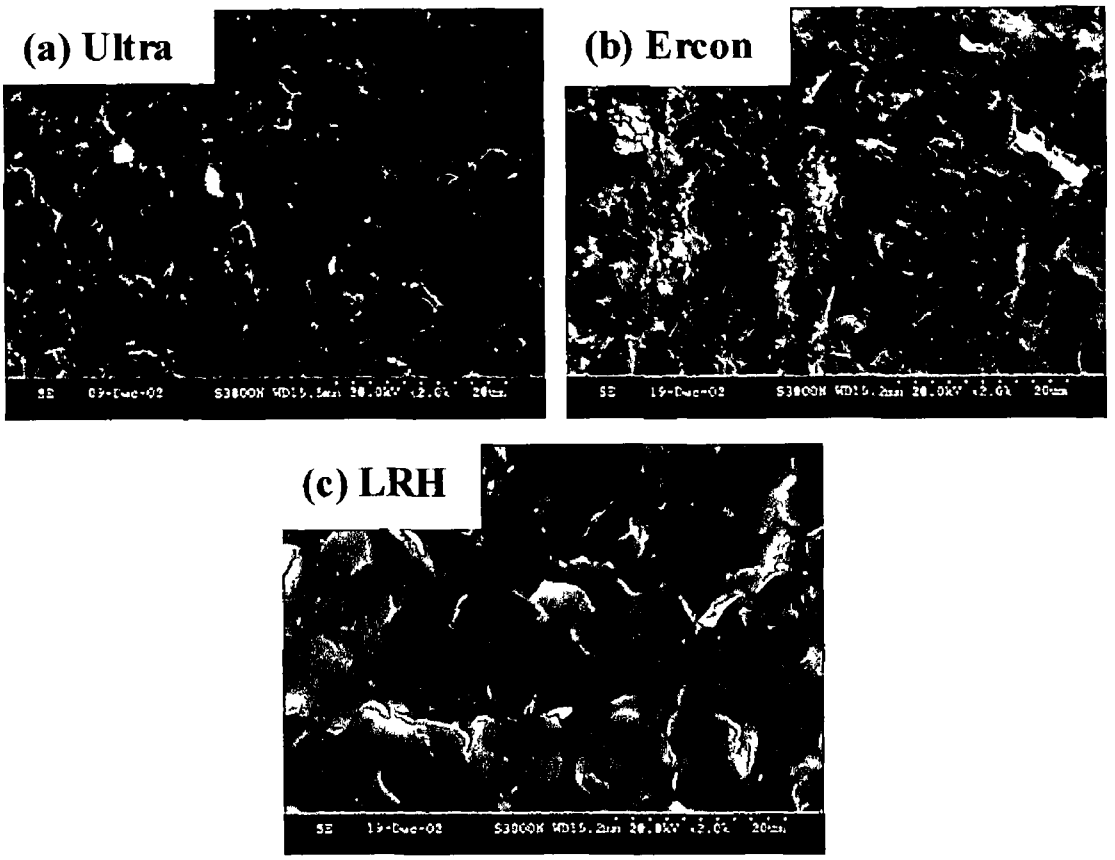


*Figure 2 14* Typical scanning electron micrographs of the (a) Ultra ink (b) LRH ink and (c) Ercon ink, each cured at 70°C for 13 minutes (2,000 X magnification)

### 2.3 2.2 Energy dispersive x-ray (EDX) analysis

EDX analysis of the carbons has shown that chlorine, oxygen and carbon are present in each of the ink formulations (*Figure 2 15*) The chlorine is present as a constituent of the binder or solvent, the presence of oxygen is due to any hydrophobic contamination and the major constituent of each of the inks is carbon (90% approx ) There was no discernible difference between the carbon content of each of the inks using EDX analysis illustrating that the severe electrochemical differences observed between the different electrodes is not due to variations in carbon compositions

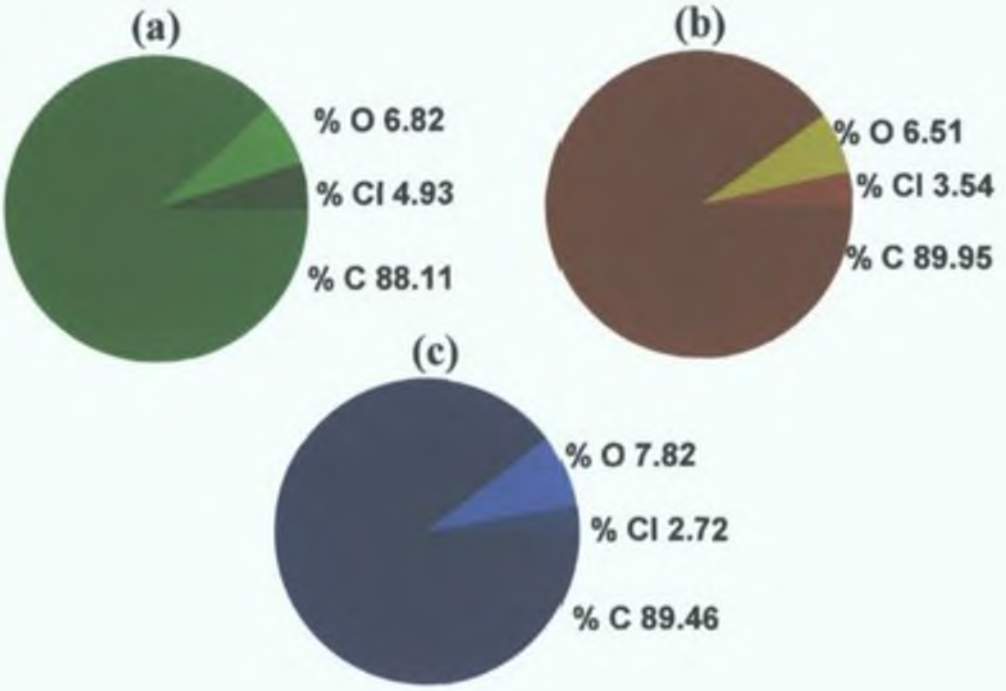


***Figure 2.15.*** Percentage elemental compositions of the major constituents of the carbon inks (a) Ultra, (b) Ercon and (c) LRH. Chlorine, oxygen and carbon content are approximately the same for each of the three inks.

### *2.3.3 Optimisation of Ultra-inH*

Although Ultra-inH did exhibit the best electrochemical and physical properties of all electrodes, for the purpose of designing an electrode suited towards amperometric sensing, there were major concerns that the Ultra™ ink for the WE was still not ideal. This was highlighted in the cyclic voltammetric study of ferrocyanide (*Section 2.3.1.1*). Attempts to decrease the $\Delta E_p$ values were done by varying the curing temperature and length of curing time of the carbon ink, and also the effect of electrochemical pre-treatment was studied.

#### 2.3.3.1 Curing parameters

Due to the composition of carbon inks, the parameters of curing can have a profound effect on their performance (Grennan *et al.*, 2001). $\Delta E_p$ values and $i_p$ values for the ferri/ferrocyanide redox couple were monitored over a range of curing

temperatures and it was found that above a temperature of 70°C, $\Delta E_p$ values increased greatly and the $i_{p\,a}$ decreased (*Figure 2.16*)

Carbon inks may be composed of three basic constituents: graphite, vinyl or epoxy-based polymeric binders and solvent to enhance the ink's affinity for the substrate in terms of adhesion, and to improve viscosity for the screen-printing process. It has been suggested that increases in curing temperature may result in evaporation of the solvent and decomposition of the polymeric binder to give a greater definition of the graphite or carbon particles. This would mean that the increases in temperature should result in an increase in the microparticulate nature of the carbon and greater definition of the graphite particle surface area (Grennan *et al*., 2001). According to this theory, electron transfer rates should increase as the graphite particle surface area becomes increasingly defined (i.e. with increasing temperature). This behaviour was not observed for the Ultra ink. Increases in temperature above 70°C resulted in reduced reaction kinetics. This demonstrates that the individual nature of the ink and its unknown constituents can have a profound effect on its characteristics. The Ultra ink seemed to maintain a very defined microparticulate character (*Figure 2.14a*), which was quite different from the Gwent electrode (Grennan *et al*., 2001). This difference in behaviour could be attributed to different solvents with different evaporation rates, different graphite particles or binders or other additives, and their relative concentrations/solubilities etc. If the viscosity of inks differ, the film thickness after a single print will most likely also differ and may cause a difference in the electrochemical and physical characteristics. Below 70°C, $\Delta E_p$ values were relatively constant. There were no resistive effects observed that one might expect if there was excess polymeric binder present at the electrode surface due to curing at lower temperatures. $i_{p\,a}$ values peaked at 70°C, and this temperature was chosen as optimum, as greatest sensitivity was exhibited at this curing temperature.

At a curing temperature of 70°C, the effect of curing time on electrode performances was monitored. Over a range of 0-20 minutes, there did not appear to be any significant effect on electrode performance. $\Delta E_p$ values for ferrocyanide did not vary significantly (*data not shown*), suggesting that curing had very little impact on the performance of the ink at all. Even at 0 min (no curing), $\Delta E_p$ was only marginally higher. This makes sense along with the curing temperature data in that up to about 70°C, there is very little gain in electrochemical performance. Heat may serve only to

physically dry the constituents of the ink. This may also suggest that any solvents present are extremely volatile or extremely non-volatile and ink-drying may he brought about by polymerisation processes rather than evaporative processes. It certainly suggests a very different composition for this Ultra ink, as opposed to the Gwent ink previously characterised (Grennan *et al.*, 2001).

Inverness Medical cure all carbon inks at 70°C for 13 minutes. Since curing temperature and time were not found to be such important factors, it was decided not to deviate from these parameters. For all future work, these curing parameters were used for the Ultra™ ink.

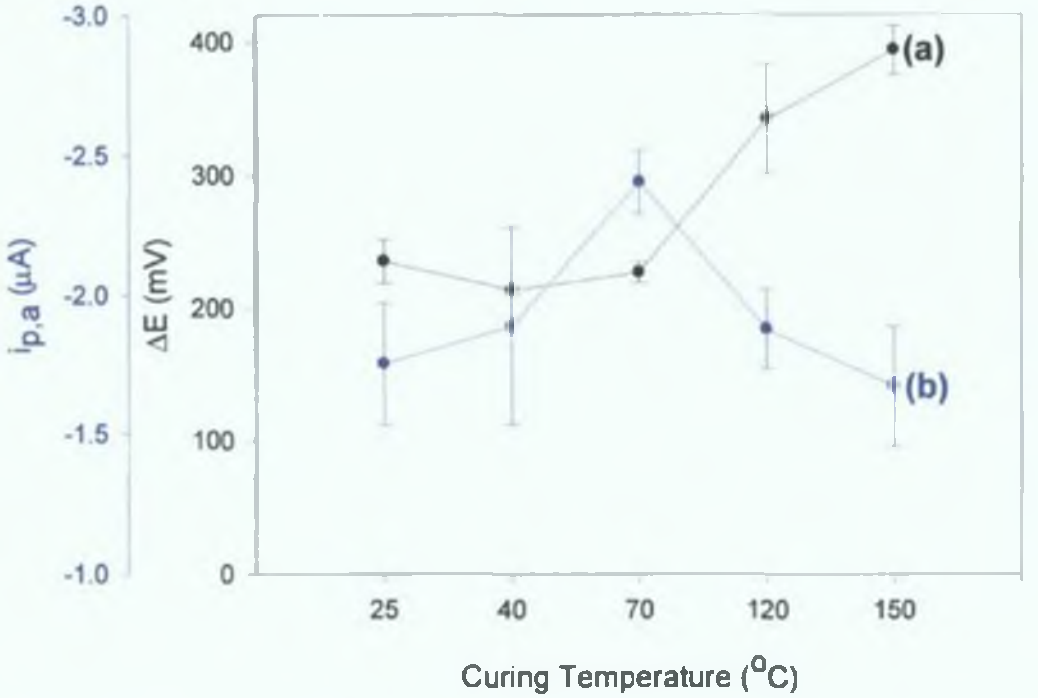


***Figure 2.16.*** (a) Mean $\Delta E_p$ values (n=4) and (b) mean $i_{p,a}$ values (n=4) for $1 \times 10^{-3}$ mol $dm^{-3}$ ferrocyanide, for varying curing temperatures of the Ultra™ ink on the Ultra-inH electrode. A curing temperature of 70°C showed optimal voltammetric performance for $\Delta E_p$ and $i_{p,a}$ values.

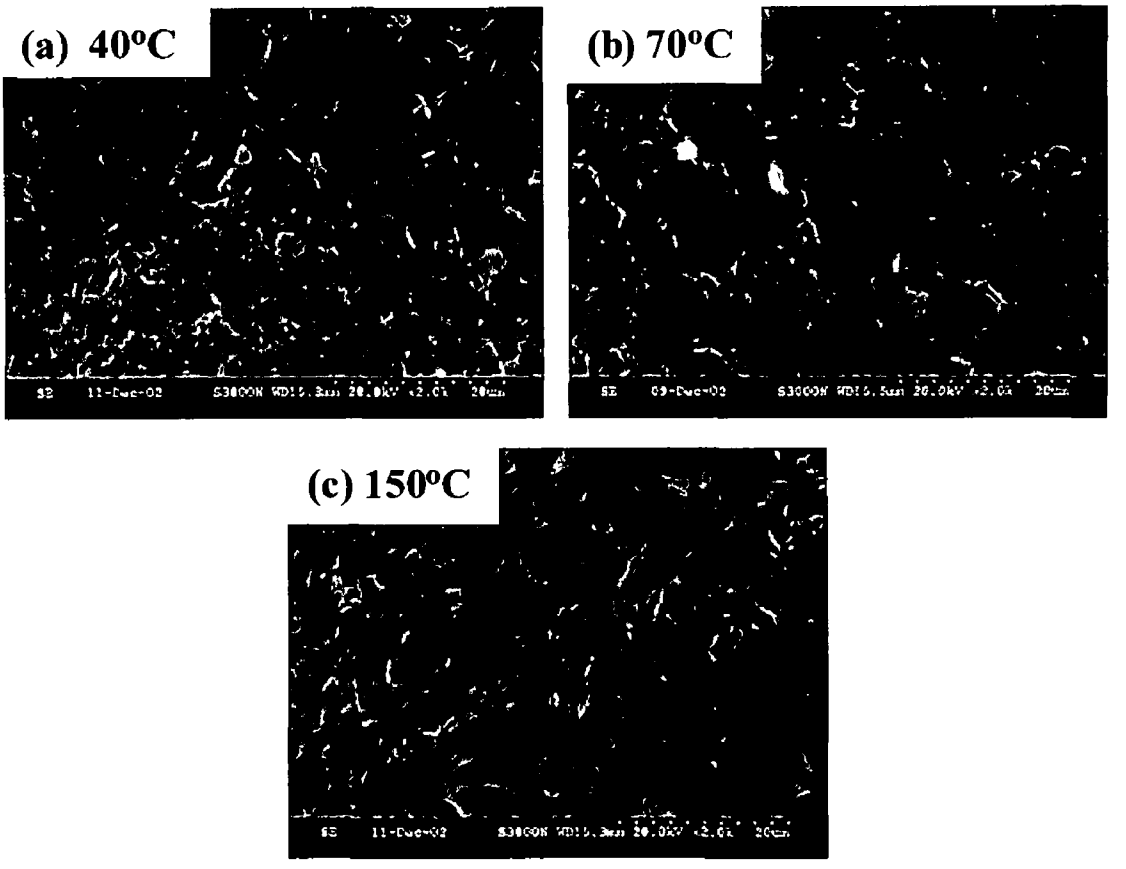


*Figure 2.17.* Typical scanning electron micrographs for the Ultra™ ink cured at various temperatures (a) 40°C, (b) 70°C and (c) 150°C for 13 minutes (2,000 X magnification ) The surface topography shows good definition of graphite particles for all curing temperatures

### 2 3 3 2 Electrochemical pre-treatment

Pre-treatment of working electrodes is a method employed by many researchers in order to enhance the electrochemical activity of their screen-printed electrodes (Gue *et al* , 2002, Wang *et al* , 1996 and Cui *et al* , 2001) It is generally agreed that pre-treatment effectively removes organic binders and contamination that occur at electrode surfaces such as carbon and gold and may bring about an increase in the numbers of chemically reactive sites on the electrode surface Wang *et al* (1996) employed an electrochemical pre-treatment method involving short pre-anodisation (30 s to 3 min m the +1 5 to +2 0 V range) of screen-printed electrodes in phosphate buffer solution (0 05 mol $dm^{-3}$) This pre-treatment method appeared to increase the surface functionalities and roughness or to remove surface contaminants and resulted in enhanced electrochemical activity Electrochemical pre-treatment of

electrodes can also be carried out by cycling the potential in acidic media Gue *et al* (2002) simply used a chemical cleaning step with sulphuric acid and hydrogen peroxide solution for gold microelectrodes This step was critical for sensor sensitivity

The electrochemical pre-treatment method of Killard *et al* (1999) has been employed in this work (*Section 2 2 5*) Cycling the screen-printed electrode in sulphuric acid (0 2 mol $dm^{-3}$) is believed to have the effect of stripping the surface of the carbon electrode Any insulative materials present at the surface may be removed The procedure may even have the effect of renewing the surface by removing the whole outer layer of the ink To assess the effect of electrode pre-treatment on the Ultra™ ink, the electrodes were subjected to varying numbers of cycles in 0 2 mol $dm^{-3}$ $H_2SO_4$, and the effect of this on electrode behaviour was examined by looking at the $Fe^{2+}/Fe^{3+}$ couple and on the first polymerisation cycle of polyaniline

By electrochemically pre-treating the Ultra electrode, its behaviour towards the ferri/ferrocyanide redox couple improved dramatically (*Figure 2 18*) $\Delta E_p$ values decreased by 50% Before pre-treatment, electrodes were exhibiting an average $\Delta E_p$ value of 222 mV (RSD = 2 01%, n = 9) After pre-treatment, this was reduced to 112 mV (RSD = 3 49%, n = 9) $i_p$ current values also increased as a result One pre-treatment cycle was sufficient to observe this behaviour Increasing the number of pre-treatment cycles did not have a significant effect Apparent heterogeneous electron transfer rate constants ($k^0$) increased from $3\ 09 \pm 0\ 06 \times 10^{-4}$ cm $s^{-1}$ (no pre-treatment) to $3\ 97 \pm 0\ 14 \times 10^{-3}$ cm $s^{-1}$ (pre-treated), a ten-fold improvement

These figures suggested that the electrochemical pre-treatment of the screen-printed electrode was of vital importance After pre-treatment, the kinetics and charge transfer rates at the Ultra-inH electrode were enhanced greatly

*Figure 2 19* shows the first polymerisation cycle of aniline onto the electrode after a varying number of pre-treatment cycles The peak at -330 mV is due to the reduction of silver in acidic solution The silver conducting path directly underneath the carbon print undergoes a redox process if it has not been completely covered with carbon As the number of pre-treatment cycles was increased, more silver became available for this oxidation process, indicating that the sulphuric acid pre-treatment step was stripping components of the carbon ink from the surface Increasing the number of pre-treatment cycles had no effect on any other aspects of

the polymerisation process Pre-treatment is a stripping procedure that appears to enhance electroactivity, through exposure of increased amounts of electroactive carbon

As the pre-treated Ultra-inH electrode appeared to be near comparable to the Gwent electrode, it was decided to use this configuration in further work involving polyaniline deposition

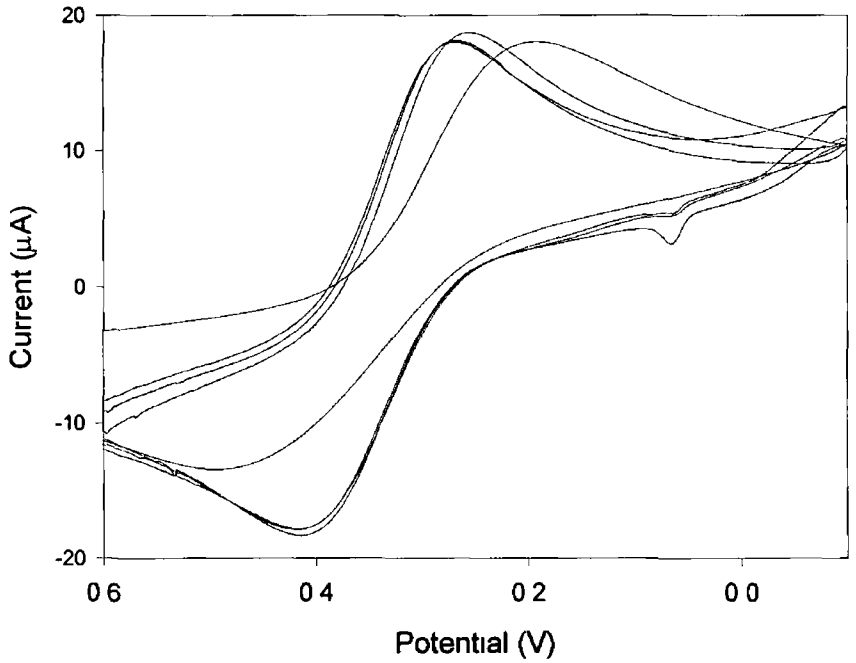


***Figure 2.18.*** Effect of pre-treatment of the Ultra-inH electrode on cyclic voltammogram of ferri/ferrocyanide No pre-treatment (black), one pre-treatment cycle (red), two pre-treatment cycles (blue), three pre-treatment cycles (green)

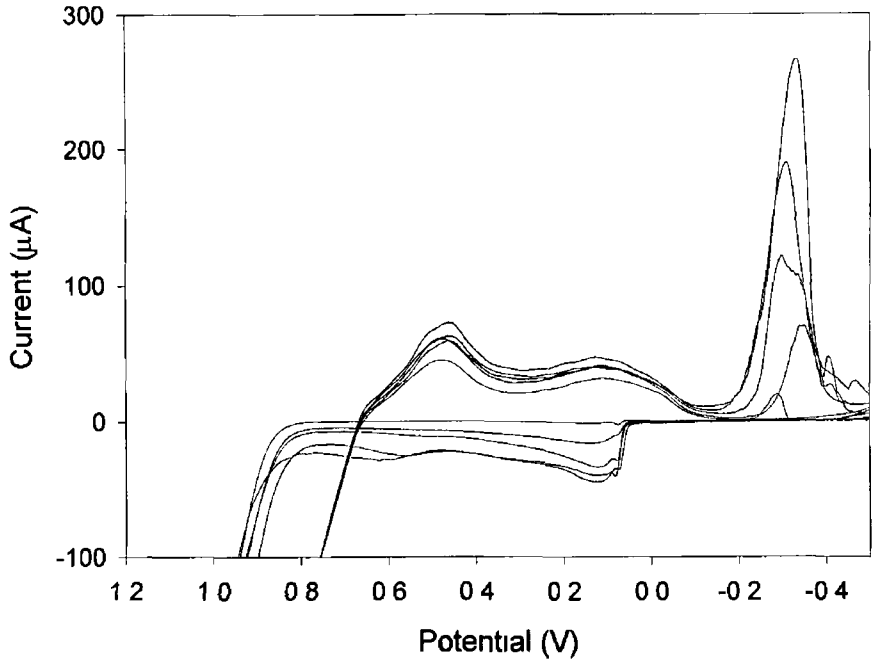


***Figure 2.19.*** First polymerisation cycle of aniline onto an Ultra-inH electrode after varying numbers of pre-treatment cycles 0 cycles (black), 1 cycle (red), 2 cycles (brown), 5 cycles (blue) and 10 cycles (green)

### *2 3 4 Behaviour of electrochemically deposited polyaniline as a function of its film thickness*

The PANI/PVS copolymer can be potentiodynamically grown to a given thickness on an electrode, provided that the charge transfer properties of the film do not become limiting The thickness is controlled by monitoring the number of scans, or current reached during deposition *Figure 2 20* shows SEM images of side profiles of electropolymerised copolymer on an Ultra-inH electrode The images illustrate the increasing thickness of the polymer layer on the electrode surface with increasing number of potentiodynamic scans Up to 10 scans, the polymer layer appears to be thin, and it is possible to differentiate between the electrode layers carbon and silver, and the polymer Single branches of polymer formed can be seen After cycling for 20 scans, the polymer layer is noticeably thicker as the single branches developed during the early scans had grown into each other Cycling the electrode for 40 scans resulted in very thick, visually dense films *Figure 2 21* shows angled SEM images of electrodeposited polyaniline of varying thickness These images demonstrate that the

polymer grows in a neat vertical fashion over the electrode, to form the porous, sponge-like, non-uniform polymer-modified electrode.

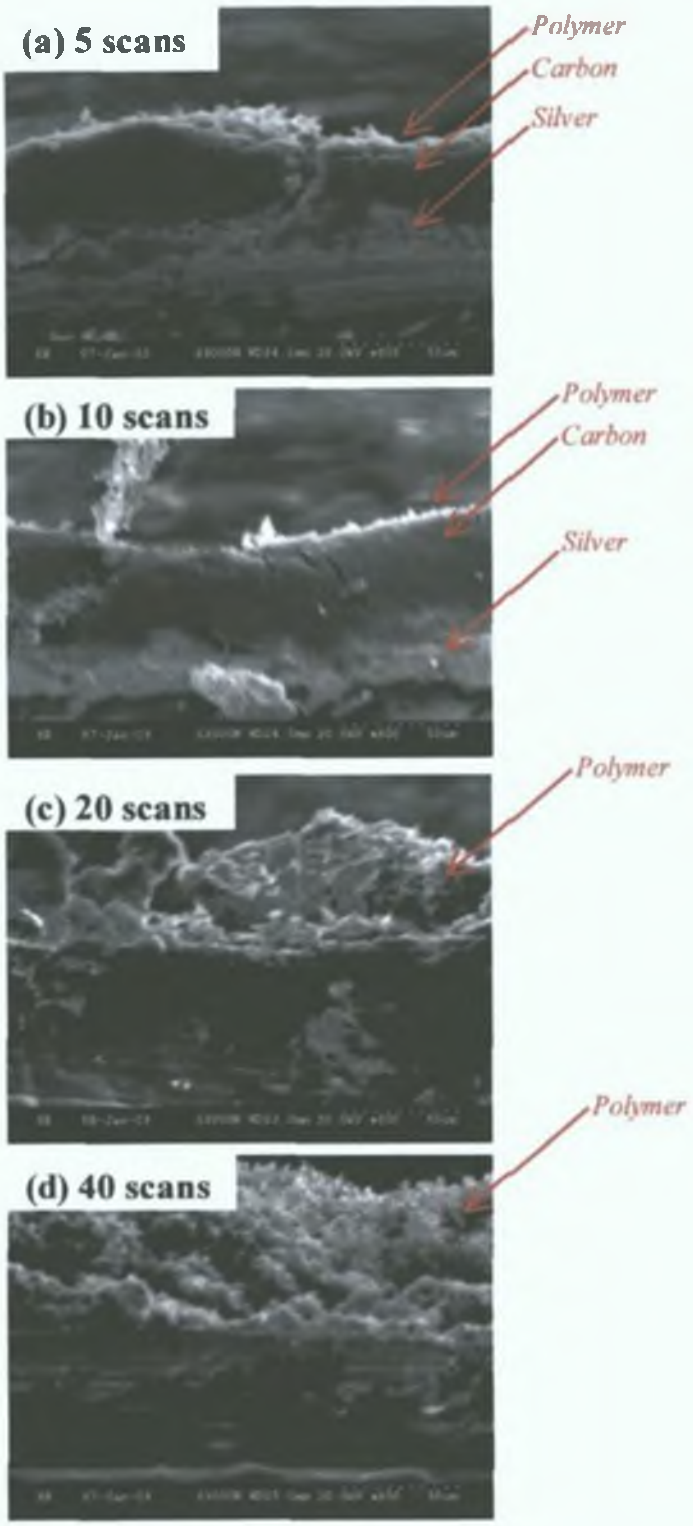


***Figure 2.20.*** Side profile scanning electron micrographs of the various thicknesses of PANI/PVS copolymer deposited on the Ultra-inH electrode (500 X magnification). Polymer thicknesses gauged by number of electropolymerisation scans.

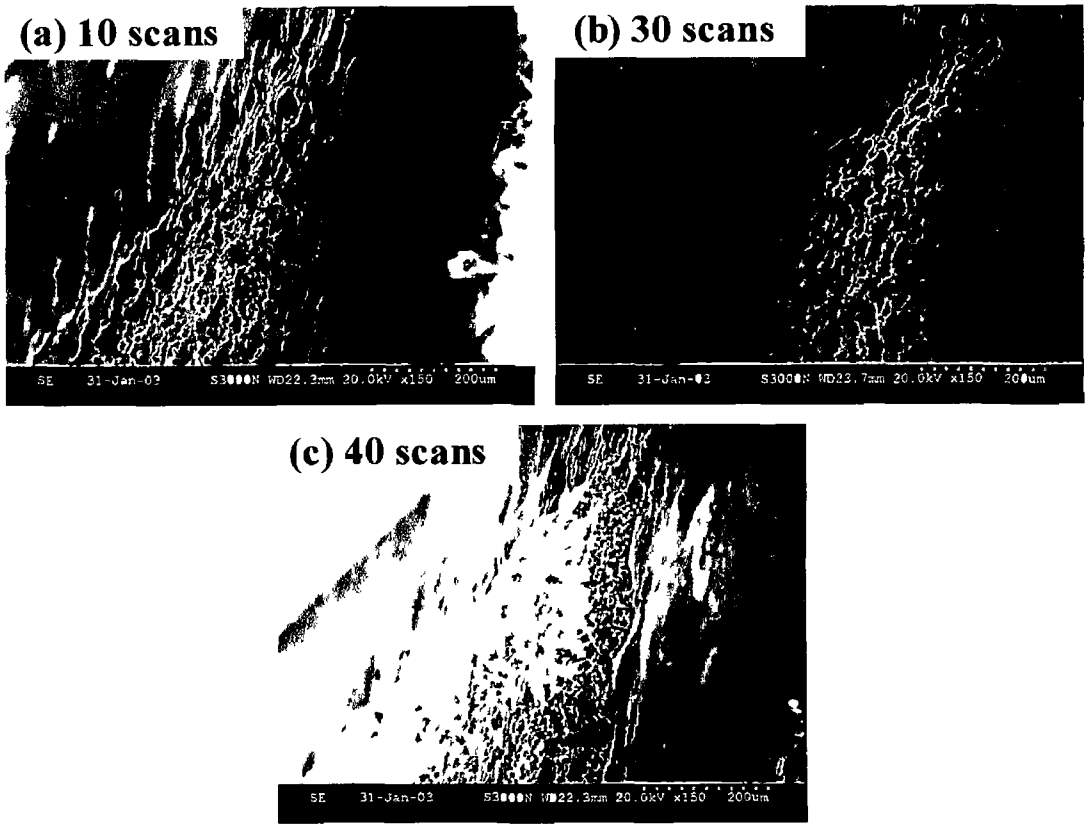


*Figure 2 21* Angled scanning electron micrographs of the various thicknesses of PANI/PVS copolymer deposited on the Ultra-inH electrode (150 X magnification) Polymer thicknesses gauged by number of electropolymerisation scans

The thickness of the polymer films can be estimated from the amount of charge, Q, necessary to switch from LM to the $LM^{+}$ (peak (a) in *Figure 2 4*) form of PANI according to *Equation 2 2* (Duic & Grigic, 2001)

$$d = \frac{Q_a M_w}{zFA\rho} \qquad \textit{Equation 2.2}$$

where $Q_a$ is the charge under the first voltammetric peak, $M_w$ is the molecular weight of aniline, z = 0 5 (number of electrons per aniline unit), A is the area of the electrode (0 09 $cm^2$), ρ is the specific density of aniline (1 02 g $cm^{-3}$), and F is Faraday's constant (96,485 C)

The method does not accommodate for the porosity factor and the counter-ion volume, but calculates the total quantity of PANI only

*Table 2 5* Charge Q and the calculated thickness of PANI films

| *No. of electro-polymerisation scans* | *$LM^{+}$ Anodic Peak Height (mA)* | *Charge Incorporated Q/(mC)* | *Calculated PANI Thickness d/(μm)* |
|---|---|---|---|
| 5 | 0 5 | 0 2 | 3 9 |
| 10 | 2 8 | 1 7 | 34 6 |
| 20 | 6 8 | 9 1 | 191 3 |
| 30 | 10 0 | 12 0 | 252 4 |
| 40 | 17 0 | 16 8 | 354 4 |

*Equation 2 2* was used to calculate thickness of the electroactive polymers shown in the SEM images in *Figure 2 20* and *2 21* Approximate polymer thickness gauged from the SEM images (using the scale on the bottom of each of the images) are all larger than those calculated using the formula This is due to the fact that the polymer layer incorporates the non-conducting vinylsulphonate polymer, which cannot be accounted for in *Equation 2 2* Also, any non-electroactive polyaniline is not included in d, polymer thickness

O'Connell *et al* (2001) reported that amperometric sensor responses do not increase with increasing thickness of polymer on the electrode surface, suggesting that the rate-determining step for catalysis occurs only at the outer polymer-solution interface However, Duic and Grigic (2001) reported a consistent increase in $i_p$ values as a function of film thickness for the redox couple hydroquinone/quinone, attributed to increases in the real surface area of the polymer Providing the redox molecules are small enough to diffuse into the polymer matrix, the bulk of the reaction may be occurring within the polymer matrix, i e at the polymer – solution interface *within* the polymer layer Increases in polymer thickness increase the available surface area of polymer within the polymer layer, thus resulting in increased $i_p$ values

Investigations into the effects of the thickness of our PANI/PVS film on amperometric behaviour are shown in this section Previous work (Iwuoha *et al*, 1997) on polyaniline-based amperometric sensors employed ten redox cycles as standard during the polymerisation process (Ten redox cycles allows the peak corresponding to the formation of the $LM^{+}$ (peak (a) in *Figure 2 4*) to reach an anodic current of approx 2 8 mA)

### 2 3.4.1 Voltammetric behaviour

Ferri/ferrocyanide was the redox system used for comparing voltammetric behaviours of different polymer thicknesses 1 mol $dm^{-3}$ HCl was used as supporting electrolyte, as polyaniline exhibits optimum conductivity in acidic media PANI/PVS was deposited on Ultra-inH electrodes to a LM $^{\bullet+}$ anodic peak height of approx 2 8 mA according to *Section 2 2 6* Cyclic voltammograms for varying concentrations of ferrocyanide were momtored in order to verify the $Fe^{2+}/Fe^{3+}$ redox peaks (*Figure 2 22*) Peak potentials were found to be $\approx$ 560 mV and 460 mV for anodic and cathodic peaks, respectively $\Delta E_p$ values of 85 mV were observed for concentrations of ferrocyanide up to $2 \times 10^{-2}$ mol $dm^{-3}$ $4 \times 10^{-2}$ mol $dm^{3}$ ferrocyanide resulted in a $\Delta E_p$ value of 126 mV

*Figure 2 23* shows that there is a very significant influence of PANI/PVS thickness ($LM^{+}$ peak height) as well as scan rate on the resulting peak potential separation It was found that $\Delta E_p$ values was higher for bare electrodes than thin polymer electrodes showing that the rate of electron transfer is higher when thin layers of PANI/PVS were deposited Electron transfer began to decrease as the polymer thickness was increased, since an increase in $\Delta E_p$ values was observed However, Mandic & Duic (1998) found that the peak separations decreased with increasing PANI film thickness for the same redox couple The reduction in the electron transfer rate for increasing thicknesses of PANI/PVS could be attributed to the lower diffusion rates of the of the ferri/ferro couple with increasing amounts of large vinylsulphonate counterions present within the polymer, which may serve to inhibit kinetics in acidic medium

Current peak values, $i_p$ exhibited a linear dependence on $\upsilon^{1/2}$, ($r^2$ = 0 9924, data not shown), suggesting a diffusion controlled process is taking place However, the fact that $\Delta E_p$ even decreases below 60 mV at low scan rates implies, however, that the reaction is not under diffusion control and that it corresponds to the reaction of a species within a layer (Mandic & Duic, 1998)

This could be a result of hexacyanoferrate (III) (molar mass 210 g $mol^{-1}$) being able to diffuse into the PANI/PVS polymer matrix, so that the location of the reaction is not only at the outer polymer-solution interface, but at the polymer-solution interface *within* the polymer layer (*Figure 2 24*) Therefore, mcreases in

currents for the $Fe^{2+}/Fe^{3+}$ couple could be explained by the increase in the available surface area of the polymer-modified electrode Gros *et al* (1997) have shown before that their PANI films doped with large inert molecules are permeable to electroactive species up to a molar mass of 200 g $mol^{-1}$ Although this phenomenon may be used to explain this increase in $i_p$ values for a small electroactive species, it cannot explain increases in current responses for much larger molecules such as proteins, as these should not be able to permeate the polymer The effect of polymer thickness on catalytic responses due to protein interactions is discussed in *Section 2 3 4 2*

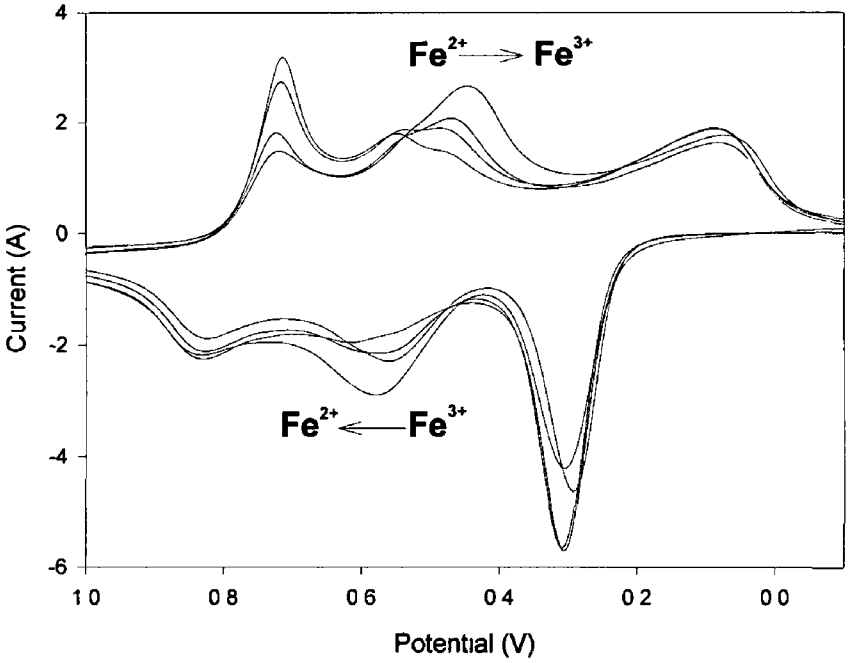


***Figure 2.22.*** Cyclic voltammograms of polyaniline-modified Ultra electrodes for varying concentrations of ferrocyanide in 1 mol $dm^{-3}$ HCl supporting electrolyte Blank (black), $1 \times 10^{2}$ (blue), $2 \times 10^{-2}$ (red), $4 \times 10^{2}$ (green) mol $dm^{-3}$ $Fe^{3+}$

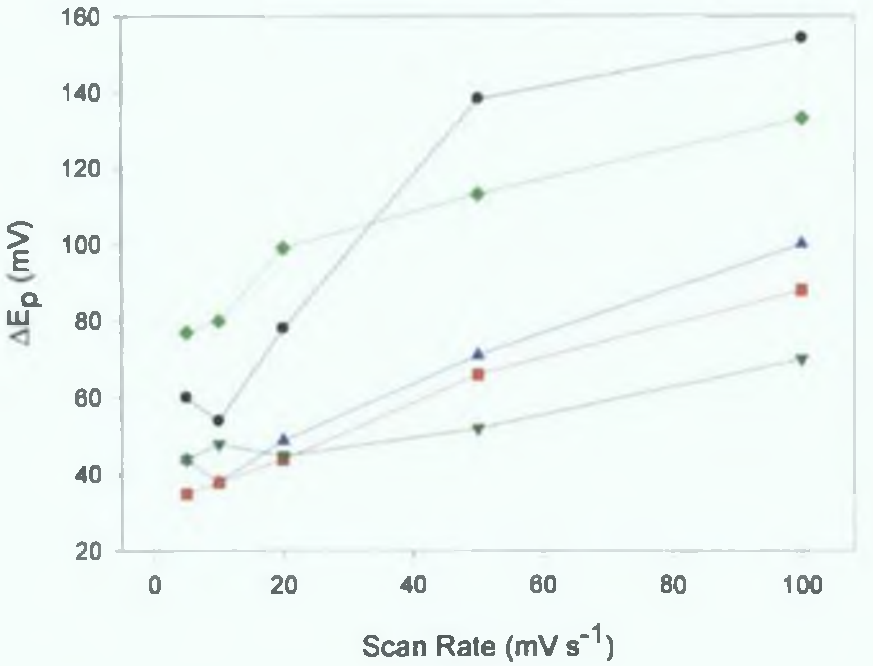


***Figure 2.23.*** Dependence of $\Delta E_p$ on scan rate for various thicknesses of the PANI/PVS copolymer layer for $2 \times 10^{-2}$ mol $dm^{-3}$ ferrocyanide in 1 mol $dm^{-3}$ HCl. Polymer thickness gauged by the current associated with $LM^{+\bullet}$ peak heights during polymerisation: 1.1 mA (dark green), 2.8 mA (red), 5.5 mA (blue), 10 mA (black) and blank (light green).

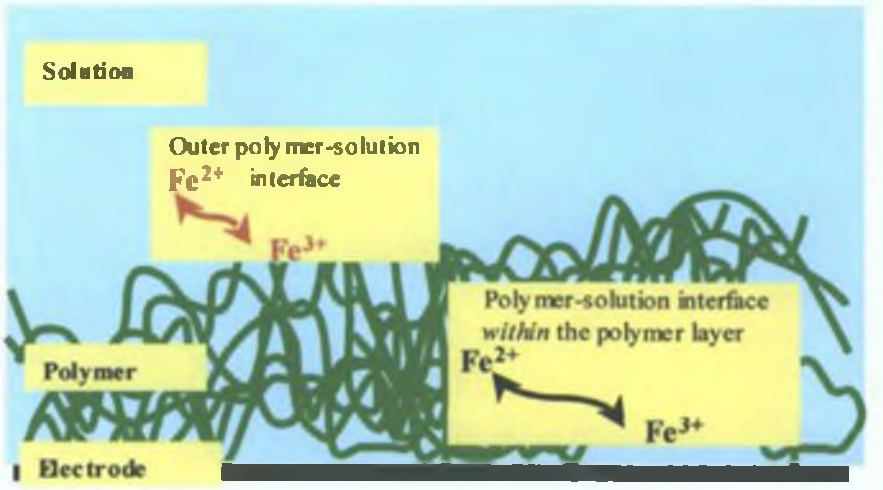


***Figure 2.24.*** Schematic of possible locations of the $Fe^{2+}/Fe^{3+}$ redox reaction. It is important to note that the concept of the reaction occurring at the polymer-solution interface within the polymer layer is only applicable to small electroactive species. Reactions for larger species should occur at the outer polymer-solution interface only.

### 2 3 4.2 Amperometric transients

Using ten redox cycles ($LM^{\bullet+}$ peak height of ≈ 2 8 mA) for deposition of polymer on pre-treated glassy carbon, the time taken to reach steady state for the amperometric experiments (*Section 2 2 10*) was typically < 1000 seconds and yielded a charging current typical of that shown in *Figure 2 25* The large peak is a direct result of the charging of the polymer This charging process occurs as a result of the oxidation of the polymer for 25 minutes before steady state experiments (*Section 2 2 9*) This charging current profile is also typical of the behaviour of previous polymer-modified screen-printed electrodes (Iwuoha *et al*, 1997) Although its relationship with electrode performance was never properly established, it was observed that the presence of this type of charging was indicative of good electrode performance (Killard & Grennan, personal communication and unpublished data)

The effect on amperometric transients of increasing the thickness of the polymer film, by cycling the potential for longer periods was monitored on the Ultra-inH electrodes (*Figure 2 26*) Ultra-inH polymer electrodes showed charging currents very different to glassy carbon and Gwent electrodes when the polymer was cycled to the same thickness of 2 8 mA $LM^{\bullet+}$ peak current Although the quantity of charge was similar, the charging profile was noisier This improved somewhat when polymer thickness was increased to 6 mA $LM^{\bullet+}$ peak current At 8 mA $LM^{\bullet+}$ peak current, the smooth charging profile was restored However, the charging currents exhibited were greater than for thinner polymers on glassy carbon and Gwent electrodes At present, there is no clear explanation why the charging characteristics of the Ultra-inH electrodes are so much poorer than their Gwent electrode counterparts, when the conditions of polymer electrodeposition appear to be comparable (equivalent number of voltammetric cycles for a given layer deposition)

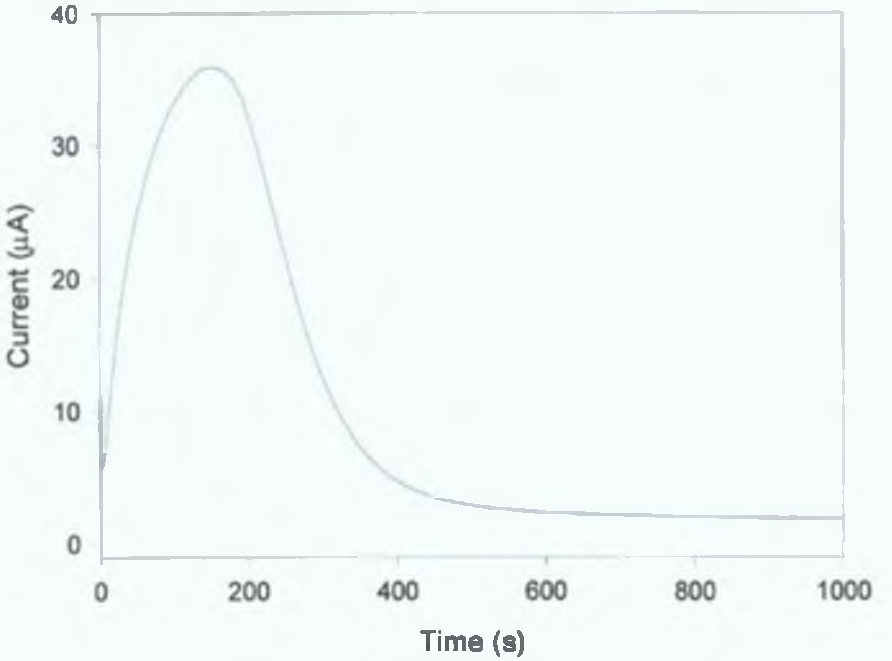


***Figure. 2.25.*** Typical charging current behaviour at a polymer-modified glassy carbon electrode at the beginning of a steady state amperometric experiment. Electrode stepped from +700 mV to –100 mV vs. Ag/AgCl.

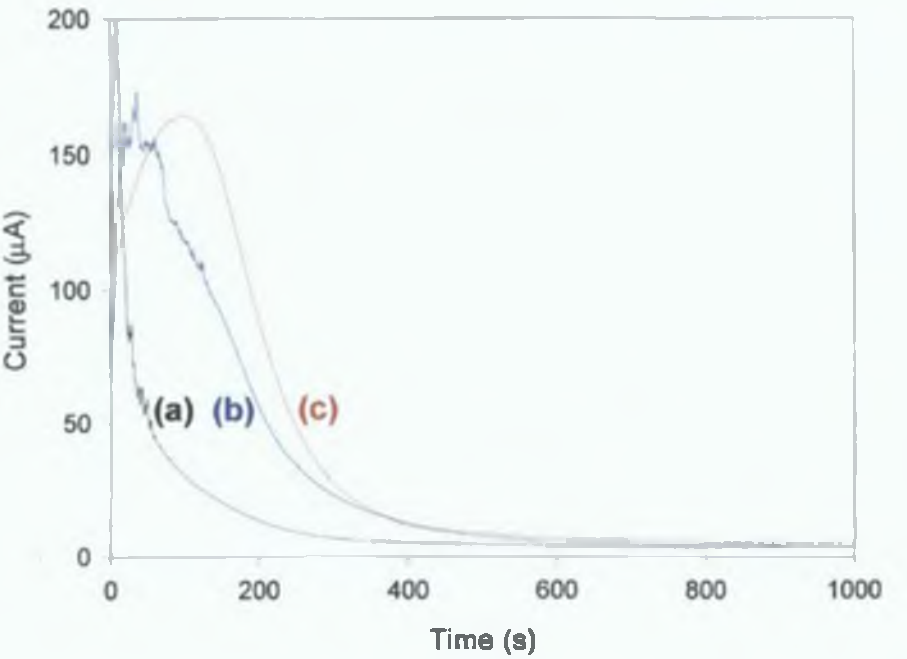


***Figure. 2.26.*** Typical charging current behaviour at Ultra-inH electrodes at the beginning of steady state amperometric experiments. $LM^{n+}$ current heights during polymerisation: (a) 2.8 mA, (b) 6 mA and (c) 8 mA. Electrode held at –100 mV vs. Ag/AgCl.

The relationship between the charging current and the polymer thickness was investigated further The integral of the charging current was used to give a value of the charge incorporated into the polymer The dependence of this charge on initial polymerisation conditions is shown in *Figure 2 27* The charge incorporated into the polymer increased linearly as the polymerisation cycle was increased This linear relationship was found not to be limiting up to a polymer deposition level of 20 mA for the peak height of $LM^{\bullet+}$ Relative standard deviations were typically 15% where n>2 The major disadvantages of thicker polymer films were higher background currents and increased response times (discussed in *Section 2 3 4 3*) The same linear charge relationship was seen for glassy carbon and Gwent carbon paste electrodes verifying that this behaviour is a property of the polymer, and not the carbon electrode (*Figure 2 27*) However, equivalent amounts of polymer deposited on the Gwent electrode, consistently incorporated slightly more charge than the Ultra electrode after 2000 s This may be due to the smaller geometric area Although equivalent amounts of polymer are deposited, polymerisation on the Gwent electrode should result in a thicker film due to the smaller electrode area Glassy carbon, which has the same electrode area as the Gwent electrode incorporates slightly lower charge Overall, however, the three electrode types do not show significant differences in their polymer thickness/charge capacity relationships However, as illustrated in *Figure 2 26*, it is the nature of the charging process that appears to be different between these electrodes Little is understood about the detailed nature of this process and further studies using techniques such as rotating disk voltammetry would be required to elucidate it more fully

Charge transfer appears to become limiting for glassy carbon during deposition of polymer at high $LM^{\bullet+}$ currents As the number of polymerisation cycles increased, the potentials for all four main peaks shifted to markedly more positive potentials, indicating that the growth of the polymer was becoming increasingly difficult Polymer depositions were not carried out above 9 mA This limiting behaviour was not observed for the screen-printed electrodes, and so thicker depositions of polymer could be monitored Once again, the reason for this is not clear

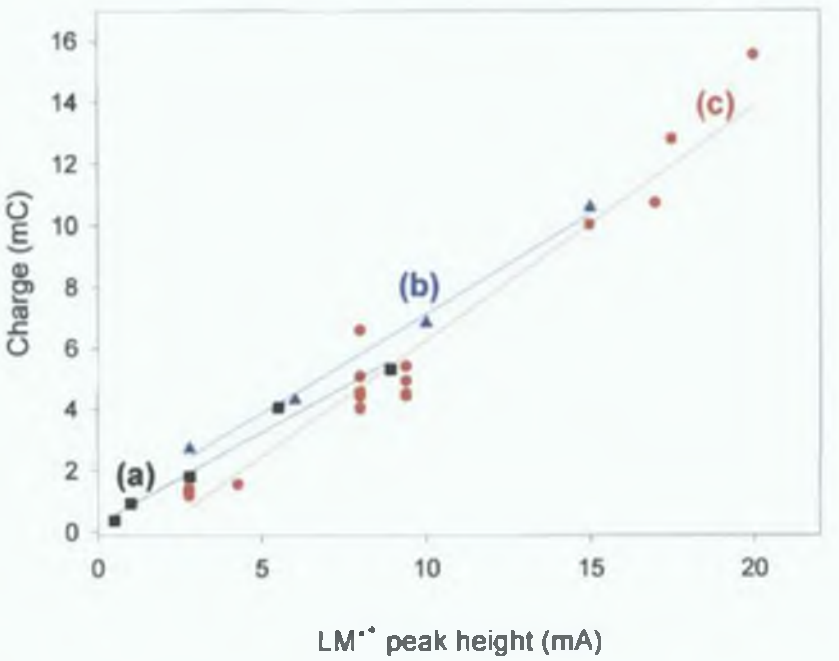


***Figure. 2.27.*** Dependence of charge incorporated into the polymer on the $LM^{\bullet+}$ peak height after depositing the polymer onto (a) glassy carbon (slope = 5.97, $r^2$ = 0.9776), (b) Gwent-inH (slope = 6.50 mC $mA^{-1}$, $r^2$ = 0.9933) and (c) Ultra-inH electrode (slope = 7.59 mC $mA^{-1}$, $r^2$ = 0.9533). Charge measured between 0 and 2000 s.

### 2.3.4.3 Background signals and response times

Background signals and time taken to reach steady state both increased as a result of increasing the thickness of the polymer on Ultra-inH electrodes (*Figure 2.28*). The thickness of the polymer was monitored in terms of charge incorporated during steady state experiments, rather than $LM^{\bullet+}$ peak height for all further discussion, since it was deduced in *Section 2.3.4.2* that the functions were linearly proportional.

Although there are definite direct relationships between both background signals and time to reach steady state and the charge of the polymer, the regression coefficients are low: $r^2$ = 0.689 and 0.612 for background and time to reach steady state respectively. This appears to be because these correlations break down above ≈ 5 mC and so this relationship does not hold for the very thickest of polymer layers.

The time taken to reach steady state in amperometric measurements has an impact on the response time of the sensor. As polymer thickness increases, time taken

to reach steady state increases, and analyte cannot be introduced into the system until later times However, increased polymer thickness appeared to be necessary to produce smoother charging currents (*Section 2 3 4 2*) on Ultra-inH electrodes The problem of long response times could, perhaps, be overcome by introducing a further potential step at the beginning of the steady state experiment This step might allow for the polymer to charge more quickly, resultmg in a dramatic reduction of response times *Figure 2 29* demonstrates this principle A standard assay was compared to an assay incorporating a step potential The step potential experiment involved holding the potential at -0 8 V for 100 seconds before stepping to the standard potential of -0 1 V The response time decreased by almost 1000 seconds No protein was immobilised on the surface of the electrode Amperometric experiments were carried out according to *Section 2 2 10* Amperometric responses were due to the addition of $H_2O_2$ (8 mmol $dm^{-3}$) to a solution of HRP (1 mg $ml^{-1}$) Further studies need to be carried out to see if steppmg the potential could result in damage or loss of immobilised protein

Another advantage of this steppmg protocol is that the background signal decreased by a factor of 30% Low background response is another important criterion when validating a quantitative methodology as the response for the lower detection limit of an assay should be at least three times the background signal Without the use of a step potential, the background noise level at mcreased levels of polymer deposition (*Figure 2 29*) could prove a major barrier in developing sensitive assays

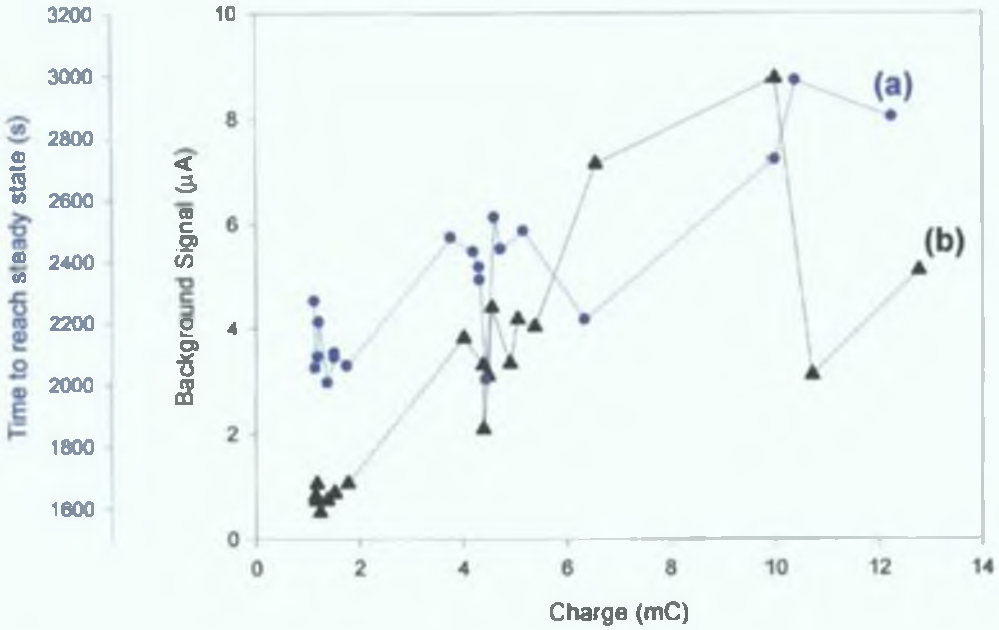


***Figure. 2.28.*** Relationship between (a) length of time to reach steady state and (b) background signals of steady state on the charge incorporated into the polymer (Ultra-inH electrode).

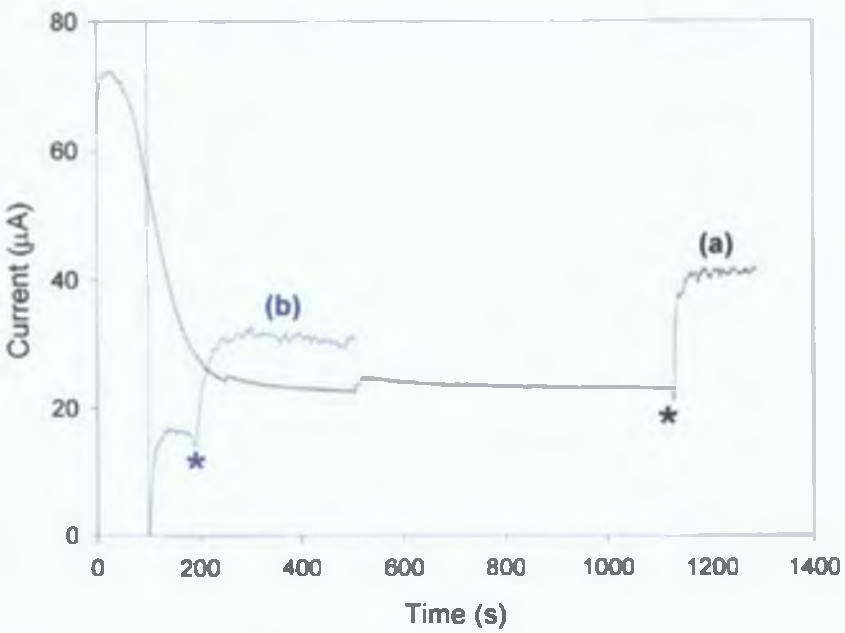


***Figure 2.29.*** (a) Potential held at -0.1 V vs. Ag/AgCl for duration of experiment. (b) Potential held at – 0.8 V vs. Ag/AgCl for 100 sec before being stepped to -0.1 V. On reaching of steady state, HRP (1 mg $ml^{-1}$) and $H_2O_2$ (8 mmol $dm^{-3}$) were added to stirred batch cell to produce the amperometric response. * Indicates addition of HRP with $H_2O_2$.

### 2 3 4 4 Performance of polyanıline ın an ımmunosensor format

Antı-bıotın (0 75 mg $ml^{-1}$) was ımmobılısed on the polymer-modıfied electrode accordıng to *Sectıon 2 2 9* HRP-labelled bıotın (15 μg $ml^{-1}$) and $H_2O_2$ (1 mmol $dm^{-3}$) were passed over the surface of polymer-modıfied electrodes upon reachmg steady state accordıng to *Sectıon 2 2 10* The film thıckness, and hence the charge ıncorporated ınto the polymer was varıed It was found that amperometrıc responses ıncreased wıth ıncreasıng amounts of polymer charge, at least to a lımıt of approxımately 6 mC, for the Ultra-ınH electrodes (*Fıgure 2 30*) Above thıs charge, responses eıther plateaued or began to dımınısh A sımılar trend was seen for glassy carbon, where the lımıtıng charge was approxımately 2 5 mC (*data not shown*) Thıs behavıour cannot be attrıbuted to varıatıons ın the real surface area of the polymer, as protein molecules are too large to permeate the polymer and so catalytıc responses should only occur at the outer polymer-solutıon ınterface Perhaps above a certaın thıckness, the passage of charge becomes too torturous and communıcatıon between electrode and the outer polymer-solutıon ınterface ıs lost Communıcatıon between the outer polymer-solutıon ınterface and the glassy carbon electrode became too torturous at very hıgh thıcknesses of polymer e g , above 2 5 mC Thıs may be due to the poorer charge transfer propertıes of the glassy carbon electrode as dıscussed ın *Sectıon 2 3 4 2*

What ıs clear from thıs work ıs that a consıderable varıatıon ın amperometrıc responses can occur as a result of changes or varıatıons ın polymer thıckness, and that maıntaınıng polymer thıckness on an electrode ıs crucıal for the generatıon of consıstent, reproducıble sıgnals

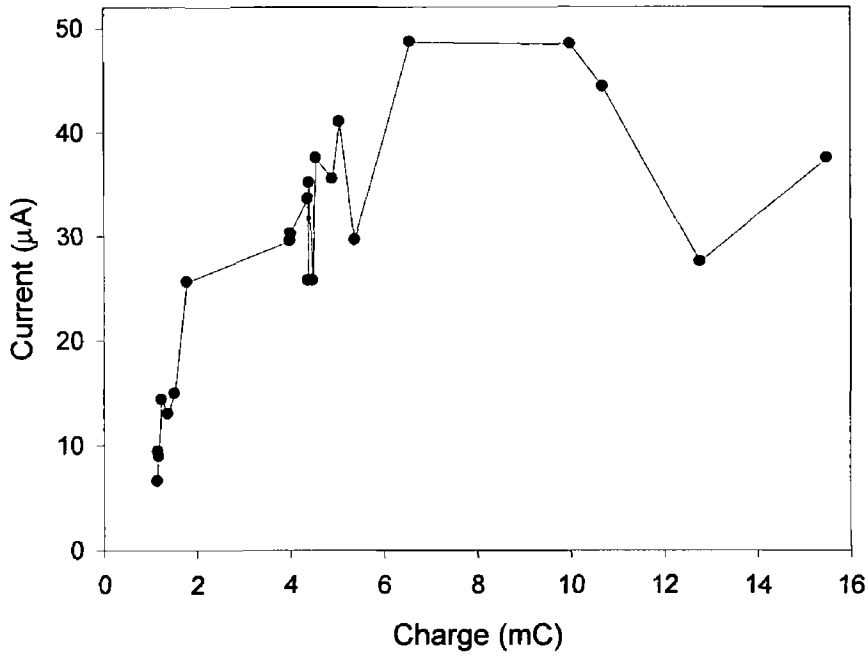


***Figure 2.30.*** Dependence of amperometric responses of the Ultra-inH electrode on polymer charge Amperometric responses were due to a biotin format

Due primarily to uncontrollable variations in the nature of the electrode and polymer, this biosensor suffers from very poor reproducibility (*Table 2 5*) Although PANI/PVS is deposited consistently according to *Section 2 2 8* to a certain $LM^+$ current level, differences in charge incorporated into the polymer are always encountered during the amperometric transients (18 49 % RSD, n = 6) The inability to control the source of the variation in this charging parameter is one of the factors affecting the reproducibility of the sensor It has been shown that charge incorporated and amperoinetric responses are proportional In theory, if the magnitude of the charge incorporated into the polymer were factored into the amperometric response, relative standard deviations should decrease This is demonstrated in Table 2 5 Anti-biotin (0 75 mg $ml^{-1}$) was immobilised on the polymer-modified electrode according to *Section 2 2 9* HRP-labelled biotin (15 μg $ml^{-1}$) and $H_2O_2$ (1 mmol $dm^{-3}$) were passed over the surface of polymer-modified electrodes upon reaching steady state according to *Section 2 2 10* Without taking the charge mto account, the % RSD was 52 99 % (n = 6) However, this figure reduced to 31 72% if charge was factored into the amperometric responses These results indicate that approx 40% of the deviation in response could be attributed to the variations in the charging current However,

there must also be other parameters contributing to the poor reproducibility of the system

Since reproducible assay work has been carried out before using the Gwent-inH electrode, with much better RSDs (Killard *et al*, 1999), the non-idealised behaviour that has been described, could be attributed in part at least to the Ultra-inH electrode, and not the assay protocol itself Although the Ultra-inH electrode was the best of the inks analysed in *Section 2 3 1*, its behaviour towards amperometric immunosensing was not seen to be ideal Despite polymer deposition on the Ultra-inH electrode being comparable to the Gwent-inH electrode, some difference in its interaction with the polymer must exist and cannot presently be defined Although attempts to characterise and correlate these variations have been made, a satisfactory solution has not been found and presently none of these inks, including Ultra™, are suitable for amperometric sensing, based on electropolymerised polyaniline

**Table 2 5** Variations in amperometric responses from the sensor When the current responses were divided by the charge incorporated, RSD values decreased by 40%

| *$LM^{+}$ peak height (mA)* | *Current response (μA)* | *Charge incorporated (mC)* | *Current / Charge* $\mu A\ mC^{-1}$ |
|---|---|---|---|
| 2 8 | 6 842 | 11 6 | 0 590 |
| 2 8 | 7 823 | 13 8 | 0 567 |
| 2 8 | 9 373 | 12 4 | 0 756 |
| 2 8 | 18 080 | 17 8 | 1 016 |
| 2 8 | 5 157 | 11 5 | 0 448 |
| 2 8 | 6 163 | 11 8 | 0 522 |
| *Average* | 8 906 | 13 15 | 0 0650 |
| *Std Dev* | 4 720 | 2 431 | 0 021 |
| *% RSD* | **52 996** | 18 489 | **31.718** |

## 2.4 CONCLUSION

Two aspects of this sensor technology were examined in this chapter the screen-printed electrode and the PANI/PVS polymer layer

Initially, commercial screen-printed electrodes were examined with a view to using them for amperometric immunosensing It was found, however, that although the working electrodes of the strips may have been suitable, the charge transfer properties of the strips were not high enough This was due to the fact that the electrode surfaces and conducting paths were too resistive and hindered the required current flow from the working electrode to the potentiostat A new in-house electrode was designed with a silver conductmg path The charge transfer properties of the electrode were not limiting, and this design was used for the electrochemical analysis of various working electrode carbon inks The inks were analysed using cyclic voltammetry, linear sweep voltammetry and amperometry and it was found that the Ultra-inH electrode had the most preferable electrochemical properties (i e a $k^0$ value of 3 09 × $10^{-4}$ cm $s^{-1}$, and a high sensitivity in the amperometric experiments) These properties were further enhanced by electrochemical pre-treatment This electrode was used for further work, with the presumption that it would be suitable for amperometric sensing on electrodeposited polyaniline

The properties of the PANI/PVS layer were examined using the Ultra-inH electrode However, it was seen that despite the optimised conductmg path and an optimum carbon ink, problems were still observed with the interfacial region of the Ultra$^{TM}$ carbon and polymer layer The charging characteristics of the polymer immobilised on Ultra-inH were poorer than those observed for a glassy carbon electrode or the Gwent-inH, when the polymer was cycled to the same thickness Characteristics of varying the thickness of the polymer layer were monitored using Ultra-inH, Gwent-inH and glassy carbon, and it was found that the charge incorporated into the polymer, background signals, response times, and amperometric responses all increased with increasing polymer thickness Since the charge incorporated into the polymer cannot currently be intrinsically controlled (on the Ultra-inH electrode), it is accounting for perhaps up to 40% of the deviation in values observed in analysis usmg the Ultra-inH electrode RSD values of up to 50% have

been observed for this system, and therefore, is not currently suitable for analytical work Such poor reproducibility has not been observed before for the electrodes produced from D14 or the glassy carbon electrode, and therefore must be attributed to the Ultra™ carbon ink

## 2.5 REFERENCES


Bard, A , Faulker, L (2001) Electrochemical Methods, Second Edition *Wiley & Sons Inc , New York*

Cao, Y , Andretta, A , Heeger, A , Smith, P (1989) Influence of chemical polymerisation conditions on the properties of polyanilme Polymer, 30 2305-2311

Casella, I , Guascito, M (1997) Electrocatalysis of ascorbic acid on the glassy carbon electrode chemically modified with polyanilme films *Electroanal* , **9** 1381-1386

Chiang, J , MacDiarmid, A (1986) 'Polyaniline' Protomc acid doping of the Emeraldine form to the metallic regime *Synth Met* , **13** 193-205

Cui, G , Yoo, J , Lee, J , Yoo, J , Uhm, J , Cha, G , Nam, H (2001) Effect of pre-treatment on the surface and electrochemical properties of screen-printed carbon paste electrodes *The Analyst*, **126** 1399-1403

Duic, L , Grigic, S (2001) The effect of polyanilme morphology on hydroquinone/quinone redox reaction *Electrochim Acta,* **46** 2795-2803

Erlenkotter, A , Kottbus, M , Chemnitius, G (2000) Flexible amperometric transducers for biosensors based on a screen-printed three electrode system *J Electroanal Chem* , **481** 82-94

Garjontye, R , Malinauskas, A (1998) Electrocatalytic reactions of hydrogen peroxide at carbon paste electrodes modified by some metal hexacyanoferrates *Sens Actuat B,* **46** 236-241

Gorton, L , Dominguez, E (2002) Electrocatalytic oxidation of NAD(P)H at mediator-modified electrodes *Rev Mol Biotech* , **82** 371-392

Grennan, K , Killard, A J , Smyth, M R (2001) Physical characterisation of a screen-printed electrode for use in an amperometric biosensor system *Electroanal* , **13** 745-750

Grennan, K , Strachan, G , Porter, A , Killard, A J , Smyth, M R (2003) Atrazine analysis using an amperometric immunosensor based on single-chain antibody fragments and regeneration-free multi-calibrant measurement *Anal Chim Acta,* **500** 28-298

Gros, P , Gibson, T , Bergel A , Comtat, M (1997) Permeability enhancement of electropolymerized thin organic films *J Electroanal Chem* , **437** 125-134

Gue, A , Tap, H , Gros, P , Maury, F (2002) A miniaturised silicon based enzymantic biosensor towards a generic structure and technology for multi-analytes assays *Sens Actuat B*, **82** 227-232

Hart, J , Wring, S (1997) Recent developments in the design and application of screen-printed electrochemical sensors for biomedical, environmental and industrial analyses *Tr Anal Chem* , **16** 89-103

Huang, X , Kok, W (1993) Conductive carbon cement as electrode matrix for cobalt phthalocyanine modified electrodes for detection on flowing systems *Anal Chim Acta,* **273** 245-253

Iwuoha, E , de Villaverde, D , Garcia, N , Smyth, M R , Pingarron, J (1997) Reactivities of organic phase biosensors 2 The amperometric behaviour of horseradish peroxidase immobilised on a platinum electrode modified with an electrosynthetic polyaniline film *Biosens Bioelectron* , **12** 749-761

Jin, G , Norrish, J , Too, C , Wallace, G (2004) Polypyrrole filament sensors for gases and vapours *Curr App Phys* , **4** 366-369

Killard, A J , Zhang, S , Zhao, H , John, R , Iwuoha, E I , Smyth, M R (1999) Development of an electrochemical flow injection immunoassay (FIIA) for the real-time monitoring of biospecific interactions *Anal Chim Acta,* **400** 109-119

Killard, A J , Micheli, L , Grennan, K , Franek, M , Kolar, V , Moscone, D , Palchetti, I , Smyth, M R (2001) Amperometric separation-free immunosensor for real-time environmental monitoring *Anal Chim Acta,* **427** 173-180

Lu, S (2004) Electrochemical determination of 8-azaguanine in human urine at a multi-carbon nanotubes modified electrode *Microchem J*, **77** 37-42

Mandic, Z , Duic, L (1996) Polyaniline as an electrocatalytic material *J Electroanal Chem* , **403** 133-141

Naudin, E , Gouerec, P , Belanger, D (1998) Electrochemcial preparation and characterisation in non-aqueous electrolyte of polyaniline electrochemically prepared from an anilinium salt *J Electroanal Chem* , **459** 1-7

Nicholson, R S (1965) Theory and application of the cyclic voltammetry of electrode reaction kinetics *Anal Chem* , **37** 1351-1355

O'Connell, P J , Gormally, C , Pravda, M , Guilbault, G G (2001) Development of an amperometric L-ascorbic acid (Vitamin C) sensor based on electropolymerised aniline for pharmaceutical and food analysis *Anal Chim Acta,* **431** 239-247

Pekmez, N , Pekmez, K , Yildiz, A (1994) Electrochemical behaviour of polyaniline films in acetonitrile *J Electroanal Chem* , **370** 223-229

Pravda, M , O'Meara, C , Guilbault, G (2001) Polishing of screen-printed electrodes improves IgG adsorption. *Talanta,* **54** 887-892

Sharma, A , Annapoorni, S , Malhotra, B (2003) Characterization of electrochemically synthesised poly(2-fluoroaniline) film and its application to glucose biosensor *Curr App Phys* , **3** 239-245

Von Stackelberg, M , Pilgram, M , Toome, V (1953) *Z Elektrochem* , **57** 342

Wallace, G , Spinks, G , Kane-Maguire, L (2003) Conductive Electroactive Polymers (2nd Ed), CRC Press, London

Wang, J , Pedrero, M , Sakslumd, H , Hammerich, O , Pingarron, J (1996) Electrochemical activation of screen-printed carbon strips *The Analyst*, **121** 345-350

Wang, J , Tian, B , Nascimento, V B , Angnes, L (1998) Performance of screen-printed carbon electrodes fabricated from different carbon inks *Electrochim Acta,* **43** 3459-3465

Zhang, S , Wright, G , Yang, Y (2000) Materials and techniques for electrochemical biosensor design and construction *Biosens Bioelectron* , **15** 273-282

Zotti, G , Cattarin, S , Comisso, N (1988) Cyclic potential sweep electropolymerisation of aniline, the role of anions in the polymerisation mechanism *J Electroanal Chem* , **177** 387-396

# Chapter 3

## Studies on the Biomolecular Immobilisation Conditions of Enzymes on a Polyaniline-Modified Screen-Printed Electrode

## 3.1 INTRODUCTION

Electrochemical biosensors are a particular class of CME, which comprise an electrode modified with a bioreagent film They combine the exquisite selectivity of biology with the processing power of modern electronics Although current research effort on biosensors is proceeding by using many different types of transduction principles, electrochemical detection offers attractive advantages over alternative transducers They can operate in turbid media and their instrumental sensitivities are comparable to optical systems With electrochemical transduction, the mass-production of low-cost, disposable electrode devices using thick and thin film technologies is possible, making electrochemical sensing systems amenable to miniaturisation and widespread application

In the study contained in this chapter, the preparation and characterisation of an amperometric, enzyme-based biosensor with potential immunosensing applications is described This amperometric biosensor has been developed previously, incorporating the electroactive polymer, polyaniline (PANI), which undergoes redox cycling, and can couple electrons directly from the enzyme active site, to the electrode surface (Killard *et al*, 1999) Construction of this sensor was achieved by electropolymerisation of polyvinylsulphonate-doped aniline onto the surface of a screen-printed carbon-paste electrode (*Chapter 2*) Biomolecules could then be doped onto the surface of the polymer by electrostatic interactions with the polymer backbone This effective biosensor format has examined the amperometric behaviour of immobilised horseradish peroxidase (Iwuoha *et al*, 1997), and has since been extended to develop rapid, single-step, separation-free immunosensors for real-time monitoring (Killard *et al*, 1999 & 2001, Grennan *et al*, 2003) The aim of this work was to utilise the polyaniline-modified screen-printed electrode, Ultra-inH, which was developed and optimised in *Chapter 2*, as the basis of an enzyme biosensor and investigate in more detail, the factors affecting the immobilisation of enzymes and antibodies to this platform

A brief introduction into biomolecules and their immobilisation methods for use in electrochemical biosensing is given in the following section The general area is introduced and discussed m relation to previous work carried out by this group and others

### *3 1 1 Biological molecules in biosensors*

Biological molecules, which are in intimate association with an electrochemical transducer can selectively recognise target analyte The recognition event may be either a biocatalytic reaction (e g enzyme-based biosensor) or a binding process (e g affinity ligand-based biosensor, when the recognition element is, for example, an antibody, DNA sequence or cell receptor) These recognition processes can be monitored quantitatively by producing a physiochemical change to be detected by the transducer Biocatalytic biosensors, based on enzymatic reactions are the most common type of electrochemical biosensors in the literature, followed by immunosensors, where antibody is used as the recognition element

Most published work on enzyme-based biosensors has targeted blood glucose monitoring (Malhotra & Chaubey, 2003) Glucose measurements were first described by Clark & Lyons (1962) in an experiment in which glucose oxidase (GOD) was entrapped at a Clark oxygen electrode using a dialysis membrane A decrease in the measured oxygen concentration was found to be proportional to glucose concentration in solution The oxidation of glucose, catalysed by glucose oxidase was the principle of measurement (*Equation 3 1*) The production of $H_2O_2$, also proportional to glucose concentration, can alternatively be monitored electrochemically (Guilbault & Lubrano, 1973)

$$\text{D-glucose} + O_2 + H_2O \xrightarrow{\text{GOD}} H_2O_2 + \text{D-gluconic acid} \qquad \textit{Equation 3 1}$$

Yellow Springs Instruments were the first company to commercialise an enzyme-based glucose biosensor in 1970 In 1987, Medisense (Abbott Laboratories) marketed the first point of care disposable glucose biosensor Since then, more similar commercial devices have followed (Roche, Johnson & Johnson) Substitution of glucose oxidase for other enzymes allows biosensors for other substances to be constructed Lactate oxidase has been used in commercial electrochemical biosensing applications for blood lactate (Lactate Analyser 640, Roche, Switzerland) Other analytes that have been electrochemically detected include cholesterol (Shumyantseva *et al* 2004), ethanol (Guzman *et al*, 2003), urea (Sant *et al*, 2003) and pesticides (Dzyadevych *et al*, 2004), to name but a few

This work focuses on a biosensor format using immobilised horseradish peroxidase (HRP). HRP is a heme-containing glycoprotein, capable of the catalytic reduction of hydrogen peroxide co-substrate. This induces a catalytic current at an electrode due to the electrochemical reduction of HRP I and HRP II, which are the two and one electron states higher than the native HRP resting state, respectively. Polyaniline is depicted as the electrocatalytic mediator in the reaction scheme shown in *Figure 3.1*.

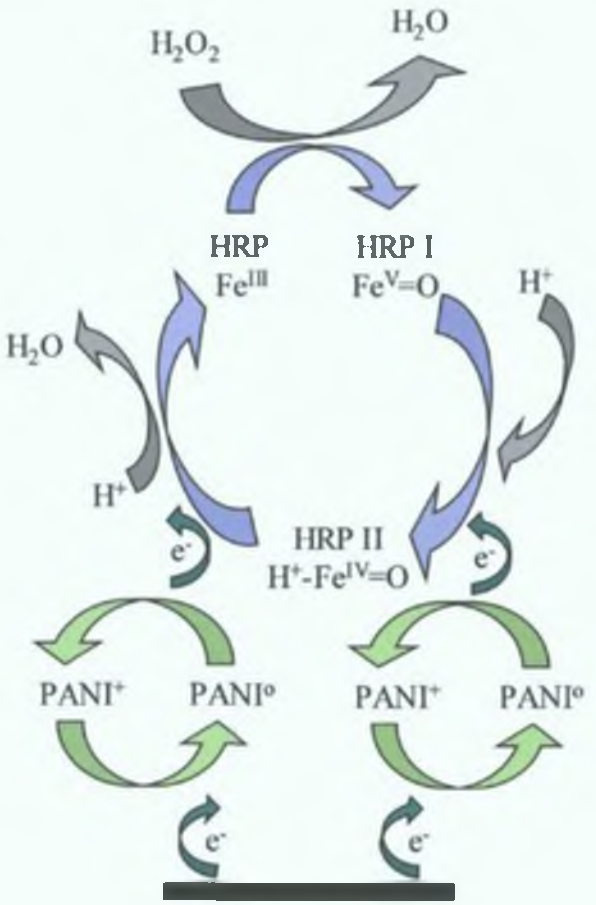


***Figure 3.1.*** The reaction cycle for the PANI/PVS/HRP electrode. Ferric HRP resting state ($Fe^{III}$), oxyferryl HRP-I ($Fe^{V}=O$), hyroxyferryl HRP-II ($Fe^{IV}$-OH) and polyleucoemeraldine/polyleucoemeraldine radical cation redox couple ($PANI^{0/+}$) participate in the peroxidase ping-pong mechanism.

The development of electrochemical immunosensors, that use antibodies as the recognition element, have also generated considerable interest. Immunosensors take advantage of the high selectivity provided by the molecular recognition properties of antibodies (Ab). Antibodies will bind selectively to their specific antigen, and tend not to bind to other antigens (Ag). This binding is extremely strong.

i.e. antibodies have very high affinities to their corresponding antigens, and as little as $10^{-18}$ M of antigen can be detected in certain immunoassays with low cross reactivity. Electrochemical detection usually requires labelling of one of the immunoreactants, usually the antigen, with enzyme to monitor the interaction. Electrochemical immunosensors have been developed to detect a wealth of analytes. Pesticides such as 2,4-dichlorophenoxyacetic acid (2,4 D) (Navrátilová & Skládal 2004) and chlorsulfuron (Dzantiev *et al.*, 2004) have recently been detected for environmental use. Clinical analytes such as carbohydrate tumour markers (Du *et al.*, 2003) and oestradiol (Pemberton *et al.*, 2004) have also been detected.

The immunosensing application for the work described here is based on a single step, separation-free electrochemical immunosensor based on a PANI/PVS/antibody-modified electrode. A schematic representation of the binding events that take place in this immunosensor is given in *Figure 3.2*. Unlike traditional immunoassay formats, there is no need to separate bound and unbound antigen since only redox reactions that are coupled to the electrode surface via the Ab-Ag interaction are capable of generating detectable signals. This immunosensor was most recently applied to the detection of the pesticide atrazine, and a detection limit of 0.1 μg $l^{-1}$ was achieved (Grennan *et al.*, 2003).

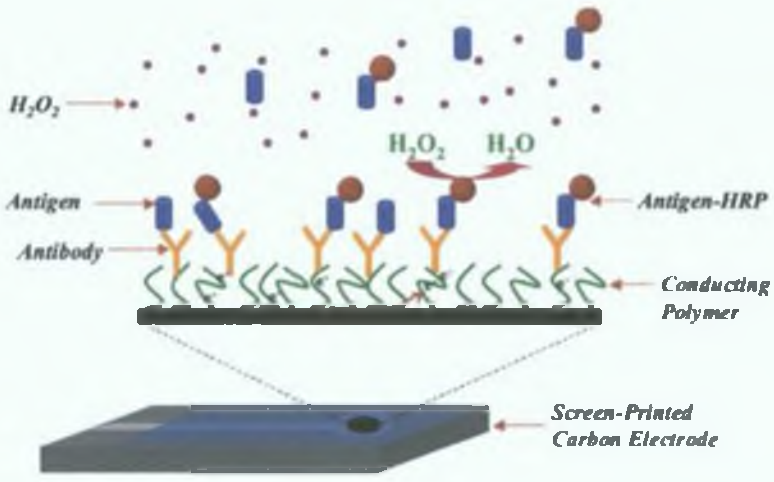


***Figure 3.2.*** Schematic diagram of the electrochemical real-time immunosensing process. Free and labelled Ag compete for binding to immobilised Ab. The interaction of $H_2O_2$ substrate with HRP produces a catalytic current, which flows from the electrode surface through the molecular wires of the conducting polymer. This response is indirectly proportional to the concentration of bound Ag. (adapted from Grennan *et al.*, 2003).

### *3 1 2 Immobilisation of the biological molecule*

The biological sensing element (e g enzyme, antibody) of a biosensor must be integrated within or intimately associated with the electrode The immobilisation process should result in a stable protein layer, where the activity of the free protein is comparable to that of the immobilised protein The pH of the immobilisation step should be carefully controlled In the case of electrode fouling, the biomolecule layer can be protected by an electro-inactive layer such as non-conducting polymer

Methods for immobilisation include adsorption, e g physisorption (Moore *et al*, 2003), crosslinking using glutaraldehyde (Fiorito & Cordoba de Torresi, 2004), and chemical coupling using for example, 1-ethyl-3-(3-dimethylaminopropyl)carbodiimide (EDC) and N-hydroxysuccinimide (NHS) for covalent attachment to a surface through its amine groups (Leonard *et al*, 2004) Covalent attachment of biological molecules to self-assembled monolayers (SAMs) has also been carried out (Chaki *et al*, 2002), where the long chain alkane thiols produce a highly packed and ordered surface that provides a membrane-like environment suitable for biomolecules In addition, manipulation of SAMs for controlled immobilisation of protein, (i e, by control of the orientation and conformation of protein), allows for facile electron transfer and low background currents Entrapment m matrices such as polymers (Rajesh *et al*, 2004) carbon pastes (Wang *et al*, 2001) and Langmuir-Blodgett films (Sharma *et al*, 2004) are also promising methods for controlled immobilisation of biomolecules In the case of this system, adsorption by electrostatic forces on an electroactive copolymer, PANI/PVS, (Killard *et al*, 1999) was the method of choice In this way, diffusion of substrates and biorecognition molecules does not have to take place into and out of a polymer matrix as traditionally occurs m polymer entrapment systems

The immobilisation matrix may function purely as a support, or may also be concerned with mediation of the signal transduction In the case of Killard *et al* (1999), protein molecules were electrostatically attached to the backbone of the electroactive copolymer PANI/PVS, by application of an oxidising potential Both enzyme-based biosensors (Iwuoha *et al*, 1997) and immunosensors (Killard *et al*, 1999 & 2001, Grennan *et al*, 2003) have been demonstrated using this immobilisation format Initially, it was assumed that the modification of the electrode

surface with an antibody was best achieved by using a high protein concentration (1 mg $ml^{-1}$), so as to maximise the mass of protein on the electrode surface, as in the case with traditional Enzyme-Linked Immunosorbent Assay (ELISA) procedures Since then, it has been shown that far from being optimal, the 1 mg $ml^{1}$ protein concentration yielded much lower catalytic signals than lower protein concentrations For a screen-printed carbon electrode (working electrode area 7 07 $mm^2$), a protein concentration of 0 6 mg $ml^{-1}$ was found to be optimal (Killard *et al* , 2001) However, the reason for this phenomenon was not understood It was hypothesised that electron transfer at the electrode surface may be more efficient at lower antibody concentrations However, further work was not carried out to investigate this theory

## 3.2 MATERIALS AND METHODS

### *3 2 1 Materials*

Horseradish peroxidase (HRP, 1,100 U/mg and 1,310 U/mg, P8672), bovine serum albumin (BSA, A-7906), and 2,2'-azino-bis(3-ethylbenzthiazoline-6-sulphonic acid) (ABTS, A-1888) were purchased from Sigma-Aldrich (Poole, Dorset, UK) Aniline was purchased from Aldrich (13,293-4), vacuum distilled and stored frozen under nitrogen 30% (v/v) hydrogen peroxide solution was purchased from Merck Polyvinylsulphonate (PVS, 27,842-4) Silver/silver chloride (Ag/AgCl) electrodes were purchased from Bioanalytical Systems Ltd (Cheshire, UK) The platinum mesh (29,809-3) was purchased from Aldrich

### *3 2 2 Buffers and solutions*

Unless otherwise stated, all electrochemical measurements were carried out in phosphate buffered saline (PBS), (0 1 mol $dm^{-3}$ phosphate, 0 137 mol $dm^{-3}$ NaCl and 2 7 mmol $dm^{-3}$ KCl), pH 6 8 All colorimetric assays were carried out in 10 mmol $dm^{-3}$ phosphate buffer, (0 33 mmol $dm^{-3}$ $KH_2PO_4$ and 0 66 mmol $dm^{-3}$ $Na_2HPO_4$), pH 7 0 Unless otherwise stated, all immunochemicals were prepared in PBS The ABTS buffer was 200 mmol $dm^{-3}$ dihydrogen phosphate and 100 mmol $dm^{-3}$ citric acid, and adjusted to pH 5 5 using concentrated NaOH

### *3.2.3 Instrumentation*

Screen printing of the Ultra-inH electrode was performed according to *Section 2 3 3* and was used for all experiments in this work All electrochemical protocols were performed either on a BAS100/W electrochemical analyser with BAS100/W software, or a CH1000 potentiostat with CH1000 software, using either cyclic voltammetry or time-based amperometric modes An Ag/AgCl reference electrode and a platinum mesh auxiliary electrode were used for bulk electrochemical experiments Electrochemical batch and flow cells were constructed according to

Killard *et al* (1999) They were composed of polycarbonate, and designed to house the screen-printed electrodes Both cells incorporated internal Ag/AgCl pseudo-reference and platinum wire auxiliary electrodes (*Chapter 2, Figure 2 6*) Cell volumes of the batch and flow cells were 2 ml and 26 µl, respectively

An ICN Flow Titertek® Multiskan PLUS microplate reader (Medical Supply Co , Ireland) was used m conjunction with Nunc Maxisorp microtiter plates (Biosciences, Ireland) for all colorimetric assays

### *3.2.4 Electrode pre-treatment procedure*

Screen-printed electrodes were placed in a solution of 0 2 mol $dm^{-3}$ $H_2SO_4$ A single voltammetric cycle was carried out between –1200 mV and +1500 mV at 100 mV $s^{-1}$ vs Ag/AgCl

### *3.2.5 Polymerisation of aniline on the electrode surface*

A solution of 186 µl aniline, 7 8 ml 1 mol $dm^{3}$ HCl, and 2 ml PVS, was degassed for 10 mm Aniline was polymerised from this solution, onto the surface of the working electrode using cyclic voltammetry A platinum mesh auxiliary and a Ag/AgCl reference electrode were used The potential was cycled between –0 5 and 1 1 V at 100 mV $s^{-1}$ for 10 cycles

### *3 2 6 Immobilisation of protein*

Following polymerisation of aniline, the electrode was transferred to a 2 ml batch cell The surface of the polymer was reduced in 2 ml of PBS (degassed for 10 min under nitrogen or argon) at –500 mV vs Ag/AgCl, sample interval of 500 ms, over 1500 s at a sensitivity of 1 $\times 10^{-4}$ A $V^{1}$ Protein was prepared m PBS prior to use Very quickly after reduction was complete, PBS buffer was removed from the cell and quickly replaced with the protein solution, not under stirring or degassing Oxidation was then performed immediately at +700 mV vs Ag/AgCl for 1500 s During this oxidation, the protein becomes electrostatically attached to the polymer

surface The protein solution was carefully recovered from the cell and re-stored for later use

### *3 2 7 Electroanalytical Procedure*

After the immobilisation of protein (*Section 3 2 6*), the electrode was housed in the flow cell Amperometric experiments were performed at –100 mV vs Ag/AgCl wire electrode, with a sample interval of 100 ms and a sensitivity of $1 \times 10^{-4}$ A $V^{-1}$ PBS was passed over the surface of the electrode at a flow rate of 10 µl $s^{-1}$ When a steady state was reached, appropriate solutions were passed over the surface of the electrode and the amperometric responses momtored

### *3.2.8 Blocking of the electrode surface with bovine serum albumin*

A range of dilutions of bovine serum albumin (BSA) beginning at 10 mg $ml^{-1}$ was prepared in PBS These solutions were used for the immobilisation of BSA on the surface of the electrode according to *Section 3 2 6* and a series of electrodes with different masses of BSA was prepared An electroanalytical procedure was performed according to *Section 2 3 8* where a solution of HRP (0 5 mg $ml^{-1}$) and $H_2O_2$ (0 8 mmol $dm^{-3}$) in PBS was passed over the surface of each electrode

### *3 2 9 Optimisation of the mass of HRP on the electrode surface*

A range of dilutions of HRP beginning at 10 mg $ml^{-1}$ was prepared in PBS These solutions were used for the immobilisation of HRP onto the surface of a series of electrodes according to *Section 3 2 6* The electroanalytical procedure was as described in *Section 3 2 7* where a solution of $H_2O_2$ (0 8 mmol $dm^{-3}$) in PBS was passed over the surface of each electrode

### *3.2.10 Colorimetric enzyme assay*

Solutions of HRP in doubling dilutions beginning at 10 mg $ml^{-1}$ were prepared in phosphate buffer, pH 7, for use as a set of calibration standards ABTS

solution (5 33 mg $ml^{-1}$) was prepared, containing $H_2O_2$ (0 3 mmol $dm^{-3}$) 20 µl of the HRP solutions were transferred to the wells of a microtitre plate with 180 µl of the ABTS solution The plate was covered with laboratory film, left in the dark for 35 min and then the absorbance read at 620 nm

Colorimetric enzyme assays were performed on the surfaces of the screen-printed electrodes according to a similar protocol In this instance, HRP-immobilised electrodes, prepared according to *Section 3 2 6*, were placed in the well of the microtitre plate along with 20 µl phosphate buffer to replace the HRP solutions in the calibration standards

## 3.3 RESULTS AND DISCUSSION

### *3.3.1 Protein binding capacity of the polymer-modified electrode*

Electrostatic adsorption was the biomolecular immobilisation method used for this work (*Section 3 2 6*) Optimisation of this technique for the biosensor had been carried out previously (Killard *et al*, 2001) This study showed that a protein solution concentration of 0 5 – 0 75 mg $ml^{-1}$ yielded the optimal amperometric signals encountered for a screen-printed electrode (geometric area 7 07 $mm^2$) However, it was not clear why this concentration yielded the optimum responses from the sensor In addition, the absence of the necessity for blocking or separation steps was not fully understood The present study used electrochemical and colorimetric techniques to elucidate the reasons why this concentration yielded optimum responses from the sensor

#### 3 3 1 1 Effect of protein concentration on sensor response

The PANI/PVS copolymer was deposited on Ultra-inH electrodes to an $LM^+$ peak height of approx 2 8 mA for all experiments These PANI/PVS electrodes were modified with a range of concentrations of BSA (*Section 3 2 8*) and the reaction between HRP (1 mg $ml^{1}$) and $H_2O_2$ (0 8 mmol $dm^{-3}$) present in the bulk solution was monitored HRP is a heme-containing glycoprotein that is capable of the catalytic reduction of hydrogen peroxide substrate A range of concentrations of HRP were also used to modify the electrode surface, and their responses to hydrogen peroxide were noted (*Figure 3 3*)

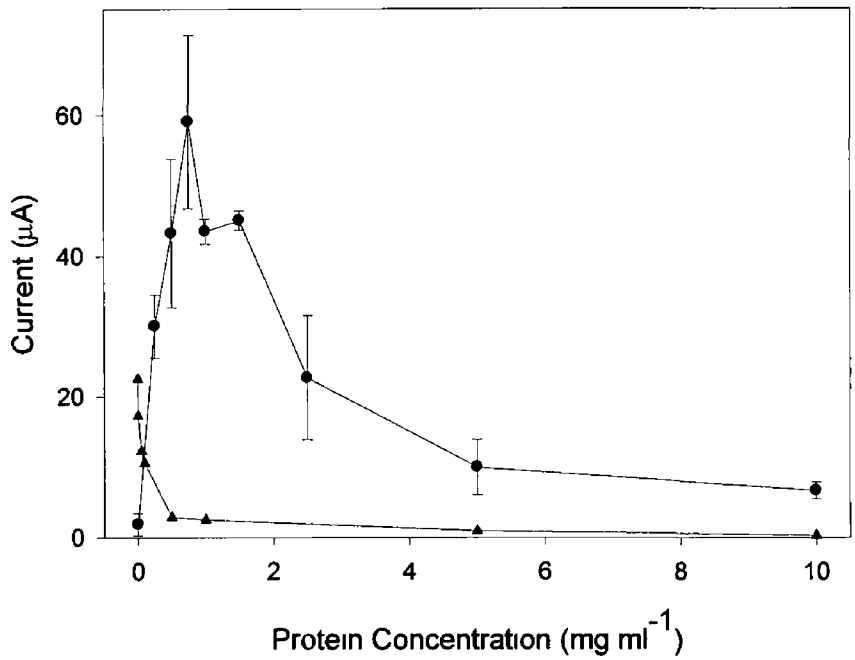


***Figure 3.3.*** Dependence of sensor response on the concentration of protein used for immobilisation Concentrations of BSA (blue line) and HRP (black line) were immobilised on the surface of an Ultra-inH electrode Amperometric responses increased as a function of concentration of HRP up to 0 75 mg $ml^{-1}$ (n=3, black) Above this concentration the responses decreased (solid black line) Concentrations of BSA immobilised were found to be inversely proportional to the amperometric responses from HRP (0 5 mg $ml^{-1}$) and $H_2O_2$ (8 mmol $dm^{3}$) m bulk solution (blue line) (n=1)

It was found that the concentration of BSA used for immobilisation was inversely proportional to the electrochemical responses from HRP and $H_2O_2$ in bulk solution Effective blocking was achieved when the immobilised protein concentration was above 0 5 mg $ml^{-1}$ When HRP was immobilised on the electrode surface at various concentrations, amperometric responses generated by $H_2O_2$ (8 mmol $dm^{-3}$) in the bulk solution peaked at 0 75 mg $ml^{-1}$, and diminished significantly above this, but decreased more gradually at lower concentrations

These data seem to suggest that this critical concentration of approximately 0 75 mg $ml^{-1}$ allowed for the effective blocking of the electrode surface from bulk solution interactions, while also providing optimal amperometric response from immobilised enzyme Killard *et al* (2001) have shown previously that optimum

responses were seen for a critical concentration of 0 6 mg $ml^{-1}$, using a Gwent-inH electrode

### 3 2 1.2 Determination of the mass of protein immobilised to the electrode surface

It is important to note that for a given concentration of protein used for immobilisation, a mass per unit area becomes electrostatically attached to the polymer-modified electrode during the immobilisation procedure However, until now, the relationship between concentration and mass had not been established Protein mass measurements on an amperometric biosensor have been carried out previously by Halliwell *et al* (2003) through radioisotope labelling of the enzyme L-lactate dehydrogenase (LDH) The radio-label did not affect the activity of this enzyme, and so it was possible to determine the enzyme mass loading on the biosensor surface In the present work, protein mass measurements were made by carrying out a set of colorimetric enzyme assays specific for HRP The purpose of using an enzyme assay rather than a protein assay to measure the mass, was that protein assays were not sensitive enough to measure the small mass of protein attached to the electrode surface, whereas enzyme-based techniques could result in signal amplification over time making them more sensitive The substrate used was ABTS with $H_2O_2$, which yields a soluble blue-green product in the presence of HRP

The kinetics of peroxidase with ABTS as a chromogen are relatively slow, allowing a reasonable time frame during which the colour can equilibrate, even at high concentrations of HRP A calibration assay was carried out on HRP in solution accordmg to *Section 3 2 10*, and a linear relationship was observed between 0 and 8 × $10^{5}$ mg $ml^{-1}$ (or between the masses of 0 and 1 6 × $10^{-5}$ mg) (*Figures 3 4a & b*)

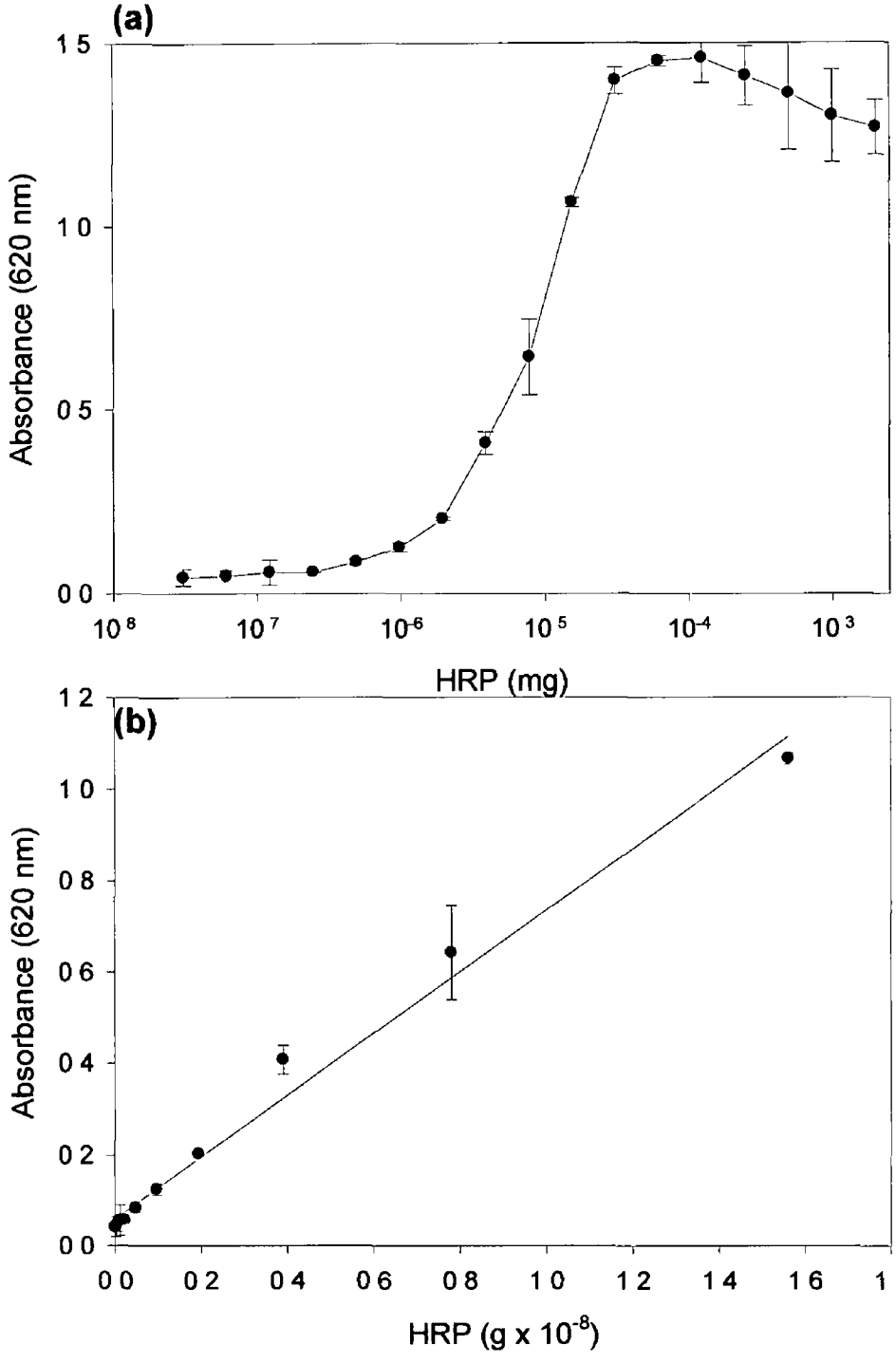


***Figure 3.4.*** Colorimetric HRP calibration assay ($n$=3) Solutions of HRP were prepared in phosphate buffer and transferred to the wells of a microtiter plate along with ABTS and $H_2O_2$ (*Section 3 2 10*) (a) Absorbance (620 nm) vs mass of HRP over a range from 0 mg to 0 002 mg (logarithmic scale) (b) Linear region of assay from 0 to 1 6 × $10^{-8}$ g ($y = 6\ 73 \times 10^{8}x + 0\ 0614$, $r^2 = 0\ 9871$)

The assay was then carried out on the surfaces of the HRP-modified electrodes All electrodes were washed extensively in PBS before the assay A logarithmic relationship for this electrode assay was observed between concentrations of 0 00625 and 0 063 mg $ml^{1}$ and was linearized (*Figure 3 5a & b*) The linear segments of these curves were used for further analysis (*Figure 3 4a & 3 5b*)

A correlation between protein mass and protein concentration could now be deduced by combining these two sets of data as absorbances corresponding to a concentration of HRP used during immobilisation could be related to a mass of HRP present on the electrode surface (For this correlation to be valid, it was assumed that the activity of immobilised enzyme was equivalent to that of enzyme in the solution phase )

The equation was calculated to be

$$y = 1\ 452 \times 10^{-8}\text{Log}x + 3\ 375 \times 10^{-8} \qquad \textit{Equation 3.2}$$

where y is the mass of HRP immobilised (g) and x is the concentration of HRP (mg $ml^{-1}$) used for immobilisation In order to convert the mass of HRP (y) in this equation to number of molecules the equation was first multiplied across by Avogradro's Number ($6\ 022 \times 10^{23}$) to give *Equation 3 3*

$$y = 8\ 74 \times 10^{15}\text{Log}x + 1\ 85 \times 10^{16} \qquad \textit{Equation 3 3}$$

*Equation 3 3* was then divided across by the molar mass of HRP (based on a molecular weight of 44,000 Da), and the equation becomes

$$y = 1\ 885 \times 10^{11}\text{Log}x + 4\ 610 \times 10^{11} \qquad \textit{Equation 3.4}$$

where y is now the number of molecules of HRP and x is the concentration of HRP (mg $ml^{-1}$) used for immobilisation By substituting x, the concentration of HRP used for immobilisation, with the optimum protein concentration of 0 75 mg $ml^{-1}$ (*Figure 3 5*), then the number of molecules of HRP that were immobilised at this concentration on the surface of the electrode would be $4\ 362 \times 10^{11}$, according to *Equation 3 4*

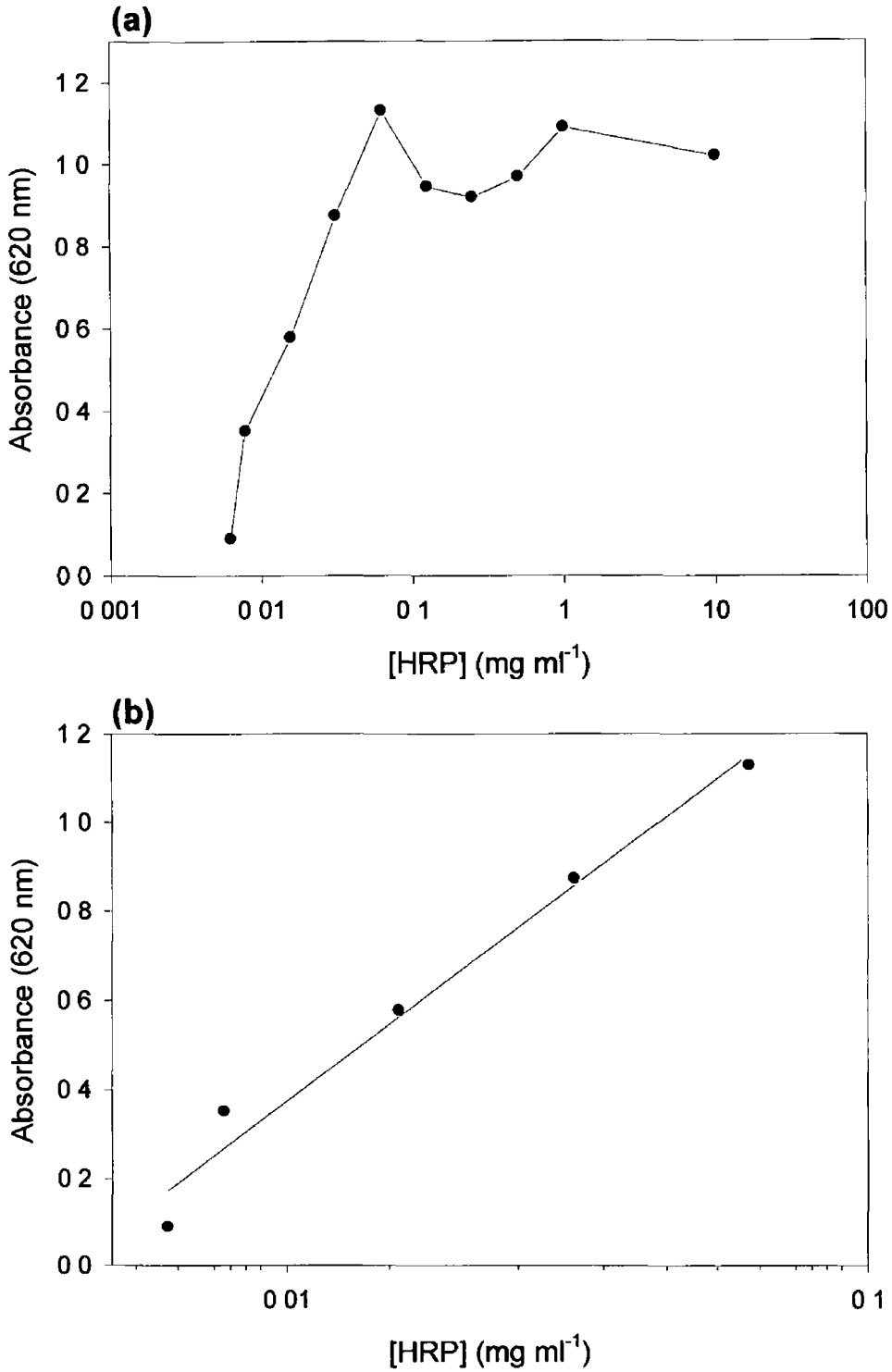


***Figure 3.5.*** Colorimetric enzyme assay of HRP-modified electrodes (n=1) HRP was immobilised onto the PANI-modified electrode The WEs were then cut from the substrate and placed in the wells of the microtiter plates with ABTS and $H_2O_2$ (*Section 3 7 10*) (a) Absorbance (620 nm) of HRP-modified electrodes from 0 to 10 mg $ml^{-1}$ (b) Linear region of assay from 0 00625 mg $ml^{-1}$ to 0 063 mg $ml^{-1}$ ($y = 0\ 9782\mathrm{Log}x + 2\ 3305, r^2 = 0\ 9777$)

Proteins such as antibodies and enzymes often have to be immobilised such that they retain their biological activity Their large size and necessary accessibility to interact with other molecules usually requires sufficient spatial separation of their binding and active sites Based on the obtained data, the next step was to elucidate the type of surface coverage being obtained at the optimum protein concentration using this electrochemical immobilisation technique The number of molecules of HRP necessary to form a monolayer on the surface of these electrodes was calculated to be $4\,237\times10^{11}$ molecules, where the radius of HRP was 26 Å (Ban & Rizzolo, 1997, Byrod *et al*, 2000) and the polymer-modified electrode area was estimated to be $9\times10^{-6}$ $m^2$, assuming an ideal flat two-dimensional electrode surface

The theoretical number of molecules of HRP required to form a monolayer at this surface can be compared to the number of molecules immobilised at optimum concentration It would appear that at this concentration, a monolayer of protein is formed at the electrode surface However, there are factors that may have introduced errors in both the methodology and the calculations Regarding methodology, significant inter-electrode variability brought about by variations during printing and polymer deposition could be a contributory factor Within the calculations, a crude assumption was made about the surface area of the polymer-modified electrode and the microscopic topology of the polymer was not taken into account In addition, the molecular weight of HRP in the literature varies from 40-44,000 Da Also, given the logarithmic relationship derived between the concentration of HRP used and the mass immobilised on the surface of the electrode, the change in mass immobilised according to *Equation 3 4* with respect to the concentration range examined is very small However, the fact that the experimental data correlates so closely with the presence of a theoretical monolayer may explain the data seen in *Figure 3 3* and in previous work by Killard *et al* (2001) At the optimal concentration of HRP (0 75 mg $ml^{-1}$), a monolayer, or very close to a monolayer appears to become immobilised at the electrode surface At concentrations above this, steric hindrance or impeded charge transfer may result from crowding of the surface with multiple layers of protein, causing significantly diminished responses

Further physical studies using scanning electrochemical microscopy (SEM) by Grennan (2003) have been used to image protein on the surface of the PANI/PVS layer A colloidal gold anti–HCGβ monoclonal antibody (MoAb), in

conjunction with a silver enhancement technique was used Uniform surface coverages of the PANI/PVS layer were obtained at a concentration of 0 625 mg $ml^{-1}$ However, patches of polymer could be observed intermittently between Ab clusters When higher concentrations were used for immobilisation, aggregation or clumping of protein was observed on electrode surfaces It was deduced that although Ab coverage was visually lower in the case for 0 625 mg $ml^{-1}$, the amperometric signals were still larger than for electrodes coated with higher concentrations of antibody This could be attributed to reduced instances of Ab clumping at lower concentrations, resulting in more effective communication between enzyme labels and electrode surfaces This study is in agreement with the theories deduced from this work

A discrepancy exists between the data for the electrochemical and colorimetric tests on immobilised HRP This is that at concentrations higher than the optimal concentrations, decreases in response were much more marked for the electrochemical data (*Figure 3 3*) than for the colorimetric data (*Figure 3 5b*) It may be the case that at concentrations above 0 75 mg $ml^{-1}$, multiple protein layers become attached, and these layers inhibit diffusion of substrate to enzyme centres close to the electrode surface or catalyse it before diffusion can occur This might result in a diminished electrochemical signal, as efficient electron transfer would not occur between these outer layers and the electrodes, whereas, in a colorimetric assay, these layers would all contribute to the signal produced (*Figure 3 6*) When multiple layers of protein are immobilised, little change in response for the colorimetric assay occurs However, this results in a significant decrease in amperometric response

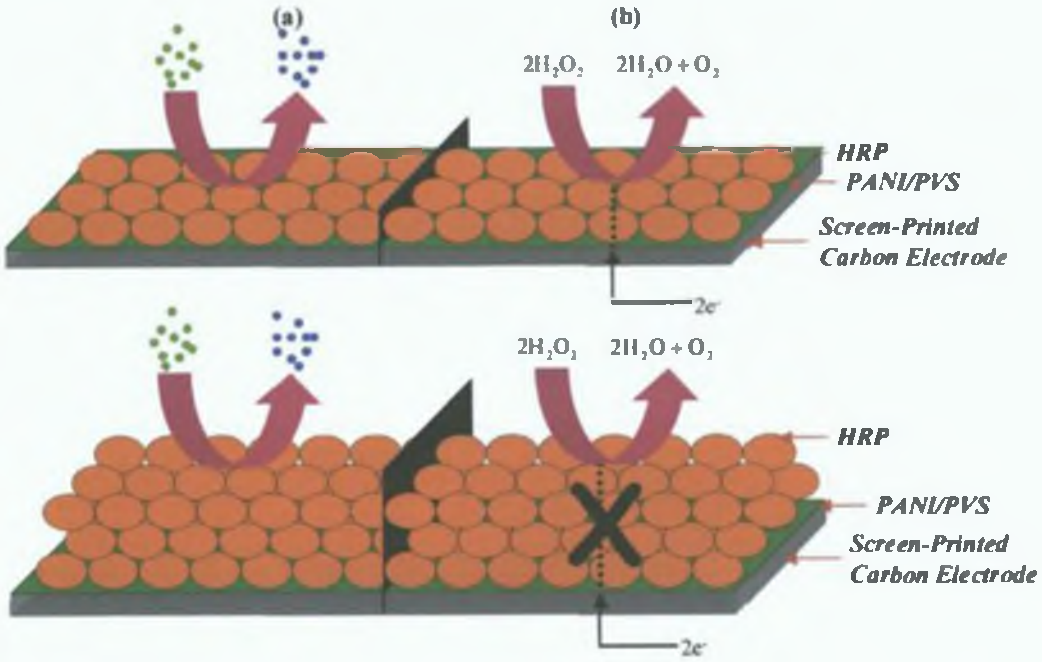


***Figure 3.6.*** Schematic diagram of the behaviour of the HRP-modified electrode surface for the colorimetric assay (a) and the amperometric assay (b). The case for a monolayer is depicted (top), when maximum absorbance and amperometric response, respectively are observed. Multi-layers are formed at higher concentrations (bottom).

It appears that from indirect electrochemical and optical measurements, at optimal conditions, a monolayer, or close to a monolayer of protein becomes deposited onto the polymer electrode, which simultaneously blocks non-specific responses from the bulk solution while providing efficient electronic interaction between the immobilised enzyme and the electrode as well as efficient mass transport of substrate to the enzyme. This understanding is essential for the application of this immobilisation technique in enzyme and antibody biosensor applications.

## 3.4 CONCLUSION

A study on a particular conducting polymer-based screen-printed electrode was carried out in order to assess optimal protein binding capacity and to elucidate why maximising the mass of protein on the surface of the polymer does not result in optimal catalytic signals This study on the protein layer was carried out using Ultra-inH electrodes It appears that from indirect electrochemical and optical measurements, at optimal conditions, a monolayer of protein becomes deposited onto the polymer electrode, which simultaneously blocks non-specific responses from the bulk solution while providing efficient electronic interaction between the immobilised enzyme and the electrode as well as efficient mass transport of substrate to the enzyme By applying a solution of bovine serum albumin at 0 75 mg $ml^{-1}$, efficient blocking of the electrode from electroactive species in the bulk solution could be achieved When the horseradish peroxidase was immobilised on the electrode, optimal amperometric responses from hydrogen peroxide reduction were achieved at approximately the same concentration The mass of enzyme immobilised at this solution concentration was determined by a colorimetric enzyme assay to be equivalent to the formation of a protein monolayer Under these conditions, amperometric responses from the immobilised layer are maximised and non-specific bulk solution interactions are minimised At higher immobilised protein concentrations, diminished amperometric responses may be due to inhibited diffusion of hydrogen peroxide to enzyme which is in electronic communication with the electrode surface, or impeded electron transfer This understanding is essential for the application of this immobilisation technique in enzyme-based and antibody-based biosensor applications

## 3.5 REFERENCES


Ban, Y , Rizzolo, L (1997) A culture model of development reveals multiple properties of RPE tight junctions *Mol Vision,* **3** 18

Byrod, G , Rydevik, B , Johansson, B , Olmarker, K (2000) Transport of epidurally applied horseradish peroxidase to the endoneurial space of dorsal root ganglia a light and electron mocroscopic study *J Periph Nervous System,* **5** 218-226

Chaki, N , Vijayamohanan, K (2002) Self-assembled monolayers as a tunable platform for biosensor applications *Biosens Bioelectron ,* **17** 1-12

Clark, L C , Lyons, C (1962) Electrode systems for continuous monitoring in cardiovascular surgery *Ann N Y Acad Sci ,* **102** 29

Du, D , Yan, F , Liu, S , Ju, H (2004) Immunological assay for carbohydrate antigen 19-9 using an electrochemical immunosensor and antigen immobilisation in titania sol-gel *J Immunol Meth ,* **283** 67-75

Dzantiev, B , Yazynina, E , Zherdev, A , Plekhanova, Y , Reshetilov, A , Chang, S , McNeil, C (2004) Determination of the herbicide chlorsulfuron by amerometric sensor based on separation-free bienzyme immunoassay *Sens Actuat B,* **98** 254-261

Dzyadevych, S , Soldatkin, A , Arkhpova, V , El'skaya, A , Chovelon, J (2004) Early-warning electrochemical biosensor system for environmental monitoring based on enzyme inhibition *Sens Actuat B, In press*

Fiorito, P , Cordoba de Torresi, S (2004) Optimized multiplayer oxalate biosensor *Talanta,* **62** 649-654

Grennan, K , Strachan, G , Porter, A , Killard, A , Smyth, M R (2003) Atrazine analysis using an amperometric immunosensor based on single-chain antibody

fragments and regeneration-free multi-calibrant measurement *Anal Chim Acta,* **500** 287-298

Grennan, K (2003) Developments in electrochemical immunosensors PhD Thesis School of Chemical Sciences, Dublin City University, Ireland

Guilbault, G , Lubrano, G (1973) An enzyme electrode for amperometric determination of glucose and lactate *Anal Chim Acta,* **64** 439-445

Guzman-Vazquez de Prada, A , Pena, N , Mena, M , Reviejo, A , Pingarron, J (2003) Graphite-Teflon composite bienzyme amperometric biosensors for alcohols *Biosens Bioelectron* , **18** 1279-1288

Halliwell, C , Simon, E , Toh, C , Bartlett, P , Cass, A (2003) A method for the determination of enzyme mass loading on an electrode surface through radioisotope labelling *Biosens Bioelectron* , **17** 965-972

Iwuoha, E , de Villaverde, D , Garcia, N , Smyth, M R , Pingarron, J (1997) Reactivities of organic phase biosensors 2 The amperometric behaviour of horseradish peroxidase immobilised on a platinum electrode modified with an electrosynthetic polyaniline film *Biosens Bioelectron* , **12** 749-761

Killard, A J , Zhang, S , Zhao, H , John, R , Iwuoha, E I , Smyth, M R (1999) Development of an electrochemical flow injection immunoassay (FIIA) for the real-time monitoring of biospecific interactions *Anal Chim Acta,* **400** 109-119

Killard, A J , Micheli, L , Grennan, K , Franek, M , Kolar, V , Moscone, D , Palchetti, I , Smyth, M R (2001) Amperometric separation-free immunosensor for real-time environmental monitoring *Anal Chim Acta,* **427** 173-180

Leonard, P , Hearty, Quinn, J , O'Kennedy, R (2004) A generic approach for the detection of whole *Listeria monocytogenes* cells in contaminated samples using surface plasmon resonance *Biosens Bioelectron* , **19** 1331-1335

Malhotra, B , Chaubey, A (2003) Biosensors for clinical diagnostics industry *Sens Actuat B,* **91** 117-127

Moore, E , Pravda, M , Guilbault, G (2003) Development of a biosensor for the quantitative detection of 2,4,6-trichloroanisole using screen-printed electrodes *Anal Chim Acta,* **484** 15-24

Navratilova, I , Skladal, P (2004) The immunosensors for measurement of 2,4-dichlorophenoxyacetic acid based on electrochemical impedance spectroscopy *Bioelectrochem* , **62** 11-18

Pemberton, R , Hart, J , Mottram, T (2004) A screen-printed electrode (SPCE)-based electrochemical immunosensor for estradiol determination in saliva *The Eighth World Conference on Biosensors* Granada, Spain 24-28 May 2004

Rajesh, S , Takashima, T , Kaneto, K (2004) Amperometric tyrosinase based biosensor using electropolymerised PTS-doped polypyrrole film as an entrapment support *Reac Func Poly* , **59** 163-169

Sant, W , Pourciel, M , Launay, J , Conto, T , Martinez, A , Boyer, P (2003) Development of chemical field effect transistors for detection of urea *Sens Actuat B* , **95** 309-314

Sharma, S , Singhal, R , Malhotra, B , Sehgal, N , Kumar, A (2004) Langmuir-Blodgett film based biosensor for estimation of galactose in milk *Electrochim Acta,* **49** 2479-2485

Shumyantseva, V , Deluca, G , Bulko, T , Carrara, S , Nicolini, C , Usanova, S , Archakov, A (2004) Cholesterol amperometric biosensor based on cytochrome P450scc *Biosens Bioelectron* , **19** 971-976

Wang, J , Mo, J , Li, S , Porter, J (2001) Comparison of oxygen-rich and mediator-based glucose-oxidase carbon-paste electrodes *Anal Chim Acta,* **441** 183-189

# Chapter 4

## A Polyaniline-Based Enzyme Biosensor Fabricated from Nanoparticles

## 4.1 INTRODUCTION

Modification of electrodes with polyanilines and other conducting polymers is commonly carried out by means of electropolymerisation of the monomer aniline from aqueous media (Gerard *et al*, 2001) As demonstrated in *Chapter 2*, modification of electrodes with polyaniline has been applied in biosensing applications (Killard *et al*, 2001), where polyanihne can act as an effective non-diffusional mediating species coupling electrons directly from the enzyme redox site to the electrode This allows for very effective direct electrical communication between the biomolecule and the electrode surface Polyaniline exhibits good environmental stability, and its electrical properties can be modified by the oxidation state of the main chain and degree of protonation for different applications including the aforementioned biosensors, microporous electrically conducting materials, anticorrosion protection of metals, chemical sensing, supporting material for catalysts etc

However, the poor processability of polyanilines has limited their exploitation in commercial applications Aniline is a carcinogenic monomer and must be distilled prior to use It is insoluble in common solvents (Cho *et al*, 2004), seriously hindering its potential In addition, acidic conditions are required for the formation of the most highly conductive form of polyaniline, which does not lend itself to entrapment of pH-sensitive materials such as proteins Chemically-prepared polyaniline is unprocessable by conventional plastic processing methods such as extrusion or injection moulding, as the polymer is infusible (Banerjee & Mandal, 1995) Processability issues such as these need to be overcome for further successful exploitation of this electrically conducting polymer *Chapter 2* highlighted some other problems associated with the use of electropolymerised PANI as a diffusionless mediator in a biosensor application Protein could not be entrapped with the polymer film as acidic conditions were used for the electropolymerisation As such, proteins had to be subsequently deposited, adding complexity to the sensor fabrication In addition, the inter-film variability was high, due to lack of ability to control the charge contained within the film These problems led to the fabrication of biosensors that were shown to be unreliable and irreproducible

Much effort has been spent improving the processability of PANI Dispersion of this polymer is one of the interesting ways to improve its processability Problems with solubility can be overcome and its processability by conventional plastic processing methods improves In addition, little or no aniline should be present in dispersions, thereby reducing its carcinogenic properties These dispersions have been studied by many research groups (Park *et al*, 2004, Somani, 2003, Gangopadhyay *et al*, 2001) PANI dispersions have been prepared by various methods such as polymerisation of aniline in micelle (Kim *et al*, 2000, 2001), emulsion (Kinlen *et al*, 1998) and reversed microemulsion (Gan *et al*, 1995) methods Polymerisation of aniline in the micelle has not generated extensive research to date despite being a facile method of synthesis It has the added benefit that coalescence and coagulation of the particles is naturally prevented by electrostatic repulsive interaction between anionic micelles Kim *et al* (2001) reported the preparation of PANI nanoparticles by oxidation with ammonium peroxydisulphate (APS) in sodium dodecyl sulphate (SDS) micellar solution The particle size was found to be of the order of 10 - 20 nm and the conductivity was in the range of 4 – 20 S $cm^{-1}$ This dispersion exhibited long-term stability, and existed as a stable solution without precipitation over several years Oh *et al* (2002) have also carried out similar work using SDS micellar solution as the polymerisation medium More recently, Han *et al* (2002) produced conducting polymer nanoparticles by introducing dodecylbenzene sulphonic acid (DBSA), which can play both the roles of dopant and surfactant in the aqueous solution This serves to increase the processability and stability of the resulting nanoparticles, and to simplify the process without additional dopants Recently, Moulton *et al* (2004) used the micelle polymerisation method developed by Han *et al* (2002) to synthesise larger quantities of the polyaniline nanodispersion (40 g) This was achieved by increasing the oxidant to monomer ratio (1 1, compared to 0 5 1) These nanoparticles were characterised as spherical particles, 10 ± 2 nm in diameter with an electrical conductivity of 15 ± 3 S $cm^{1}$

This work investigates these polyaniline nanoparticles, synthesised by Moulton *et al* (2004), as an alternative non-diffusional mediating species in biosensing to the PANI/PVS co-polymer discussed in *Chapter 2* The nanoparticles are readily dispersed in aqueous media which helps overcome some of the processability issues associated with polyaniline Modification of electrodes can be readily done from this aqueous dispersion, where the nanoparticles can be deposited

by electrochemical or drop-coating methods Nanodimensional conducting polymers have been shown to exhibit unique properties such as greater conductivity and more rapid electrochemical switching speeds (Innis & Wallace, 2002) Nanoscale materials offer bulk solution handling characteristics with nanoscale material control, and in the case of biosensors, can be combined with biomolecular species at this point, or subsequent to their fabrication on an electrode surface

In this work, the polyaniline nanoparticles - referred to as *nano*PANI/DBSA in this section - were successfully electrodeposited on the surface of carbon electrodes by means of cyclic voltammetry, to form nanostructured films These electrodeposited polymer nanoparticles were examined by Scanning Electron Microscopy (SEM), Atomic Force Microscopy (AFM), spectroelectrochemistry and profilometry Biomolecules were combined with these films m a number of ways Physical techniques have shown that the nanostructured films possess properties which allow for uniform adsorption of protem to take place The biosensor performance has been characterised using horseradish peroxidase (HRP) with the catalytic substrate hydrogen peroxide ($H_2O_2$) This sensor exhibited higher signal-to-background ratios (S/B) and quicker response times than the PANI/PVS biosensor configuration discussed in *Chapter 2*

Drop-coating of the *nano*PANI/DBSA onto screen-printed electrodes for biosensor development was also investigated By drop-coating a mixed solution of an enzyme and nanoparticles, a simple fabrication method for a biosensor was developed The S/B of this sensor was comparable to the sensor developed using electrodeposited nanoparticles, but has the added advantage of ease of fabrication, a method that would lend itself to techniques such as ink-jet printing for mass production of biosensors

## 4.2 MATERIALS AND METHODS

### *4 2.1 Materials*

Polyanilme dodecylbenzene sulphonic acid nanoparticles (*nano*PANI/DBSA) were synthesised according to a previously published procedure (Moulton *et al*, 2004) by Simon Moulton, IPRC, University of Wollongong, Australia Horseradish peroxidase (HRP, 232-668-6) was purchased from Biozyme Laboratories (South Wales, UK) Bovine serum albumin (BSA, A-7906), 2,2'-azmo-bis(3-ethylbenzthiazolme-6-sulphonic acid) (ABTS, A-1888), and silver enhancer kit (SE-100) were purchased from Sigma-Aldrich (Poole, Dorset, UK) Human chorionic gonadotropin (HCGβ) monoclonal antibody (MoAb) labelled to colloidal gold (62-H25) was purchased from Fitzgerald Industries International (MA, USA) 30% (v/v) hydrogen peroxide solution was purchased from Merck Glassy carbon and silver/silver chloride (Ag/AgCl) electrodes were purchased from Bioanalytical Systems Ltd (Cheshire, UK) The platinum mesh (29,809-3) was purchased from Aldrich

### *4.2.2 Buffers and solutions*

Unless otherwise stated, all electrochemical measurements were carried out in phosphate buffered saline (PBS), (0 1 mol $dm^{-3}$ phosphate, 0 137 mol $dm^{3}$ NaCl and 2 7 mmol $dm^{-3}$ KCl), pH 6 8 Colorimetric assays were carried out in 10 mmol $dm^{-3}$ phosphate buffer, (0 33 mmol $dm^{-3}$ $KH_2PO_4$ and 0 66 mmol $dm^{-3}$ $Na_2HPO_4$), pH 7 0 The ABTS buffer was 200 mmol $dm^{-3}$ dihydrogen phosphate and 100 mmol $dm^{3}$ citric acid, and adjusted to pH 5 5 using concentrated NaOH

### *4.2.3 Instrumentation*

All electrochemical protocols were performed either on a BAS100/W electrochemical analyser with BAS100/W software, or a CH1000 potentiostat with CH1000 software, using either cyclic voltammetry or time-based amperometric

modes A Ag/AgCl reference electrode and a platinum mesh auxiliary electrode were used for bulk electrochemical experiments Scanning electron microscopy (SEM) was performed with a Hitachi S 3000N scanning electron microscope An acceleration voltage of 20 kV was employed Atomic Force Microscopy (AFM) was performed with a Dimension 3100 (Digital Instruments) in contact mode All AFM measurements were carried out by Orawan Ngamna at the IPRI, Wollongong, Australia Profilometer readings were taken with a Dektak V-220-Si Stylus Profilometer (Veeco Instruments Ltd , Cambridge, UK) Spectroelectrochemistry was carried out with a Varian Cary UV-Vis spectrophotometer (JVA Analytical Ltd )

### *4.2.4 Electrodeposition of nanoPANI/DBSA*

Glassy carbon working electrodes (area 0 07 $cm^2$) were cleaned by successive polishing on aqueous slurries of 1 μm, 0 3 μm and 0 05 μm alumina powder, followed by ultrasonic cleaning in Milli-Q water for ten minutes Indium tin oxide (ITO) glass was cleaned by sonicating in acetone for 10 min *Nano*PANI/DBSA (5 5 4 % w/w ratio) was made up with distilled water and electrodeposited from this solution onto the surface of the working electrode (glassy carbon or ITO), using cyclic voltammetry (CV) The potential was cycled between –500 mV and 1100 mV vs Ag/AgCl at 100 mV $s^{-1}$ for the required number of cycles

### *4.2.5 Electrostatic immobilisation of protein*

Following electrodeposition of the *nano*PANI/DBSA, the electrode was transferred to a batch cell The surface of the polymer was reduced in PBS (degassed for 10 min under mtrogen) at –500 mV vs Ag/AgCl, over 1500 s at a sensitivity of 1 × $10^{-4}$ A $V^{-1}$ Protein was prepared m PBS prior to use Very quickly after reduction was complete, PBS buffer was removed from the cell and quickly replaced with the protein solution, not under stirring or degassing Oxidation was then performed immediately at +700 mV vs Ag/AgCl for 1500 s During this oxidation, the protein becomes electrostatically attached to the polymer surface The protein solution was carefully recovered from the cell and re-stored for later use

### *4.2 6 Real-time monitoring of protein interactions in the batch cell*

After the immobilisation of protein, the electrode was placed in PBS buffer in a batch cell Amperometric experiments were performed at –100 mV vs Ag/AgCl, with a sample interval of 100 ms and a sensitivity of $1 \times 10^{-4}$ A $V^{-1}$ $H_2O_2$ (8 mmol $dm^{-3}$) was added once the current had reached steady state

### *4.2.7 Blocking of the electrode surface with bovine serum albumin*

A range of dilutions of bovine serum albumin (BSA) beginning at 10 mg $ml^{-1}$ was prepared in PBS These solutions were used for the immobilisation of BSA on the surface of the electrode An electroanalytical procedure was performed where a solution of HRP (0 5 mg $ml^{-1}$) and $H_2O_2$ (8 mmol $dm^{-3}$) in PBS was added to the stirred buffer solution

### *4.2.8 Optimisation of the mass of HRP on the electrode surface*

A range of dilutions of HRP beginning at 10 mg $ml^{-1}$ was prepared in PBS These solutions were used for the immobilisation of HRP onto the surface of a series of electrodes An electroanalytical procedure was performed where a solution of $H_2O_2$ (Final concentration 8 mmol $dm^{-3}$) in PBS was added to the stirred buffer solution

### *4.2.9 Silver enhancement of gold-labelled HCGβ MoAb on nanoPANI/DBSA-modified electrodes*

Colloidal gold-labelled HCGβ MoAb of varying concentrations was electrostatically deposited onto the surface of the polymer film according to *Section 4 2 5* The films were allowed to dry Equal volumes (1 ml) of solutions A (silver salt) and B (initator) from the silver enhancer kit were mixed together immediately before use, and applied onto the surface of the electrode After 6 min, the solution was removed, and potassium thiosulphate (2 5 % (w/v), 20 µl) was then dropped on the surface for 2 min in order to stop the silver reaction

### *4 2 10 Drop-Coating of nanoPANI/DBSA biosensors*

*Nano*PANI/DBSA was dispersed with distilled water at the required concentration pH adjustment was carried out at this point if necessary HRP was then added at the required concentration to the dispersion, and the resulting mixture was drop-coated onto pre-treated Gwent-inH electrodes and allowed to dry overnight at 4°C over silica gel Amperometric measurements were carried out according to *Section 4 2 6*

## 4.3 RESULTS AND DISCUSSION

Aqueous dispersions of polyaniline nanoparticles were prepared as described in *Section 4 2 4* Particle sizes were previously determined to be of the order of 10 nm (Moulton *et al*, 2004) Dispersions of these nanoparticles were found to be stable for at least two months

Electrodeposition of *nano*PANI/DBSA dispersions was successfully carried out on carbon electrodes It was possible to electrodeposit this material onto both glassy carbon, and screen-printed carbon electrodes (Gwent-inH) However, glassy carbon was used as the working electrode due to the greater reliability of it over the screen-printed electrodes for fundamental studies These electrodeposited nanoparticles were characterised, and examined as an alternative platform to the PANI/PVS film (*Chapter 2*) in a working biosensor

In addition to electrodeposition, drop-coating of the *nano*PANI/DBSA dispersion was also carried out onto pre-treated Gwent-inH electrodes Preliminary work was carried out on this type of modified electrode in order to determine the suitability of the material for single-step biosensor fabrication

Attempts to deposit PANI/DBSA from aniline monomer in the presence of DBSA acid was also attempted as an alternative method for modifying the electrode surface with PANI However, mixing aniline and DBSA (1 1) in aqueous medium resulted in a white, highly viscous material, due to the formation of the insoluble crystalline anilinium-DBSA complex (Haba *et al*, 2002) Reducing the ratio of DBSA did serve to decrease the viscosity However, the pH of this solution increased as a result For example, at a monomer acid ratio of 1 0 6, the pH of the mixture was measured at 5 6 Electropolymerisation of PANI at pH higher than 4 is not possible as the nucleation step is an oxidative process requiring protons (*Chapter 2, Figure 2 2*) Although it was possible to deposit PANI/DBSA onto glassy carbon at a monomer acid ratio of 1 1, the SEM images of the resulting films were patchy and inhomogeneous, and not suitable for further work As a result, all further work was based on *nano*PANI/DBSA

### *4.3.1 Electrodeposition of nanoPANI/DBSA onto glassy carbon electrodes*

Cyclic voltammetry was the method used for electrodeposition of the *nano*PANI/DBSA emeraldine salt (ES) nanodispersion onto glassy carbon electrodes (*Figure 4.1*). *Figure 4.1a* shows a typical voltammetric electrodeposition of the *nano*PANI/DBSA onto glassy carbon for 10 cycles. This electrodeposition process showed typical PANI redox behaviour, similar to that observed from the PANI/PVS system in *Chapter 2*, undergoing two distinct redox processes, also observed for the PANI/PVS system. Current responses increased on subsequent scans indicating that the nanoparticles aggregated/assembled on the glassy carbon electrode surface. The oxidation peaks were assigned to the oxidation of leucoemeraldine (LM) to its radical cation, ($LM^{\bullet+}$) (a), and $LM^{+}$ to emeraldine (EM) (b). The reduction peaks were assigned to the reduction of EM to its emeraldine radical cation ($EM^{+}$) (c) and $EM^{\bullet+}$ to LM (d). A third redox couple was observed at about +600 mV when just 10 voltammetric cycles were employed. This was attributed to the formation of *p*-benzoquinone and hydroquinone as side products (Sadik & Wallace, 1993). These degradation peaks were no longer observed after 30 voltammetric cycles (*Figure 4.1b*), as the PANI redox couples dominated the CV. Shifts in peak potentials began to occur after a number of cycles (*Figure 4.1b*). This may be the result of increased resistance of the electrode, as the film deposited becomes thicker. Currents reached for the electrodeposition (30 cycles) of the nanoparticles can be seen to be in the order of hundreds of $\mu A\ cm^{-2}$. This is in contrast to the PANI/PVS system where $mA\ cm^{-2}$ current levels were reached after just 10 cycles (*Chapter 2*).

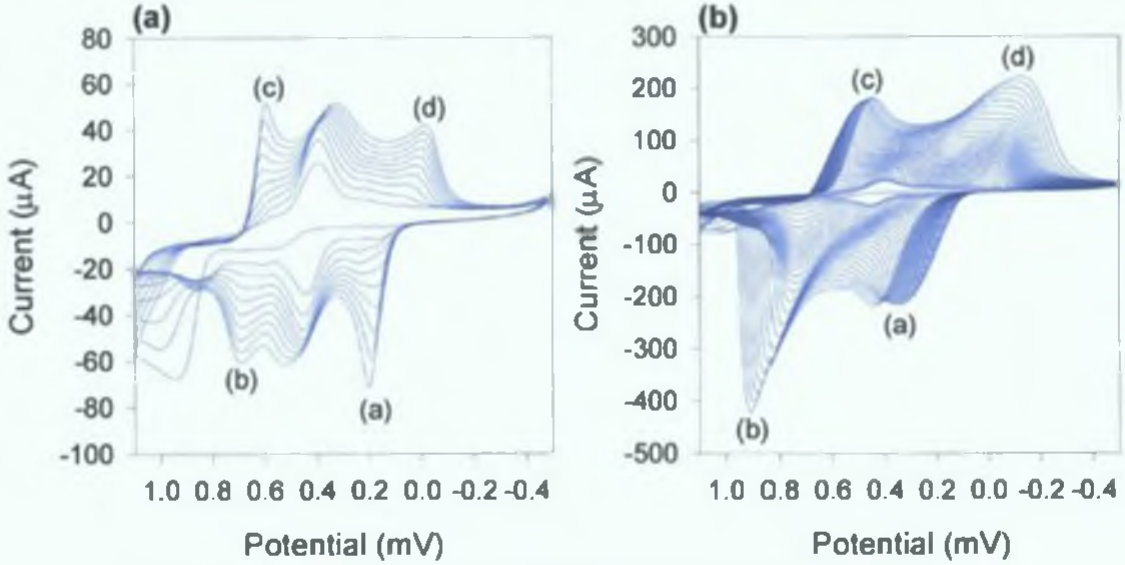


***Figure 4.1.*** Electrodeposition of *nano*PANI/DBSA (5.54 % w/w) film onto a glassy carbon electrode (0.07 $cm^2$). (a) 10 and (b) 30 voltammetric cycles. Scan rate: 100 $mV\ s^{-1}$.

Different concentrations of the *nano*PANI/DBSA dispersion were used for electrodeposition (10 cycles), in order to examine its effect on the growth of the film. CVs of these electrodeposited films were carried out in HCl (1 mol $dm^{-3}$) and a plot of the $EM^{+\bullet}$ peak current against dispersion concentration is given in *Figure 4.2*. It was seen that below dispersion concentrations of 5.54 % w/w, the peak current heights were quite low, showing that there was not sufficient electrical connectivity between the PANI molecules for effective inter-communication. Increasing the concentration to 5.54 % w/w, a sharp increase was observed in peak current. This is the critical concentration for the *nano*PANI/DBSA redox centres to interact, and hence produce much larger peak currents. Increasing the concentration above values of 5.54 % w/w resulted in increases in peak height. However, above 7 % w/w, the slope of the graph began to decrease, indicating that inhibition of charge transfer was occurring in these films. Hence, for all further electrodepositions, 5.54 % w/w was used.

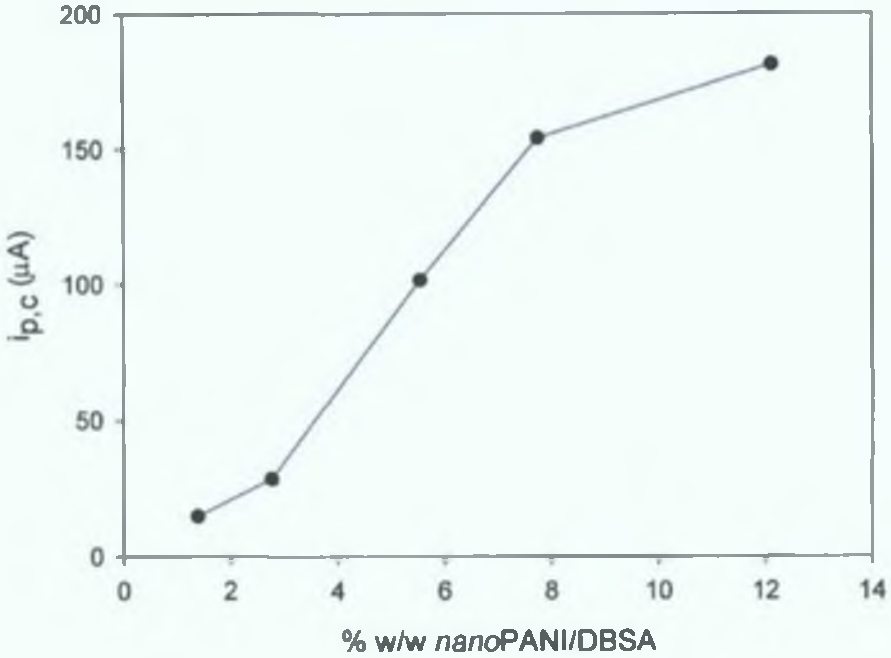


***Figure 4.2.*** Dependence of cathodic peak current ($i_{p,c}$). (Peak (c) in *Figure 4.1a*), on concentration (% w/w) of *nano*PANI/DBSA used for electrodeposition on glassy carbon electrodes.

### *4.3.2 Characterisation of electrodeposited nanoPANI/DBSA*

Preliminary profilometry results indicated that the electrodeposited film from *nano*PANI/DBSA (30 cycles) was approximately 350 nm thick on glassy carbon (0.07 $cm^2$). This was about 100-times less than those synthesised from PANI/PVS (using only 10 voltammetric cycles) (*Chapter 2*). SEM studies also showed the drastically smoother electrodeposited film of *nano*PANI/DBSA compared to the electropolymerised film of PANI/PVS (*Figure 4.3*). Literature reports (Do & Chang, 2004; Sharma *et al.*, 2003) that electropolymerised polyaniline films grown from acidic media, usually result in a sponge-like, branched, porous-structure, high-surface area polymer film (*Figure 4.3a*). Since electrodeposition of nanoparticles involves deposition of preformed polymer, no nucleation or branching occurs and a more ordered deposit results (*Figure 4.3b*). The white sphere is presumed to be excess DBSA.

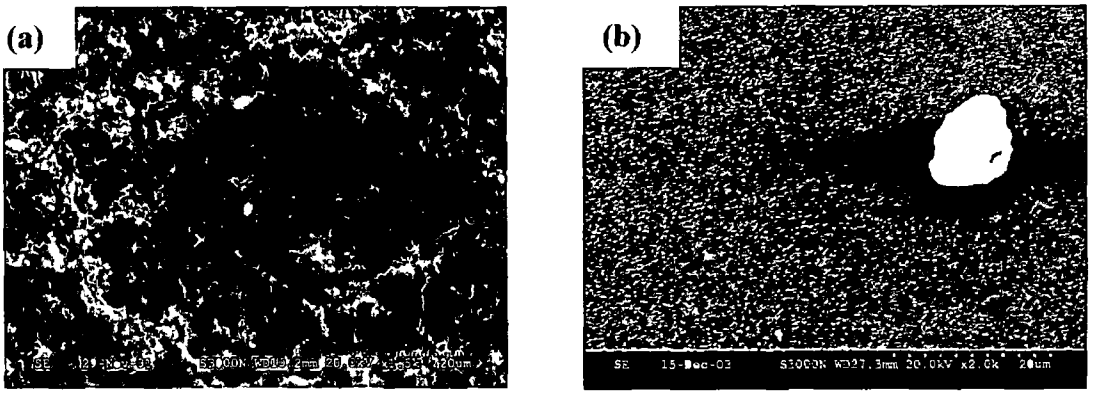


***Figure 4.3*** Typical scanning electron micrograph of (a) PANI/PVS electropolymerised on a glassy carbon electrode surface (20 cycles) (1500 X magnification) (b) *nano*PANI/DBSA (5 54 % w/w) electrodeposited on a glassy carbon electrode surface (30 cycles) (2500 X magnification)

AFM was also employed to characterise surface morphology of the electrodeposited *nano*PANI/DBSA film (*Figure 4 4*) The AFM images shows nanoPANI/DBSA films after different numbers of electrodeposition cycles Each of the films are characterised by uniform arrays of PANI/DBSA nodules The roughness of the film however, depends on the number of cycles employed for the electrodeposition process The roughness calculations for the electrodeposited films formed with various voltammetric cycles were calculated (*Table 4 1*) Root mean square average of height deviations were taken from the mean data plane as the formulation below

$$\frac{\sqrt{\sum Z_i^2}}{n}$$

Where Z is the height (nm) and n is the no of data points taken

As the number of cycles increased, the roughness of the films also mcreased up to 30 cycles At 40 cycles the roughness decreased, possibly due to the aggregation of individual nodules to form a continuous film

***Table 4 1*** Roughness calculations for *nano*PANI/DBSA films electrodeposited onto glassy carbon as a function of number of voltammetric cycles

| *Number of Cycles* | *RMS (nm)* |
|---|---|
| 10 | 24 74 |
| 20 | 83 19 |
| 30 | 115 55 |
| 40 | 86 66 |

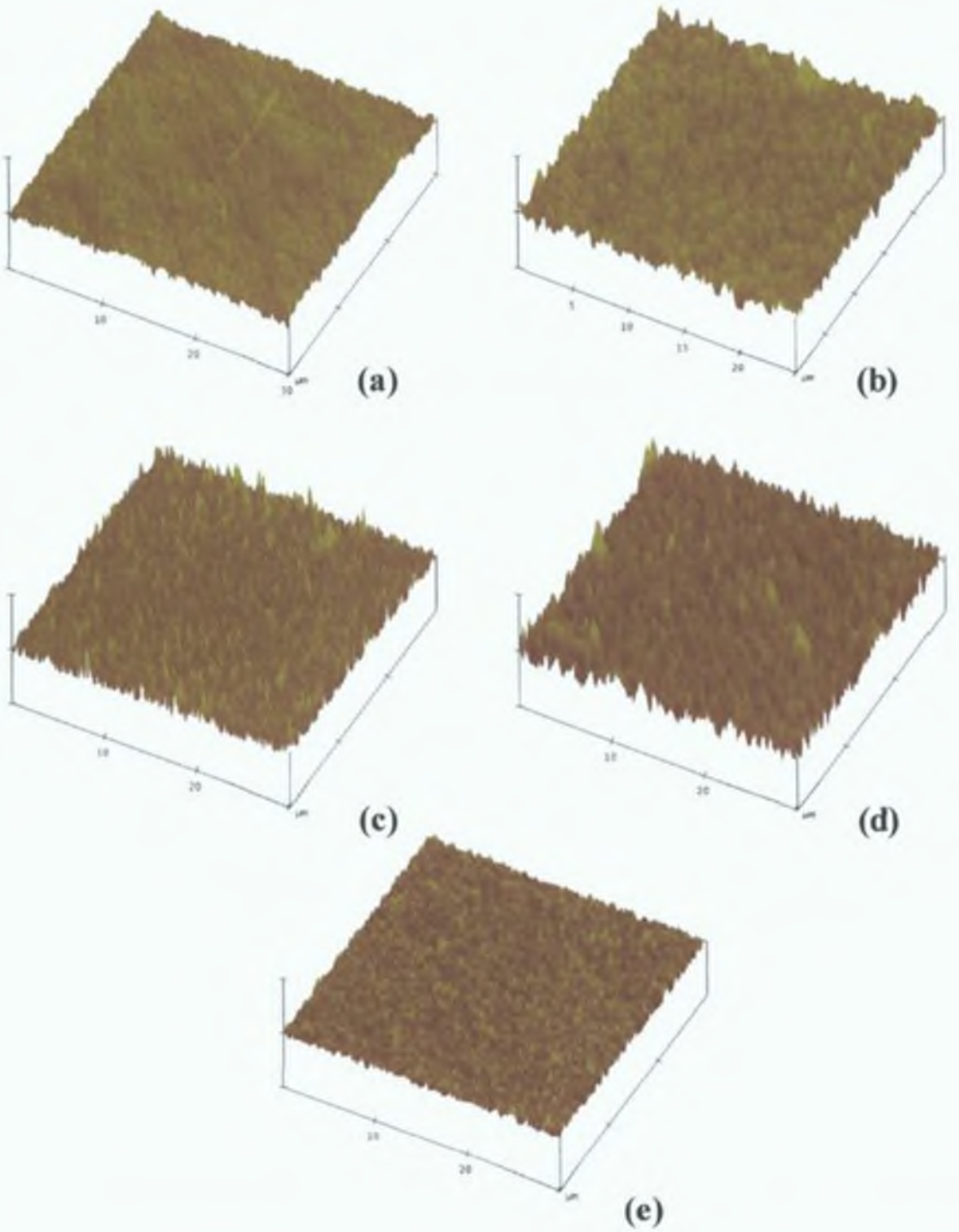


***Figure 4.4.*** AFM 3-D images (30 × 30 μm) of *nano*PANI/DBSA (5.54 % w/w) electrodeposited on a glassy carbon electrode surface. (a) glassy carbon, (b) 10, (c) 20, (d) 30, (e) 40 voltammetric cycles.

Spectroelectrochemistry of the *nano*PANI/DBSA film was carried out on films electrodeposited onto ITO-coated glass (80 cycles) in order to investigate the electronic properties of the film UV-Vis absorption spectra (*Figure 4 5*) contained the three characteristic absorption bands of doped PANI observed at about 330 nm, 420 nm and 750 nm (Haba *et al*, 1999) The first absorption band arises from electron transitions within the benzenoid segments and is assigned to a $\pi$-$\pi^*$ transition The second absorption band represents the protonation stage of the PANI chains This band is most prominent when the film is held at negative potentials (-500 mV), and decreases in intensity as the film becomes oxidized (or deprotonated) The absorption band in the visible region around 750 nm is assigned to the presence of polarons, which are the dominant charge carriers in polyanilme This peak is not present when the film is fully reduced (-500 mV), as the polymer chains are fully protonated This spectroscopic investigation shows that the *nano*PANI/DBSA electrodeposited from aqueous media exhibited typical PANI characteristics in the UV and visible regions

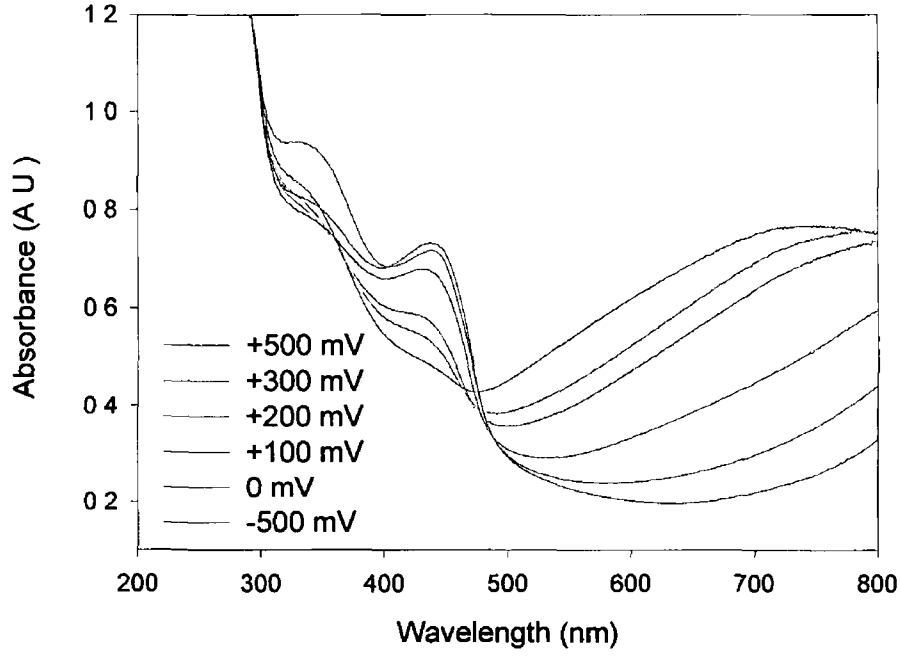


***Figure 4.5.*** Spectroelectrochemistry of *nano*PANI/DBSA film on ITO glass (80 voltammetric deposition cycles) UV-Vis scans were carried out in phosphate buffer, pH 6 8, while the potential was held constant for each scan over the range –500 mV to +1100 mV

### *4.3.3 Optimisation of electrodeposited nanoPANI/DBSA film for use in biosensing*

Preliminary biosensing work was performed on surfaces modified by electrodeposition from 5.54 % w/w *nano*PANI/DBSA initially using 10 voltammetric cycles. HRP (0.1 mg $ml^{-1}$) was electrostatically immobilised onto the modified electrode surface according to *Section 4.2.5*. The amperometric response obtained from addition of $H_2O_2$ (8 mmol $dm^{-3}$) is shown in *Figure 4.6*. The applied potential of –100mV was chosen in order to directly compare the amperometric response of the *nano*PANI/DBSA sensor with the previously reported PANI/PVS biosensor (*Chapter 2*). The background current density (5.7 μA $cm^{-2}$) was much lower than obtained previously (42.4 μA $cm^{-2}$) using the PANI/PVS copolymer. Response times of less than 1 s were observed.

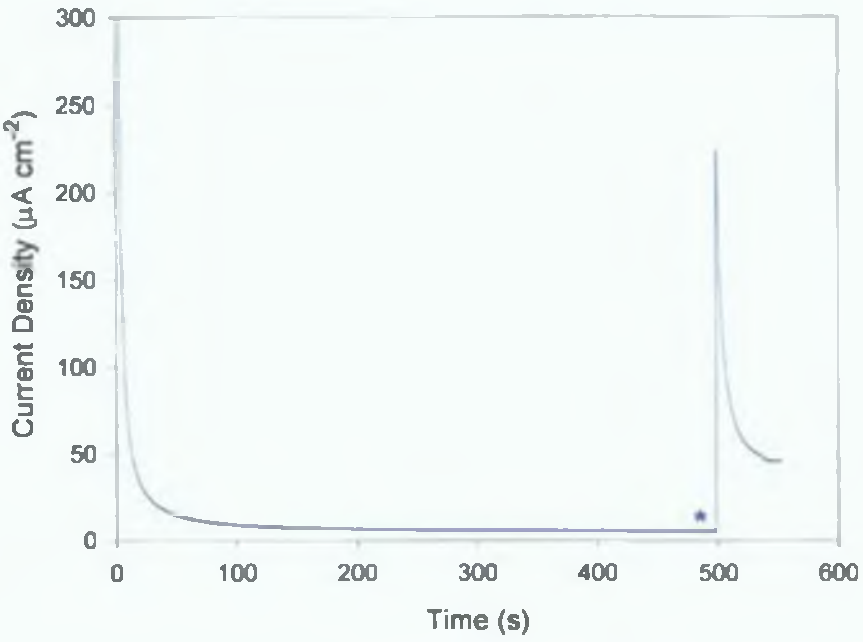


***Figure 4.6.*** Amperometric response of electrodeposited *nano*PANI/DBSA sensor modified with HRP (0.1 mg $ml^{-1}$). Potential held at –100 mV vs. Ag/AgCl. * Indicates addition of $H_2O_2$ (Final concentration: 8 mmol $dm^{-3}$).

#### 4.3.3.1 Optimisation of protein mass on the surface

Immobilisation of both BSA and HRP onto the surface of the *nano*PANI/DBSA polymer film was achieved *via* electrostatic interactions.

Investigations into the process of protein immobilisation using amperometric and SEM techniques was carried out Amperometric response as a function of enzyme immobilisation is shown in *Figure 4 7* Optimal amperometric responses were achieved when HRP was immobilised on the electrode surface at a concentration of 0 1 mg $ml^{-1}$ Amperometric responses increased as a function of concentration of HRP up to the optimal concentration of 0 1 mg $ml^{-1}$ Above this concentration the responses decreased, possibly due to steric hindrance of the enzyme or the presence of impeded charge transfer due to multiple protein layers To confirm the recorded signal response was due to the catalytic interaction between $H_2O_2$ and HRP, BSA was electrostatically immobilised to the *nano*PANI/DBSA surface By electrostatically applying a sufficient amount of BSA to the electrode, efficient blocking of the electrode surface from any electrochemically detectable reactions in bulk solution should be achieved This occurred when BSA was used at concentration levels between 0 1 mg $ml^{-1}$ and 10 mg $ml^{-1}$ (*Figure 4 7*) Concentrations of BSA immobilised were found to be inversely proportional to the amperometric responses from HRP and $H_2O_2$ in bulk solution

A similar trend was observed previously using the PANI/PVS platform (*Chapter 3*) However, in the work reported here, optimum catalytic signals were obtained using a protein immobilisation concentration approximately six times lower than our previous formats, showing that a much more efficient deposition of protein is achieved on the *nano*PANI/DBSA nanoparticulate surface than the PANI/PVS surface

The absolute mass of enzyme immobilized at the solution concentration of 0 1 mg $ml^{-1}$ was determined by a colorimetric enzyme assay (*Chapter 3*), and was calculated to be $5\,0 \pm 4\,4 \times 10^{11}$ molecules Assuming an ideal flat two-dimensional *nano*PANI/DBSA surface with an area of $7\,07 \times 10^{-6}$ $m^2$, the theoretical number of molecules of HRP (radius 26 Å) necessary to form a monolayer on the surface of these electrodes was estimated to be $3\,33 \times 10^{11}$ molecules This theoretical number of molecules of HRP required to form a monolayer at this surface can be compared to the number of molecules immobilised at optimum concentration (0 1 mg $ml^{-1}$) Therefore, it would appear that at this concentration, roughly a monolayer of protein is formed at the surface In comparison to the PANI/PVS formats previously developed (*Chapter 3*), both optimum catalytic signals and monolayer formation for the *nano*PANI/DBSA platform occur when the concentration of protein for

immobilisation is six-fold lower. This extra efficiency of the nanoparticulate system leads to a more economic biosensor in terms of protein reagents.

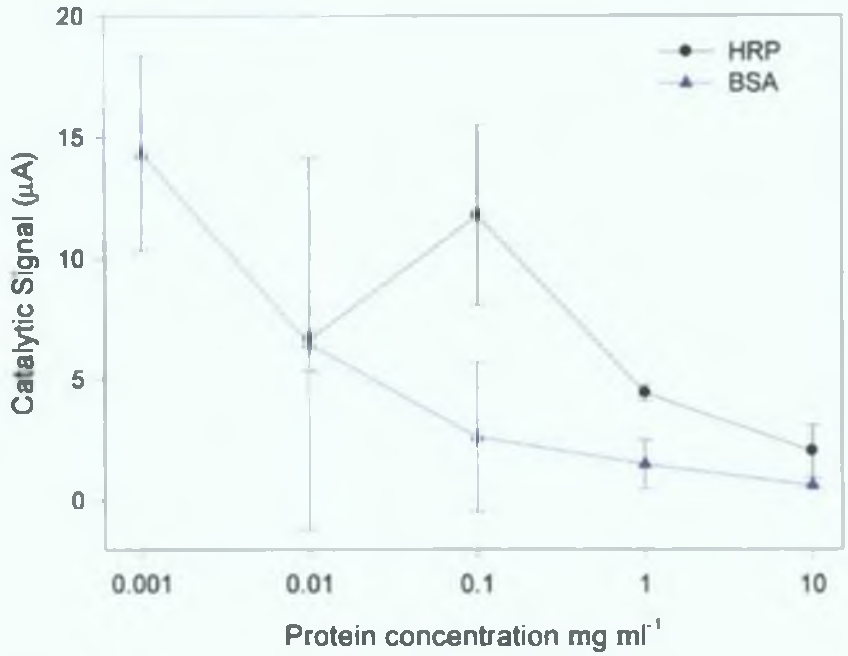


***Figure 4.7.*** Dependence of sensor response on the concentration of both BSA (blue line) and HRP (black line) used for immobilisation. Amperometric responses increased as a function of concentration of HRP up to 0.1 mg $ml^{-1}$ (n=3). Above this concentration the responses decreased. Concentrations of BSA immobilised were found to be inversely proportional to the amperometric responses from HRP and $H_2O_2$ in bulk solution (n=3).

Although AFM and SEM could provide adequate surface information as to the overall topography of protein films, the resolution of individual proteins or groups of proteins is not possible (Grennan, 2003). However, through the use of proteins conjugated to a non-fading, electron-dense particle such as gold, it was possible to indirectly visualise the distribution of proteins. A colloidal gold-labelled HCGβ MoAb was used as a model for the visualisation of protein on the *nano*PANI/DBSA film. HCGβ MoAbs conjugated to colloidal gold particles were employed as a model, with a view to imaging the topography of protein layers on *nano*PANI/DBSA modified glassy carbon. All gold-labelled-protein-modified surfaces were enhanced with silver, in order to visualise the gold label. This silver enhancement process caused the reduction of silver ions, resulting in the precipitation of metallic silver

around the gold particles, so as to enlarge the gold particles for better visualisation (Grennan, 2003)

*Figure 4 8* contains the images of colloidal gold-labelled HCGβ MoAb electrostatically immobilised on the surface of *nano*PANI/DBSA films (5 54 % w/w, 30 voltammetric cycles) A trend of increasing surface coverage was observed as the concentration of protein used for immobilisation was increased At a level of 0 001 mg $ml^{-1}$, low surface coverage was observed This surface coverage increased gradually until 10 mg $ml^{-1}$, which had a very dense layer of protein covering the polymer layer These images showed that protein was uniformly distributed over the surface of the *nano*PANI/DBSA film and no clustering was evident This is in contrast to the topographical results obtained for the protein-modified PANI/PVS surface, where high concentrations of protein resulted in aggregation and clumping of protein on the PANI/PVS surface with intermittent patches of the underlying polymer still visible (Grennan, 2003) These contrasting results must be attributed to the very different polyaniline films One reason may be that the morphology of the spongy PANI/PVS surface may hinder the immobilisation process of the protein In addition, there may be irregular patches of electro-inactive PANI/PVS within the film where protein may not adhere to during the electrostatic immobilisation, and so must cluster on the electroactive PANI areas of the film The *nano*PANI/DBSA film has a smoother morphology, and the electroactivity within the film may be more homogeneous As such, from these SEM results, the *nano*PANI/DBSA provides a more favourable platform for the immobilisation of protein

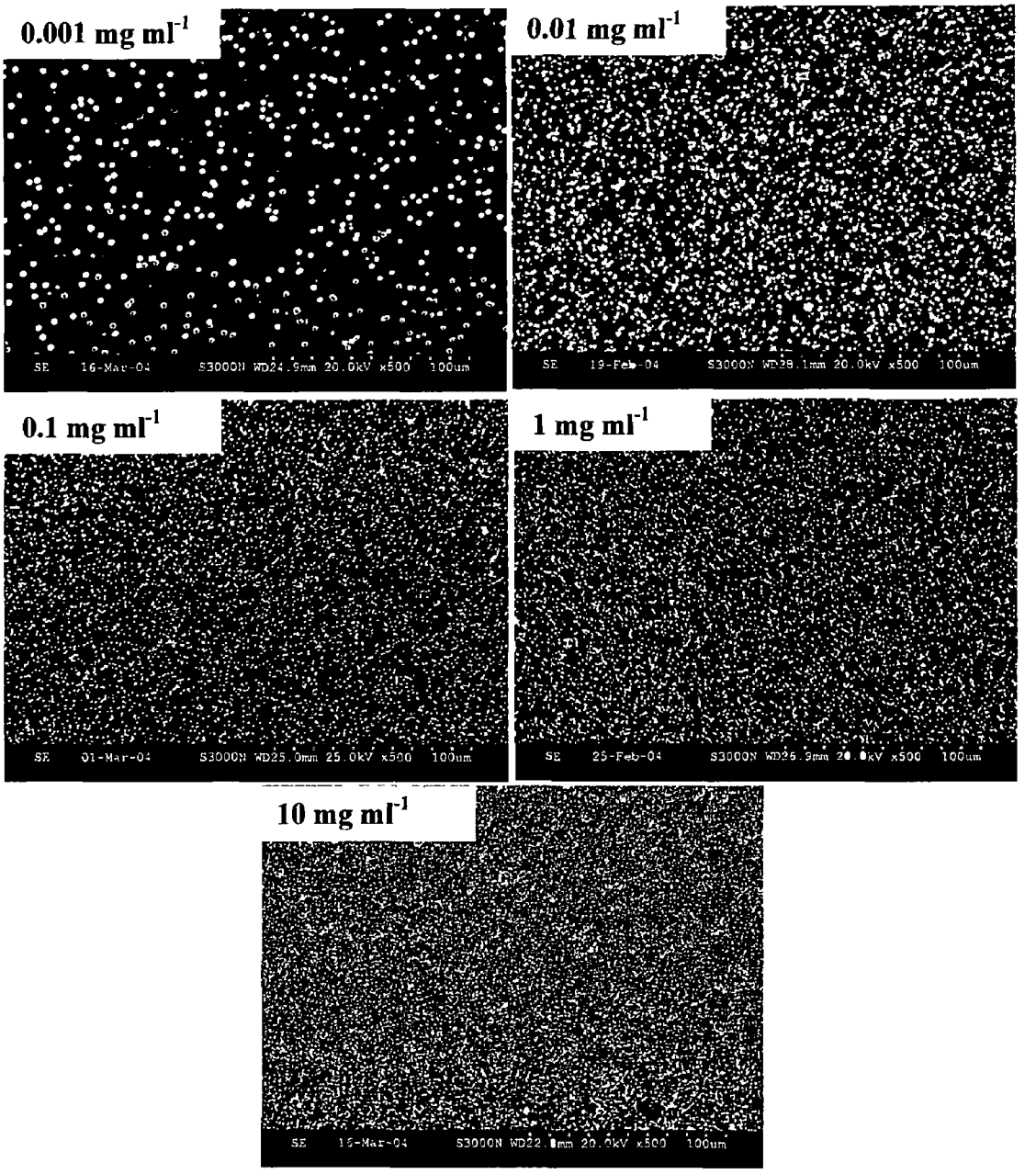


***Figure 4 8*** SEM images of *nano*PANI/DBSA films with varying concentrations of electrostatically immobilised HCGβ MoAb-Colloidal Gold The protein can be seen to be uniformly distributed over the surfaces, with the coverage increasing for increasing concentrations All surfaces were silver-enhanced in order to be able to visualise the protein gold label (500 X magnification)

### 4 3 3 2 Optimisation of the *nano*PANI/DBSA film thickness

By varying the thickness of film using different numbers of electrodeposition cycles, the charge held within the film should vary *Figure 4 9* shows a graph of the dependence of catalytic response of immobilised HRP to $H_2O_2$ (8 mmol $dm^{-3}$) on the number of cycles used for electrodeposition Up to a limit of 30 cycles, the catalytic response to $H_2O_2$ increases Above 30 cycles, the current response was seen to decrease This was due to the thicker polymer film hindering the electron transfer properties between the electrode surface and the bulk solution This result is in agreement with the AFM data (*Table 4 1 & Figure 4 4*), which seems to indicate 30 cycles as optimum for film performance

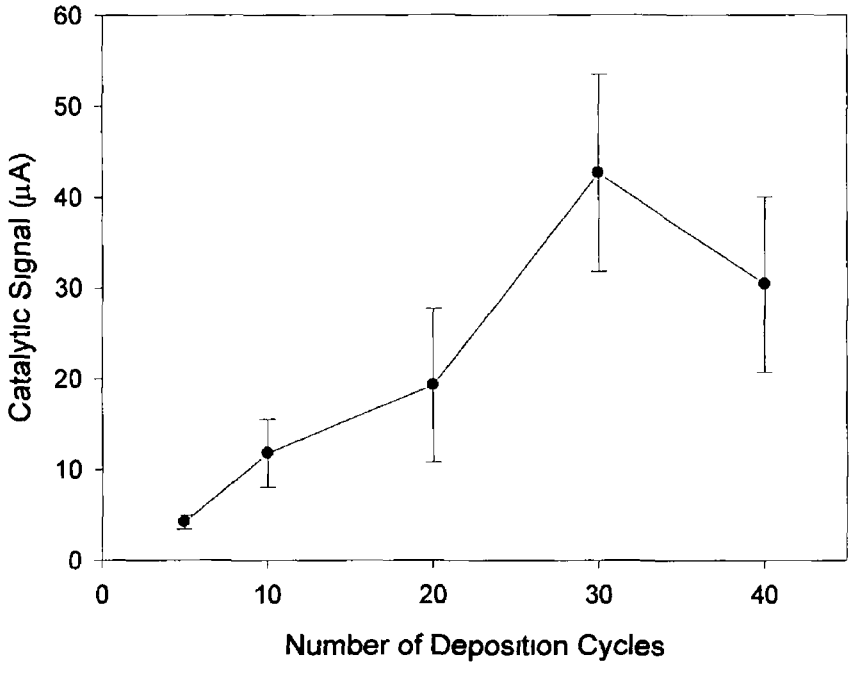


***Figure 4.9.*** Relationship between amperometric response and number of cycles used for electrodeposition of the *nano*PANI/DBSA film HRP (0 1 mg $ml^{-1}$) was electrostatically immobilised on the polymer films of varying thicknesses, and the recorded amperometric response was due to its catalytic interaction with $H_2O_2$ (8 mmol $dm^{-3}$) Maximum signal response was achieved when the number of deposition cycles was 30

### 4 3 3 3 Comparison of electrodeposited *nano*PANI/DBSA with PANI/PVS for use in biosensing

Finally, the characteristics of the optimised *nano*PANI/DBSA film were compared directly to the PANI/PVS film in terms of a platform for biosensing As stated previously, the *nano*PANI/DBSA film seemed more efficient in terms of protein immobilisation and required a concentration of protein six-fold lower than the PANI/PVS layer for monolayer coverage Although the net signal of the *nano*PANI/DBSA sensor (42 ± 11 μA) to $H_2O_2$ (8 mmol $dm^{-3}$) was just half of the signal achieved with PANI/PVS sensor (71 ± 14 μA), the S/B ratio was three times greater for the *nano*PANI/DBSA sensor (61 ±3 vs 17 ± 14) S/B ratios determine the sensitivity of the sensor, and therefore the *nano*PANI/DBSA sensor should have a lower limit of detection than the PANI/PVS sensor The response time for the optimised *nano*PANI/DBSA biosensor (0 62 ± 0 04 s) was at least one order of magnitude lower than that of the PANI/PVS biosensor (9 46 ± 4 12 s) These data show that the *nano*PANI/DBSA was more powerful as a biosensor platform, due to its highly ordered nanostructure, thinner layer, and the consequent uniform and efficient immobilisation of enzyme

### *4 3.4 Drop-coating of nanoPANI/DBSA onto screen-printed electrodes*

Drop-coating of the *nano*PANI/DBSA dispersion onto electrodes was carried out as an alternative deposition method to the electropolymerisation Electropolymerisation is not a technique applicable to mass production of biosensors Drop-coating (or casting) is a simpler method of electrode modification that, combined with screen-printed electrodes, would be amenable to mass production In addition, enzyme could be drop-coated either simultaneously or sequentially in order to develop a very simple method for fabrication of a biosensor

In order to examine this approach, various compositions of *nano*PANI/DBSA (20 μl) were first drop-coated onto Gwent-inH screen-printed electrodes (SPEs) and allowed to dry overnight over silica gel *Figure 4 10* shows the CVs in HCl (1 mol $dm^{-3}$) of compositions ranging from 5% to 40% w/w It can be seen that 5% and 10% compositions resulted in low currents, and the electrochemistry

of the underlying silver track of the SPEs dominated the voltammograms Increasing the concentration to 5 54 % resulted in much higher currents, where the electrochemistry of the PANI dominated Increasing the concentration to 40% resulted in only a negligible increase in current Therefore, 5 54 % w/w was chosen for all further work This optimum nanoparticle dispersion concentration was found to be the same as for the electrodeposition method The drop-coated electrodes, however, did not display such well-defined electrochemistry This observed poor electrochemistry may have been related to the thicker films that resulted from drop-coating as compared to electrodeposition No profilometry studies were carried out on these films, but could be estimated to be approximately 1000-times thicker than electrodeposited films, from a comparison of the voltammetric peak heights in HCl (1 mol $dm^{-3}$)

The volume of PANI/DBSA used for the drop-coating was varied to see if peak definition could be improved *Figure 4 11* shows that smaller volumes of PANI/DBSA (5 54 % w/w) resulted in more defined electrochemistry, which was more optimal, despite losing magnitude in current 5 µl showed the most well-defined peaks This was attributed to the thinness of the films that would result from using lower drop-coating volumes However, even at these volumes, the quality of PANI electrochemistry in HCl is still not ideal Drop-coating may not result in a continuous polymer chain as the nanoparticles may not aggregate on the electrode surface in an ordered fashion, as occurs for the electrodeposition method, which may reduce the quality of the charge propagation throughout the film and hence the electrochemistry It was not possible to deposit films using lower volumes than 5 µl, as these volumes did not cover the surface of the electrode adequately However, thinner films could be physically created by controlled deposition techniques such as ink-jet printing and spin-coating

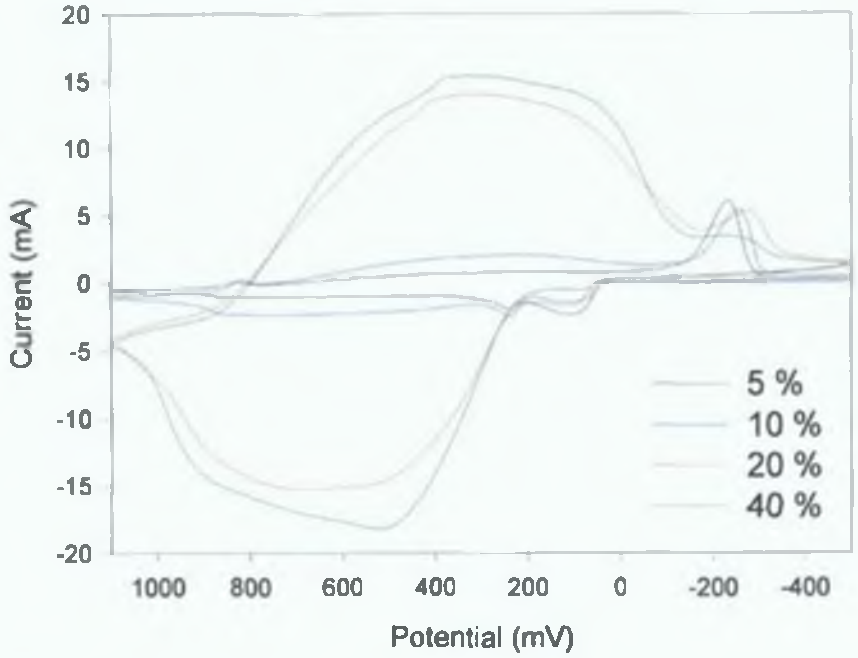


***Figure 4.10.*** CVs in HCl (1 mol $dm^{-3}$) for various compositions (% w/w) of *nano*PANI/DBSA drop-coated onto Gwent-inH screen-printed electrodes.

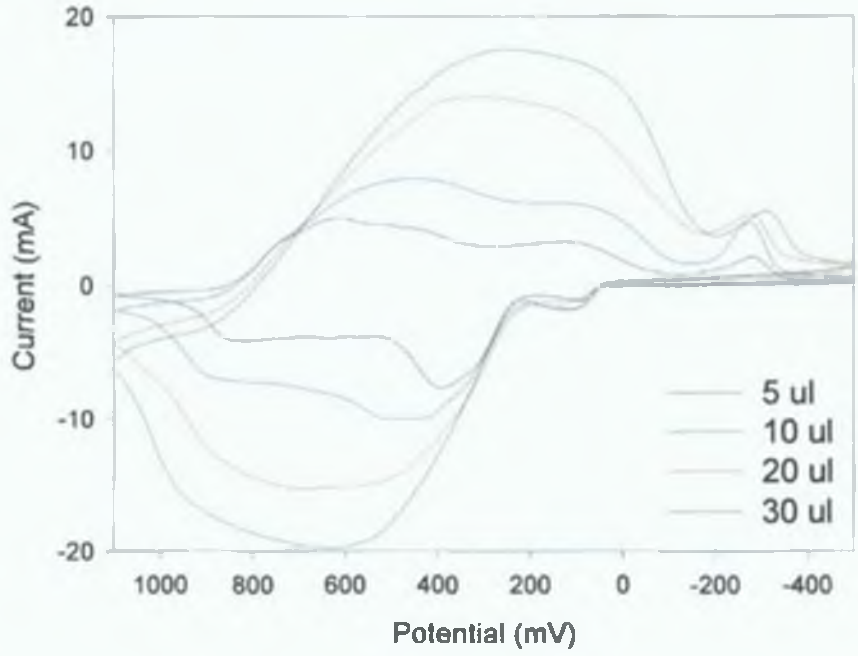


***Figure 4.11.*** CVs in HCl (1 mol $dm^{-3}$) for various volumes of *nano*PANI/DBSA (5.54 % w/w) drop-coated on Gwent-inH screen-printed electrodes. All electrodes were dried overnight at 4°C over silica gel.

The drying conditions of the drop-coated films needed to be investigated, as the films drop-coated with lower volumes were more fragile, and formed cracks upon drying Different drying conditions were used m order to try to strengthen the film Drying under vacuum over silica gel, and drying at 4°C, also over silica gel, were both explored It was observed that the films dried at 4°C were most stable, perhaps due to the slower drying process that would occur rather than at room temperature *Figure 4 12* shows a digital image of the *nano*PANI/DBSA film (5 µl) on a screen-printed electrode dried over silica gel at 4°C overnight The layer appears smooth and homogenous, with no apparent cracking

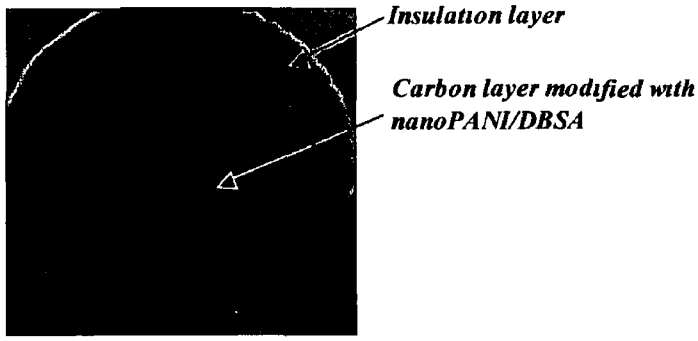


***Figure 4.12.*** Digital image of *nano*PANI/DBSA drop-coated (5 µl) onto a SPE and dried over silica gel at 4°C overnight

Incorporation of HRP into the film was then carried out m order to construct a working biosensor for $H_2O_2$ Three methods of protein immobilisation were examined (1) pre-mixing the HRP with the dispersion before drop-coating, (2) post-drop coating of the HRP onto the dried *nano*PANI/DBSA film and (3) electrostatic immobilisation of HRP All of the electrodes were tested in a stirred batch format using amperometry where the potential was held at −100 mV vs Ag/AgCl wire $H_2O_2$ was added once the current had reached steady state (*Section 4 2 6*) The immobilisation methods used, and the catalytic signals achieved upon addition of $H_2O_2$ are summarised in *Table 4 2*

It can be seen that pre-mixing HRP with *nano*PANI/DBSA did not yield any measurable signal upon addition of $H_2O_2$ However, when the pH of the nanoparticle solution was adjusted *before* addition of HRP, a high net catalytic signal was achieved Voltammetric studies in HCl (1 mol $dm^{-3}$) showed that there was little or no effect on the polyaniline electrochemistry of the films after pH adjustment (*data not shown*) Post-drop coating HRP (1 mg $ml^{-1}$) did not achieve such high catalytic

currents The PANI-mediated mechanism of the catalytic reduction of $H_2O_2$ was much more pronounced when HRP and *nano*PANI/DBSA were drop-coated simultaneously Electrostatic immobilisation of the HRP yielded net signals approximately half of that achieved with the pre-mixing method (with pH adjustment) This could be the result of a much lower mass of HRP immobilised on this electrode compared with electrodes where HRP was drop-coated There may also be charge inhibition as a result of the use of such a high concentration (1 mg $ml^{-1}$) of HRP for the electrostatic adsorption (*Section 4 3 3*) However, this immobilisation technique was not explored further, as ultimately it added too much complexity to the biosensor fabrication process Hence, the simpler process of premixing (with pH adjustment) was used for all further investigations This method, as well as yielding the highest catalytic signals, also has the advantage of being the simplest method for incorporating protein, and could be developed further with techniques such as ink-jet printing

***Table 4 2*** Summary of the conditions used for the different HRP immobilisation methods with their net signals and S/B ratios for catalytic reduction of $H_2O_2$ according to *Section 4 2 6*

| ***NanoPANI/DBSA drop-coating conditions*** | ***Immobilisation method of HRP*** | ***Net Signal*** | ***S/B*** | ***n*** |
|---|---|---|---|---|
| 5 54 % w/w, 20 µl | Pre-mixed with nanoparticles (1 mg $ml^{-1}$) | - | S/N < 1 | 3 |
| 5 54 % w/w, 20 µl, pH adjusted to 7 0 using conc NaOH | Pre-mixed with nanoparticles (1 mg $ml^{-1}$) | 32 02 ± 7 16 | 8 81 ± 4 13 | 3 |
| 5 54 % w/w, 20 µl | Post drop-coat (1 mg $ml^{-1}$) 10 µl | 6 46 ± 0 94 | 3 22 ± 1 06 | 3 |
| 5 54 % w/w, 20 µl | Electrostatic (1 mg $ml^{-1}$) | 17 24 ± 16 43 | 7 35 ± 9 23 | 2 |

Using the premixing method (with pH adjustment) for immobilisation of HRP, the concentration of HRP was varied over the range 0 to 50 mg $ml^{-1}$ in order to determine the optimum working concentration A plot of catalytic response from $H_2O_2$ (8 mmol $dm^{3}$) is plotted against HRP concentration in *Figure 4 13* Catalytic responses increased as the concentration was varied from 0 to 20 mg $ml^{-1}$ Above HRP concentrations of 20 mg $ml^{-1}$, the catalytic response was seen to decrease due to

excess HRP At these high concentrations, the efficiency of the charge transfer between the redox sites of the HRP and the PANI decreased, possibly due to steric hindrance within the films This demonstrated that the HRP was responsible for the catalytic reduction of $H_2O_2$ and that when immobilised within the *nano*PANI/DBSA film could yield measurable signals Although 20 mg ml $^{1}$ was seen to be the optimum concentration, this level was too high to work with m terms of enzyme consumption Therefore 5 mg ml $^{1}$ was used for all further work The net signal at this level of HRP was 34 23 ± 10 03 μA, with a corresponding signal S/B ratio of 24 94 ± 3 4 These values were comparable to those obtained using the electrodeposited *nano*PANI/DBSA where the HRP was electrostatically immobilised However, the drop-coated biosensor was much easier to prepare, just by casting a mixed solution of enzyme and nanoparticles, without any electrochemical steps This drop-coated biosensor will be investigated further for single step fabrication of an ink-jet printable biosensor

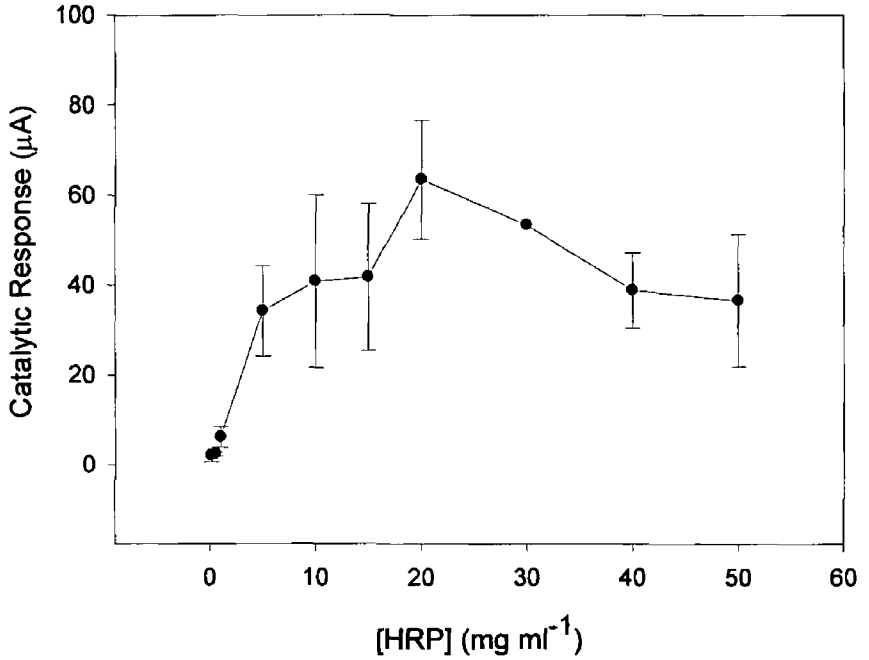


***Figure 4 13.*** Dependence of catalytic response of drop-coated *nano*PANI/DBSA biosensor on HRP concentration The nanoparticle dispersion (5 54 % w/w) was adjusted to pH 7 0 to which different concentrations of HRP (0 – 50 mg $ml^{-1}$) were added These were drop-coated onto SPEs (5 μl), and allowed to dry overnight at 4°C over silica gel (n = 3)

## 4.4 CONCLUSION

The present study illustrates deposition of polyaniline nanoparticles on carbon electrodes for use in novel biosensor fabrication techniques Two methods of deposition of *nano*PANI/DBSA were investigated (1) electrodeposition and (2) drop-coating

By electrodeposition of the nanoparticles on glassy carbon, a uniform, highly ordered, nanometric, nanostructured polyaniline film resulted This uniform surface showed improved enzyme deposition characteristics and better S/B ratios than when polyaniline is electrochemically deposited from bulk monomer solutions It is hoped that this system will lead to modified electrode platforms with improved processability and functionality over previous methods

A second, simpler drop-coating method for deposition of nanoparticles onto screen-printed electrodes was also investigated HRP was incorporated into the nanoparticle dispersion before drop-coating in order to develop a single-step fabrication method for a biosensor The signal to background was comparable to the biosensor fabricated from electrodeposited films and the drop-coated sensor was much easier to fabricate, with no electrochemical steps

Further work could include development of the electrodeposited *nano*PANI/DBSA on screen-printed electrodes, and integration of this system into a separation-free immunosensor, that has been previously developed by Killard *et al* (2001) using the PANI/PVS system The drop-coated system could be developed further with the use of ink-jet printing technology Ink-jet printing will bring this sensor to a more sophisticated fabrication level, lending itself to single-step mass production of enzyme biosensors

## 4.5 REFERENCES


Banerjee, P , Mandal, B (1995) Blends of HCl-doped polyaniline nanoparticles and poly(vinyl chloride) with extremely low percolation threshold – a morphology study *Synth Met*, **74** 257-261

Cho, M , Park, S , Hwang, J , Choi, H (2004) Synthesis and electrical properties of polymer composites with polyanilme nanoparticles *Mater Sci Eng C*, **24** 15-18

Do, J , Chang, W (2004) Amperometric nitrogen dioxide gas sensor based on Pan/Au/Nafion prepared by constant current and cyclic voltammetry methods *Sens Actuat B*, **101** 97-106

Gan, L , Zhang, L , Chan, H , Chew, C (1995) Preparation of conducting polyaniline-coated barium sulfate nanoparticles in inverse microemulsions *Mater Chem Phys*, **40** 94-98

Gangopdhyay, R , De, A , Ghosh, G (2001) Polyaniline-poly(vinyl alcohol) conducting composite material with easy processability and novel application potential *Synth Met*, **123** 21-31

Gerard, M , Chaubey, A , Malhotra, B (2002) Application of conductmg polymers to biosensors *Biosens Bioelectron*, **17** 345-359

Grennan, K (2003) Developments in electrochemical immunosensors PhD Thesis School of Chemical Sciences, Dublin City Umversity, Ireland

Haba, Y , Segal, E , Narkis, M , Titelman, G , Siegmann, A (1999) Polymerization of aniline in the presence of DBSA in an aqueous dispersion *Synth Met*, **106** 59-66

Han, M , Cho, S , Oh, S , Im, S (2002) Preparation and characterisation of polyaniline nanoparticles synthesised from DBSA micellar solution *Synth Met*, **126** 53-60

Innis, P , Wallace, G (2002) Inherently conducting polymer nanostructures *J Nanosci Nanotech* , **2** 441-451

Killard, A J , Micheli, L , Grennan, K , Franek, M , Kolar, V , Moscone, D , Palchetti, I , Smyth, M R (2001) Amperometric separation-free immunosensor for real-time environmental monitoring *Anal Chim Acta,* **427** 173-180

Kim, B , Oh, S , Han, M , Im, S (2000) Preparation of polyanilme nanoparticles in micellar solutions as polymersation medium *Langmuir,* **16** 5841-5845

Kim, B , Oh, S , Han, M , Im, S (2001) Synthesis and characterisation of polyanilme nanoparticles in SDS micellar solutions *Synth Met* , **122** 297-304

Kinlen, P , Liu, J , Dmg, Y , Graham, C , Remsen, E (1998) Emulsion polymerisation process for organically soluble and electrically conducting polyaniline *Macromol* , **31** 1735-1744

Moulton, S , Innis, P , Kane-Maguire, L , Ngamna, O , Wallace, G (2004) Polymerisation and characterisation of conducting polyanilme nanoparticle dispersions *Curr App Phys* , 4 402-406

Oh, S , Im, S (2002) Electroconductive polymer nanoparticles preparation and characterisation of PANI and PEDOT nanoparticles *Curr App Phys* , **2** 273-277

Park, S , Cho, M , Choi, H (2004) Synthesis and electrical characteristics of polyaniline nanoparticles and their polymeric composite *Curr App Phys , In press*

Sadik, O , Wallace, G (1993) Pulsed amperometric detection of proteins using antibody containing conducting polymers *Anal Chim Acta,* **279** 209-212

Sharma, A , Annapoorni, S , Malhotra, B (2003) Characterisation of electrochemically synthesised poly(2-fluoroaniline) film and its application to glucose biosensor *Curr App Phys* , **3** 239-245

Somani, P (2003) Synthesis and characterisation of polyaniline dispersions *Mater Chem Phys* , **77** 81-85

# Chapter 5

## Electrocatalytic Biosensor Device based on a Cyclopentadienylnickel(II) Thiolato Schiff Base Spontaneously Adsorbed on Gold

## 5.1 INTRODUCTION

Modification of electrodes by spontaneous adsorption has received widespread attraction in the fabrication of effective surfaces suitable in catalysis (Stolarczyk *et al*, 2003), molecule or ion recognition (Yantasee *et al*, 2004), and electron transfer (Jun & Beng, 2004) The easy and reliable fabrication procedure, rapid response, enhanced sensitivity and selectivity are the advantages of these types of modified electrodes Different spontaneous adsorption strategies have been employed on electrode surfaces, such as Langmuir–Blodgett (LB) transfer (Wilke & Baruzzi, 2002) and self-assembly techniques (Vergheese & Berchmans, 2004) Although LB films formed by physisorption of amphiphiles have been applied successfully to sensors, they are thermodynamically unstable and consequently, minor changes m temperature, or exposure to solvent can ruin their two dimensional structure (Chaki & Vijayamohanan, 2002) Self-assembled monolayer (SAM) formation, pioneered by Nuzzo and Allara in 1983, has emerged as a simpler, low-cost and more powerful method of forming solid ultra-thin films of organosulphur compounds and their derivatives onto noble metals Other formats have also been developed recently such as silane-based monolayers on silicon (Hamelmann *et al*, 2004), glass (Elmore *et al*, 2004), and metal oxide (Lee & Laibims, 1998) substrates From an electrochemistry viewpoint, the most important class of SAM is formed by chemisorption of thiolates on gold These SAMs form stable, well-packed and highly ordered ultra-thin films Apart from gold, other metals such as silver, platinum and copper may also serve as substrate materials for organosulphur SAMs However, the reasons why gold is most popular for thiol SAMs are that it is a relatively stable inert metal that does not have a stable oxide under ambient conditions and it possesses a strong specific interaction with sulphur that allows the formation of monolayers m the presence of many other functional groups (Ozoemena & Nykong, 2003)

Spontaneous adsorption of complexes on gold electrodes has yielded very promising results m the field of electroanalytical chemistry Electrodes modified in this way can be the basis of the molecular design of interfaces for special application leading to several applications including chemical sensing, control of surface properties such as wettability and friction, patterning and semiconductor passivation

These types of modified electrodes are very promising for the construction of electrochemical biosensors for various reasons Firstly, since they use only the bare minimum resources, (e g a monolayer comprised of $10^{13}$ molecules $cm^{-2}$), miniaturisation is easy Also, they can enhance selectivity and sensitivity, improve response time and decrease over-potential (Raj & Ohsaka, 2001), and along with the chemical stability of the layer, even after its coupling with immobilised molecules, gives them potential in biosensor applications

The preparation of the spontaneously adsorbed layers on electrodes is simple The desired substrate just has to be dipped in the required dilute solution for a specific time followed by thorough washing with the same solvent and drying Gas phase evaporation of the adsorbent has also been used as a method to form good monolayers (Xiao *et al*, 2001) Several factors affect the formation and packing density of monolayers, like the nature and roughness of the substrate, the solvent, the nature of the adsorbate, temperature and the concentration of the adsorbate Both cleanliness and the crystalline nature of the substrate also play a crucial role in determining the compactness of the layer For most substrates, rigorous cleaning procedures and substrate pre-treatment are necessary before spontaneous adsorption will occur Rigorous polishing, followed by subjection of the electrode to a fresh Piranha solution ($H_2SO_4$/30% v/v $H_2O_2$ = 3 1) and further cycling in dilute $H_2SO_4$ for verification of cleanliness is the most cited method in the literature However, other methods such as flame annealing (Krings *et al*, 2003) and the use of plasma cleaner under argon plasma (Stine *et al*, 1999) have also been used SAM formation, in particular, uses a very dilute solution gives ordered monolayers, whereas a high concentration and long-time (6 days) favour multi-layer formation (Chaki *et al*, 2002) Thiol, sulphide and disulphide are commonly adsorbed from high purity solvents such as ethanol, hexane, acetonitrile, etc (Chaki *et al*, 2002) Mixed monolayers can be achieved by using a solution containing two or more thiol compounds This unique finding can be exploited in such a way that steric hindrance between bulky molecules can be avoided (*Figure 5 1*) Chain length is another important parameter as dense monolayers can be obtained by controlling the chain length This results in a total suppression of reactions at the electrode surface However, if the complex is relatively short in length, either electron tunnelling across the layer, or penetration of electroactive species through defects in the layer occurs and electrochemical reaction can proceed at the electrode Phenyl and biphenyl

systems show good packing due to π - π interactions, but they are less stable than that of long chain alkanethiols (Aslam *et al.*, 2001). The influence of conjugated π-bonds on the electronic molecular conductivity has been investigated by Krings *et al.* (2003). Conjugated thiols have the ability to block oxide formation and oxygen evolution but can allow for high reaction rates for redox systems in the electrolyte solution.

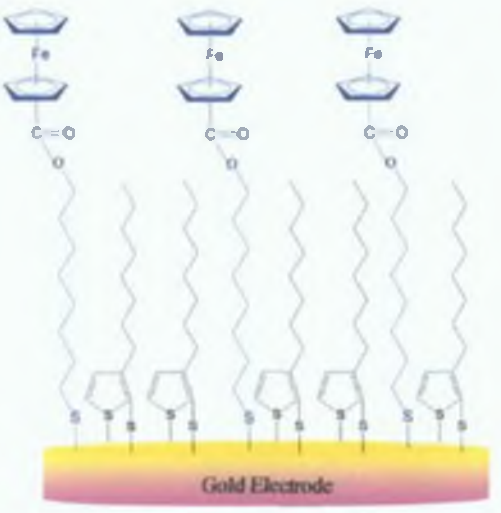


***Figure 5.1.*** Schematic of a mixed monolayer prepared from a molar ratio of 2-mercapto-3-*n*-octylthiophene and ferrocene-terminated alkanethiol (Peng *et al.*, 2004) (optimum molar ratio: 9:1). The mixed monolayer contains electroactive Fc centers which are spaced sufficiently apart so that they do not interact with each other. The alkylthiophene acts as a spacer between the electroactive sites.

Since a spontaneously adsorbed layer can serve as an layer between a noble metal surface and a species present in solution or vapour phase, its advantages for utilisation towards molecular recognition (or chemical sensing) are clear. Selectivity offered by biomolecules such as enzymes, antibodies and nucleic acids or even organised systems such as whole cells can be exploited in conjunction with spontaneously adsorbed layers to produce a biosensor. Also, a control over the orientation of the biomolecule allows tremendous flexibility in design.

Enzyme immobilisation on spontaneously adsorbed layers has been extensively studied. The traditional techniques such as direct covalent attachment, cross-linking and adsorption have all been used to date. Direct covalent attachment may be the most promising technique amongst these due to the stability of the resultant bond (Gooding & Hibbert, 1999). A popular and highly versatile method for

covalently attaching proteins to a spontaneously adsorbed layer is by using carbodiimide coupling which couples amines to carboxylic acid Martele *et al* (2003) used this approach for immobilising GOD and HRP to a gold electrode In order to increase sensitivity, multilayers were formed by consecutive adsorption of polycations and negatively charged proteins Direct covalent attachment was compared to the non-covalent methods of adsorption (Ge & Lisdat, 2002) and cross-linking (Campuzano *et al* , 2002) for cytochrome *c* and GOD, respectively Both papers found that the non-covalent immobilisation methods yielded higher electron transfer rate constants for the respective redox proteins

One of the important advantages of these types of biosensors is that their stability coupled with the behaviour of electroactive complexes as selective electron-tunnelling or 'gates' makes them suitable as substrates for monitoring biomolecular reactions Alkanethiols have been modified to include electroactive moieties (for mediator or electron transfer function), so that adsorbed layer can be used for electrical wiring or communication between redox-active enzymes and the electrode surface Several of these alkanethiols functionalised with electron transfer mediators have been used for biosensing Campuzano *et al* (2002) used an alkanethiol modified withtetrathiafulvalene and glucose oxidase for glucose detection Li *et al* (1997) used a viologen-functionalised SAM, modified with HRP for peroxide detection Xu *et al* (2003) recently used self-assembling gold nanoparticles on thiol-functionalised poly(styrene-*co*-acrylic acid) nanospheres as a simple platform for a biosensing HRP was immobilised on surface of the nanoparticles and the sensor displayed an electrocatalytic response to the reduction of peroxide without the need for an additional mediator All of these mediated SAM surfaces provide the conduction pathways necessary, and allow efficient electron-tunnelling, which makes it possible to realise direct electron-transfer from the enzymes or proteins to the electrode surface

The present work describes a novel cyclopentadienylnickel(II) compound $[Ni(SC_6H_4C(H)NC_6H_4OCH_2CH_2SMe)(\eta^5\text{-}C_5H_5)]_2$ as the active redox centre for a spontaneously adsorbed layer This was in part due to the reversible redox behaviour found for such compounds For example, Ho *et al* (1990) have found that compounds of the type $[Ni(cp)_2(SR)_2]$, where R = Ph or $PhCH_2$, (Ph = phenyl) have reversible redox couples at low positive potentials Recently, the study has been extended by

Moutloali (2003) to Schiff base analogues of the compounds mentioned in the work of Ho *et al* (1990) and similar results were obtained These complexes exhibit low positive redox potentials and are inert to moisture and air, thus making them suitable candidates for spontaneous adsorption on electrodes for sensor applications In this work, the electrochemical behaviour of the cyclopentadienylnickel(II) thiolato Schiff base compound, $[Ni(SC_6H_4C(H)NC_6H_4OCH_2CH_2SMe)(\eta^5\text{-}C_5H_5)]_2$, was probed in solution, and its spontaneously adsorbed analogue was interrogated using electrochemical techniques To assess its efficiency in an electrocatalytic biosensor device, horseradish peroxidase was electrostatically applied to the surface of the spontaneously adsorbed layer for the amperometric detection of hydrogen peroxide

## 5.2 MATERIALS AND METHODS

### *5.2.1 Materials*

Tetrabutylammonium tetrafluoroborate ([n-$Bu_4N$][$BF_4$], 21,796-4), horseradish peroxidase (HRP, 1,110 U/mg, P6782) and 30% (v/v) hydrogen peroxide solution (31642) were purchased from Sigma-Aldrich Dichloromethane and acetone were purchased from B & M Scientific (South Africa) All other reagents were of analytical grade and were used as obtained from the suppliers without further purification All complexes were prepared by Dr Moutloali (University of the Western Cape, South Africa) Complexes [$Ni(SC_6H_4C(H)NC_6H_4OC_nH_{2n+1})(\eta^5$-cp)]$_2$, where cp = cyclopentadienyl (*Figure 5 2* [1]), and [$Ni(SC_6H_4C(H)NC_6H_4OC_nH_{2n+1})(\eta^5$-dtc)]$_2$, where dtc = diethyldithiocarbamato (*Figure 5 2* [2]) were prepared as described by Moutlaoli (2003) The complex [$Ni(SC_6H_4C(H)NC_6H_4OCH_2CH_2SMe)(\eta^5$-$C_5H_5)]_2$ (*Figure 5 2* [3]) was prepared as described by Morrin *et al* (2004) A brief description of this synthesis is given in *Section 5 2 3* All reactions were performed under a nitrogen atmosphere, but the air and moisture stable complexes that were formed were worked-up in air

### *5 2.2 Buffers and solutions*

All electrochemical measurements were carried out in phosphate buffered saline (PBS), (0 1 mol $dm^{-3}$ phosphate, 0 137 mol $dm^{-3}$ NaCl and 2 7 mmol $dm^{-3}$ KCl), pH 7 4, unless otherwise stated

### *5.2 3 Synthesis of [$Ni(SC_6H_4C(H)NC_6H_4OCH_2CH_2SMe)(\eta^5$-$C_5H_5)]_2$*

4-hydroxybenzaldehyde (1 0 g, 8 19 mmol $dm^{-3}$) was dissolved in acetone and then charged with finely ground $K_2CO_3$ (5 g) 1-chloroethylmethylsulphide (1 82 ml, 16 38 mmol $dm^{-3}$) was added to the mixture The reaction mixture was refluxed for 48 h The mixture was filtered and the solvent removed from filtrate to leave a pale orange-yellow liquid ($OHCC_6H_4OCH_2CH_2SMe$)

4-aminothiophenol (0 34 g, 2 71 mmol $dm^{-3}$) and $OHCC_6H_4OCH_2CH_2SMe$ (0 5 ml, 2 71 mmol $dm^{-3}$) were dissolved in toluene (50 ml) Acetic acid (2 drops) was added to the solution and the reaction left for 18 h at room temperature Solvent was removed from the solution to leave a yellow residue which was crystallized from $CH_2Cl_2$ hexane (1 3) mixture at –15 °C $HSC_6H_4C(H)NC_6H_4OCH_2CH_2SMe$ was isolated as a yellow precipitate

A mixture of $HSC_6H_4C(H)NC_6H_4OCH_2CH_2SMe$ (0 3 g, 0 99 mmol $dm^{-3}$) and nickelocene (0 19g, 0 99 mmol $dm^{-3}$) were dissolved in toluene (40 ml) to give a green solution The reaction was left for 18 h and the colour gradually turned brown-black The mixture was filtered and the filtrate concentrated to half the original volume and hexane (40 ml) added The solution was stored at –15 °C to form the black precipitate ($[Ni(SC_6H_4C(H)NC_6H_4OCH_2CH_2SMe)(\eta^5\text{-}C_5H_5)]_2$) (*Figure 5 2* [3]) Yield = 0 11 g, 24% $^1$H NMR ($CDCl_3$) δ 8 44 (s, 2H, C(H)N), 8 10 (d, 4H, $J_{HH}$ = 8 6 Hz, $C(H)C_6H_4$), 7 88 (d, 4H, $J_{HH}$ = 8 6 Hz, $NC_6H_4$), 7 04 (dd, 8H, $SC_6H_4$, $OC_6H_4$), 4 63 (s, 10H, $C_5H_5$), 4 24 (t, 4H, $OCH_2$), 2 94 (t, 4H, $SCH_2$), 2 25 (s, 6H, $SCH_3$) Anal calcd for $C_{42}H_{42}N_2O_2S_4Ni_2$ C, 58 22, H, 4 97, N, 3 23 % Found C, 58 61, H, 4 55, N, 3 59 % $^1$H NMR spectra of [3] available in *Section 5 5*

### *5.2 4 Instrumentation*

All experiments were carried out at the University of the Western Cape, South Africa Electrochemical protocols were performed on a BAS 50/W electrochemical analyser with BAS 50/W software, using either cyclic voltammetry (CV), Osteryoung square wave voltammetry (OSWV), or time-based amperometric modes A conventional three electrode system was employed The working electrodes were glassy carbon (diam 1 5 mm, Cypress Systems) and gold (diam 1 mm, Cypress Systems) Silver/silver chloride (Ag/AgCl) and a platinum wire were used as reference and auxiliary electrodes, respectively

[1]

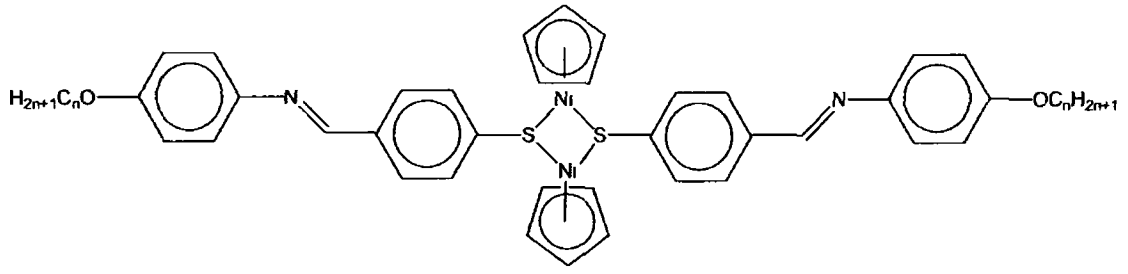


n = 4, 14, 16

[2]

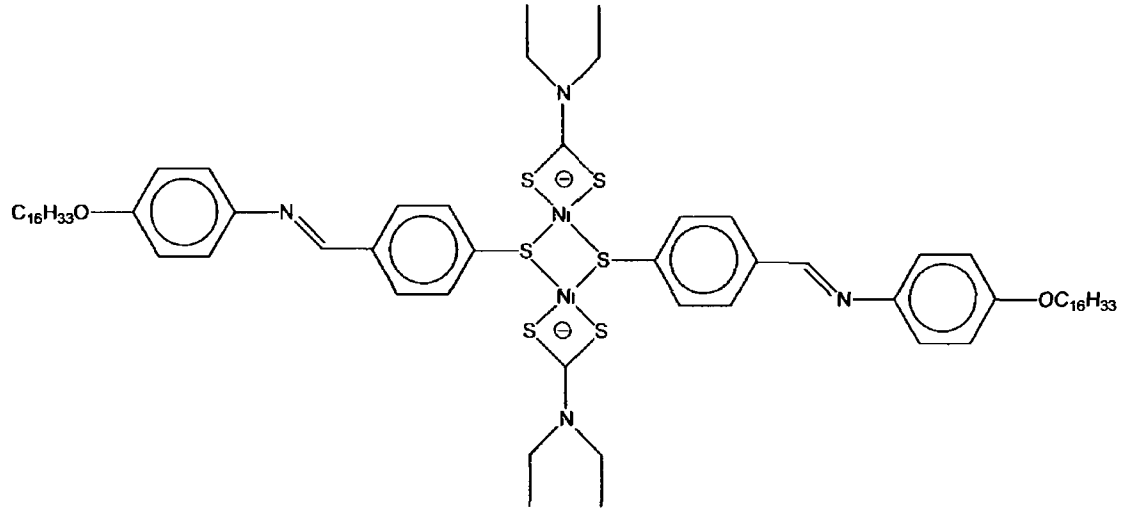


[3]

***Figure 5 2.*** Structures of thiolato Schiff bases used for electrochemical analysis [1] and [2] were characterised electrochemically, and [3] was subsequently designed for use in an electrocatalytically active spontaneously adsorbed layer

### *5 2.5 Electrochemical characterisation of nickel(II) $\mu_2$-thiolato Schiff base compounds*

Prior to use, glassy carbon electrodes were first polished on aqueous slurries of 1 μm, 0 3 μm and 0 05 μm alumina powder, and rinsed thoroughly in both deionised water and acetone

All cyclic voltammograms were carried out at scan rates of 50 mV $s^{-1}$, unless otherwise stated Square wave voltammograms were carried out using a step potential of 4 mV, an amplitude of 25 mV, and a frequency of 15 Hz Potential step chronocoulometry was carried out using a pulse width of 2 5 s

### *5.2.6 Spontaneous adsorption of cyclopentadienylnickel(II) thiolato Schiff base on gold electrode*

Prior to use, gold electrodes were first polished on aqueous slurries of 1 μm, 0 3 μm and 0 05 μm alumina powder After thorough rinsing in deionised water followed by acetone, the electrodes were etched for about 5 min in a hot 'Piranha' solution {1 3 (v/v) 30 % $H_2O_2$ and concentrated $H_2SO_4$} and rinsed again with copious amounts of deionised water and then deposition solvent, $CH_2Cl_2$ (Caution Piranha's solution is a powerful oxidising agent and reacts violently with organic compounds It is necessary to prepare solution under fumehood conditions and protects hands with gloves) Finally the electrode was placed in a solution of 0 5 mol $dm^{-3}$ $H_2SO_4$ and 10 voltammetric cycles were carried out between –1200 mV and +1500 mV at 50 mV $s^{-1}$ vs Ag/AgCl Following this pre-treatment, the electrode was rinsed with $CH_2Cl_2$, and immediately placed in a 1 ml solution of [3] ($1 \times 10^{-3}$ mol $dm^{-3}$) for 24 h at room temperature Upon removal from the $CH_2Cl_2$ deposition solution, the electrode was thoroughly rinsed with $CH_2Cl_2$ Finally, in order to observe redox activity of the spontaneously adsorbed layer, a single voltammetric cycle in 0 1 mol $dm^{-3}$ NaOH between –200 mV and +600 mV vs Ag/AgCl was required

### *5 2.7 Electrostatic immobilisation of HRP*

Following electrode modification, the electrode was transferred to a 1 ml batch cell The electrode was oxidised in 0 1 mol $dm^{-3}$ phosphate buffer solution, pH 7 4, in the presence of HRP (1 mg $ml^{-1}$) at +700 mV vs Ag/AgCl, sample interval of 500 ms, over 1500 s at a sensitivity of $1 \times 10^{-9}$ A $V^{-1}$ During this oxidation, the enzyme becomes electrostatically attached to the modified electrode surface The enzyme solution was carefully recovered from the cell, and re-stored for later use

### *5.2.8 Real-time monitoring enzyme/substrate interactions in a batch cell*

After the immobilisation of HRP (*Section 5 2 7*), the electrode was transferred to a 1 ml batch cell Amperometric experiments were performed at –100 mV vs Ag/AgCl wire electrode, with a sample interval of 100 ms and a sensitivity of $1 \times 10^{-4}$ A $V^{-1}$ in phosphate buffer, pH 7 4 $H_2O_2$ was added to the cell as required

## 5.3 RESULTS AND DISCUSSION

### *5 3 1 Electrochemistry of nickel(II) $\mu_2$-thiolato Schiff base compounds*

Cyclic voltammetry was used to investigate the redox electrochemistry of two types of nickel(II) $\mu_2$-thiolato Schiff base compounds of the form $[Ni(SC_6H_4C(H)NC_6H_4OC_nH_{2n+1})(\eta^5\text{-}C_5H_5)]_2$ [1], and $[Ni(SC_6H_4C(H)NC_6H_4OC_nH_{2n+1})(\eta^5\text{-dtc})]_2$ [2] (*Scheme 5 1*) Both compounds exhibited starkly different electrochemistry due to the different natures of the substituents on their metal centres While the cyclopentadienyl (cp) complexes exhibited reversible to quasi-reversible behaviour (dependent on alkoxy chain length) for the most favourable nickel redox transition, Ni(II)/Ni(III), no electrochemistry corresponding to this couple was observed for diethyldithiocarbamato (dtc) complexes Two additional redox couples, attributable to Ni(I)/Ni(II) and Ni(III)/Ni(IV), could also be observed electrochemically, and exhibited different behaviour dependent on the class of compound This behaviour will be discussed and rationalised in this section

Initially, square wave voltammetry (OSWV) was carried out for [1, *n=16*] and [2, *n=16*] in order to elucidate their respective redox activities (*Figure 5 3*) While three sets of redox peaks were observed for [1] (*Figure 5 3a*), only two couples were observed for [2] (*Figure 5 3b*) In addition, [1] displayed greater reversibility than [2], for the peaks observed, showing that the cp attached to the Ni in [1], had greater polarisable or stabilisation properties than when dtc was bound to the Ni as in [2]

The first redox couple, (i), observed for both types of complexes had half-wave potential ($E_{1/2}$) values of –1052 mV and –892 mV for [1] (*Figure 5 3a*) and [2] (*Figure 5 3b*), respectively This was attributed to the Ni(I)/Ni(II) redox couple This redox couple is reversible for [1] and irreversible for [2] A second couple, (ii), Ni(II)/Ni(III) was redox active only in [1] Little or no redox activity occurred for [2] A third redox process, (iii), occurred with $E_{1/2}$ values of +833 mV and +760 mV for [1] and [2], respectively This was seen to be irreversible for both types of complexes and was attributed to Ni(III)/Ni(IV) electrochemistry

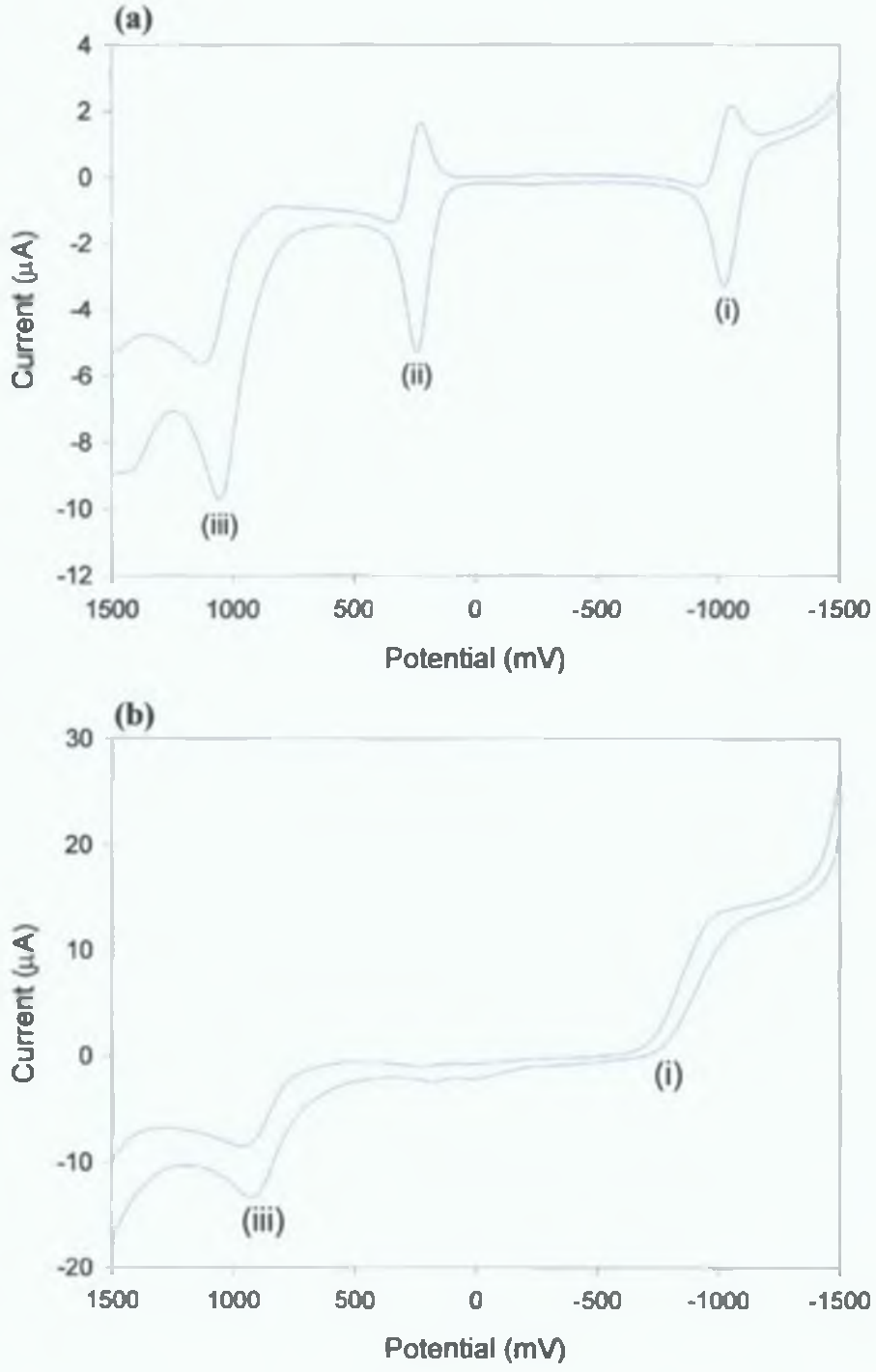


***Figure 5.3.*** Anodic square wave voltammogram for (a) [1] and (b) [2], ($1 \times 10^{-3}$ mol $dm^{-3}$), identifying the Ni redox active regions. Redox peaks were assigned as (i) Ni(I)/Ni(II), (ii) Ni(II)/Ni(III) and (iii) Ni(III)/Ni(IV) (Moutloali, 2003).

The observed differences in the electrochemistry cannot be explained solely by examining the electrochemical properties of these complexes as both carry a negative charge The irreversibility of the redox couples in the dtc complexes may be explained with the possibility that a chemical step follows the electrochemical process, i e , an EC mechanism

Bowmaker *et al* (1982) have studied a series of nickel(II) bis(dialkydithiocarbamate) complexes, $Ni(R_2NCS_2)_2$, and found that at best the complexes exhibit a quasi-reversible one-electron redox behaviour In the complexes studied by Bowmaker, the peak current ratios of the reverse to the forward scans varies from 0 77 to 0 94 for scan rates in the range of 50 to 200 mV $s^{-1}$ Thus, the reversibility increased on increasing the scan rate, a diagnostic feature of an irreversible process They reasoned that the behaviour was due to the species that was initially formed in the electrochemical process changing to some other form or decomposing to products that are not reoxidized at the same potential as the original species Analysis of the variation in current ratios to scan rates showed that the electrochemical process was followed by a first order chemical process or EC mechanism This may also be what occurs in the dtc complexes in this instance, where the lack of reversibility may be due to a chemical process rapidly following the electrochemical process

Electrochemical studies on [2] were abandoned at this stage, due to its electrochemical instability Further kinetic studies were undertaken to monitor the behaviour of [1], which behaved much more ideally Cyclic voltammetric scan rate studies were carried out for each of the redox couples observed in *Figure 5 3a* Both the Ni(I)/Ni(II) and the Ni(II)/Ni(III) redox couples were shown to behave as typical diffusion-limited species when $i_{p\,a}$ was plotted against $\upsilon^{1/2}$, with $r^2$ values of 0 997 and 0 985, respectively However, the third couple, which was shown to be irreversible, did not display this linear dependence on $\upsilon^{1/2}$ This redox couple was not kinetically stable (*data not shown*) when multiple cycles were carried out at a single scan rate, indicating a more complex mechanism or instability An explanation such as an EC mechanism could explain its behaviour

Due to the low potential required for the Ni(II)/Ni(III) redox couple, and therefore its potential usefulness as a mediator in applications such as biosensors, a rigorous electrochemical analysis of this redox couple was carried out The alkoxy

chain length was varied so that n = 4, 14 and 16. The effect of varying the length of this substituent was monitored.

CVs were carried out in the potential range –200 mV to +600 mV at a scan rate of 50 mV $s^{-1}$ (*Figure 5.4*). The electrochemistry of the Ni(II)/Ni(III) redox couple was within this range for all chain lengths analysed. [1, *n=4*] showed an additional peak at approximately +400 mV. This may just be due to an unstable interfering species present in that particular sample, as it was the only complex where this was observed.

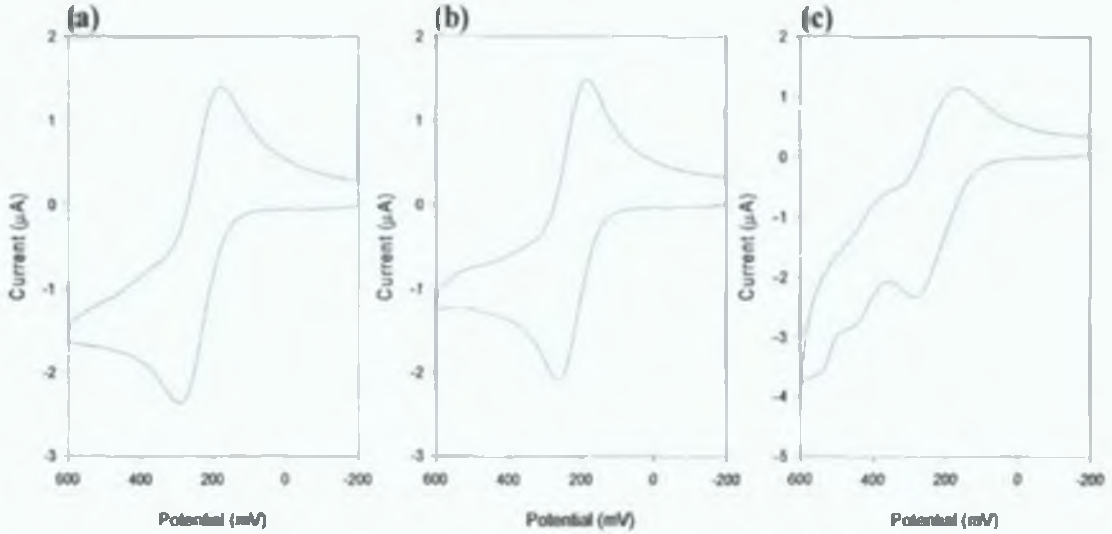


***Figure 5.4.*** Cyclic voltammograms for complexes (a) [1, *n=16*], (b) [1, *n=14*], and (c) [1, *n=4*] ($2 \times 10^{-3}$ mol $dm^{-3}$), from –200 to +600 mV. Scan rate: 50 mV $s^{-1}$.

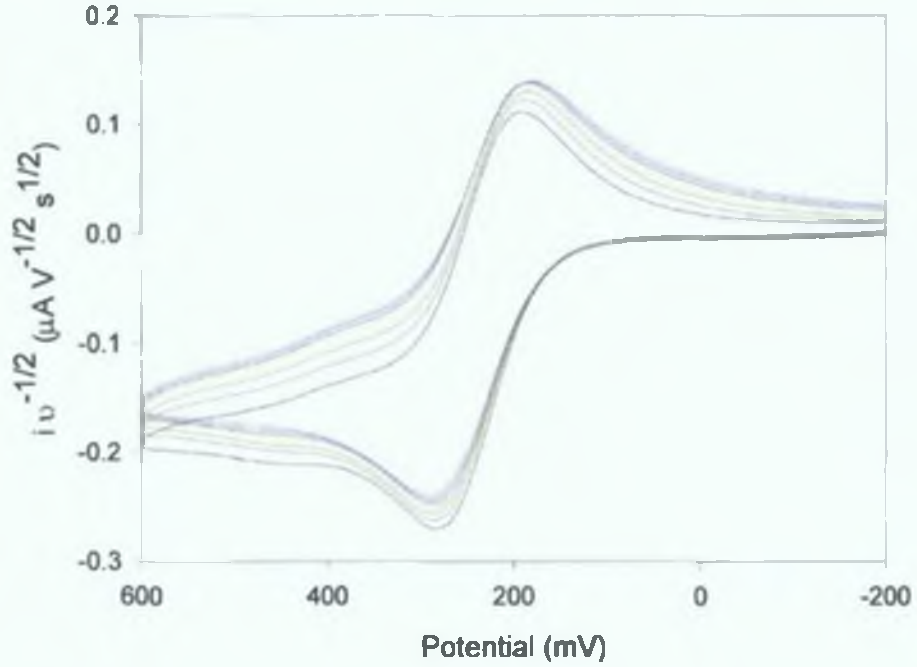


***Figure 5.5.*** Normalised currents for the change of rate of diffusion for scan rates ranging from 30 mV $s^{-1}$ (black) to 100 mV $s^{-1}$ (light blue) for complex [1, *n=16*].

***Table 5.1.*** Table of CV parameters for [1] with varying chain lengths. Scan rate: 100 mV $s^{-1}$.

| *n* | $E_{1/2}$ *(mV)* | $\Delta E_p$ *(mV)* | $i_{p,a}/i_{p,c}$ |
|---|---|---|---|
| 16 | 229 (± 12) | 61 (± 3) | 0.874 (± 0.048) |
| 14 | 227 (± 4) | 90 (± 9) | 0.955 (± 0.016) |
| 4 | 207 (± 5) | 104 (± 7) | 0.774 (± 0.077) |

$E_{1/2}$ values for the Ni(II)/Ni(III) redox couple were dependent on the alkoxy chain length (Table 5.1). Values for the longer alkoxy chain lengths, n = 16 and 14, were +229 (± 12) mV and +227 (± 4) mV, respectively. However, when n was decreased to 4, $E_{1/2}$ decreased to a value of +207 (± 5) mV, demonstrating that shorter alkoxy chain nickel(II) $\mu_2$-thiolato Schiff base compounds undergo redox reaction more easily. Increases in chain length serve to increase the overall stability of the complex, making it more difficult to oxidize.

$\Delta E_p$ values were also dependent on chain length. $\Delta E_p$ values increased as the chain length was decreased. For example, [1, *n=16*] had a $\Delta E_p$ value of 61 (± 3)

mV, [1, *n=14*] of 90 (± 9) mV, while [1, *n=4*] had a value of 104 (± 7) mV For a reversible process, $\Delta E_p$ values of 59 mV are expected for n electrons transferred Values of $\Delta E_p$ greater than 80 mV are usually associated with quasi-reversible redox behaviour Therefore, [1, *n=16*] can be termed reversible, but increasing quasi-reversible behaviour was observed for [1, *n=14*] and [1, *n=4*], where the chain length of the ligand was decreased In addition to $\Delta E_p$ values, reversibility of redox reactions can also be determined by the peak current ratios ($i_{p\,a}/i_{p\,c}$) A ratio of $i_{p\,a}/i_{p\,c}$ equal to unity is a measure of reversibility This ratio should also approach unity for quasi-reversible systems provided $\alpha_a = \alpha_c = 0\,5$ (where $\alpha$ is the transfer coefficient Subscripts a and c indicate anodic and cathodic processes, respectively) (Kemp, 2001) Ratios much lower than unity signify irreversible redox behaviour *Table 5 1* shows both $\Delta E_p$ and $i_{p\,a}/i_{p\,c}$ ratios for each of the complexes studied, and confirms the reversibility of [1, *n=16*] and quasi-reversibility of [1, *n=14*] and [1, *n=4*] for the Ni(II)/Ni(III) redox process, assuming $\alpha_c = \alpha_a = 0\,5$

A plot of $-i_{p\,a}\,\upsilon^{-1/2}$ vs potential can be carried out to determine the reversibility of a redox reaction For reversible systems, such normalized voltammograms should superimpose at all sweep rates *Figure 5 5* demonstrates the ideal reversibility of the Ni(II)/Ni(III) electrochemistry in [1, *n=16*]

Tafel analysis (Kemp, 2001) was used to deduce the number of electrons transferred for each of the complexes CVs were performed at slow scan rates (e g 5 mV $s^{-1}$) in order to ensure the redox reaction was mass transfer controlled, and no kinetic limitations were present Plots of ln i vs potential were then plotted, and the Tafel region identified Linearity outside the Tafel region is lost due to diffusion control

The slope of this plot was

$$\text{slope} = \frac{n\alpha_a F}{RT} \qquad \textit{Equation 5 2}$$

where R is the gas constant, T is the temperature in Kelvin, n is the number of electrons transferred, $\alpha_a$ is the anodic transfer coefficient and F is the Faraday's constant

Taking $\alpha_a$ to be 0 5, (ideal), the number of electrons transferred was calculated All Tafel plots gave values of approximately 1 (*Table 5 2*) for the number

of electrons transferred *Figure 5 6* shows a typical Tafel plot for [1, n=14], where the number of electrons transferred was found to be 1 12

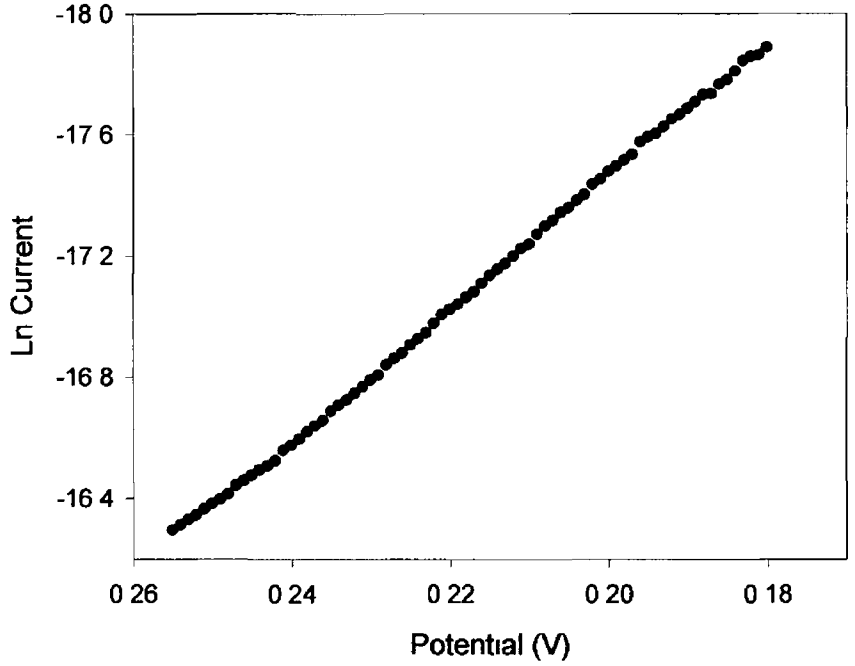


***Figure 5.6.*** Anodic Tafel plot for [1, n=14] Cyclic voltammogram carried out at 5 mV $s^{-1}$

Rate constants were calculated using chronocoulometry (Kemp, 2001) Chronocoulometric responses governed wholly or partially by the interfacial charge transfer kinetics were used, by using step potentials insufficiently extreme to enforce diffusion-controlled electrolysis throughout the experimental time domain In other words, steps were made to the potential in the rising portion of the sampled cyclic voltammogram The calculation of the rate constants was done by analysis of this charge (Q) vs time data When Q was plotted as a function of $t^{1/2}$, the data asymptotes to the straight line

$$Q = \frac{4nFA\vec{k}}{\pi} C(t_L^{1/2} t^{1/2} - t_L) \qquad \textit{Equation 5 3}$$

where *n* is the number of electrons transferred, A is the electrode area ($cm^2$) F is the Faraday's constant, C is the bulk concentration of the redox active species (mol $cm^{-3}$), $t_L^{1/2}$ is the intercept on the x-axis and $\vec{k}$ is the rate constant for the anodic process (cm $s^{-1}$)

Q is plotted as a function of $t^{1/2}$, over a range of concentrations at a constant step potential as in *Figure 5.7.*

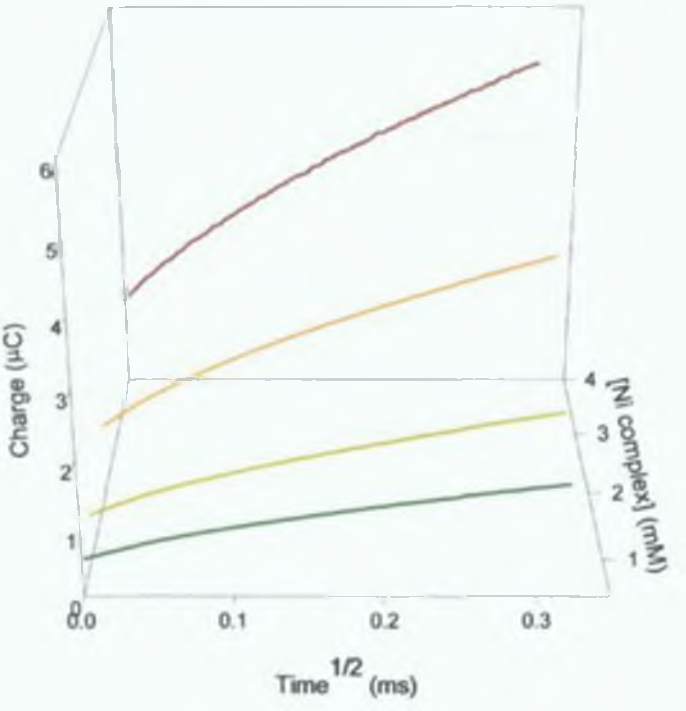


***Figure 5.7.*** Chronocoulometric plots showing the variation in concentration of Ni(II) of [1] as a function of charge and time (Step potential: +240 mV).

The slopes of these plots, m, (from *Figure 5.7*) are given by:

$$m = \frac{4nFA}{\pi} \bar{k} t_L^{1/2} C \qquad \textit{Equation 5.4}$$

By plotting these slopes as functions of $t_L^{1/2}C$, a value for $\bar{k}$ can be obtained.

The slopes of these plots, m, are given by:

$$m = \frac{4nFA}{\pi} \bar{k} t_L^{1/2} C \qquad \textit{Equation 5.4}$$

By plotting these slopes as functions of $t_L^{1/2}C$, a value for $\bar{k}$ can be obtained.

$\vec{k}$ is a function of potential according to the equation

$$\log \vec{k} = \log k^{\theta} - \frac{\alpha nF}{2.3RT}(E - E_{1/2}) \qquad \textit{Equation 5.5}$$

where $\vec{k}$ is the rate constant for the anodic process, $k^0$ is the true standard heterogeneous rate constant, R is the gas constant, T is the temperature in Kelvin, n is the number of electrons transferred, $\alpha$ is the transfer coefficient and F is the Faraday's constant

Therefore, a plot of log k vs $(E - E_{1/2})$ should therefore be linear, with an intercept of log $k^0$ (*Figure 5.8*) $k^0$ values for each of the complexes are given in *Table 5.2*

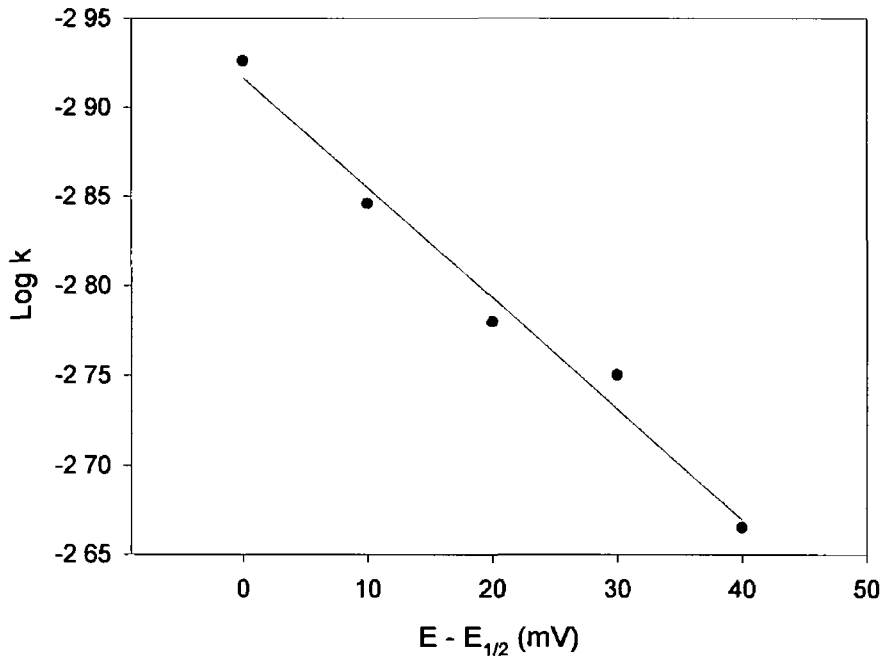


***Figure 5.8*** Plot of log k vs $(E - E_{1/2})$ for calculation of $k^0$ for [1] (y = -0.006x – 5.1541, $r^2 = 0.9718$)

The rate constants varied according to the chain length [1, *n=16*] which could be termed reversible from its CV parameters, yielded the highest rate constant ($5.1 \times 10^{-2}$ cm $s^{-1}$) [1, *n=14*] was approximately 2.5 times lower than [1, *n=16*] with a value of $1.5 \times 10^{-2}$ cm $s^{-1}$, while [1, *n=4*] was almost one order of magnitude lower than [1, *n=16*] ($0.5 \times 10^{-2}$ cm $s^{-1}$) Since the polarisability of the complex increases

with increasing chain length, the stabilization energy increases, which enhances the electron transfer rates

Diffusion coefficients, $D^0$, were calculated using potential step chronocoulometry Potential steps were taken from where insignificant electrolysis takes place in the solution, to a potential sufficient to enforce a diffusion-limited current throughout the experimental time domain In all cases, the potential was stepped from 0 mV to +600 mV The integrated form of the Cottrell equation gives the cumulative charge passed in oxidising the diffusing reactant

$$Q = \frac{2nFAD^{0\,1/2}Ct^{1/2}}{\pi^{1/2}} \qquad \textit{Equation 5 6}$$

Diffusion coefficients were shown to be independent of chain length All diffusion coefficients were measured in the same solvent ($CH_2Cl_2$) and as such were similar in magnitude ($\approx 1 \times 10^{-6}$ cm$^2$ s$^{-1}$)

***Table 5 2*** Table of calculated kinetic data for [1] with varying chain lengths

| *n* | *Calculated no of $e^-$ transferred* | *$k^0$ ($\times 10^2$ cm s$^{-1}$)* | *$D^0$ ($\times 10^6$ cm$^2$ s$^{-1}$)* |
|---|---|---|---|
| 16 | 1 1 | 5 1 | 8 7 |
| 14 | 1 1 | 1 5 | 9 3 |
| 4 | 1 4 | 0 5 | 5 1 |

### *5 3 2 Electrochemistry of a thiol-derivatised cyclopentadienylnickel(II) thiolato Schiff base compound [3]*

As the cyclopentadienylnickel(II) thiolato Schiff base compounds exhibited reversible electrochemistry at low positive potentials, modification of an electrode surface could be carried out with complexes of this type in order to develop an electrocatalytically active electrode surface A derivatised cyclopentadienylnickel(II) thiolato Schiff base, $[Ni(SC_6H_4C(H)NC_6H_4OCH_2CH_2SMe)(\eta^5\text{-}C_5H_5)]_2$ (*Figure 5 2*, [3]),was synthesised for spontaneous adsorption on a gold electrode The redox properties of this original

complex were initially studied in solution under stationary conditions at a gold disk electrode using cyclic voltammetry and square wave voltammetry in $CH_2Cl_2$ containing 0 1 mol $dm^{-3}$ [n-$Bu_4N$][$BF_4$] The concentration employed for the experiments was $2 \times 10^{-3}$ mol $dm^{-3}$

The CV shows a prominent redox wave with an $E_{1/2}$ value of +203 mV vs Ag/AgCl using a scan rate of 50 mV $s^{-1}$, which was attributed to the Ni(II)/Ni(III) redox couple (*Figure 5 9*) Sweeping the electrode through potentials outside of its potential window can deteriorate the behaviour of the system, due to formation of oxides or hydrogen evolution at the working electrode Therefore, although the Ni(II)/Ni(III) redox peaks appeared only to be quasi-reversible under these conditions, it was shown to be reversible when the potential was swept over a narrower range to isolate this redox couple (*Figure 5 10*) The purpose of sweeping the potential over a wide range was to survey all the electrochemistry of the complex It was seen that the Ni(II)/Ni(III) redox electrochemistry was the only activity present in the complex warranting further characterisation *Figure 5 10* is a cyclic voltammogram of the Ni(II)/Ni(III) redox couple Peak current was proportional to $\upsilon^{-1/2}$ ($r^2$ = 0 9998), and $\Delta E_p$ did not change with varying $\upsilon$ The redox couple was seen to be reversible at scan rates from 20 mV $s^{-1}$ to 250 mV $s^{-1}$ The peak potential difference ($\Delta E_p$) was 110 mV, and the anodic to cathodic peak current ratio ($i_{p\,a}/i_{p,c}$) was 1 05 ($\upsilon$ = 50 mV $s^{-1}$) These data suggest that the Ni(II)/Ni(III) redox couple behaved as a quasi-reversible redox couple Due to this Ni(II) Schiff base's strong redox properties, in conjunction with its methyl sulphide end-groups, the complex was further investigated in order to determine whether it could be spontaneously adsorbed onto a gold electrode to form an electrocatalytically active layer

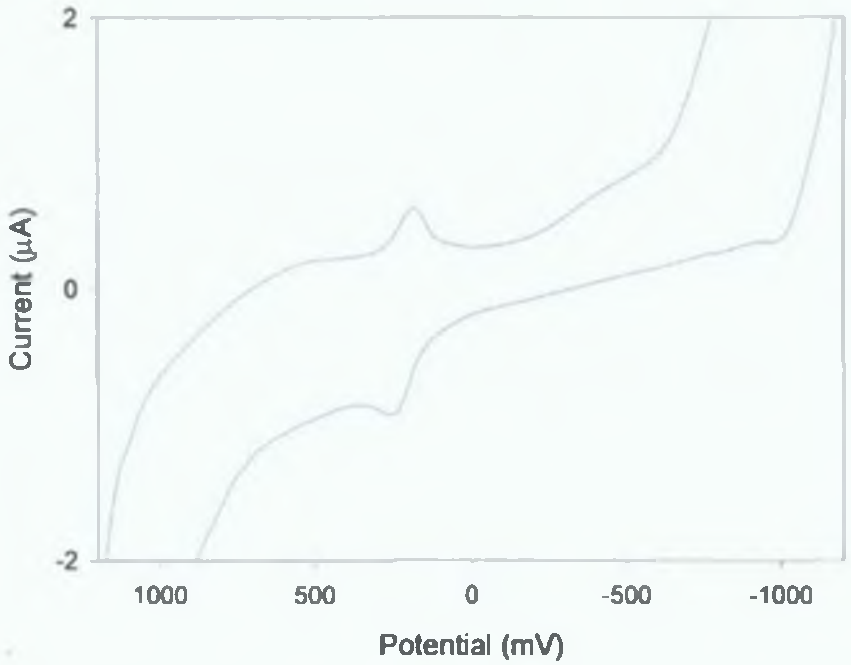


***Figure 5.9.*** Cyclic voltammogram for $[Ni(SC_6H_4C(H)NC_6H_4OCH_2CH_2SMe)(\eta^5\text{-}C_5H_5)]_2$ ($2 \times 10^{-3}$ mol $dm^{-3}$) on a 1.0 mm diameter bare gold disk electrode in $CH_2Cl_2$ containing 0.1 mol $dm^{-3}$ $[n\text{-}Bu_4N][BF_4]$. Scan rate: 50 mV $s^{-1}$.

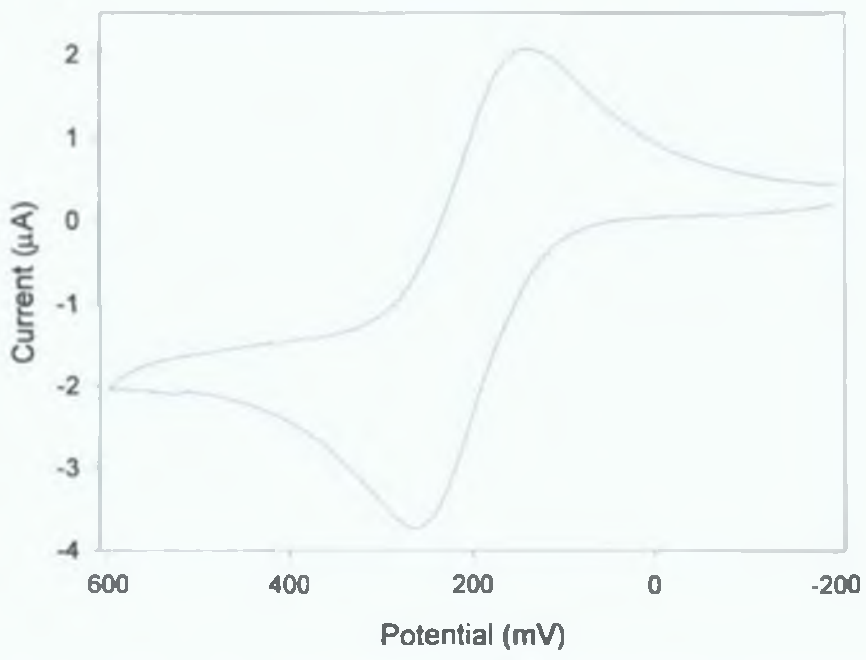


***Figure 5.10.*** Cyclic voltammogram for $[Ni(SC_6H_4C(H)NC_6H_4OCH_2CH_2SMe)(\eta^5\text{-}C_5H_5)]_2$ ($2 \times 10^{-3}$ mol $dm^{-3}$) from –200 mV to +600 mV. Scan Rate: 50 mV $s^{-1}$.

### 5.3.3 *Electrochemical characterisation of a thiol-derivatised cyclopentadienylnickel(II) thiolato Schiff base compound on gold*

In order to avoid oxidative S-S coupling in the thiol complex (Tour *et al.*, 1990), the thiol end groups were protected by a methyl group. However, before this spontaneously adsorbed complex exhibited measurable redox activity, it required voltammetric cycling in 0.1 mol $dm^{-3}$ NaOH, from –200 mV to +600 mV at 50 mV $s^{-1}$. *Figure 5.11* shows the CVs in 0.1 mol $dm^{-3}$ phosphate buffer solution, pH 7.4, before and after cycling in alkaline conditions. Prior to cycling in NaOH solution, the modified electrode showed little or no redox activity with respect to the Ni(II) metal centres. After a single cycle in NaOH, a set of quasi-reversible redox peaks, attributed to Ni oxidation and reduction was observed. When the number of cycles in 0.1 mol $dm^{-3}$ NaOH was increased, the areas under the anodic and cathodic peaks continued to grow, demonstrating that the number of redox active molecules on the surface of the electrode must have been increasing. Stability was reached after about 7 cycles in NaOH, and no further improvement in the peak heights was observed. The reason for this behaviour is unknown.

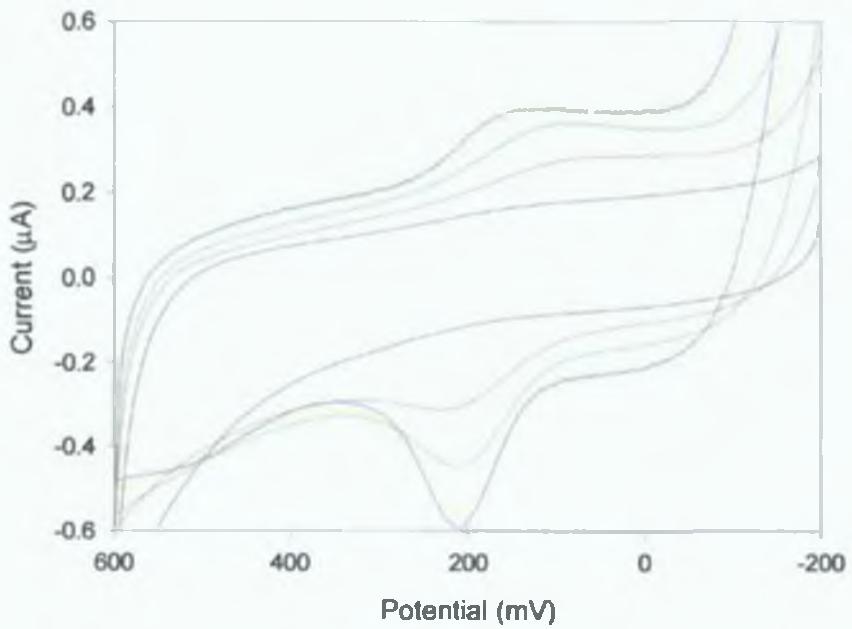


***Figure 5.11.*** CVs of the NaOH-treated spontaneously adsorbed layer on a Au electrode in 0.1 mol $dm^{-3}$ phosphate buffer, pH 7.4. Before cycling in NaOH (black), after 1 cycle (red), 3 cycles (green), 7 cycles (yellow) and 15 cycles (blue) in NaOH. Scan rate: 50 mV $s^{-1}$.

Verification that it was indeed the spontaneously adsorbed layer exhibiting the observed electrochemistry was carried out with a scan rate study It was observed that anodic current ($i_{p\,a}$) was directly proportional to scan rate, $\upsilon$, consistent with that anticipated for an electrochemical reaction involving a surface confined species ($r^2$ = 0 9997)

For the case of uniformly distributed non-interacting redox centres, located the same distance from the surface of the electrode, for reversible electron transfer reactions, the anodic and cathodic peaks in a CV, are at exactly the same potential, i e $\Delta E_p$ = 0 mV Any deviation from this can be assigned to either non-uniformity of the distribution of the redox centres with respect to their distance to the electrode surface, their interactions (e g electrostatic repulsions) or to the irreversibility of the charge transfer process involved (Krysinski *et al*, 1999) Given that in solution, the redox process approaches almost ideal behaviour, (*Figure 5 10*), the quasi-reversible nature (*Figure 5 11*) of the adsorbed complex must be attributed to non-uniformity on the surface, or molecular interactions within the adsorbed layer

Taking the number of electrons transferred to be one, the surface concentration, $\Gamma$, of the nickel redox centres observed from the graphical integration of the anodic wave (Li & Li, 2003) was found to be 3 10 × $10^{-11}$ mol $cm^{-2}$ This value is quite low, relative to other reported electroactive spontaneously adsorbed layers Li *et al* (1997) reported a surface coverage of 3 13 × $10^{-10}$ mol $cm^{-2}$ for their viologen-thiol self-assembled monolayer and Ozoemena & Nyokong (2002) reported a value of 1 0 × $10^{-10}$ mol $cm^{-2}$ for the surface coverage of a monolayer of octabutylthiophthalocyaninatoiron(II) The spontaneously adsorbed layer reported here has an estimated surface coverage one order of magnitude lower than these This would indicate that there is perhaps sub-monolayer coverage of the electrode surface, or that maybe not all the nickel groups adsorbed on the electrode surface are electroactive

### *5.3 4 Electrocatalytic reduction of $H_2O_2$ at the modified electrode*

The objective of this investigation was to develop a suitably modified electrode for the immobilisation of protein, in order to fabricate an electrocatalytic

sensor device where the Ni(II) centre of the thiolato Schiff base would behave as an electrocatalytic, non-diffusional mediator HRP was used as model enzyme HRP was electrostatically attached to the modified electrode surface by application of an oxidising potential in the presence of HRP (1 mg $ml^{-1}$), to electrostatically adsorb the enzyme to the surface (Iwuoha *et al*, (1997), Morrin *et al*, (2003)) *Figure 5 12a* depicts the CVs of the HRP/Ni(II)-modified electrode in phosphate buffer (pH 7 4), with no $H_2O_2$ present, in the presence of 50 μM $H_2O_2$, and 100 μM $H_2O_2$, under anaerobic conditions The CVs were performed at a scan rate of 5 mV $s^{-1}$ Despite the high background currents in the CVs, electrocatalytic production of the Ni(II) was seen An enhancement of the cathodic Ni(II) peak current was observed in the presence of $H_2O_2$, consistent with an electrocatalytic effect (Ruzgas *et al*, 1996) This electrocatalytic effect was not as clear for the anodic peak However, a small decrease in height was observed, providing extra evidence that the electro-produced Ni(II) was effectively consumed in the enzyme catalysis There was negligible shift in peak potential on addition of $H_2O_2$ The same experiment was also monitored using the square wave technique The voltammograms in *Figure 5 12b* represent the net current (difference between forward and reverse currents) when the electrode was scanned anodically The high background currents observed in the CVs were eliminated and the decrease in peak current heights upon additions of $H_2O_2$ was much more pronounced when compared with those observed in CV This was attributed to the high sensitivity of the square wave technique Electrocatalysis of the Ni(II) was verified with this result

In order to confirm the role of the HRP, cyclic voltammograms were carried out on a HRP-free surface CVs were run before and after addition of $H_2O_2$ While little or no change in the cathodic peak was observed, an increase m anodic peak current occurred (data not shown) This result indicates that the Ni(II)-modified electrode surface may have the ability to oxidise $H_2O_2$ However, for the purposes of this report, it can be said that Ni(II) complex alone cannot reduce the $H_2O_2$, and that HRP is playing an active role

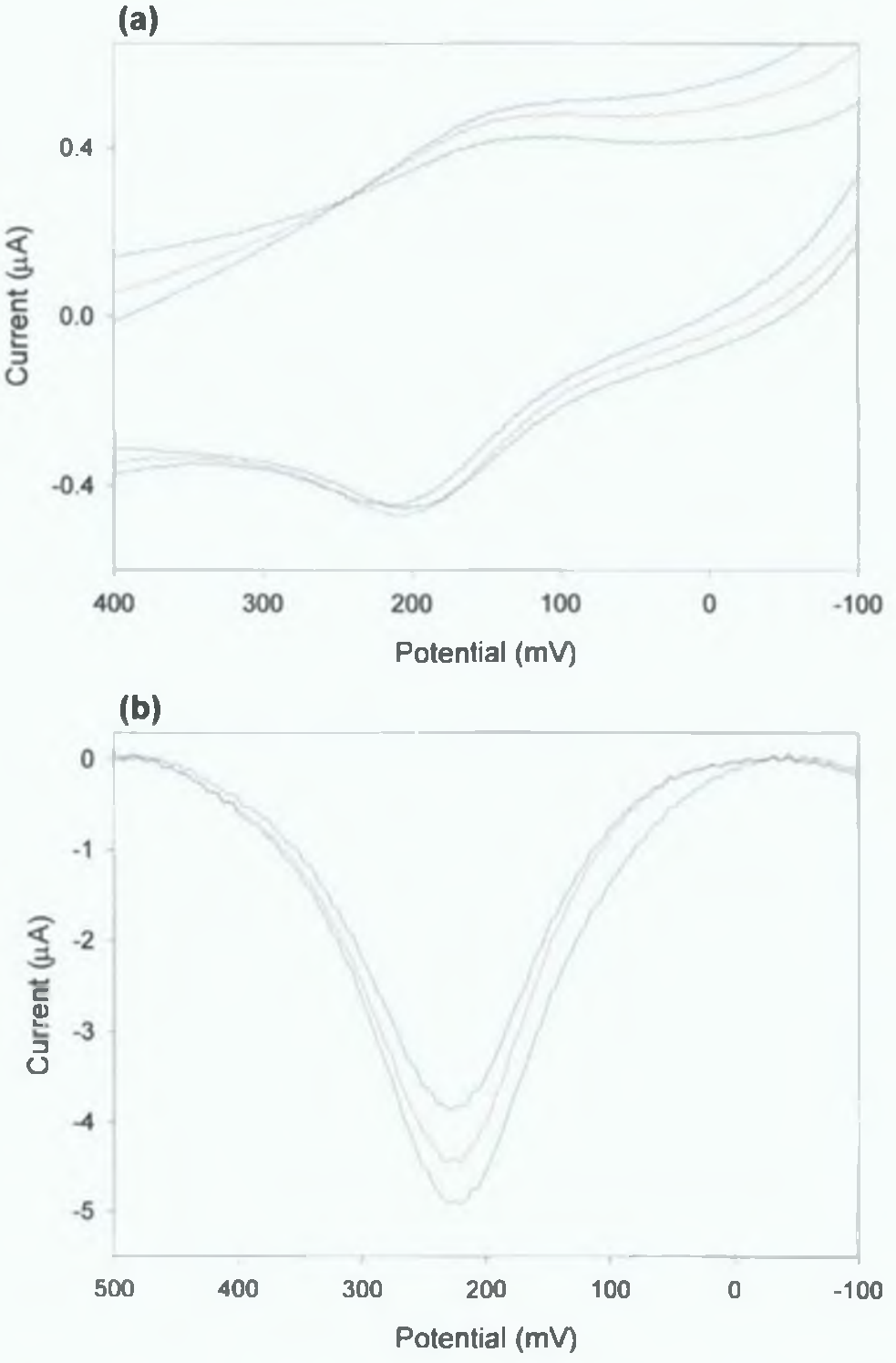


***Figure 5.12.*** (a) Cyclic (scan rate: 50 mV $s^{-1}$) and (b) anodic square wave (4 mV step potential, 25 mV amplitude, 15 Hz frequency) voltammograms of HRP/Ni(II)-modified Au electrode in 0.1 mol $dm^{-3}$ phosphate buffer, pH 7.4 for 0 μmol $dm^{-3}$ (green line), 50 μmol $dm^{-3}$ (red line) and 100 μmol $dm^{-3}$ (blue line) $H_2O_2$.

Current responses obtained by the electrocatalytic reduction of $H_2O_2$ by HRP were monitored using steady state amperometry Successive additions of $H_2O_2$ (6 25 μmol dm $^{3}$) to a stirred buffer solution (0 1 mol $dm^{-3}$ phosphate buffer solution, pH 7 4) were carried out The effect of applied potential on the catalytic signal and background current of the sensor was tested in the range between +200 mV and –300 mV vs Ag/AgCl An optimum ratio of catalytic signal-to-background noise was obtained at a potential of +200 mV Using an applied potential more positive than +200 mV resulted in oxidation current, due to oxidation of the peroxide by the modified electrode *Figure 5 13* is the peroxide calibration curve for the HRP/Ni(II)-modified electrode where the potential was held at +200 mV The sensor exhibited typical Michaelis-Menten kinetics The limit of detection was found to be 6 25 μmol $dm^{-3}$, based on a signal-to-background (S/B) level of 3 The apparent Michaelis-Menten constant, $K_m^{app}$, was calculated to be 27 3 μmol $dm^{-3}$, and the maximum current, $I_{max}$, was 678 2 nA $cm^{-2}$ *Figure 5 13* (inset) shows the steady state response observed for the reduction of $H_2O_2$ at the HRP/Ni(II)-modified electrode in a stirred batch system, in real-time A stable current response was obtained a few seconds after each $H_2O_2$ addition The response time of the sensor was less than 15 s (*Figure 5 13 (inset)*) These are modest characteristics compared to other systems based on electrocatalytic biosensing of $H_2O_2$ For example, enzyme electrodes based on conductmg polymers display particularly high sensitivities with detection limits in the submicromolar range reached Gaspar *et al* (2000) recently designed an impressive peroxidase biosensor based on a novel redox polymer that reached detection limits for $H_2O_2$ of 25 nmol $dm^{-3}$ The authors reported a $K_m^{app}$ of 386 μmol $dm^{-3}$ Other groups have also reported very sensitive peroxidase biosensors based on electrocatalytic surfaces (Tatsuma *et al*, 1992, Torriero *et al*, 2003) Although our novel approach has not yet reached these detection limits, it does provide advantages over other techniques in that the manner m which the modified electrode is prepared is an extremely versatile and simple approach for functionalising the electrode surface This technique can be improved upon by attempts to mcrease the electroactive nature of the Ni(II) molecules, and by optimising working parameters for enzyme catalysis, such as enzyme loading on the surface of the adsorbed layer, pH, adaptation to a flow cell etc

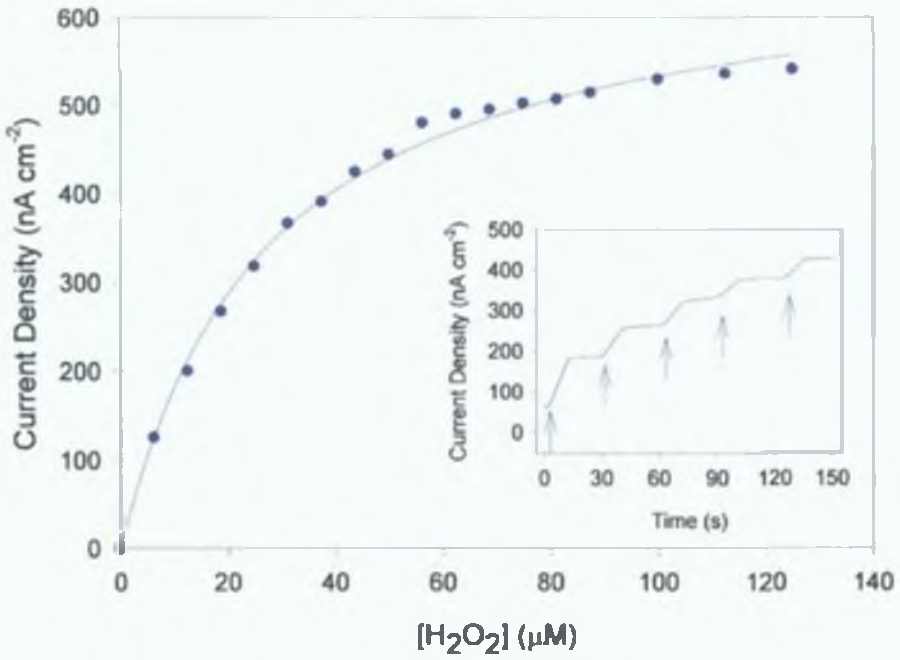


***Figure 5.13.*** The $H_2O_2$ response curve of the HRP/Ni(II) modified Au electrode at +200 mV vs Ag/AgCl in 0.1 mol $dm^{-3}$ phosphate buffer, pH 7.4. Inset: Steady state amperogram of the HRP/Ni(II) modified electrode. Each arrow indicates the addition of 6.25 μmol $dm^{-3}$ $H_2O_2$. (WE diameter: 1.0 mm).

## 5.4 CONCLUSION

The fabrication of a modified electrode based on spontaneous adsorption of a novel cyclopentadienylnickel(II) thiolato Schiff base complex, on a gold electrode is reported for the first time It was found that the spontaneously adsorbed layer required an activation cycle in 0 1 mol $dm^{-3}$ NaOH before effective electron communication between the monolayer and the gold surface was obtained The spontaneously adsorbed layer provided effective blocking of faradaic processes arising from gold surface oxidation The adsorbed layer yielded quasi-reversible electrochemistry with an $E_{1/2}$ value of +202 mV in 0 1 mol $dm^{-3}$ phosphate buffer, pH 7 4 This quasi-reversibility was attributed to non-uniformity of the layer, or molecular interactions between the molecules The surface concentration, Γ, of the nickel redox centres was found to be 1 548 × $10^{-11}$ mol $cm^{-2}$ Electrocatalytic reduction of $H_2O_2$ at a HRP/Ni(II)-modified electrode was observed It was observed using CV and OSWV, that the electro-produced Ni(II) complex was effectively consumed in the enzyme catalysis Steady state amperometry was used to evaluate enzyme kinetics of the biosensor $K_m^{app}$ was found to be 27 3 μmol $dm^{-3}$ and $I_{max}$, was 678 2 nA $cm^{-2}$ The limit of detection was 6 3 μmol $dm^{-3}$ Attempts to increase the electroactivity of the spontaneously adsorbed layer by manipulation of the surface using a mixed layer approach, or by alteration of the complex itself, will help to improve upon the working parameters of this biosensor Optimisation of the enzyme parameters will also improve the characteristics of this novel peroxidase-based biosensor These preliminary results support the view that cyclopentadienylnickel(II) thiolate spontaneously adsorbed layers could prove promising for developing novel electrocatalytic assemblies, especially practical for use in tailoring a variety of amperometric biosensor devices

## 5.5 APPENDIX

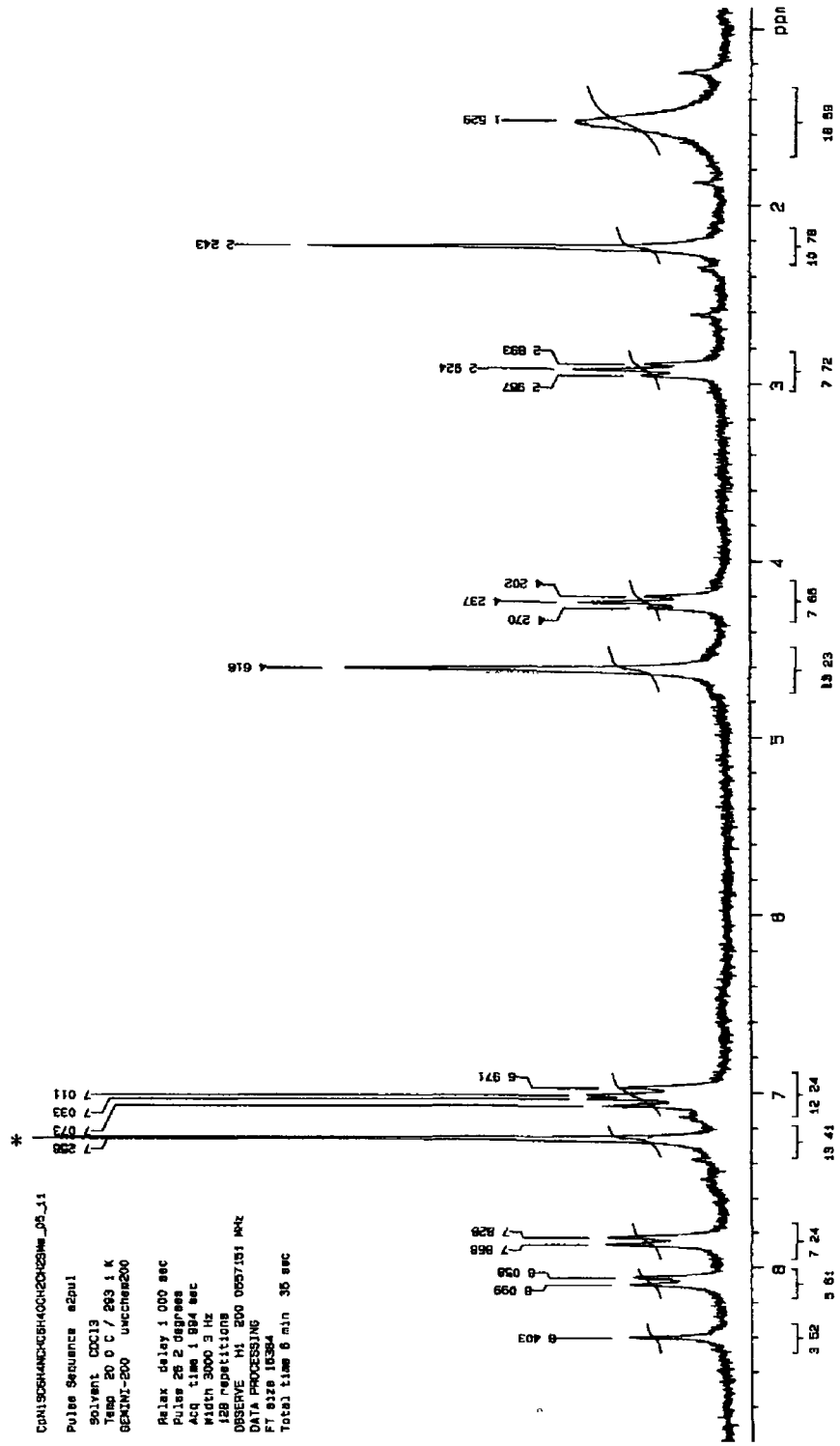

$^1$H NMR spectrum of $[Ni(SC_6H_4C(H)NC_6H_4OCH_2CH_2SMe)(\eta^5\text{-}C_5H_5)]_2$ *Represents residual $CH_2Cl_2$ in the complex

## 5.6 REFERENCES


Aslam, M , Bandyopadhyay, K , Vijayamohanan, K , Lakshminarayanan, V (2001) Comparative behaviour of aromatic disulfide and deselemde monolayers on polycrystalline gold using cyclic voltammetry, STM and quartz crystal microbalance *J Colloid Inter Sci* , **234** 410-417

Bowmaker, G , Boyd, P , Campbell, G (1982) Spectroelectrochemistry of nickel complexes Voltammetric and ESR studies of the redox reaction of phosphine-dithiolate and phosphine-catecholate complexes of nickel *Inorg Chem* , **21** 2403-2412

Bowmaker, G , Boyd, P , Campbell, G (1983) Electrochemical and ESR studies of the reactions of nickel(II), palladium(II), and platmum(II) complexes of 1,2-diphenyl-1,2-ethenedithiolate(2-)-S,S' *Inorg Chem* , **22** 1208-1213

Chaki, N , Vijayamohanan, K (2002) Self-assembled monolayers as a tunable platform for biosensor applications *Biosens Bioelectron* , **17** 1-12

Campuzano, S , Galvez, R , M Pedrero, M , Manuel de Villena, F , Pingarron, J M (2002) Preparation, characterisation and application of alkanethiol self-assembled modified with tetrathiafulvalene and glucose oxidase at a gold disk electrode *J Electroanal Chem.*, **526** 92-100

Elmore, D , Chase, D , Liu, Y , Rabolt, J (2004) Infrared spectroscopy and spectroscopic imaging of n-propyl trichlorosilane monolayer films self-assembled on glass substrates *Vib Spec* , **34** 37-45

Gaspar, S , Popescu, I , Gazaryan, I , Bautista, G , Sakharov, I , Mattiasson, B , Csoregi, E (2000) Biosensors based on novel plant peroxidases a comparative study *Electrochim Acta,* **46** 255-264

Ge, B , Lisdat, F (2002) Superoxide sensor based on cytochrome c immobilised on mixed-thiol SAM with a new calibration method *Anal Chim Acta*, **454** 53-64

Gooding, J , Hibbert, D (1999) The application of alkanethiol self-assembled monolayers to enzyme electrodes *Tr Anal Chem* , **18** 525-533

Hamelmann, F , Heinzmann, U , Siemeling, U , Bretthauer, F , Vor der Bruggen, J (2004) Light-stimulated switching of azobenzene-containmg self-assembled monolayers *App Sur Sci* , **222** 1-5

Ho, N , Mak, T , Luh, T (1990) Reductive cleavage of the C-S bond in $[Ni_2(cp)_2(\mu\text{-}SR)_2](cp=C_5H_5)$ by $LiAlH_4$ Crystal structures of $[Ni_2(cp)_2(\mu\text{-}SPh)_2]$ and $[Ni_2(cp)_2\{\mu\text{-}o\text{-}(SCH_2)_2\text{-}C_6H_4\}]$ *J Chem Soc Dalton Trans* , **12** 3591-3595

Iwuoha, E I , Villaverde, D S , Garcia, N P , Smyth, M R , Pingarron, J M (1997) Reactivities of organic phase biosensors 2 The amperometric behaviour of horseradish peroxidase immobilised on a platinum electrode modified with an electrosynthetic polyaniline film *Biosens Bioelectron.*, **12** 749-761

Jun, Y , Beng, K (2004) Electrochemical study of monolayers of heterocyclic thiols self-assembled on polycrystalline gold electrode the effect of solution pH on redox kinetics *Electrochem Comm* , **6** 87-90

Kemp (2001) Instrumental Methods in Electrochemistry *Horwood Publishing, Chichester, England*

Krings, N , Strehblow, H , Kohnert, J , Martin H (2003) Investigations on the monolayer structure of thiol SAMs and the influence of conjugated $\pi$-bonds on the electronic molecular conductivity *Electrochim Acta*, **49** 167-174

Krysinski, P , Brzostowska-Smolska, M , Mazur, M (1999) Incorporation of redox molecules into the monolayer modified electrodes *Mater Sci Eng C*, **8-9** 551-557

Lee, S , Laibnis, P (1998) Protein-resistant coatings for glass and metal oxide surfaces derived from oligo(ethylene glycol)-terminated alkyltrichloroalkanes *Biomater* , **468** 170-179

Li, D , Li, J , (2003) Self-assembly of 4-ferrocene thiophenol capped electroactive gold nanoparticles onto gold electrode *Surface Science,* **522** 105-111

Li, J , Yan, J , Deng, Q , Cheng, G , Dong S (1997) Viologen-thiol self-assembled monolayers for immobilised horseradish peroxidase at gold electrode surface *Electrochim Acta,* **42** 961-967

Martele, Y , Callewaert, K , Naessens, K , Van Daele, P , Baets, R , Schacht, E (2003) Controlled patterning of biomolecules on solid surfaces *Mater Sci Eng C,* **23** 341-345

Morrin, A , Guzman, A , Killard, A J , Pingarron, J , Smyth, M R (2003) Characterisation of horseradish peroxidase immobilisation on an electrochemical biosensor by colorimetric and amperometric techniques *Biosens Bioelectron* , **18** 715-720

Morrin, A , Moutloali, R M , Killard, A J , Smyth, M R , Darkwa, J , Iwuoha E (2004) Electro-Catalytic Sensor Devices (I) Cyclopentadienylnickel(II) thiolato Schiff base monolayer self-assembled on gold *Talanta,* **64** 30-38
Moutloali, R M , (2003) PhD thesis, University of the Western Cape

Nuzzo, R , Allara, D (1983) Adsorption of bifunctional organic disulphides on gold surfaces *J Am Chem Soc* , **105** 4481-4483

Ozoemena, K , Nyokong, T (2002) Voltammetric characterisation of the self-assembled monolayer (SAM) of octabutylthiophthalocyaninatoiron(II) a potential electrochemical sensor *Electrochim Acta,* **47** 4035-4043

Ozoemena, K , Nyokong, T (2003) Electrochemical behaviour of thiol-derivatised zinc (II) phthalocyanine complexes and their self-immobilised films at gold electrodes *Microchem J*, **75** 241-247

Peng, Z , Qu, X , Dong, S (2004) Co-assembly of ferrocene-terminated and alkylthiophene thiols on gold and its redox chemistry modulated by surfactant adsorption *J Electroanal Chem*, **563** 291-298

Raj, C , Ohsaka, T (2001) Electroanalysis of ascorbate and dopamine at a gold electrode modified with a positively charges self-assembled monolayer *Electroanal Chem* , **496** 44-49

Ruzgas, T , Csoregi, E , Emmeus, J , Gorton, L , Marko-Varga, G (1996) Peroxidase-modified electrodes Fundamentals and applicçation *Anal Chim Acta*, **30** 123-138

Stine, K , Andrauskas, D , Khan, A , Forgo, P , D'Souza, V (1999) Electrochemical study of self-assembled monolayers of a β-cyclodextrin methyl sulphide covalently linked to anthraquinone *J Electroanal Chem*, **465** 209-218

Stolarczyk, K , Bilewicz, R , Siegfried, L , Kaden, T (2003) The dual role of self-assembled monolayers of a tetrazamacrocyclic copper (II) complex m ascorbate oxidation catalysis *Inorg Chim Acta*, **348** 129-134

Tatsuma, T , Gondaira, M , Wantanabe, T (1992) Peroxidase-incorporated polypyrrole membrane electrodes *Anal Chem* , **64** 1183

Torriero, A , Salinas, E , Battaglini, F , Raba, J (2003) Milk lactate determination with a rotating bioreactor based on an electron transfer mediated by osmium complexes incorporating a continuous-flow/stopped-flow system *Anal Chim Acta*, **498** 155-163

Tour, J , Jones, L , Pearson, D , Lamba, J , Burgin, T , Whitesides, G , Allara, D , Parikh, A (1995) Self-assembled monolayers and multilayers of conjugated thiols, alpha, omega-dithiols, and thioacetyl-containing adsorbates Understanding attachments between potential molecular wires and gold surfaces *J Am Chem Soc*, **117** 9529-9534

Tour, J , Rawlett, A , Kazaki, M , Yao, Y , Jagessar, R , Dirk, S , Price, D , Reed, M , Zhou, C , Chen, J , Wang, W , Campbell, I (2001) Synthesis and preliminary testing of molecular wires and devices *Chem Eur J*, **7** 5118

Vergheese, M , Berchmans, S (2004) Evaluation of monolayers formed from mercaptobenzenethiazole and decanethiol as sensing platforms *Chem Phys* , **83** 229-238

Wilke, N , Baruzzi, M (2002) Comparative analysis of the charge transfer processes of the $Ru(NH_3)_6^{2+}$ and $Fe(CN)_6^{3-}/Fe(CN)_6^{4-}$ redox couples on glassy carbon electrode surfaces *J Electroanal Chem* , **537** 67-76

Xiao, X , Wang, B , Zhang, C , Yang, Z , Loy, M (2001) Thermal annealing effect of alkanethiol monolayers on Au(III) in air *Surf Sci* , **472** 41-50

Xu, S , Han, X (2003) A novel method to construct a third-generation biosensor self-assembling gold nanoparticles on thiol-functionalised poly(styrene-co-acryhc acid) nanospheres *Biosens Bioelectron* , **19** 117-1120

Yantasee, W , Lin, Y , Fryxell, G , Busche, B (2004) Simultaneous detection of cadmium, copper and lead using a carbon paste electrode modified with carbomoylphosphonic acid self-assembled monolayer on mesoporous silica (SAMMS) *Anal Chim Acta*, **502** 207-212

# Chapter 6

## Organic Phase Cyclopentadienylnickel(II) Thiolate Chemical Sensor for Electrochemical Determination of Sulphur Dioxide

## 6.1 INTRODUCTION

Research and development of gas sensors has increased in recent years as a result of new market opportunities, novel materials and improved fabrication technologies. Considerable progress has been made with optical and metal oxide semi-conductor devices but problems of selectivity with regard to detection of organic vapours or gases can be a serious encumbrance (Saini *et al.*, 1995). Within the last decade, the availability of microcontroller chips with prices below $1 have stimulated more complex gas sensor systems, usually tagged as electronic noses (Kohl, 2001). One of the first successful applications - the identification of solvents by a set of electrochemical cells - is still available as a module of the 'Lennartz Moses II', electronic nose (http://www.lennartz-electronic.de), also featuring semi-conductor and microgravimetric gas sensors.

Gas sensor technology encompasses many different operating principles such as metal oxide semi-conductor films, conducting polymers, gas field-effect transistors (FETs) and electrochemical gas cells. Each of these formats has its own merits and drawbacks. Some have been commercialised and can be seen on the market today.

Semi-conducting metal oxide (SMO) sensors consist of a metal oxide semi-conducting film (e.g. $SnO_2$, $WO_3$, ZnO, CuO, $In_2O_3$) coated onto a ceramic substrate (e.g. alumina). Most often the device contains a heating element. Oxygen from the air is dissolved in the semi-conductor's lattice, setting its electrical resistance to background level. During the measurement, the volatile molecules are adsorbed at the surface of the semi-conductor device where they undergo a redox reaction causing a modification to the conductivity of the device. This change in conductivity is taken as the response of the system to that particular gas sample. Metal oxides investigated to date are non-selective (Tomchenko *et al.*, 2003). Methods to improve selectivity have been successfully employed during the last decades such as optimisation of operating temperature, bulk/surface doping and use of molecular filters (Ampuero & Bosset, 2003). The implementation of an array of SMO sensors combined with appropriate pattern recognition and classification tools is a promising technique to compensate for the

drawback of non-selectivity It has been shown by many research teams that a sensor matrix based on several SMO materials can provide a specific and unique response pattern for different chemical species or mixtures of species using pattern recognition techniques such as principal component analysis (PCA) (Santos *et al*, 2004, Zhu *et al*, 2004)

Conducting organic polymers have also been used as semi-conducting materials for gas sensing They are usually deposited onto a substrate between two gold plated electrodes and upon interaction with volatile molecules, a reversible change of the device's conductivity is observed The inherent poor reproducibility in manufacturing polymer sensors, however, is a huge drawback (Ampuero *et al*, 2003)

Another sensing technology is based on field effect transistors (FETs), or ion-selective electrodes FETs are semi-conductor devices that exhibit low noise, consume low power, and can be interfaced to electronic circuits with ease They can be used as solid state potentiometric transducers, and can be used as components of low-cost and miniaturised sensor arrays Ebarvia *et al* (2001) developed a very sensitive ion selective FET (ISFET) for $SO_2$ The gate surface of the FET was coated with a thin film of a hydrogel containing $NaHSO_3$ as electrolyte The $SO_2$ diffused through a Teflon film covering the hydrogel, which produced a pH change The sensor exhibited a very good limit of detection (2 ppb) The high sensitivity of the sensor was attributed to the reduced volume of electrolyte at the surface of the ISFET

Electrochemical gas sensors based on amperometric cells occupy a large sector of the gas sensing field, and sensors of this type specific to gases such as CO, $NH_3$, $SO_2$, NO and $NO_2$ are on the market today (Hodgson *et al*, 1999) The amperometric sensor is based on porous precious metal electrodes chemically or vacuum deposited onto a Nafion ion exchange membrane The metal electrode is directly exposed to the gas phase, while the back of the membrane is in contact with an internal compartment containing an electrolyte solution in which counter and reference electrodes are placed (*Figure 6 1*) The design of these cells is well suited to miniaturisation and readily adaptable to *in situ* analysis, and at the same time has been shown to give fast responses and high sensitivities (due to the linear dependence of response on concentration) (Hodgson *et al*, 1999)

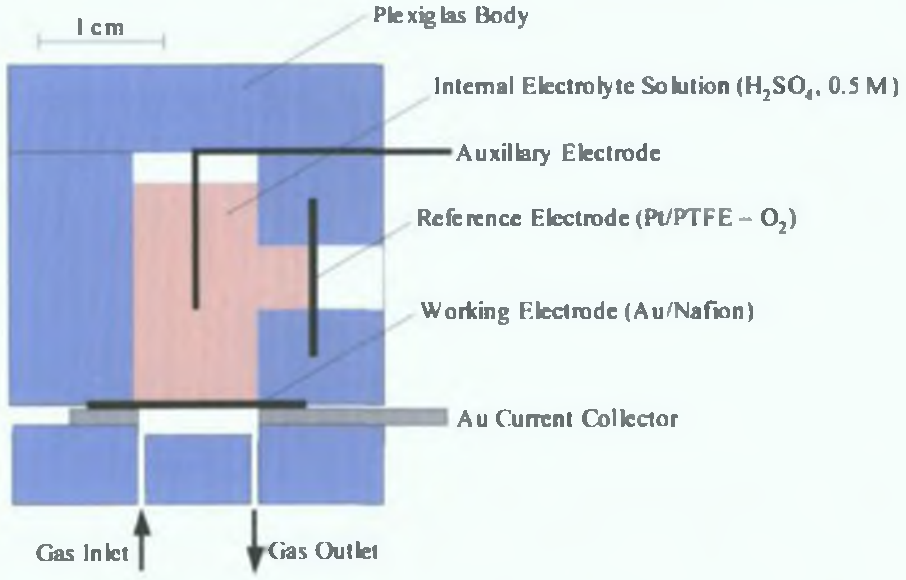


***Figure 6.1.*** Schematic of an amperometric gas sensor (Knake & Hauser, 2003). Scale 1.7:1. The working electrode is located at the bottom to allow direct mounting on top of the gas manifold while the $Pt/O_2$ reference is exposed to ambient air.

Sulphur dioxide emission is directly related to combustion processes such as the burning of fossil fuels and biomass and can also be formed in the atmosphere by the oxidation of reduced sulphur compounds. It is one of the most important atmospheric pollutants (Milani & Cardoso, 2003). Sulphur gases are important in atmospheric chemistry due to their role in the genesis of acid precipitation and degradation of atmospheric visibility. Environmental and health hazards associated with sulphur dioxide pollution mandates that atmospheric sulphur dioxide is stringently monitored in many countries (Ferrari & Salisbury, 1999). The European Commission has published a new directive (96/62/CE), setting the limit of $SO_2$ present in the atmospheric environment at 0.125 ppb. This limit needs to be met by January 2005 in all EU countries. There are currently a number of methods and instruments available to monitor $SO_2$ levels in the air. These include ultraviolet fluorescence (Schwarz *et al.*, 1974), flame photometry (Hisamatsu *et al.*, 1989), ion chromatography (Krochmal & Kalina, 1997), conductimetric measurements and electrolytic conductivity detection (Dasgupta & Kar, 1995). However, the above methods are in general laborious and time-consuming, which make it necessary for new methods to be developed.

Electrochemical gas sensors have been developed in recent years to detect $SO_2$ To date, the focus has been placed on potentiometric sensors, such as FET (field effect transistors) (Ebarvia *et al*, 2001), and amperometric sensors, which involve monitoring redox changes of sulphur dioxide (Chiou & Chou, 2002) Indirect electrochemical oxidation of $SO_2$ (Shi *et al*, 2001), which involves the oxidation of $SO_2$ at the modified electrode to sulphate has also been used However, this indirect measurement of $SO_2$ has a potential drawback, in that the modified electrode used has to be sensitive to intermediate $HSO_3^-$ or $SO_3^{2-}$ in the electrochemical cell A sensor that responds directly to $SO_2$ detection would have no such drawback Metal thiolates in general, and cyclopentadienyl nickel thiolates in particular that can complex with $SO_2$, offer such an alternative

Complex formation between $SO_2$ and metal thiolates is very well documented (Eller & Kubas, 1977, Shaver & Plouffe, 1992, Darensbourg *et al*, 1994, Darkwa *et al*, 1998, Kovacs, 2001, Moloto *et al*, 2004) This chemistry attracts attention primarily because of environmental concerns and the potential use of such reactions to develop sulphur dioxide scrubbers or sensors Three main reaction types of sulphur dioxide with metal complexes are known The best studied of these reactions is the coordination of $SO_2$ to a metal centre (Kubas & Ryan, 1986) The second reaction type is insertion of $SO_2$ into a bond formed by a central metal atom and another atom such as carbon (Li *et al*, 2003, Yang & Burton, 2000, Kubas, 1994) Also, Rys *et al* (2002) recently reported the insertion of $SO_2$ into S–S bonds in $Mo(\eta^5\text{-}C_5H_5)_2S_2$ to form $Mo(\eta^5\text{-}C_5H_5)_2S_3O_2$ This constitutes the first example of sulphur dioxide insertion into the S–S bond The third reaction type involves the binding of sulphur dioxide to a soft atom in a ligand, usually sulphur (Shaver & Plouffe, 1992, Eller & Kubas, 1977) The soft atom in a ligand binds the sulphur dioxide by donating electrons into empty d-orbitals of the sulphur atom of the sulphur dioxide, in a reaction where the soft atom in the ligand behaves as a Lewis base Such bonds are inherently weak and generally lead to unstable sulphur dioxide adducts compared to compounds formed *via* type 1 and type 2 reactions

Ligand-bound $SO_2$ is generally found for late-transition metal thiolato complexes These are either $SO_2$ bound to the sulphur atom of a bidentate thiolato ligand complex (Darensbourg *et al*, 1994) or $SO_2$ bound to the sulphur atom of a monodentate

thiolato ligand complex (Shaver & Plouffe, 1992, Darkwa *et al*, 1998) which are cyclopentadienyl metal complexes Shaver & Plouffe were the first to report the reversible binding of $SO_2$ to the sulphur atom of a cyclopentadienyl metal thiolato phosphine complex in 1992, and showed that the weak sulphur–sulphur interaction is responsible for the reversibility The isoelectronic nickel analogues reported by Darkwa *et al* (1998) show similar reversibility but are too labile to allow solids to be isolated and characterized As such, unequivocal characterisation of the $NiS(SO_2)R$ adducts is still lacking It is, however, possible to use analytical techniques to establish the formation of labile $SO_2$ adducts $^1H$ NMR spectroscopy has been used as a tool for detecting $SO_2$ adduct formation This is based on electronic changes that occur upon adduct formation and hence changes in chemical shift It is therefore possible that the electronic changes that occur when $SO_2$ adducts are formed, can give a different electrochemical response to that of the complex, and allow $SO_2$ to be detected electrochemically A direct method in which an electrochemical response is generated by a stable $SO_2$ adduct *via* a change in potential could be desirable since it should not suffer from interferences like other reported electrochemical techniques

This study reports a novel electrochemical technique for $SO_2$ detection based on its interaction with Ni(II) thiolato complexes Preliminary results showed that many of the Ni(II) complexes investigated possess stable $SO_2$ adducts which can allow their use in electrochemical $SO_2$ sensing using cyclic voltammetry Electrochemical, UV-Vis and $^1H$ NMR spectroscopic analyses showed that the formation of $SO_2$ adducts caused the perturbation of the electronic density of the Ni centre, (indicated by shifts in the $E_{1/2}$ values of the Ni(II)/(III) redox couple) was dependent on $SO_2$ concentration One of the Ni(II) thiolato complexes investigated is particularly attractive for $SO_2$ sensing, as the end groups of the complex (MeS) allows for adsorption onto inert metals (*Chapter 5*), which could lead to the development of a conceptually novel modified electrode for $SO_2$ sensing

## 6.2 MATERIALS AND METHODS

### *6 2 1 Materials*

All preparations were carried out in reagent grade solvents Dichloromethane used for electrochemical experiments was refluxed twice over $P_2O_5$ for 24 h, distilled under nitrogen and stored over activated molecular sieves All complexes were prepared by Dr Moutloali (University of the Western Cape, South Africa) Complexes $[Ni(RP)(\eta^5\text{-}C_5H_5)\text{-}(SC_6H_4X\text{-}4)]$ (R = tributyl ($Bu_3$), triphenyl ($Ph_3$), X = F, Cl, Br, $NH_2$) (*Figure 6 2* [1]) were prepared as described by Darkwa *et al* (1998) and Moloto *et al* (2004) Complexes $[Ni(PBu_3)(\eta^5\text{-}C_5H_5)(SC_6H_4C(H)NC_6H_4X\text{-}4)]$ (X = F, Me, OMe) (*Figure 6 2* [2]) were prepared as described by Nevondo *et al* (2000) Complexes $[Ni(\eta^5\text{-}C_5H_5)(\mu_2\text{-}SC_6H_4X\text{-}4)]_2$ (X = F, $NH_2$) (*Figure 6 2* [3]) were prepared as described by Moutloali (2003) The complex $[Ni(SC_6H_4C(H)NC_6H_4OCH_2CH_2SMe)(\eta^5\text{-}C_5H_5)]_2$ (*Figure 6 2* [4]) was prepared as described by Morrin *et al* (2004) (for a brief description, see *Section 5 2 1*) All reactions were performed under a nitrogen atmosphere, but the air and moisture stable complexes that were formed were prepared in air Sulphurous acid (24,762-6) and $SO_2$, 99 9+% (29, 569-8) were purchased from Sigma-Aldrich Mixed gases (13 6 % $CO_2$, 1 % $SO_2$, 56% $O_2$, Bal $N_2$) (340208) and $CO_2$ were purchased from BOC gases

### *6 2 2 Instrumentation*

Elemental analyses were carried out at the University of the Western Cape using a CARLO EBER CHN analyser $^1H$ NMR spectra were recorded on a Varian Gemini 2000 spectrometer at 200 00 MHz and referenced internally to residual $CDCl_3$ at 7 26 ppm UV–Vis absorbance measurements were recorded at room temperature on a UV/VIS 920 spectrometer (GBC Scientific Instruments, Australia) The electrochemistry measurements were performed with a BAS 50/W potentiostat A conventional three-electrode system was used, consisting of a glassy carbon working electrode (1 mm

diameter), a silver/silver chloride (Ag/AgCl) reference electrode and a platinum wire auxiliary electrode The experiments were carried out in dichloromethane at room temperature under an argon atmosphere with tetrabutylammomum tetrafluroborate ([n-$Bu_4N$][$BF_4$], 0 1 mol $dm^{-3}$) as electrolyte A Hamilton SampleLock syringe (50 µl) was used for quantitative measurements of $SO_2$ gas

### *6 2 3 Cyclic voltammetry*

Prior to use, the glassy carbon electrode was cleaned by successive polishing on aqueous slurries of 1 µm, 0 3 µm and 0 05 µm alumina powder, followed by thorough rinsing in de-ionised water The electrode was then placed in solution containing Ni complex (2 mmol $dm^3$, unless otherwise stated), under argon atmosphere The choice of solvent was $CH_2Cl_2$, which contained 0 1 mol $dm^3$ [n-$Bu_4N$][$BF_4$] as supporting electrolyte Voltammograms were obtained at a scan rate of 50 mV $s^1$ under diffusion-limited conditions

### *6 2 4 Ni complex screening*

After performing the initial voltammetric experiment, the electrode was removed and polished $SO_2$ was bubbled through the complex for 1 min approximately, and immediately after, another voltammetric experiment was carried out using experimental conditions in *Section 6 2 3*

### *6 2 5 Quantitative measurement of $SO_2$ using $SO_2$ gas as an analyte source*

Quantitative measurements of $SO_2$ were carried out on complexes [1], [3] and [4] After performing the initial voltammetric experiment, the electrode was removed and polished A known quantity of $SO_2$ was injected into the solution measured with a gastight syringe The solution was then shaken vigorously and a voltammogram was carried out using experimental conditions in *Section 6 2 3* This procedure was repeated a

number of times until the solution of complex became saturated with $SO_2$, i e , when no further change in the voltammogram was observed

### *6 2 6 Quantitative measurement of $SO_2$ using $H_2SO_3$ as an analyte source*

Quantitative measurements of $SO_2$ were carried out on complexes [1], [3] and [4] After performing the initial voltammogram, the electrode was removed and polished A known quantity of sulphurous acid was added to the solution, the solution was shaken vigorously and a voltammogram was carried out using experimental conditions in *Section 6 2 3* This procedure was repeated a number of times until the solution of complex became saturated with $SO_2$, i e , when no further change in the voltammogram was observed

[1]

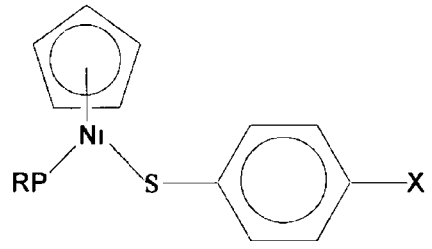


R = $Bu_3$, $Ph_3$
X= $NH_2$, Cl, F, Br

[2]

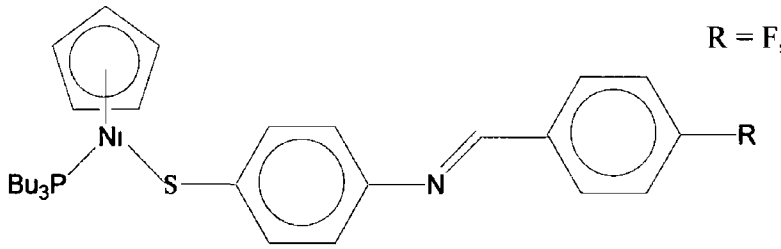


R = F, Me, OMe

[3]

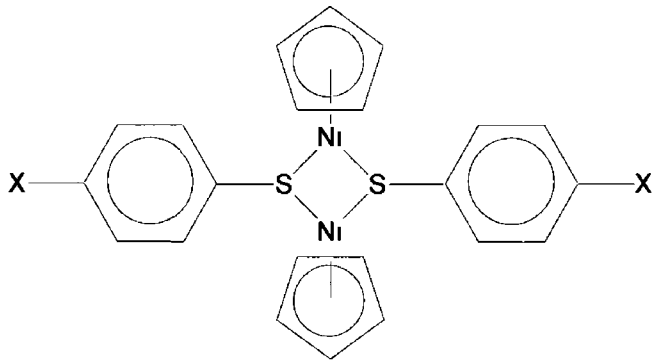


X = F, $NH_2$

[4]

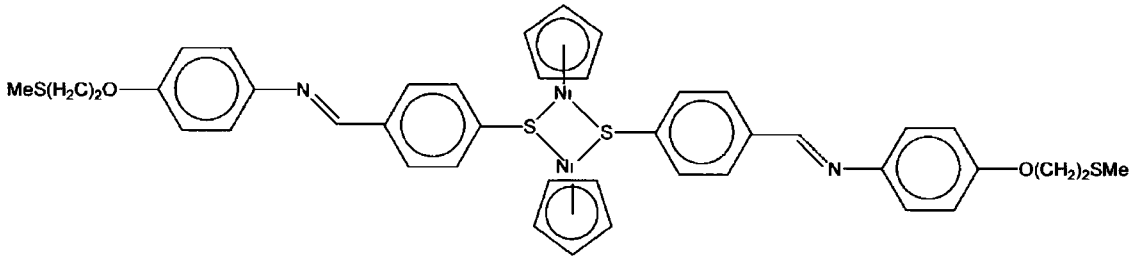


*Figure 6 2* Structures of complexes screened as potential materials for $SO_2$ sensing

## 6.3 RESULTS AND DISCUSSION

### *6 3 1 Electrochemical screening of [Ni(PR)($\eta^5$-$C_5H_5$)($SC_6H_4X$)] [1]*

Cyclopentadienylnickel phosphine complexes with simple thiolate ligands, [Ni($PR_3$)($\eta^5$-$C_5H_5$)($SC_6H_4X$)] [1], where R = $Bu_3$ and $Ph_3$, and X = $NH_2$, F, Cl and Br, were the initial set of complexes to be interrogated Complexes where R = $Bu_3$, formed $SO_2$ adducts in solution, initially observed by a distinct colour change from a dark brown to a reddish colour after bubbling excess $SO_2$ through the solutions (*Figure 6 3*) This colour change on formation of the adduct was also observed by Shaver & Plouffe (1992) and Kovacs *et al* (2001) Further evidence and mechanism for this adduct formation was gathered from electrochemistry, $^1$H NMR and UV-Vis spectroscopy and literature

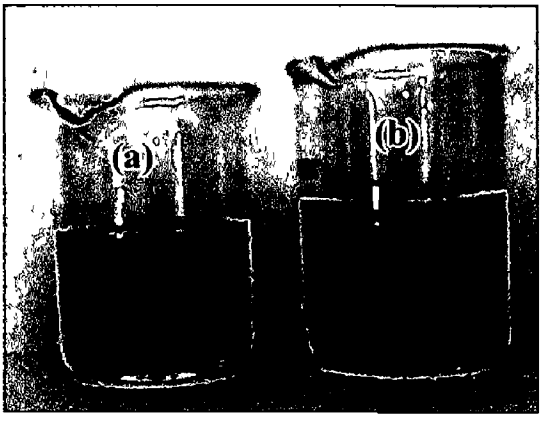


***Figure 6 3*** Images of (a) the dark brown solution of [Ni($PBu_3$)($\eta^5$-$C_5H_5$)($SC_6H_4NH_2$)] and (b) the red solution of its $SO_2$ adduct

Quasi-reversible electrochemistry of the Ni(II)/(III) redox couple before and after formation of the $SO_2$ adducts (*Figure 6 4*) was observed for all complexes where R = $Bu_3$ However, this electrochemistry became irreversible when R was changed to $Ph_3$ (data not shown) Although both phosphines are electron rich, the increased stability of the Ph groups stabilized by its resonance structure makes the $PPh_3$ ligand a weaker donor

of electrons to facilitate redox reaction. When the phenyl group was substituted for a butyl, electron donation to the metal centre was much easier, facilitating the redox reaction. As shown in the data in *Section 6.3.4. Table 6.1.*, the ratio of the cyclic voltammetric anodic to cathodic peak currents ($i_{p,a}/i_{p,c}$) was approximately unity in both the thiolate complexes and their sulphur dioxide adducts. The peak separation $\Delta E_p$ ($\Delta E_p = E_{p,a}-E_{p,c}$) values ranged from 59 mV for [Ni(PBu$_3$)($\eta^5$-C$_5$H$_5$)(SC$_6$H$_4$F-4)] to 119 mV for [Ni(PBu$_3$)($\eta^5$-C$_5$H$_5$)(SC$_6$H$_4$Cl-4)], as would be expected for quasi-reversible diffusion-controlled electrochemical processes. However, within limits of experimental error, the $\Delta E_p$ values for each compound remained essentially the same before and after $SO_2$ adduct formation. This shows that the faradaic process being observed in both $SO_2$-free and $SO_2$-containing compound was the same, namely the diffusion-controlled Ni(II)/(III) electrochemistry of the [Ni(PBu$_3$)($\eta^5$-C$_5$H$_5$)(SC$_6$H$_4$X-4)] (X = F, Cl, Br, NH$_2$).

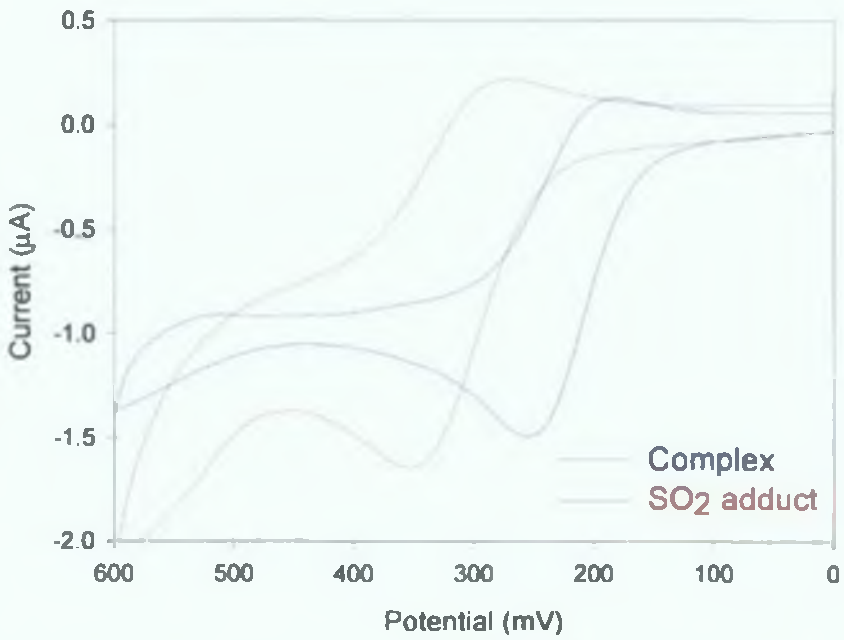


***Figure 6.4.*** Cyclic voltammograms for [Ni(BuP$_3$)($\eta^5$-C$_5$H$_5$)(SC$_6$H$_4$NH$_2$)] and its $SO_2$ adduct (adduct formed by bubbling $SO_2$ through the complex).

As shown in *Section 6.3.4. Table 6.1*, the half wave potentials ($E_{1/2}$) of the $SO_2$ adducts were generally higher than for the thiolate complexes by up to 60 mV vs.

Ag/AgCl for the case of $[Ni(PBu_3)(\eta^5\text{-}C_5H_5)(SC_6H_4NH_2\text{-}4)]$, which is indicative of the perturbation of the redox properties of the metal centre by the binding of $SO_2$ The magnitude of the half-wave potential shift ($E_{1/2\ Shift}$) varied with the substituent on the thiolate ligand in the order F > $NH_2$ > Br ≅ Cl The $NH_2$ ($E_{1/2\ Shift}$ = 57 mV) and F ($E_{1/2\ Shift}$ = 60 mV) substituents exhibited the largest shift in $E_{1/2}$ after $SO_2$ binding The data suggests a relationship between the electron withdrawing ability of the substituent and the $E_{1/2}$ of the complex This was verified by the analysis of the Hammett constants of the substituents The Hammett substituent constant ($\sigma_p$) reflects a molecule's intrinsic reactivity, related to the electronic effect of differing substituents This constant is related to the oxidizing ability of a molecule and so is reasonable to expect a correlation between $E_{1/2}$ and Hammett (Hansch *et al*, 1991) *Figure 6 5* shows that the $E_{1/2}$ value of the compounds varied in accordance with the value of the Hammett constant of the substituent in the para-position of the thiolate ligand $\sigma_p$ values of the $SO_2$ adduct increase in the order Br ≅ Cl > F > $NH_2$ It is important to emphasise that Br and Cl substituents which have the same $\sigma_p$ value of 0 23, show remarkable similarity in their $E_{1/2}$ values for the $SO_2$ adducts ($E_{1/2\ Br}$ = 413 mV and $E_{1/2\ Cl}$ = 412 mV), even though the $E_{1/2}$ values of their $SO_2$-free analogues differ by up to 47 mV This behaviour of Br- and Cl-substituted $SO_2$ adducts confirms the observed linear relationship between $\sigma_p$ and $E_{1/2}$ as shown in *Figure 6 5* It has been proposed that $SO_2$ adducts of $[Ni(PBu_3)(\eta^5\text{-}C_5H_5)(SC_6H_4X\text{-}4)]$ have the $SO_2$ bonded to the sulphur of the thiolate ligand (Darkwa *et al*, 1998) Since the value of $\sigma_p$ is a measure of the electron-withdrawing ability of the substituent in the para-position of the benzene ring to which the sulphur donor atom is attached, the increased $E_{1/2}$ of the $SO_2$ adducts confirms the behaviour of $SO_2$ as a Lewis acid that binds to the thiolate sulphur by accepting electrons This bonding mode in turn reduces electron density at the metal centre, hence the increase in half-wave potentials of $SO_2$ adducts

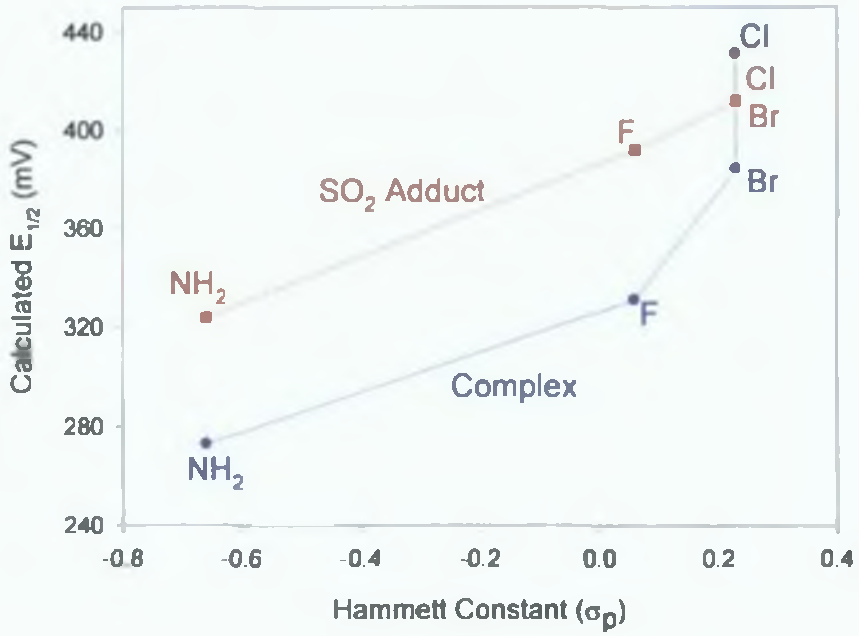


***Figure 6.5.*** The dependence of $E_{1/2}$ of $[Ni(PBu_3)(\eta^5\text{-}C_5H_5)(SC_6H_4X\text{-}4)]$ (X = $NH_2$, F, Cl, Br) complexes and their $SO_2$ adducts on the Hammett constants of the para-substituents on the thiolate ligand.

$^1H$ NMR showed that the cyclopentadienyl (cp) singlet attached to the Ni(II) center for $PBu_3$ ligand complexes, was observed at 5.15 ppm in the original spectrum (*Figure 6.6a*), but shifted downfield to a value of 5.53, upon exposure to $SO_2$ (*Figure 6.6b*). This deshielding effect resulted from a decrease in electron density around the Ni centre, which in turn drew electron density from the cyclopentadienyl group. This effect was also observed for both sets of doublets on the benzene ring. The downfield doublets can be assigned to the protons close to the electro-negative substituents and the upfield doublets to the protons next to the sulphur. The protons near the sulphur atom have upfield shifts in the $SO_2$ adducts (6.416 and 6.377 ppm shifted to 6.601 and 6.562 ppm, respectively). This implies that the $SO_2$ is bound to the sulphur of the ligand and draws electron density from this sulphur and hence from the nearest protons. The other set of protons experience little electron density changes, resulting in only slight changes in chemical shifts. The $^1H$ NMR spectrum reverted back to its original spectrum after two

hours in air (*Figure* 6.6c), demonstrating the reversibility of this labile bond. However, under $SO_2$ atmosphere, the adduct remained stable.

UV-Vis spectra for $[Ni(PBu_3)(\eta^5\text{-}C_5H_5)(SC_6H_4NH_2)]$ are shown in *Figure 6.7*. It shows increases in absorption and shifts in absorption wavelength on the formation of $SO_2$ adduct of the complex. In the UV region (*Figure 6.7a*), the absorption bands of the complex at 260 and 320 nm were replaced by one strong band at 290 nm ($Abs_{(290\ nm)} \approx 2A_{(260\ nm)}$ and $4.5Abs_{(320\ nm)}$) after $SO_2$ adduct formation. These transitions in the UV region are ligand-based and indicate the attachment of $SO_2$ to a site on the ligand. In the visible region (*Figure 6.7b*), the δ-δ transition of the Ni centre is seen at about 400 nm. This shifts only slightly to about 390 nm ($Abs_{(390\ nm)} \approx 3Abs_{(400\ nm)}$) after adduct formation, indicating that it is most likely that the $SO_2$ is not directly bonded to the metal and the electronic state of the metal is only affected secondarily.

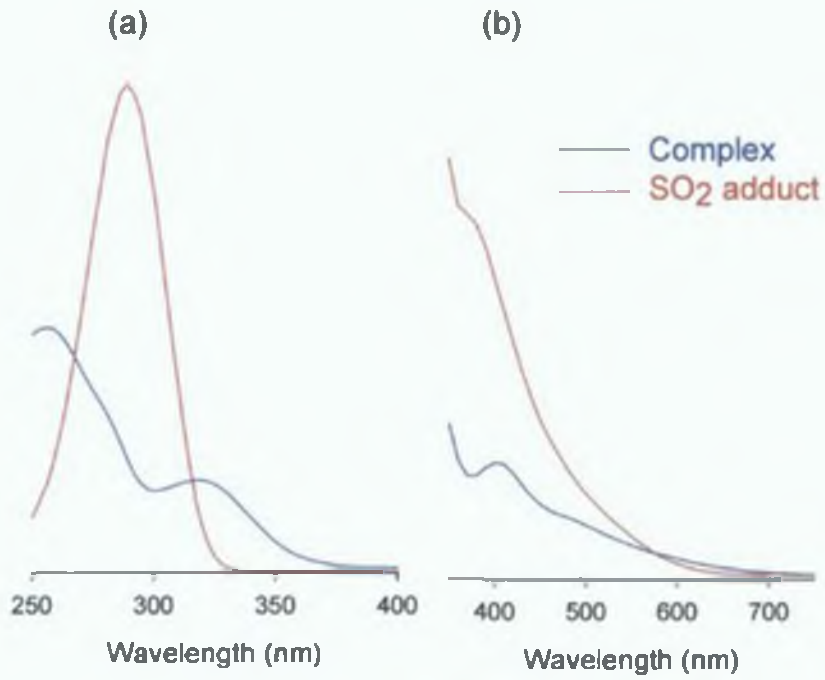


***Figure 6.7.*** UV-Vis spectra for $[Ni(PBu_3)(\eta^5\text{-}C_5H_5)(\mu_2\text{-}SC_6H_4NH_2)]$. (a) UV region showing the ligand-based transitions and (b) visible region showing the metal transition.

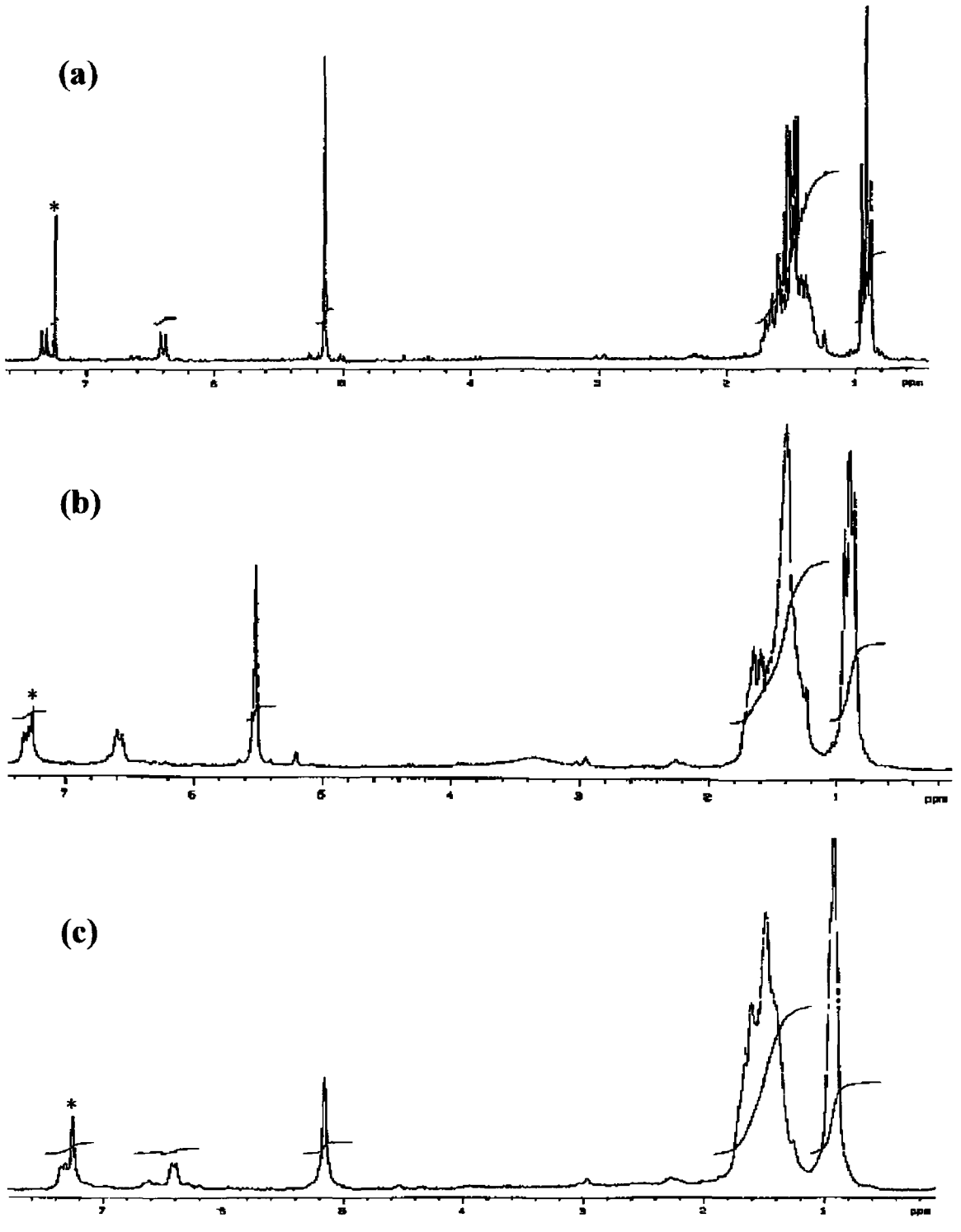


*Figure 6 6* $^{1}H$ NMR spectra of (a) $[Ni(PBu_3)(\eta^5\text{-}C_5H_5)(SC_6H_4NH_2\text{-}4)]$, (b) its $SO_2$ adduct, and (c) 2 h after adduct formation *Represents residual $CH_2Cl_2$ in each of the complexes

*Figure 6 8* represents a schematic of where $SO_2$ attaches to the complex $SO_2$ probably acts as a Lewis acid and forms a bond with the lone pairs of the coordinated S attached to the metal centre Shaver *et al* (1992) have shown that the transition metal thiolates $CpRu(PPh_3)_2S\text{-}4\text{-}C_6H_4Me$) form labile adducts with $SO_2$ at the sulphur atoms Eller and Kubas (1977) have also demonstrated this adduct formation with copper(I) complexes of the type $Cu(PR_3)_n(SR')$ Crystallographic data has been given as the evidence for adduct formation in these papers To date, attempts to recrystallise the $SO_2$ adducts of the cyclopentadienylnickel(II) thiolate have not been successful, due to the extreme lability of the $SO_2$ bond

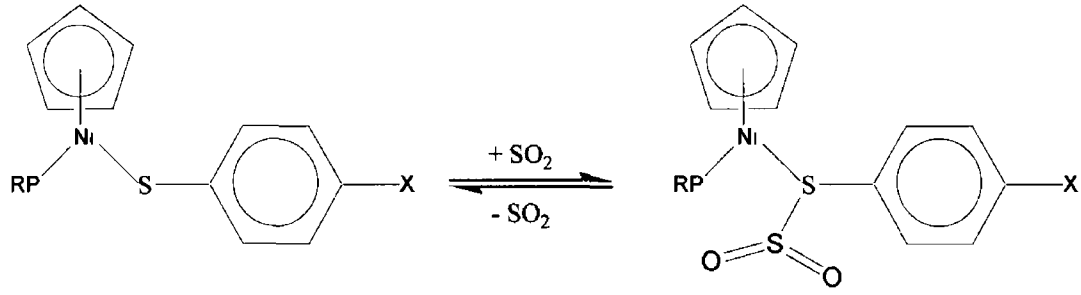


***Figure 6 8*** Proposed reversible reaction for formation of the $SO_2$ adduct for [1]

### *6 3 2 Electrochemical screening of $[Ni(PBu_3)(\eta^5\text{-}C_5H_5)(SC_6H_4C(H)NC_6H_4R)]_2$ [2]*

Other cyclopentadienylnickel(II) phosphino complexes were also examined, $[Ni(PBu_3)(\eta^5\text{-}C_5H_5)(SC_6H_4C(H)NC_6H_4R)]_2$ where R = F, Me and OMe [2] , in which the substituent on the thiolate ligand had an imine functionality forming a Schiff base Despite a noticeable colour change when $SO_2$ was bubbled through solutions of [2], there was no adduct formation but rather the complexes decomposed Evidence for this decomposition was gathered from electrochemical data and $^1H$ NMR

Typical voltammograms of these compounds are shown in *Figure 6 9* for $[Ni(PBu_3)(\eta^5\text{-}C_5H_5)(SC_6H_4C(H)NC_6H_4CH_3\text{-}4]$ and its $SO_2$ adduct Electrochemical data for F, $OCH_3$ and $CH_3$ substituents of the $SO_2$-free complex are contained in *Section 6 3 4, Table 6 1* The compounds exhibited the quasi-reversible electrochemistry ($i_{p\,a}/i_{p\,c}$ values

are approximately unity and the $\Delta E_p$ values for X = F and $OCH_3$ are within 59 ± 6 mV) of a diffusion-controlled system, as has been reported for related compounds (Nevondo *et al*, 2000) $E_{1/2}$ values of the complexes are 345, 326 and 351 mV vs Ag/AgCl for the F, $OCH_3$ and $CH_3$ substituents, respectively The maximum difference between any of the complexes was just 25 mV This is due to the fact that the R group cannot influence the metal centre as in [1], due to the presence of the imine functionality that could absorb the electronic effects of the R group In contrast to [1], the electrochemistry of the Ni centre deteriorated on bubbling of $SO_2$, indicating decomposition of the complexes (*Figure 6 9*)

*Figure 6 10a & b* show the $^1H$ NMR spectra of the complex before and after addition of $SO_2$, respectively The cp singlet, originally at 5 273 ppm, shifted as expected to 5 528 ppm, after bubbling $SO_2$ through the sample This downfield shift was due to the deshielding of the cp, as discussed for [1] A singlet attributable to the imine group on the ligand was initially observed at 8 479 ppm This imine group remained intact after bubbling of $SO_2$ The most crucial observation in the spectrum after $SO_2$ was the formation of an aldehyde functional group, indicated by the peak at 9 986 ppm The spectrum was run again after 5 days (*Figure 6 10c*), and it was observed that the cp singlet was no longer present and the imine singlet had disappeared The aldehyde was still detectable, showing that the products formed after bubbling $SO_2$ were irreversible

*Figure 6 11* represents the proposed scheme for the decomposition of [2] on addition of $SO_2$ Although an adduct is probably formed through the sulphur attached to the Ni, an aldehyde is also formed through the splitting of the complex at the imine site The adduct is an unstable species, as it is not detectable through electrochemistry, and $^1H$ NMR data showed that it fully decomposed over time Since this complex type does not form stable (or electrochemically detectable) $SO_2$ adducts, it would be unsuitable as an $SO_2$ sensor material based on well-defined electrochemistry of both the complex and adduct

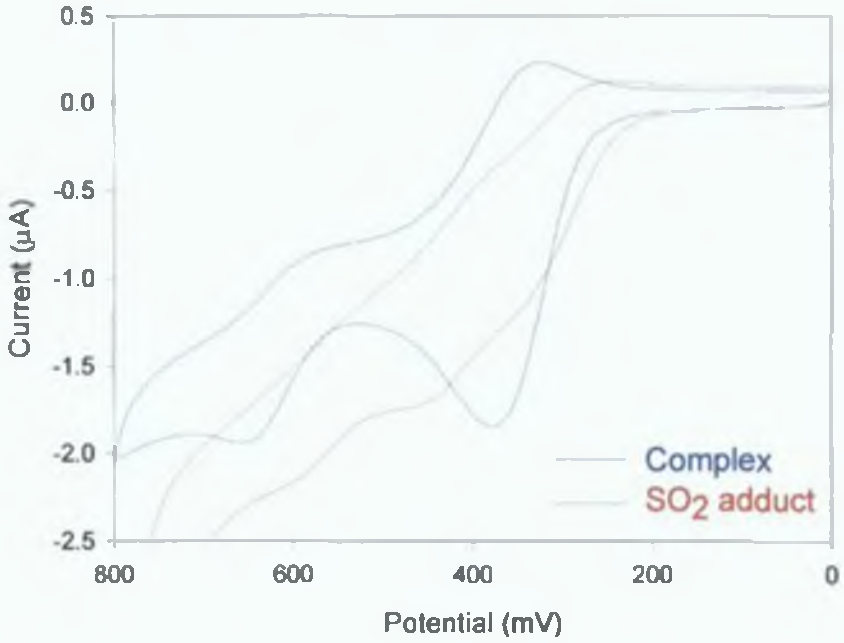


***Figure 6.9.*** Cyclic voltammograms for the complex $[Ni(\eta^5\text{-}C_5H_5)(\mu_2\text{-}SC_6H_4NC(H)C_6H_4CH_3)]_2$ before and after bubbling of $SO_2$. An electrochemically detectable $SO_2$ adduct was not observed.

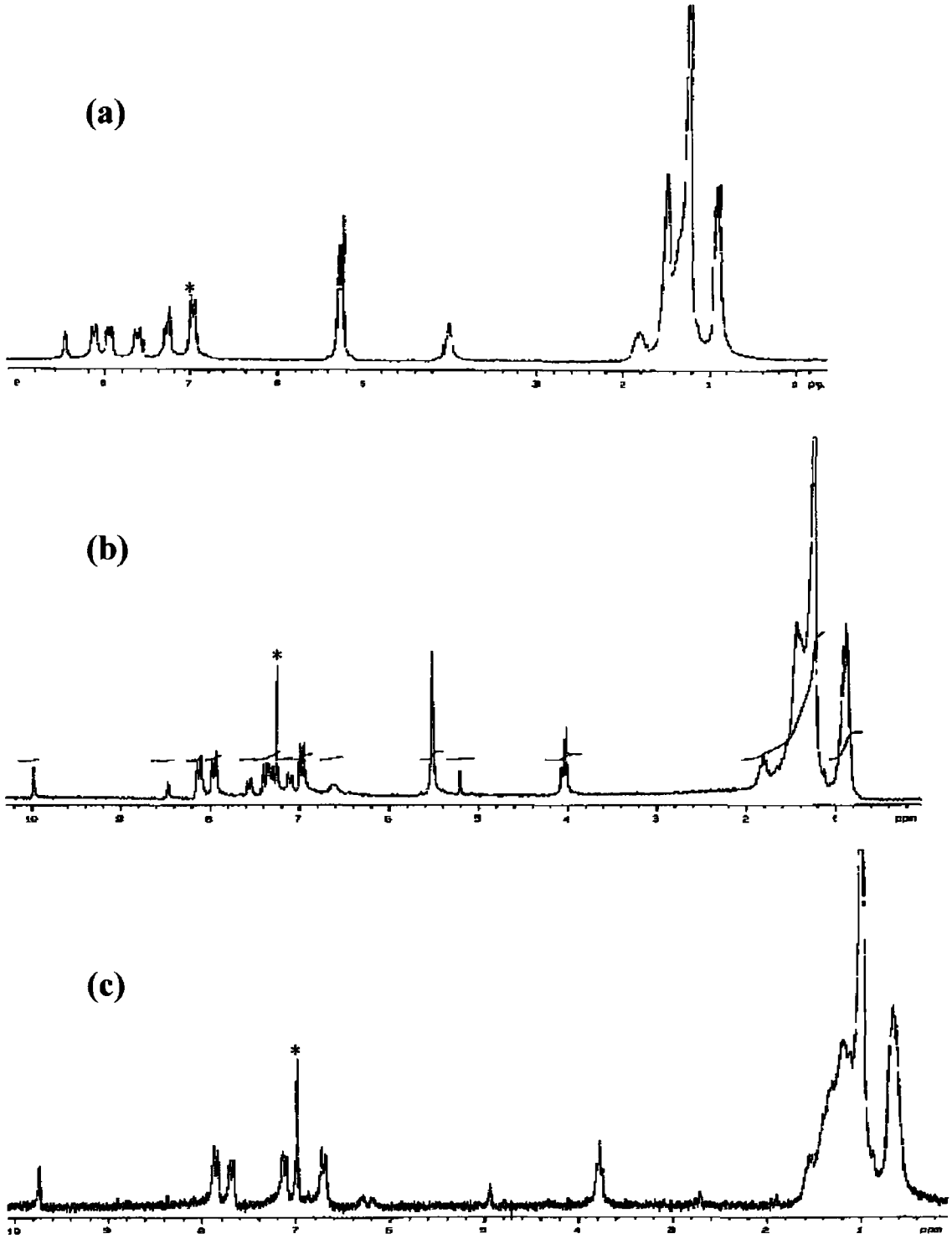


*Figure 6 10.* $^{1}H$ NMR spectra of (a) $[Ni(PBu_3)(\eta^5\text{-}C_5H_5)(SC_6H_4NH_2\text{-}4)]$, (b) its $SO_2$ adduct, and (c) 2 h after adduct formation * Represents residual $CH_2Cl_2$ in each of the complexes

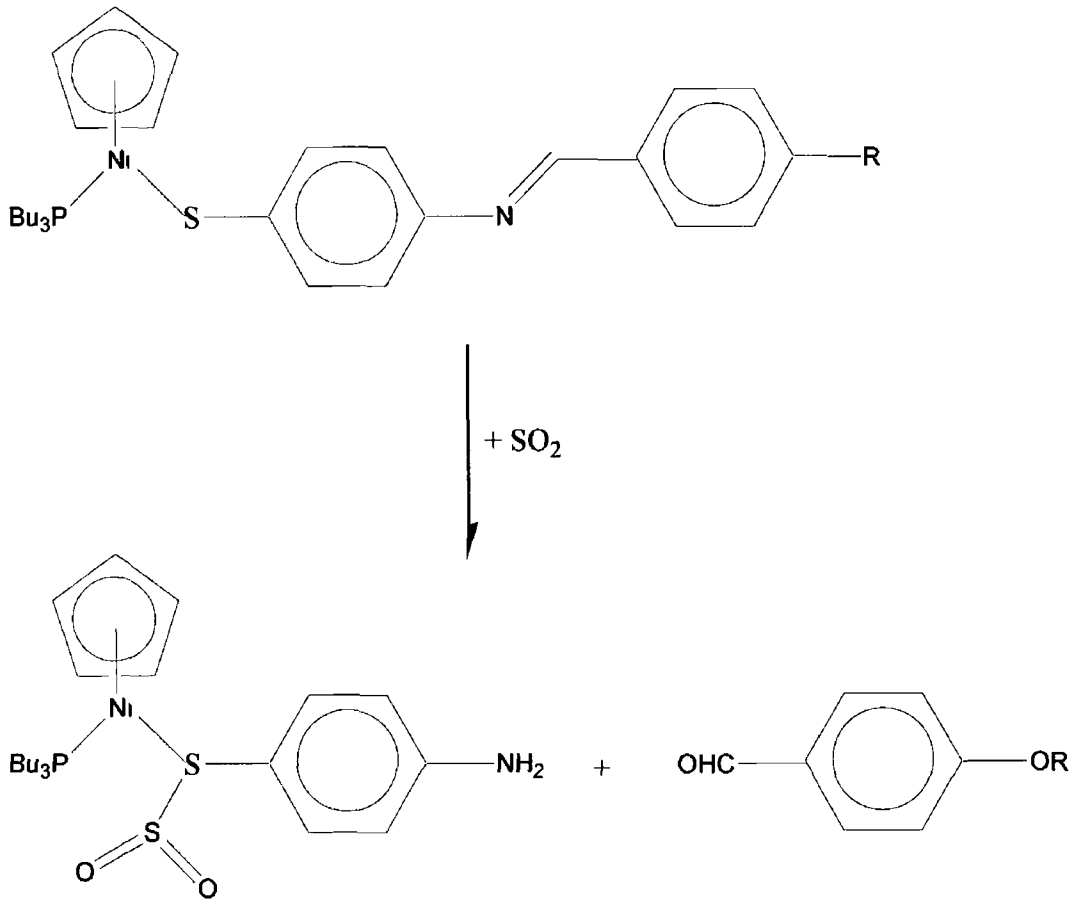


***Figure 6 11*** Proposed reaction of [2] with $SO_2$ where decomposition of the complex occurs to form an unstable adduct and aldehyde

### *6 3 3 Electrochemical screening of [Ni($\eta^5$-$C_5H_5$)($\mu_2$-$SC_6H_4X$-4)]$_2$ [3]*

[Ni($\eta^5$-$C_5H_5$)($\mu_2$-$SC_6H_4X$-4)]$_2$, where X = F and $NH_2$ [3] were the third set of cyclopentadienylnickel(II) thiolato complexes to be screened as potential $SO_2$ sensors These Schiff base complexes do not contain tributylphosphine, in contrast to [1] and [2] but have symmetrical bridging about the Ni-S bond (*Figure 6 2*) Each ligand contains one benzene ring with the X group attached in the para - position On bubbling of $SO_2$, distinct colour changes were observed for both complexes, indicative of adduct formation The binding mode for the $SO_2$ adduct should be different from that of [1],

since the coordinated sulphur that served as a point of attachment for the $SO_2$ in [1], no longer has a lone pair of electrons available for donation

Quasi-reversible, diffusion-controlled electrochemistry of Ni(II)/(III) before and after formation of the $SO_2$ adducts was observed ($\Delta E_p$ values were below 100 mV and $i_{pa}/i_{pc}$ values approached unity, *Section 6 3 4, Table 6 1*) In accordance with the behaviour of [1], the electrochemistry of [2] was radically different depending on the nature of the X group attached $E_{1/2}$ of the complex increased from + 69 mV to +292 mV when X was changed from $NH_2$ to F, rationalized by the decrease in electron density around the Ni centres This same trend was observed for [1] and can be explained both by trend in Hammett constants and the electron-donating and electron-withdrawing properties of the respective X groups

Of these complexes, only where X = F, an electrochemically detectable $SO_2$ adduct was formed, which yielded a $E_{1/2}$ shift of 52 mV The direction of this shift was negative, opposite to that observed in [1] (*Figure 6 12a*) Peak currents increased marginally upon adduct formation Little or no change in $E_{1/2}$ was observed when X = $NH_2$ between complex and adduct (*Figure 6 12b*) However, a dramatic decrease in current for the Ni redox couple and an irreversible anodic peak was observed ($E_{1/2}$ = + 400 mV) on formation of the $SO_2$ adduct This is in contrast to the behaviour of [1] whereby both the F and the $NH_2$ complexes yielded comparable $E_{1/2}$ shifts This behaviour would indicate that the electron rich metal centre of [2] requires stabilization on formation of the adduct which can only be obtained with an electron-withdrawing end group such as F

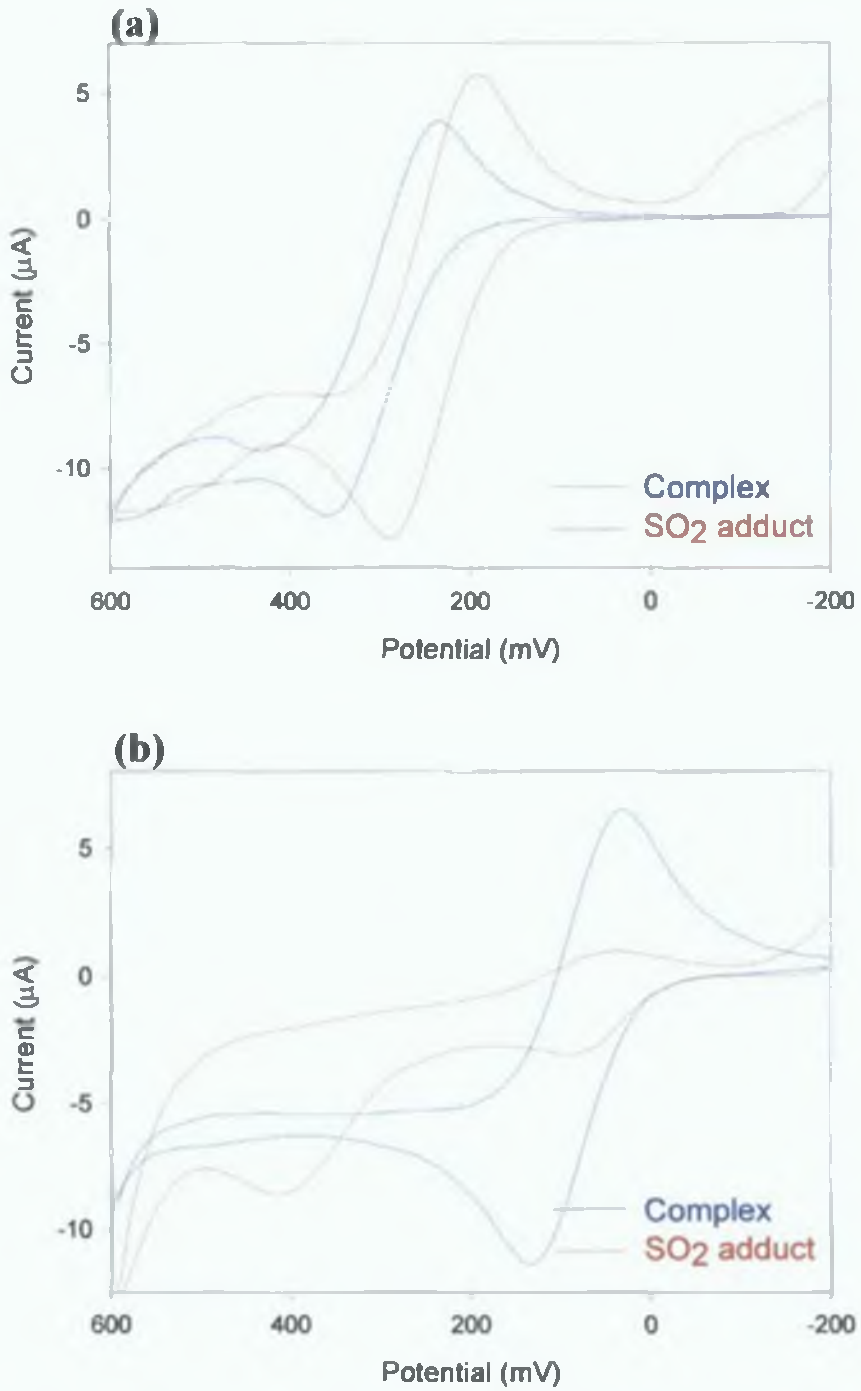


***Figure 6.12.*** Cyclic voltammograms for complexes (a) $[Ni(\eta^5\text{-}C_5H_5)(\mu_2\text{-}SC_6H_4F\text{-}4)]_2$ and (b) $[Ni(\eta^5\text{-}C_5H_5)(\mu_2\text{-}SC_6H_4NH_2\text{-}4)]_2$ and their respective $SO_2$ adducts.

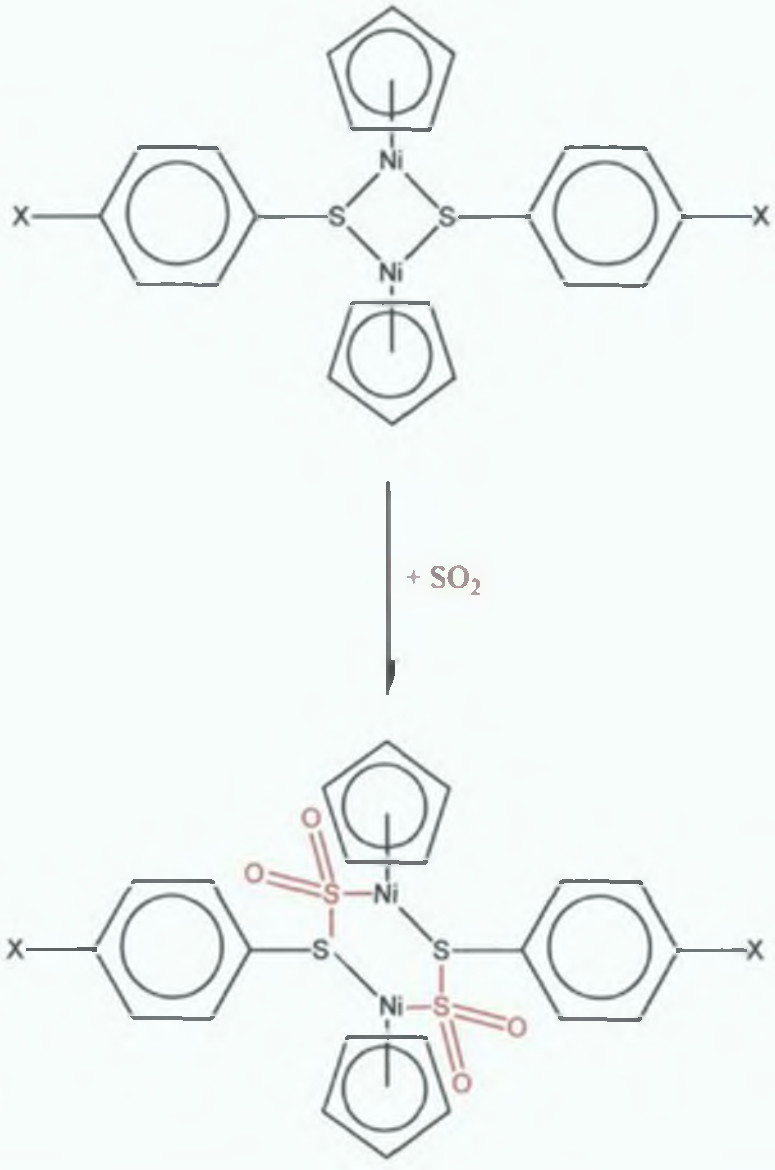


***Figure 6.13.*** Insertion reaction for $SO_2$ adduct formation hypothesized for [3].

No further information was gathered from $^1H$ NMR or UV-Vis spectroscopy. The proposed insertion reaction is given in *Figure 6.13* whereby insertion of $SO_2$ into the Ni-S dative bond is hypothesized. This would serve to increase the electron density around the proximal Ni centres, and thus explain the observed negative shifts in $E_{1/2}$ (*Figures 6.12a & b*). The stability or the reversibility of this adduct has not been investigated to date.

### *6 3 4 Electrochemical screening of [Ni(SC$_6$H$_4$NC(H)C$_6$H$_4$OCH$_2$CH$_2$SMe)($\eta^5$-C$_5$H$_5$)]$_2$ [4]*

[Ni(SC$_6$H$_4$NC(H)C$_6$H$_4$OCH$_2$CH$_2$SMe)($\eta^5$-C$_5$H$_5$)]$_2$ [4], also screened for potential $SO_2$ detection, was similar to [3] in that it had symmetrical bridging about the Ni-S bond In this case each ligand contained an imine functionality, forming a Schiff base as in [2], and possessed a methyl sulphide end group On bubbling of $SO_2$, distinct colour changes were observed, indicative of adduct formation

Quasi-reversible electrochemistry of the Ni centre before and after formation of the $SO_2$ adduct (*Figure 6 14*, *Table 6 1*) was observed with $\Delta$Ep values of 82 mV and 61 mV, respectively $i_{pa}/i_{pc}$ was approximately unity for both complex and adduct The shift in $E_{1/2}$ of this complex on formation of the $SO_2$ adduct was 84 mV in the negative direction An insertion reaction for adduct formation as for [3] can similarly be applied for this complex, thus explaining the negative shift

Complexes [1] and [3] can potentially only detect dissolved $SO_2$ in bulk organic phase in their present states as they contain no functionalities to allow for stable adsorption onto a solid surface However, it has been demonstrated that [4] can be applied to the surface of a gold electrode to produce a stable SAM (self-assembled monolayer) through the methyl sulphide end-groups (*Chapter 5*) This property could lend itself to a unique modified electrode surface capable of $SO_2$ adduct formation and hence a solid phase electrochemical sensor applicable to aqueous, non-aqueous and gaseous samples This was not tested in this present work

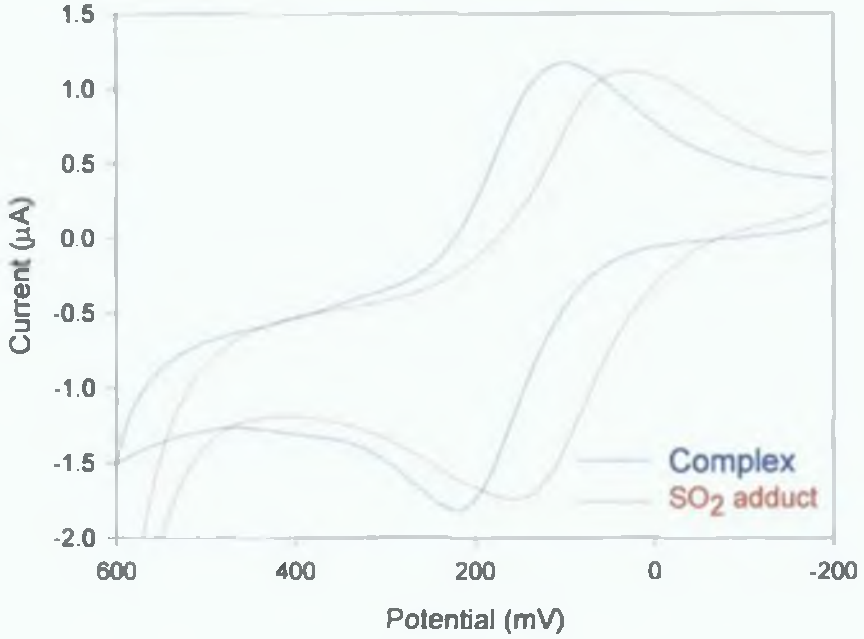


***Figure 6.14.*** Cyclic voltammograms for [4] and its corresponding $SO_2$ adduct. A negative shift of 67 mV in $E_{1/2}$ was observed after formation of the $SO_2$ adduct.

*Table 6 1* Summary of electrochemical data for all of the complexes screened for $SO_2$ adduct formation

| *Sensor material* | $E_{p,a}(mV)$ | $E_{p,c}(mV)$ | $\Delta E_p(mV)$ | $E_{1/2}$ (mV) | $i_{p,a}/i_{p,c}$ |
|---|---|---|---|---|---|
| ***Complexes and $SO_2$ Adducts [1]*** | | | | | |
| $[Ni(PBu_3)(\eta^5\text{-}C_5H_5)(SC_6H_4NH_2\text{-}4)]$ | 283 | 223 | 59 | 256 | 1 50 |
| $[Ni(PBu_3)(\eta^5\text{-}C_5H_5)(SC_6H_4NH_2\text{-}4)]SO_2$ | 342 | 283 | 59 | 313 | 1 34 |
| $[Ni(PBu_3)(\eta^5\text{-}C_5H_5)(SC_6H_4F\text{-}4)]$ | 359 | 302 | 57 | 331 | 1 07 |
| $[Ni(PBu_3)(\eta^5\text{-}C_5H_5)(SC_6H_4F\text{-}4)]SO_2$ | 422 | 359 | 63 | 391 | 1 22 |
| $[Ni(PBu_3)(\eta^5\text{-}C_5H_5)(SC_6H_4Br\text{-}4)]$ | 434 | 333 | 101 | 384 | 1 08 |
| $[Ni(PBu_3)(\eta^5\text{-}C_5H_5)(SC_6H_4Br\text{-}4)]SO_2$ | 461 | 364 | 97 | 413 | 1 15 |
| $[Ni(PBu_3)(\eta^5\text{-}C_5H_5)(SC_6H_4Cl\text{-}4)]$ | 488 | 374 | 114 | 431 | 0 91 |
| $[Ni(PBu_3)(\eta^5\text{-}C_5H_5)(SC_6H_4Cl\text{-}4)]SO_2$ | 471 | 352 | 119 | 412 | 1 08 |
| ***Complexes [2]*** | | | | | |
| $[Ni(PBu_3)(\eta^5\text{-}C_5H_5)(SC_6H_4C(H)NC_6H_4F\text{-}4)]$ | 376 | 313 | 64 | 345 | 1 10 |
| $[Ni(PBu_3)(\eta^5\text{-}C_5H_5)(SC_6H_4C(H)NC_6H_4OCH_3\text{-}4]$ | 354 | 297 | 57 | 326 | 1 04 |
| $[Ni(PBu_3)(\eta^5\text{-}C_5H_5)(SC_6H_4C(H)NC_6H_4CH_3\text{-}4]$ | 369 | 332 | 37 | 351 | 1 01 |

| *Sensor material* | $E_{p,a}$*(mV)* | $E_{p,c}$*(mV)* | $\Delta E_p$*(mV)* | $E_{1/2}$ *(mV)* | $i_{p,a}/i_{p,c}$ |
|---|---|---|---|---|---|
| ***Complexes and $SO_2$ adducts [3]*** | | | | | |
| $Ni(\eta^5\text{-}C_5H_5)(\mu_2\text{-}SC_6H_4NH_2\text{-}4)]_2$ | 107 | 28 | 79 | 69 | 1 03 |
| $[Ni(\eta^5\text{-}C_5H_5)(\mu_2\text{-}SC_6H_4NH_2\text{-}4)]_2SO_2$ | 82 | 59 | 23 | 71 | 1 68 |
| $[Ni(\eta^5\text{-}C_5H_5)(\mu_2\text{-}SC_6H_4F\text{-}4)]_2$ | 340 | 244 | 96 | 292 | 0 64 |
| $[Ni(\eta^5\text{-}C_5H_5)(\mu_2\text{-}SC_6H_4F\text{-}4)]_2SO_2$ | 281 | 198 | 83 | 240 | 0 83 |
| ***Complex and $SO_2$ adduct [4]*** | | | | | |
| $[Ni(SC_6H_4C(H)NC_6H_4OCH_2CH_2SMe)(\eta^5\text{-}C_5H_5)]_2$ | 241 | 159 | 82 | 200 | 0 93 |
| $[Ni(SC_6H_4C(H)NC_6H_4OCH_2CH_2SMe)(\eta^5\text{-}C_5H_5)]_2SO_2$ | 146 | 85 | 61 | 116 | 1 31 |

### *6 3 5 Behaviour of complexes as quantitative sensing materials for $SO_2$*

The screening results of the previous sections demonstrated that complexes [1], [3] and [4] possess well-defined electrochemistry, and can adsorb $SO_2$ to form adducts exhibiting redox electrochemistry different to that of the original complex This unique property warranted further work to investigate whether or not these complexes could be used to detect $SO_2$ quantitatively by electrochemical means By adding sufficiently small quantities of $SO_2$ to degassed solutions of selected complexes, $E_p$ values of the Ni centres were measured using cyclic voltammetry after each addition

Three of the above complexes were chosen for further analysis [1], where $X=NH_2$, [3], where X=F, and [4] Each of these complexes were shown to exhibit stable $SO_2$ adducts (*Section 6 2 1 – 6 2 4*), where the peak potentials of [1] shifted in the positive direction, and [3] and [4] in the negative direction

Two sources of $SO_2$ were used liquid $H_2SO_3$ and $SO_2$ gas, according to *Sections 6 2 5* and *6 2 6*, and the results from these methods were compared Liquid $SO_2$, sulphurous acid, $H_2SO_3$, is known to provide $SO_2$ in equilibrium with acid but is immiscible with $CH_2Cl_2$ The distribution coefficient for $SO_2$ between the aqueous and

organic phase was not known, and so arbitrary scales were used for these calibration curves An absolute scale (ppm) was possible when $SO_2$ gas was used as analyte (injected into solution by means of a gas tight syringe), assuming ideal gas conditions

It was found that all complexes examined were highly sensitive to $SO_2$ and began forming electrochemically detectable $SO_2$ adducts at very low levels of analyte All complexes were seen to respond linearly in the ppm range to $SO_2$ until a given saturation point (probably when all of the molecules had reacted with the $SO_2$) Each of the examined complexes possessed different sensitivities and linear ranges towards $SO_2$, implying that each of the complexes may be suited towards different commercial applications

*Figure 6 15* shows CVs as increasing amounts of $H_2SO_3$ are added to a solution of $[Ni(\eta^5\text{-}C_5H_5)(\mu_2\text{-}SC_6H_4F)]_2$ (Type [3]) The redox potential shifted gradually as expected in the negative direction with increasing amounts of analyte, showing that $SO_2$ present in the sulphurous acid was effectively being transferred into the organic phase and gradually forming the desired adduct $^1$H NMR was also carried out to provide further verification of adduct formation (data not shown)

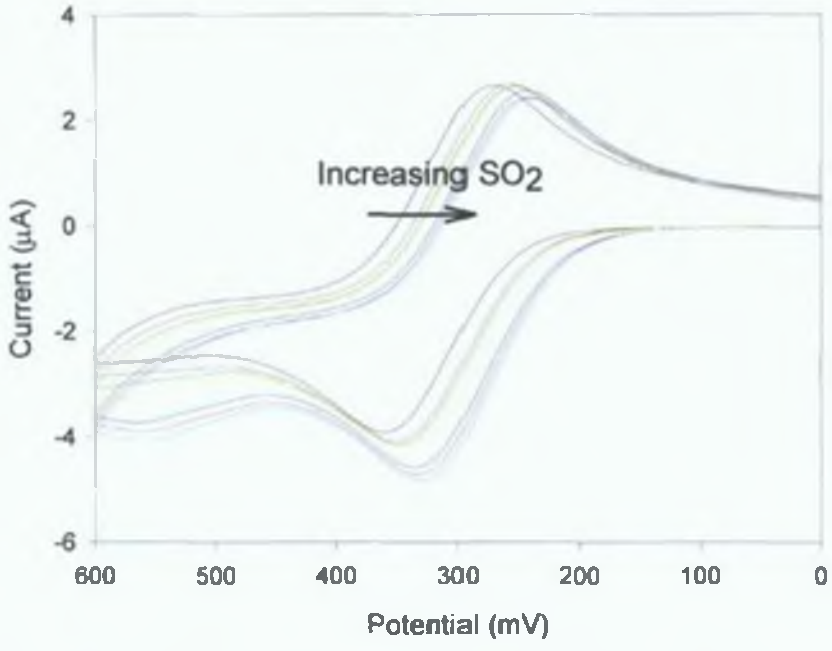


***Figure 6.15.*** Cyclic voltammograms after successive additions of $H_2SO_3$ to a solution of $[Ni(\eta^5\text{-}C_5H_5)(\mu_2\text{-}SC_6H_4F)]_2$ (2 mmol $dm^{-3}$). The CVs depict the gradual shift in $E_p$ values as increasing amounts of $S0_2$ adduct formed.

*Figures 6.16-6.18* show the calibration plots for each of the complexes using $H_2SO_3$ and $SO_2$ gas as analyte sources. All complexes were used at a concentration level of 2 mmol $dm^{-3}$ and the anodic peak potential was monitored in all cases. Liquid and gaseous sources of analyte provided similar trends in the calibration curves, illustrating that these complexes can sense $SO_2$ in organic phase, and also in non-miscible liquids (i.e. aqueous phase), provided a distribution coefficient for $SO_2$ between the two phases was known.

When gaseous $SO_2$ was used as analyte, the $[Ni(PBu_3)(\eta^5\text{-}C_5H_5)(SC_6H_4NH_2\text{-}4]$ (Type [1]) sensor system gave the widest linear relationship between $E_{p,a}$ and $[SO_2]$, from 700 to < 2000 ppm (mg $l^{-1}$) with an $r^2$ value of 0.993 for gaseous $SO_2$. *Figure 6.16a* & b show the calibration plots. It can be seen that both plots exhibit similar trends where $E_{p,a}$ experienced an initial shift in the negative direction for low levels of adduct formation. At a level of 700 ppm, the direction of the shift changed and began to increase linearly with increased amounts of $SO_2$ to give a wide linear range over two orders of

magnitude (*Figure 6 16a*) The sensitivity of the complex over this range was 0 02 mV ppm $^{1}$ using gaseous samples The initial decrease in $E_{pa}$ could result in false positive readings, a potential problem associated with this thiolato complex This decrease in $E_{pa}$ was not observed in the initial screening of the complexes as complete saturation of the complexes with $SO_2$ was carried out An explanation for it is not known, as decreases in $E_{pa}$ would indicate increases in electron density around the Ni centres According to the hypothesized mechanism (*Figure 6 8*), however, the Ni centre's electron density decreased Isolation of the adduct may provide further insight into a complete mechanism of adduct formation

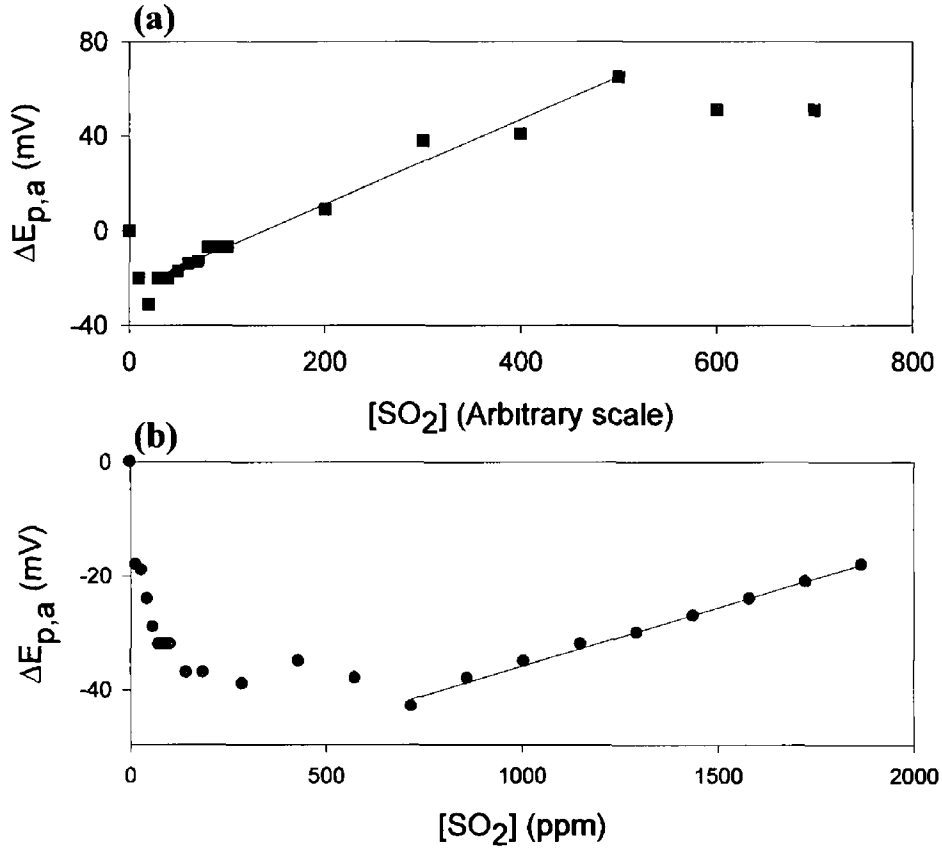


***Figure 6 16*** Calibration plots for quantitative measurement of $SO_2$ with $[Ni(PBu_3)(\mu_2\text{-}SC_6H_4NH_2)]$ (2 mmol $dm^{-3}$) using (a) liquid $H_2SO_3$ and (b) $SO_2$ gas as sources of analyte

$[Ni(\eta^5\text{-}C_5H_5)(\mu_2\text{-}SC_6H_4F\text{-}4)]_2$ (Type [3]) had the lowest saturation point resulting in a narrow linear range (0 – 20 ppm) with $r^2$ values of 0 989 for gaseous

samples Calibration curves for $[Ni(\eta^5\text{-}C_5H_5)(\mu_2\text{-}SC_6H_4F)]_2$ are given in *Figure 6 17* Consistent linear shifts in $E_{p\,a}$ in the negative direction, as expected, were observed using both $H_2SO_3$ and $SO_2$ gas as sources for analyte Although the linear range of this complex is narrow (*Figure* 6 17b), it would still have applications for detection of $SO_2$ in the environment at very low levels It was seen to be more sensitive than [1] with a slope of 0 88 mV $ppm^{-1}$ for gaseous samples

$[Ni(SC_6H_4NC(H)C_6H_4OCH_2CH_2SMe)(\eta^5\text{-}C_5H_5)]_2$ (Type [4]) displayed linearity between 140 and 550 ppm using $SO_2$ gas as analyte ($r^2$ = 0 963) Consistent linear shifts in $E_{p,a}$ in the negative direction, as expected, were observed using both $H_2SO_3$ and $SO_2$ gas as sources for analyte (*Figure 6 18a & b*) $E_{p\,a}$ values of the metal centre remained unchanged for additions of $SO_2$ up to a level of 140 ppm, demonstrating that this complex required a minimum amount of $SO_2$ before its adduct could form (or be electrochemically detected) Above concentrations of 550 ppm, the $SO_2$ adduct was fully formed, and no further change in potential was observed (*Figure 6 18b*) The sensitivity of this complex was 0 090 mV $ppm^{1}$, which was the highest sensitivity observed for any of the complexes It does not, however, have the advantage of being able to detect $SO_2$ at very low levels as in [3], nor has the capability of [1], where it can detect the species over such a wide linear range However, it has a distinct advantage over the other complexes as it has been shown to be possible to bind this molecule to the surface of a gold electrode via the thiol end groups (*Chapter 5*) This unique property of the complex may allow for development of a very novel solid phase sensor for $SO_2$

The trends observed for each of these complexes indicate that very different mechanisms are used for formation of adduct Isolation of these adducts must be carried out in order to verify the sites of attachment of $SO_2$ for adduct formation Investigations into the mechanisms are also required in order to elucidate the intermediate products that are generated

The results of this section demonstrate that each of these complexes could potentially be used as a sensor material for quantitative analysis of $SO_2$ It has been demonstrated that $SO_2$ can be detected in both immiscible liquid samples (provided there is a distribution coefficient for $SO_2$ between the two phases) and gaseous samples The variation in linear ranges and sensitivities suggest that potential applications would be

different for each complex. While [3] and [4] could potentially be suited towards high precision measurements at low concentrations of $SO_2$, [1] would be better suited to qualitative measurements of the gas towards the middle to upper end of the ppm scale. A device incorporating more than one of these sensor materials, covering the different ranges, would yield a wider measurement range, and have the capacity to eliminate false positives.

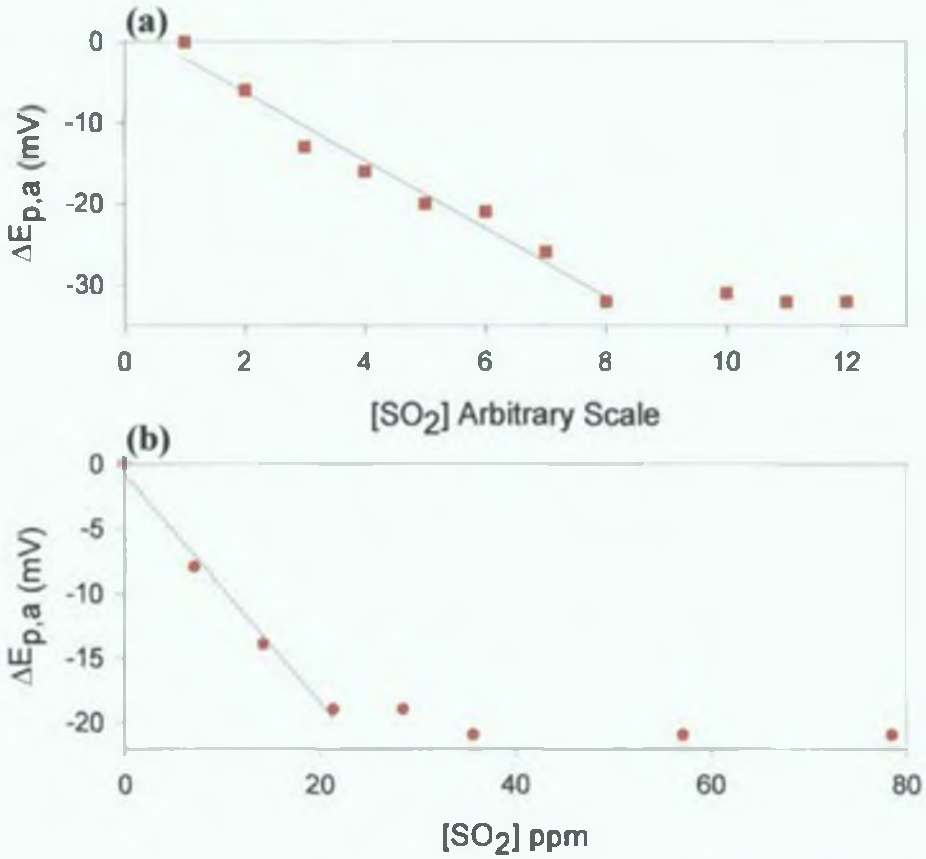


***Figure 6.17.*** Calibration plots for quantitative measurement of $SO_2$ with $[Ni(\eta^5\text{-}C_5H_5)(\mu_2\text{-}SC_6H_4F\text{-}4)]_2$ (2 mmol $dm^{-3}$) using (a) liquid $H_2SO_3$ and (b) $SO_2$ gas as sources of analyte.

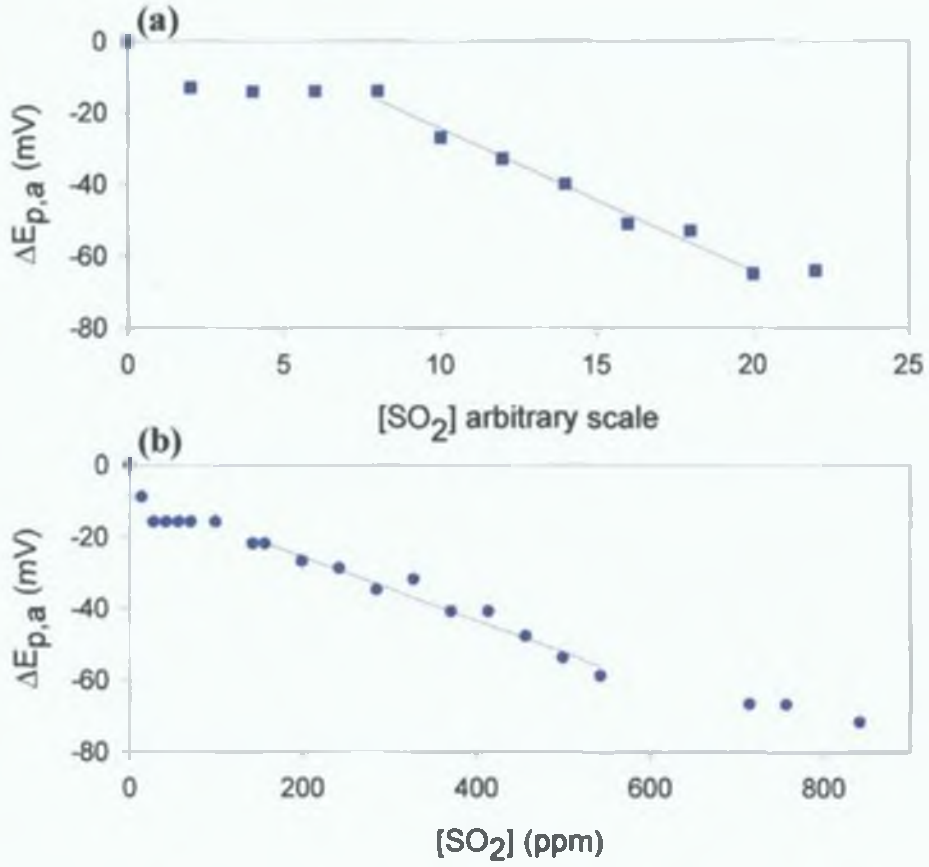


***Figure 6.18.*** Calibration plots for quantitative measurement of $SO_2$ with $[Ni(SC_6H_4NC(H)C_6H_4O)CH_2CH_2SMe)(\eta^5\text{-}C_5H_5)]_2$ (2 mmol $dm^{-3}$) using (a) liquid $H_2SO_3$ and (b) $SO_2$ gas as sources of analyte.

### *6.3.6 Interference studies*

A major problem often encountered with electrochemical sensors is the lack of selectivity towards electroactive species (Saini *et al.*, 1995). One major advantage of this novel sensor is that other matrix gaseous species should not interfere, unless they exhibit electrochemistry in the same region as the complex, or that they affect the electrochemistry of the complex in a manner similar to the $SO_2$ molecule by attaching to some point on the complex. Since the molecules of interest such as $H_2S$, CO, $CO_2$, NO, $NO_2$, $O_2$, $N_2$ and $NH_3$ are generally not redox active in the potential region of interest

(-200 – 600 mV), the major concern should be whether or not these molecules can distort the electrochemistry of the thiolato complexes by complexation

Influences of some interfering gases on shifts in $E_p$ values of the complexes were evaluated by running CVs of the complex (2 mmol $dm^{-3}$), saturating of solutions by bubbling with $N_2$, $H_2S$ and $CO_2$ for 1 min approx , and then running the CV again to monitor any shifts in potential Both $H_2S$ and $CO_2$ were chosen for their similarities in structure to $SO_2$ It was thought that these molecules may bind to the thiolato complex in a manner similar to $SO_2$ Other gases such as nitrogen oxides could also be potential interferents, but were not used in this study

It was observed that when $H_2S$ was bubbled through the solution, the redox activity of the complex disappeared immediately After leaving a solution of complex with $H_2S$ gas present over a period of 2 days, a black precipitate was observed, indicative of metal sulphide formation (Cotton & Wilkinson, 1988) Analysis of this precipitate by IR would confirm this suspicion $H_2S$ contamination is a serious drawback of this type of sensor, and if $H_2S$ was present at high levels in a given matrix, electrochemical sensing using the Ni(II) thiolato complexes would not be possible

*Figure 6 19* depicts a bar chart of the effect of saturation of solutions with $CO_2$, $N_2$ and $SO_2$ on $[Ni(PBu_3)(\eta^5\text{-}C_5H_5)(SC_6H_4C(H)NC_6H_4F)]_2$ (Type [3]) The electrochemistry remained defined, and there were neglible potential shifts for $CO_2$ and $N_2$ While the shifts in $E_{p\,a}$ values for $SO_2$ is $118 \pm 21$ mV, the shifts for $CO_2$ and $N_2$ were just $6 \pm 8$ and $9 \pm 15$ mV, respectively These values show that there is no binding of $CO_2$ or $N_2$ to the complex, and neither gas distorts the electrochemistry of the metal centres, and therefore do not pose as major interferences

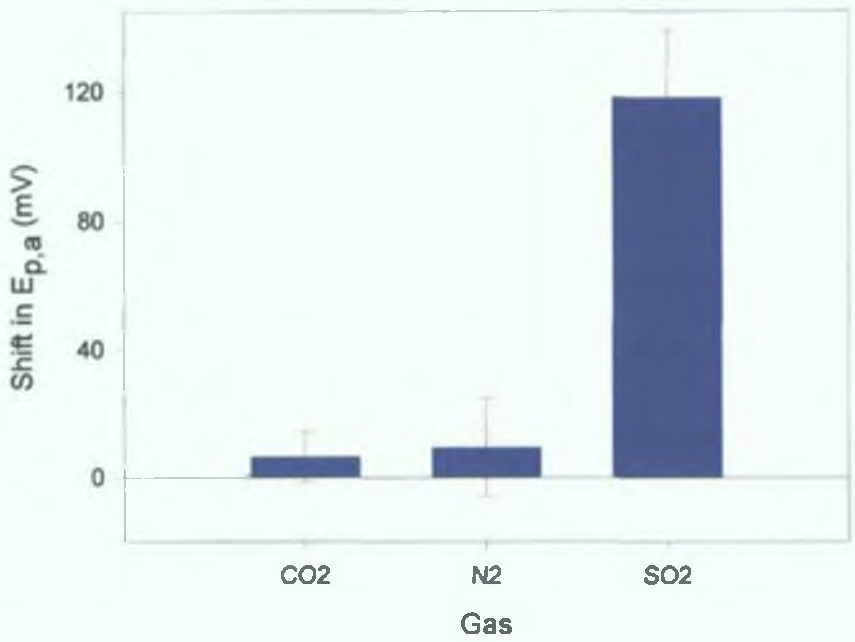


***Figure 6.19.*** Bar chart of the effects of two potential interfering gases, $CO_2$ and $N_2$, on $E_{p,a}$ compared to $SO_2$.

## 6.4 CONCLUSION

This work presents preliminary data that shows particular types of cyclopentadienyl nickel complexes form reversible $SO_2$ adducts that can be detected electrochemically Electrochemistry, $^1H$ NMR and UV-Vis spectroscopy were used as methods of characterisation for both complexes and adducts Cyclopentadienylnickel phosphine complexes with simple thiolate ligands [1], exhibited defined electrochemistry where $E_{1/2}$ values varied depending on the substituent on the thiolate ligand in the order F > $NH_2$ > Br ≅ Cl attached These complexes formed $SO_2$ adducts that possessed defined electrochemistry different to that of the original complex The potential shift was most apparent for the –F and the –$NH_2$ complexes $^1H$ NMR spectroscopic data showed all chemical shifts after $SO_2$ adduct formation to shift downfield, which is diagnostic of the thiolato sulphur atom acting as a Lewis base in binding the $SO_2$ Time dependent $^1H$ NMR data showed the adduct to be labile UV-Vis verified the attachment of $SO_2$ to a ligand site, rather than the metal

Complex [2], a cyclopentadienylnickel(II) phosphino Schiff base, did not form an $SO_2$ adduct but rather decomposed in the presence of $SO_2$ Although the complex itself exhibited quasi-reversible electrochemistry of the Ni centre, in the presence of $SO_2$ this behaviour was lost The major difference in the $^1H$ NMR spectrum of this complex before and after adding $SO_2$ was the presence of an aldehyde peak, indicating decomposition The Schiff base must split at the imine site on the ligand to generate the aldehyde

Complex [3], nickel thiolato complexes, with ligand substituents –F and $NH_2$, formed $SO_2$ adducts that possessed electrochemistry different to that of the original complexes The fluoro complex possessed the best electrochemical characteristics of the $SO_2$ adduct It is thought an insertion mechanism occurs for adduct formation in these complexes where cleavage of the Ni-S dative bond occurs by insertion of $SO_2$ A similar mechanism has been hypothesised for complex [4], a cyclopentadienylnickel(II) thiolato Schiff Base containing a MeS end group No $^1H$ NMR or UV-Vis data were obtained for

complexes [3] and [4] to date The stability and reversibility of these adducts has not yet been elucidated

Further investigations were carried out in order to determine whether or not these complexes could be used to detect $SO_2$ quantitatively by electrochemical means It was found that complexes [1], [3] and [4] were all quantitatively sensitive to $SO_2$ and began forming electrochemically detectable $SO_2$ adducts at very low levels of analyte Both liquid and gaseous sources of analyte provided similar trends in the calibration curves, illustrating that these complexes could sense $SO_2$ in organic phase, and also in non-miscible liquids (i e aqueous phase), provided a distribution coefficient for $SO_2$ between the two phases was known

Each of the complexes responded linearly in the ppm range using gaseous $SO_2$ until a given saturation point (probably when all of the molecules had reacted with the $SO_2$) Complex [1] where X = $NH_2$ had the widest linear range of 700-2000 ppm when $SO_2$ was added as gaseous analyte The lowest linear range (0 – 20 ppm) was seen for [3], where X = F Complex [4] had a linear range between 140 and 550 ppm Sensitivity varied between the complexes, with [3] being the most sensitive (0 88 mV $ppm^{-1}$) A device incorporating more than one of these sensor materials would also serve to yield a wider measurement range, and also have the capacity to eliminate false positives

None of the complexes examined were capable of detecting $SO_2$ in the sub or low ppb range using cyclic voltammetry Legislation requires $SO_2$ sensing techniques to detect sub-ppb levels in the environment In order to achieve this sensitivity, a full investigation would be necessary into the pathways required for $SO_2$ adduct formation Investigations into the effects of varying the metal centre on the magnitude of potential shift could also be examined With information such as this, it may be possible to tailor a material suitable for $SO_2$ detection at sub-ppb levels The materials examined in this work may be more suited to fields such as $SO_2$ detection in combustion gases, where higher levels of $SO_2$ would be expected to be present

Within limits of experimental error, $CO_2$, $N_2$ and $O_2$ do not interfere with the detection of $SO_2$ with the sensor system However, the presence of $H_2S$ leads to the formation of nickel sulphide and as such, distorts the electrochemistry of the Ni centre

severely The effect of nitrogen oxides, other potential interferents, was not covered in this study

Complex [4] may have the most potential as a sensor material due to its methyl sulphide end group Modification of gold electrodes with this material can be carried out through self-assembly of the methyl sulphide end-groups (*Chapter 5*) Unlike the other complexes in their present states, the solution phase adduct formation may be extended to surface bound adduct formation This would allow direct sensing of $SO_2$ in gaseous form Modifications of complexes [1] and [3] to include thiol or methyl sulphide end-groups could also be carried out, and depending on the resulting electrochemistry of these new complexes, these materials could also be integrated into promising solid phase sensors for $SO_2$

## 6.5 REFERENCES


Ampuero, S , Bosset, J (2003) The electronic nose applied to dairy products a review *Sens Actuat B,* **94** 1-12

Chiou, C , Chou, T (2002) Amperometric $SO_2$ gas sensors based on solid polymer electrolytes *Sens Actuat B,* **87** 1-7

Cotton, F , Wilkinson G (1988) Advanced Organic Chemistry, Fifth Edition *Wiley-Interscience, United States* pp 743

Darensbourg, M , Tuntulani, T , Rebenspies, J (1994) Sulphur site adducts of sulphur dioxide in nickel-bound thiolates and their conversion to sulphate *Inorg Chem* , **33** 611-613

Darkwa, J , Moutloali, R , Nyokong, T (1998) Reversible sulphur dioxide reactions with cyclopentadienylnickel(II) organochalcogenide complexes *J Organomet Chem* , **564** 37-45

Dasgupta, P , Kar, S (1995) Measurement of gases by a suppressed conductometric capillary electrophoresis separation system *Anal Chem* , 67 3853-3860

Ebarvia, B , Binag, C , Sevilla III, F (2001) Surface and potentiometric properties of a $SO_2$ sensor based on a hydrogel coated pH-FET *Sens Actuat B,* **76** 644-652

Eller, P , Kubas, G (1977) Sulphur dioxide adducts of organophosphinecopper(I) mercaptide, phenoxide, and selenolate complexes coordinated SR-, OR-, and SeR- as Lewis bases *J Am Chem Soc* , **99** 4346-4351

Ferrari, L , Salisbury, J (1999) Australian National Environmental Health Forum Monographs, Air Series No 4 pp 14

Hansch, C , Leo, A , Taft, R (1991) A survey of Hammett substituents constants and resonance and field parameters *Chem Rev* , **91** 165-195

Hisamatsu, Y , Ping, L , Dasgupta, P (1989) Measurement of trace levels of atmospheric sulphur dioxide with a gold film sensor *J Air Waste Man Assoc* , **39** 975-980

Hodgson, A , Jacquinot, P , Jordan, L , Hauser, P (1999) Amperometric gas sensors with detection limits in the low ppb range *Anal Chim Acta,* **393** 43-48

Knake, R , Hauser, P (2003) Portable instrument for electrochemical gas sensing *Anal Chim Acta,* **500** 145-153

Kohl, D (2001) Function and applications of gas sensors *J Phys D Appl Phys* , **34** R125-R149

Kovacs, I , Pearson, C , Shaver, A (2001) Preparation of ruthenium silanethiolato complexes and their reactions with sulphur dioxide, possible models for the activation of $SO_2$ in the homogeneously catalysed Claus reaction *J Organomet Chem* , **596** 193-203

Krochmal D , Kalina, A (1997) A method of nitrogen dioxide and sulphur dioxide determination on ambient air by use of passive samplers and ion chromatography *Atmos Environ* , **31** 3473-3479

Kubas, G (1994) Chemical transformations and facile disproportionation of sulphur dioxide on transition metal complexes *Acc Chem Res* , **27** 183-190

Kubas, G , Ryan, R (1986) Activation of $H_2$ and $SO_2$ by Mo and W complexes first examples of molecular $-H_2$ complexes, $SO_2$ insertion into metal hydride bonds, and homogeneous hydrogenation of $SO_2$ *Polyhed*, **5** 473-485

Li, K , Guzei, I , Darkwa, J (2003) Insertion of sulfur dioxide into metal-carbon bonds of chloro(methyl)palladium complexes *Polyhed*, **22** 805-810

Milam, M , Cardoso, A (2003) Construction and performance of a drop cell for the nephelometric determination of sulphur dioxide *Microchem J*, **74** 75-82

Moloto, M , Nelana, S , Moutloali, M , Guzei, I , Darkwa, J (2004) Cyclopentadienylnickel thiolate complexes synthesis, molecular structures and electrochemical detection of sulphur dioxide adducts *J Organomet Chem*, **689** 387-394

Morrin, A , Moutloali, R , Killard, A J , Smyth, M R , Iwuoha, E , Darkwa, J (2004) Electro-Catalytic Sensor Devices (I) Cyclopentadienylnickel(II) Thiolato Schiff Base Monolayer Self-Assembled on Gold *Talanta*, **64** 30-38

Moutloali, R (2003) Thiolato Schiff base complexes of nickel and palladium as mesogens and molecular wires PhD Thesis School of Chemistry, University of the Western Cape, South Africa

Nevondo, F , Crouch, A , Darkwa, J (2000) Synthesis and characterisation of thiolato Schiff base nickel(II) complexes X-Ray structures of Ni($\eta$5-$C_5H_5$)($PPh_4$)($SC_6H_4N$=$CHC_6H_4$Br-4') Ni($\eta$5-$C_5H_5$)($PPh_4$)($SC_6H_4N$=$CHC_6H_4CH_3$-4') *J Chem Soc Dalton Trans*, **43** 43-50

Rys, A , Lebuis, A , Shaver, A , Harpp, D (2002) Insertion of SO2 into the S-S bond of $Cp_2MoS_2$ and $Cp_2MoS_2O$ to give molybdocene dithiosulphate and bis(*O*-alkylthiosulphates) *Inorg Chem*, **41** 3653-3655

Saini, S , Surareungchai, W , Turner, A (1995) Preliminary investigation of a bioelectrochemical sensor for the detection of phenol vapours *Biosens Bioelectron*, **10** 945-957

Santos, J , Garcia, M , Aleixandre, M , Horrillo, M , Gutierrez, J , Sayago, I , Fernandez, M , Ares, L (2004) Electronic nose for the identification of pig feeding and ripening times in Iberian hams *Meat Sci* , **66** 727-732

Schwarz, F , Okabe, H , Whittaker, J (1974) Fluorescence detection of sulphur dioxide in air at the parts per billions level *Anal Chem* , **28** 1024-1028

Shaver, A , Plouffe, P -Y (1992) Possible cooperative bonding between the ruthenium-bonded and sulphur-bonded $SO_2$ groups in $CpRu(PPh_3)(SO_2)[S(SO_2\text{-}4\text{-}C_6H_4Me]$ *Inorg Chem* , **31** 1823-1826

Shi, G , Luo, M , Xue, J , Xian, Y , Jin, L , Jin, J -Y (2001) The study of $PVP/Pd/IrO_2$ modified sensor for amperometric determination of sulphur dioxide *Talanta,* **55** 241-247

Tomchenko, A , Harmer, G , Marquis, B , Allen, J (2003) Semi-conducting metal oxide sensor array for the selective determination of combustion gases *Sens Actuat B,* **93** 126-134

Yang, Z , Burton, D (2000) A novel double insertion of the difluoromethylenecopper into the carbon-copper bond of perfluoroaryl- and perfluorovinylcopper reagents preparation, mechanism and applications of the new fluorinated copper reagents *J Fluorine Chem* , **102** 89-103

Zhu, L , Seburg, R , Tsai, E , Puech, S , Mifsud, J (2004) Flavour analysis in a pharmaceutical oral solution formulation using an electronic nose *J Pharm Biomed Sci* , **34** 453-461

# Chapter 7

## Future Developments

## 7.1 FURTHER DEVELOPMENT OF ELECTROANALYTICAL MATERIALS FOR BIOSENSORS (CHAPTERS 2, 3 & 4)

Electroanalytical sensors and biosensors provide an exciting and achievable opportunity to perform biomedical, environmental and industrial analyses away from a centralised laboratory Screen-printed electrodes in particular can combine ease of use and portability with simple, inexpensive fabrication techniques The modest cost of screen-printed electrodes has further enhanced their desirability because it allows the devices to become disposable Recent years have seen a tremendous increase in the focus on screen printing as an inexpensive electrode production method Screen printing can be used to print whole electrode systems with reference and auxiliary electrodes, each with their own tailored characteristics They can be made cheaply, and with a high degree of precision They can be used to produce a wide range of electrode geometries (either as arrays or single electrodes) It has been researched to date as a method of planar electrode fabrication Chapter 1 demonstrated the versatility of the screen-printing technique, where different planar electrode configurations were utilised, along with different inks All electrodes were characterised in terms of electrochemical behaviour, and it was seen that, in line with other studies, the Gwent D14 ink was certainly the best material for amperometric biosensor development

Porous electrodes possess several advantageous properties over planar electrodes suitable for electroanalysis For example, reticulated vitreous carbon (RVC), claimed to possess several advantages over planar electrodes, is characterised by an open pore structure of random carbon struts with a void volume as high as 90 – 97% (Pena *et al*, 2001) It has a low resistance to flow, and a very high area-to-volume ratio Moreover, the microporous nature of RVC facilitates mass transport of the electroactive species to the electrode surface, potentially resulting in a high coulometric efficiency and low detection limits Electroanalytical applications for porous carbon materials such as RVC have been realised, using non-disposable solid carbon rods (Dimakis *et al*, 2002, Serra *et al*, 2002) However, to the author's

knowledge, screen printing has not been utilised to date for the development of porous carbon materials Many templating protocols have been documented in recent years for development of nano- or micro- porous electrodes For some biosensing applications, micro- or even macro-porous electrodes are required for easy diffusion of large molecular weight species through the carbon structure The next step in this research could be to move away from the planar electrode configuration, and towards macro-porous 3-dimensional electrode configurations Transferring of this porous templatmg technology to screen-printed electrodes would involve introducing regular porous spheres such as colloidal particles, silica or polymer latex spheres, into the ink before printing The spheres would then be removed under conditions that do not impact on the carbon ink, subsequent to printing and curing of the ink Silica spheres can be removed from a solid framework with aqueous hydrofluoric acid (HF) solution while removal of latex can be carried out by either calcination, or by extraction with a suitable solvent, e g , tetrahydrofuran (THF)/acetone

Development of this technique could result in non-ordered macro-porous disposable three-dimensional carbon electrodes, with large mcreases in surface area-to-volume ratios The high surface area is an important advantage for their potential use in biosensors, as a consequence of the high protein mass loading capacity expected Miniaturisation of electrodes is more difficult with amperometric techniques as the response is dependent on electrode area Introducing a third dimension allows small lateral dimensions of the electrode to be used without loss of response Alternatively, the increase in surface area can be of significant benefit in systems which utilise surface-confined interactions such as immunosensors Here, the increase in electrode surface area allows for immobilisation of greater quantities of immunoreagents, again leading to improvements in signal-to-background ratios In addition, utilisation of the porous electrode as a thin layer cell would allow for very high linear flow rates and high rates of mass transport of the reactive species to the electrode surface These properties would supersede the present planar electrodes m terms of space-time yields and normalised space velocities

Properties of the copolymer PANI/PVS as a non-diffusional mediator for a biosensor were investigated in the second part of *Chapter 2* Electropolymerised using cyclic voltammetry onto screen-printed electrodes, the growth of the polymer was found to be highly irreproducible in terms of charge capacity For PANI biosensing applications, this leads to high irreproducibility in quantitative data The charge

incorporated into the polymer was factored into sensor responses, and although the coefficient of variation was reduced significantly, it remains at a level of 30% Fundamental research on the growth of this polymer is required to elucidate the other factors relating to the polymer's unpredictable behaviour Other electrochemical techniques such as galvanostatic and potentiostatic methods need to be investigated in order to see if more precise control can be achieved over the growth of the polymer Additionally, variations in electrochemical cell geometry should be investigated and the effect of varying the IR drop on the polymerisation process could be studied This would require production of a controlled geometry electrochemical cell The polymerisation of PANI is also known to be temperature dependent, and so it is important to carry out electrochemical polymerisations under temperature-controlled conditions The goal here is to produce PANI/PVS electrode surfaces with significantly improved reproducibility

Although the electropolymerisation of PANI as a method of deposition is good for laboratory-based research, ultimately this technique needs to be replaced with cheaper, mass fabrication methods Electropolymerisation is not easily amenable to production techniques *Chapter 4* investigated the properties of nanoparticulate PANI dispersions using two deposition methods electrodeposition and drop-coating It was found that the electrodeposition of the nanoparticles onto an electrode surface led to a very highly ordered, nanostructured polymer film In terms of enzyme biosensing, this film would be highly competitive with the PANI/PVS system in terms of analytical characteristics, with a very efficient protein immobilisation capability This electrodeposited nanoparticulate system will be investigated as an alternative platform to the PANI/PVS system (Killard *et al*, 1999) for future bio- and immuno-sensor developments in our group

Drop-coating of the nanoparticles was also investigated as a promising method of modifying electrodes, with a view to biosensor development Casting of films holds much more potential than electrodeposition in terms of ease of fabrication and mass production The drop-coating technique was explored, as it was easy to perform in the laboratory Following this study, more sophisticated casting methods such as spin-coating or ink-jet printing could be used The most successful drop-coating protocol was a single-step biosensor fabrication technique where enzyme was incorporated into PANI nanoparticle dispersions for simultaneous drop-coating onto electrodes This drop-coated biosensor possessed reasonable analytical characteristics

However, the inherent thickness of the polymer film due to the method of deposition inhibited its potential A more sophisticated deposition method is required in order to deposit thinner, more homogeneous films Spin-coating is a possible technique Again, however, it is not amenable to large-scale development Ink-jet printing is an established technique that allows fluids to be deposited with low volume, great accuracy and at high speed These features would attribute great flexibility in terms of the design components of a biosensor device Volumes in the picolitre range can be deposited, thereby making the technique a cost-effective approach to large-scale sensor production The accurate deposition of protein-containing inks onto screen-printed carbon working electrodes would transfer the drop-coating protocol from manual deposition to large-scale production by mechanical methods Successful development of this technique could, in the future replace electrochemical deposition processes, eliminating the complexity, inconvenience and time delays associated with electrochemical deposition processes if suitably high quality films could be produced In addition, very little wastage would be associated with the ink-jet printing of expensive or valuable protein solutions, illustrating the economical benefits of this proposed process Simultaneous or sequential deposition of protein and other electrode components could be readily achieved with this versatile method Multi-analyte sensors could also be manufactured with ease In addition, the control of the size of the droplets deposited would mean that the manufacture of microelectrodes would also be feasible A single reference to the ink-jet printing of enzyme composites has been reported in the literature (Newman & Turner, 1992) However, this biosensor required the addition of external electron transfer mediators To the author's knowledge, ink-jet printing has not been applied to date for the production of mediatorless conducting polymer-based biosensors

Finally, formation of porous PANI films using a similar approach to that discussed for the carbon screen-printed electrodes could also be investigated These polymer films would have all the benefits that were discussed earlier for carbon electrodes, such as high surface areas and high coulometric efficiency This research should initially focus on the development of porous electropolymerised or electrodeposited polymer films Although this moves away from the idea of a printable biosensor, it would be interesting to explore as a technique that could eventually be further developed with techniques such as ink-jet printing

*Chapter 3* explored the electrostatic deposition method of protein on the surface of the PANI/PVS films This technique is once again only amenable to laboratory-based research, and it is not a method suited towards mass production Despite this, much can be elucidated in terms of optimum protein behaviour This work theorized on the concept of approximate monolayer formation for optimum charge transfer between immobilised enzyme and the PANI layer However, although this colorimetric investigation was in agreement with the imaging of gold-labelled protein on the surface by Grennan (2003), neither method was direct Direct imaging of a protein-modified PANI layer had been investigated using scanning electrochemical microscopy (SECM) previously, but due to the roughness of the surface it was unsuccessful The *nano*PANI/DBSA showed a much smoother morphology to the PANI/PVS system (*Chapter 4*), and as such, SECM imaging on this protein-modified surface may provide a direct visualisation of immobilised protein Combined scanning electrochemical-atomic force microscopy (SECM-AFM), (Macpherson & Unwin, 2000), a recently developed technique could also be used for simultaneous topographical and electrochemical measurements of the protein-modified polymer surface Understanding of the protein-modified electrode surface is critical for the production of high quality biosensor systems, and further investigation is still required to elucidate more precisely the mechanisms and processes involved

In the processes involving HRP alone, further studies could be performed on the effect of orientation of the protein at the electrode surface Since HRP interacts both with the bulk (through diffusion of $H_2O_2$) and the electrode (through electron transfer), the interplay of these two processes is critical to the performance of mediated reduction of hydrogen peroxide However, which process is the most critical could be determined by the controlled orientation of all proteins at the electrode surface Such control could be achieved *via* a combination of new surface immobilisation techniques and protein engineering Once again, such fundamental studies will also lead to improvements in biosensor performance

The situation becomes more complex when dealing with an antibody-antigen interaction Now, at least two species are involved The effect of orientation of the antibody and the electrode surface, and its interaction with an enzyme-labelled species plays a critical role in sensor response Such orientated immobilisation studies would again yield extremely valuable information as to the fundamental processes involved, again with the knock-on benefit of improved sensor configurations

As a result of the work performed in these chapters, work is foreseen involving carbon ink development, printing techniques and physical and analytical characterisation To achieve the goal of a viable mass-producible bio- or immuno-sensor device, fundamental studies on fabrication technologies, electrode design and a complete characterisation of the modified electrode would be necessary

## 7.2 NOVEL DEVELOPMENT OF ELECTROCATALYTIC SELF-ASSEMBLED MONOLAYERS (CHAPTER 5)

The work in this chapter focussed on another biosensor development approach – spontaneous adsorption A cyclopentadienylnickel(II) thiolato Schiff base was shown to spontaneously adsorb on gold to yield a redox active layer of the thiolato Schiff base This monolayer exhibited surface-confined quasi-reversible electrochemistry of the nickel(II) centre Further work is required to improve the kinetics of the Ni(II) centre of the complex Investigations into the effects of varying the chain length, increasing the number of conjugated π–bonds and perhaps utilising a mixed monolayer approach m order to minimise steric hindrance, may all serve to improve the kinetics of this electroactive layer

HRP immobilisation onto the Ni(II) layer was carried out by electrostatic adsorption Electrocatalytic reduction of $H_2O_2$ was observed, and the electroproduced Ni(II) was effectively consumed in enzyme catalysis This immobilisation method results in a random non-oriented distribution of protein across the surface, resulting in non-optimised conditions for charge transfer between the redox centre of the HRP and the Ni(II) sites In addition, an inherent irreproducibility is associated with this technique A variety of other immobilisation techniques are available that could be utilised in order to develop a more ordered protein layer One class of spontaneously adsorbed layers (usually self-assembled monolayers) useful for immobilising proteins uses alkanethiolates terminally functionalised with a biotin moiety The biotin binds streptavidin, which in turn permits the immobilisation of biotin-labelled proteins This is widely used as a method for oriented immobilisation, but has disadvantages as this modification procedure can lead to denaturation of the protein In addition, and the presence of multiple sites on the protein available for modification results in loss of control over the orientation of the protein after immobilisation Another approach would be to generate an adsorbed layer functionalised with nitrilotriacetic acid (NTA) or other macrocyclics that when complexed with Ni(II), would selectively bind to proteins labelled with a histidine tag (His-tag) This method of immobilisation could control the orientation of the immobilised protein such that the active site would be

accessible to molecules in solution An NTA-functionalised SAM has previously been used before as a regenerable surface for protein immobilisation, where surface plasmon resonance (SPR) was used to study the interaction of bound His-tagged protein with molecules in solution (Sigal *et al*, 1996) Since Ni(II) complexes with conjugated backbones have been shown to behave as non-diffusional mediators, a novel NTA-functionalised conjugated complex that could spontaneously adsorb could stem from this work An adsorbed layer of this functionalised compound could complex with Ni(II) which could serve as the electrocatalytic centre of the layer and also be used as a site for protein immobilisation In theory, this type of dual-purpose layer could both mediate and promote oriented immobilisation of His-tagged redox active proteins Fundamental information on electron transfer rates could be gauged from this format, in addition to data on the interaction of bound His-tagged proteins with molecules in solution Studies such as these could lead to the development of a novel electrochemical biosensor platform, as well as serving to give practical improvements to current biosensor designs

This NTA-Ni procedure could also be applicable as an alternative immobilisation technique to electrostatic adsorption, used for the PANI systems in *Chapters 2, 3 & 4* NTA could be entrapped within the polymer films during growth, and could subsequently complex with Ni(II) to produce active sites for the oriented immobilisation of engineered His-tagged enzymes or antibodies

## 7.3 TOWARDS DIRECT ELECTROCHEMICAL SENSING OF SULPHUR DIOXIDE (CHAPTER 6)

Sulphur dioxide coordination to metal complexes attracts attention because of its potential use in developing $SO_2$ sensors or scrubbers This chapter dealt with some fundamental research on a novel electrochemical sensor for $SO_2$ It was shown that particular types of cyclopentadienylnickel(II) complexes form reversible $SO_2$ adducts that can be detected electrochemically All of this work was carried out in solution phase, using cyclic voltammetry to monitor changes in potential shifts These compounds have the potential to be developed as amperometric sensors that could allow direct electrochemical detection of $SO_2$ without having to oxidise the $SO_2$ to sulphate before detection

In order for further development, more fundamental work is required in order to gain a better insight into the electronic properties of the thiolato complexes used and their capabilities and limitations for forming $SO_2$ adducts The effects of ligand variation and metal substitution on the complexes need to be examined in detail with the aim of establishing conditions where maximum electrochemical shifts can be observed upon adduct formation By using techniques such as electrochemistry, UV-Vis and $^1H$ NMR, the influence of the electron density of the metal centre could be elucidated In this work, two different adduct formation mechanisms were proposed for two different types of complexes, i e , attachment to $SO_2$ to the S attached to a metal bond, and insertion of $SO_2$ into a metal sulphur bond Synthesis of a an extended range of complexes so that both of these reactions could be studied in more detail is necessary m order to confirm these postulated reactions The effect of the substituents on the ligands should also be explored

The lability of the $SO_2$ adducts has prevented isolation of solid $SO_2$ adducts for structural characterisation However, work could be carried out to isolate the complex after $SO_2$ desorption It is possible that some irreversible structural changes occur for the complexes that would give direct evidence to the proposed $SO_2$ adduct formation reactions given within *Chapter 6*

It has yet to be investigated whether $SO_2$ adduct formation could be followed by chronoamperometry If this was possible, rates of adduct formation and dissociation could be determined These parameters would be important in order to determine the quality of different complexes for further sensor work

The use of ligand substituents such thiol or methyl thiolato could prove instrumental in terms of developing a solid phase $SO_2$ sensor Complex [4] possessed methyl sulphide end groups that could be used for self-assembly on gold The self-assembly of this complex was carried out in *Chapter 5*, and further work needs to be carried out in order to see if a SAM of this complex could withstand reversible $SO_2$ absorption If this was shown to be possible, solution phase adduct formation could thus be easily extended to surface-bound adduct formation This would lead to an advancement from indirect to direct electrochemical detection of $SO_2$ in the chemical sensing field

## 7.4 SUMMARY AND GENERAL OUTLOOK

On completion of the work proposed in this chapter, significant benefits could be foreseen for the electroanalytical field in general The successful development of macro-porous screen-printed electrodes could add to the many benefits of the screen printing technique, for biosensor applications in particular Additional fundamental studies of polyaniline as a non-diffusional mediator in biosensing should also advance the credibility of it as an effective part of a biosensor system The improvements in the processability characteristics of polyaniline to date, could lead to polyaniline-modified electrodes that are reliable and easy to fabricate

While many biosensors have attained the required detection limits for a range of analytes of medical, environmental or industrial significance, the main obstacle in their path to widespread use and acceptance is the inability or impracticality in producing such systems on a large scale The work described in this chapter proposes a feasible alternative to the time consuming and complex nature of biosensor preparation Although the printing techniques put forward are established and widely used techniques in other manufacturing areas, they are only beginning to infiltrate the electroanalytical field Their adaptation to the biosensor field is both reasonable and uncomplicated Screen printing is already the method of choice for the production of sensors for the monitoring of blood sugar levels in diabetes patients Ink-jet printing is a non-contact printing process that is simple to install, occupies minimal production line space and can be situated on line The entire production process is appealing from a manufacturing point of view and has the potential to create a niche in the market place for cheap, disposable sensor devices

Recently, the bonding of enzymes to self-assembled monolayers of alkanethiols on gold surfaces has begun to receive attention as a robust method of constructing biosensors where precise control over the orientation and distribution of the enzyme is afforded However, in terms of electrochemical biosensing, either direct electron transfer needs to be possible between the enzyme and the electrode, or an external mediator needs to be employed for biosensor devices The development of a SAM that could behave electrocatalytically and simultaneously orientate protein would lead to a very effective platform for monitoring both catalytic and binding

protein interactions electrochemically The method outlined would be applicable to any protein that could be genetically engineered with a His-tag This surface could be used for studying reaction and binding kinetics of proteins for biosensor development devices, where the method of immobilisation would ensure control over the immobilised protein such that the active site would be accessible to molecules in solution The electrocatalytic properties of the proposed SAM would ensure that under the correct conditions, electrochemical signals could be achieved for all proteins with active redox centres The impact of such a device would be significant There is no electrochemical device to date that would rival the optical BIAcore™ system in terms of sensitivity and versatility However, with the development of very sophisticated electrocatalytic SAMs, cheap electrochemical devices could eventually compete with optical bench-top systems presently on the market

In addition to biosensors, the development of the proposed chemical sensor for direct $SO_2$ sensing, would impact on the chemical sensing market To date, no sensitive direct amperometric technique has been commercialised for $SO_2$ detection New directives from the European Commission demands stringent monitoring of this gas and although there are techniques available, they are time-consuming, laborious and expensive The sensor proposed in this work, based on a SAM, would be cost-effective and simplistic

In conclusion, several different electrode modification schemes have been proposed in this chapter for application in electroanalytical devices In combination with the research carried out in this thesis and powerful analytical tools available, extended research into these proposed ideas could benefit the electroanalytical field, in particular, bio- and chemical sensing, immensely

## 7.4 REFERENCES


Dimakis, V , Gavalas, V , Chaniotakis, N (2002) Polyelectrolyte-stabilized biosensors based on macroporous carbon electrode *Anal Chim Acta,* **467** 217-223

Grennan, K (2003) Developments in electrochemical immunosensors PhD Thesis School of Chemical Sciences, Dublin City University, Ireland

Killard, A J , Zhang, S , Zhao, H , John, R , Iwuoha, E I , Smyth, M R (1999) Development of an electrochemical flow injection immunoassay (FIIA) for the real-time monitoring of biospecific interactions *Anal Chim Acta,* **400** 109-119

Macpherson, J , Unwin, P (2000) Combined scanning electrochemical-atomic force microscopy *Anal Chem* , **15** 276-285

Newman, J , Turner, P (1992) Ink-jet printing for the fabrication of amperometric glucose biosensors *Anal Chim Acta,* **262** 13-17

Serra, B , Jimenez, S , Mena, M , Reviejo, A , Pingarron, J (2002) Composite electrochemical biosensors a true comparison of three different electrode matrices for the construction of amperometric tyrosinase biosensors *Biosens Bioelectron* , **17** 217-226

Sigal, G , Bamdad, C , Barberis, A , Strominger, J , Whitesides, G (1996) A self-assembled monolayer for the binding and study of histidine-tagged proteins by surface plasmon resonance *Anal Chem* , **68** 490-497

# LIST OF PUBLICATIONS AND PRESENTATIONS

## PAPERS

- Aoife Morrin, Alicia Guzman, Anthony J Killard, Jose M Pingarron, Malcolm R Smyth (2002)
  *'Characterisation of horseradish peroxidase immobilisation on an electrochemical biosensor by colorimetric and amperometric techniques'*
  Biosens Bioelectron , **18** 715-720

- Aoife Morrin, Anthony J Killard, Malcolm R Smyth (2003)
  *'Electrochemical characterisation of commercial and home-made screen-printed carbon electrodes'*
  Anal Lett , **36** 2021-2039

- Aoife Morrin, Richard M Moutloali, Anthony J Killard, Malcolm R Smyth, James Darkwa, Emmanuel Iwuoha (2004)
  *'Organic phase cyclopentadienylnickel thiolate sensor system for electrochemical determination of sulfur dioxide'*
  Electroanalysis, In press

- Aoife Morrin, Richard M Moutloali, Anthony J Killard, Malcolm R Smyth, James Darkwa, Emmanuel Iwuoha (2004)
  *'Electro-Catalytic Sensor Devices (I) Cyclopentadienylnickel(II) Thiolato Schiff Base Monolayer Self-Assembled on Gold'*
  Talanta, **64** 30-38

- Emmanuel Iwuoha, Avril R Wilhams-Dottin, Lincoln A Hall, Aoife Morrin, Gretta N Mathebe, Malcolm R Smyth, Anthony J Killard (2004)
  *'Electrochemistry and application of novel monosubstituted squarate electron-transfer mediator in a glucose oxidase-doped poly(phenol) sensor'*
  Pure App Chem , **76** 789-799

- Aoife Morrin, Orawan Ngamna, Anthony J Killard, Simon Moulton, Malcolm R Smyth, Gordon G Wallace (2004)
  *'A polyaniline based enzyme biosensor fabricated from nanoparticles'*
  Submitted to Electroanalysis

## POSTER PRESENTATIONS

- **Analytical Research Forum Incorporating Research and Development Topics**
  University of East Anglia, Norwich, UK, 16-18 July 2001
  *'Immunoelectrochemical methods of hormone analysis'*
  Aoife Morrin, Malcolm R Smyth, Anthony J Killard

- **2nd Annual Conference on Analytical Sciences in Ireland**
  Institute of Technology, Tallaght, Dublin 24, Ireland, 4-5 April 2002
  *'Elucidation of the mode of action of a conductive polymer-based electrochemical immunosensor'*
  Aoife Morrin, Anthony J Killard, Malcolm R Smyth

- **Biosensors 2002 The 7th World Conference on Biosensors**
  Kyoto, Japan, 15-17 May 2002
  *'Elucidation of the mode of action of a conductive polymer-based electrochemical immunosensor'*
  Aoife Morrin, Alicia Guzman, Jose M Pingarron, Anthony J Killard, Malcolm R Smyth

- **Analytical Research Forum Incorporating Research and Development Topics**

  Kingston University, Kingston upon Thames, London, UK, 15-17 July 2002

  *'Elucidation of the mode of action of a conductive polymer-based electrochemical immunosensor'*

  Aoife Morrin, Alicia Guzman, Jose M Pingarron, Anthony J Killard, Malcolm R Smyth

- **The Inaugural Conference of the Southern and Eastern Africa Network of Analytical Chemists (SEANAC)**

  Gaborone, Botswana, 7-10 July 2003

  *'High performance electrocatalytic nanosensor devices (I) Cyclopentadienylnickel(II) thiolato Schiff base monolayer self-assembled on gold'*

  Aoife Morrin, Richard M Moutloali, Anthony J Killard, Malcolm R Smyth, James Darkwa, Emmanuel Iwuoha

- **Cape Organometallic Symposium**

  Morganhof, Stellenbosch, South Africa, 30 July 2003

  *'Development of a highly sensitive electrochemical $SO_2$ sensor based on $SO_2$ adduct formation from cyclopentadienyl nickel(II) thiolato complexes'*

  Aoife Morrin, Richard M Moutloali, Anthony J Killard, Malcolm R Smyth, James Darkwa, Emmanuel Iwuoha

- **10th International Conference on Electroanalysis, European Society for Electroanalytical Chemistry (ESEAC)**

  National University of Galway, Ireland, 6-10 June 2004

  *'Application of nanoparticulate conducting polyaniline in nanofilm biosensor technology'*

  Aoife Morrin, Orawan Ngamna, Anthony J Killard, Simon Moulton, Malcolm R Smyth, Gordon G Wallace (2004)